รายงานวิจัยฉบับสมบูรณ์

งานวิจัยและพัฒนาระบบอบแห้งไม้ยางพาราเชิงพาณิชย์โดยใช้ไมโครเวฟชนิดป้อนคลื่นหลายตำแหน่งที่ไม่สมมาตรร่วมกับระบบลมร้อนและสายพานลำเลียงอย่างต่อเนื่อง

(Research and Development on the Commercialized Wood Drier Using a Combined Unsymmetrical Multi-Feed Microwave and Hot Air-Continuous Belt System)

โดย ศาสตราจารย์ ดร.ผดุงศักดิ์ รัตนเดโช

12 กันยายน 2554

สัญญาเลขที่ IUG5280012

รายงานวิจัยฉบับสมบูรณ์

งานวิจัยและพัฒนาระบบอบแห้งไม้ยางพาราเชิงพาณิชย์โดยใช้ไมโครเวฟชนิดป้อนคลื่นหลายตำแหน่งที่ไม่สมมาตรร่วมกับระบบลมร้อนและสายพานลำเลียงอย่างต่อเนื่อง

(Research and Development on the Commercialized Wood Drier Using a Combined Unsymmetrical Multi-Feed Microwave and Hot Air-Continuous Belt System)

โดย ศาสตราจารย์ ดร.ผดุงศักดิ์ รัตนเดโช

สนับสนุนโดยสำนักงานกองทุนสนับสนุนการวิจัย (สกว.)

(ความเห็นในรายงานนี้เป็นของผู้วิจัย สกว. ไม่จำเป็นต้องเห็นด้วยเสมอ)

หน้าสรุปโครงการ (Executive Summary)
"โครงการการสร้างกำลังคนเพื่อพัฒนาอุตสาหกรรม"

1. **ชื่อโครงการ**

งานวิจัยและพัฒนาระบบอบแห้งไม้ยางพาราเชิงพาณิชย์โดยใช้ไมโครเวฟชนิดป้อนคลื่นหลายตำแหน่งที่ไม่สมมาตรร่วมกับระบบลมร้อนและสายพานลำเลียงอย่างต่อเนื่อง
(Research and Development on the Commercialized Wood Drier Using a Combined Unsymmetrical Multi-Feed Microwave and Hot Air-Continuous Belt System)

2. **ชื่อหัวหน้าโครงการ หน่วยงานที่สังกัด ที่อยู่ หมายเลขโทรศัพท์ โทรสาร และ** e-mail

รองศาสตราจารย์ ดร. ผดุงศักดิ์ รัตนเดโช
หน่วยวิจัยเพื่อการใช้ประโยชน์จากไมโครเวฟในงานวิศวกรรม (R.C.M.E.)
ภาควิชาวิศวกรรมเครื่องกล คณะวิศวกรรมศาสตร์
มหาวิทยาลัยธรรมศาสตร์ ศูนย์รังสิต คลองหลวง ปทุมธานี
หมายเลขโทรศัพท์ 02-564-3001-9 ต่อ 3153 โทรสาร 02-564-3010
E-mail ratphadu@engr.tu.ac.th

3. **สาขาอุตสาหกรรมที่ทำการวิจัย**

อุตสาหกรรมการแปรรูปผลิตภัณฑ์ทางการเกษตร
อุตสาหกรรมอาหาร
อุตสาหกรรมแปรรูปพลังงาน

4. **คำหลัก** (keyword) **ของโครงการวิจัย** (3 – 5 **คำ**)

กระบวนการอบแห้ง ไมโครเวฟ ไม้ยางพารา ผลิตภัณฑ์ทางการเกษตร

5. **งบประมาณทั้งโครงการ** 3,000,000 **บาท (ระดับที่** 3)

6. **ระยะเวลาดำเนินงาน** 2 **ปี**

7. ได้เสนอโครงการนี้หรือโครงการที่มีส่วนเหมือนกับเรื่องนี้บางส่วนเพื่อขอทุนต่อแหล่งทุนอื่นที่ใดบ้าง

☐ **ไม่ได้เสนอต่อแหล่งทุนอื่น**

☐ **เสนอต่อ** _____

ชื่อโครงการที่เสนอ _____

กำหนดทราบผล (หรือสถานภาพเท่าที่ทราบ)_____

8. ความเชื่อมโยงกับหุ้นส่วนวิจัยในภาคอุตสาหกรรม

8.1 ชื่อผู้ประกอบการที่เป็นหุ้นส่วนวิจัยในภาคอุตสาหกรรม

บริษัท ศรีพิพัฒน์เอ็นจิเนียริ่งจำกัด (ซึ่งเป็นผู้ประกอบการที่ให้ความร่วมมือเป็นอย่างดีในโครงการแรก (ระดับที่ 3) ที่เคยอนุมัติโดย สกว. "งานวิจัยและพัฒนาระบบอบแห้งอเนกประสงค์เชิงพาณิชย์ โดยใช้ ไมโครเวฟ ร่วมระบบสุญญากาศ; กรณีศึกษา: ผลิตภัณฑ์ที่มีคุณภาพสูง"

ประเภทธุรกิจ งานด้านวิศวกรรม ขายเครื่องมือและระบบทางวิศวกรรม

ผู้รับผิดชอบโครงการ นายมงคล ใบโพธิ์วงศ์

ตำแหน่ง Chief Executive

ที่อยู่ 165/1 ซอย สุขุมวิท 93 ถ. สุขุมวิท แขวงบางจาก เขตพระโขนง กรุงเทพ 10260

โทรศัพท์ 02-331-9103

โทรสาร 02-333-0061

โทรศัพท์มือถือ 01-908-1261

การสนับสนุนจากภาคอุตสาหกรรม

1. In cash มูลค่า 150,000 บาท

2. In kind (ระยะการดำเนินการ 6 เดือน)***

2.1 อุปกรณ์เครื่องมือ ในการทำชิ้นส่วนและอะไหล่ประกอบเครื่อง (คิดประเมินเป็นค่าเช่าต่อเดือน)

- เครื่องพับ	คิดเป็นมูลค่า 270,000 บาท
- เครื่องเชื่อมอาร์กอน	คิดเป็นมูลค่า 18,000 บาท
- เครื่องกลึง	คิดเป็นมูลค่า 192,000 บาท
- อุปกรณ์ในการผลิตชิ้นส่วนประกอบเครื่อง	คิดเป็นมูลค่า 150,000 บาท

โดยอุปกรณ์เครื่องมือทั้งหมดตั้งอยู่ใน บ.ศรีพิพัฒน์เอ็นจิเนียริ่ง จำกัด

2.2 บุคลากรร่วมงาน จำนวน 6 คน คิดเป็นมูลค่า 360,000 บาท (คิดประเมินจากเงินเดือน)

*** ส่วนสนับสนุนที่นอกเหนือจากงบประมาณ 3 ล้านบาท

8.2 ระดับความร่วมมือกับหุ้นส่วน (เลือกข้อใดข้อหนึ่ง)

☐ **ภาคอุตสาหกรรมให้การสนับสนุนงบประมาณเพื่อการวิจัย** (in cash) **มาระยะเวลาหนึ่งแล้ว (กรุณาสรุปแนวทางและรูปแบบความร่วมมือที่ผ่านมา)**

- ให้งบประมาณมาสร้างเครื่องต้นแบบระดับ Pilot Scale

☐ **ภาคอุตสาหกรรมให้การสนับสนุนด้านสถานที่ โครงสร้างพื้นฐาน เครื่องมือ วัสดุสำหรับการวิจัย ฯลฯ** (in kind) **มาระยะเวลาหนึ่งแล้ว**
(กรุณาสรุปแนวทางและรูปแบบความร่วมมือที่ผ่านมา)

- ทำการขึ้นรูปวัสดุโดยใช้วัสดุและเครื่องมือภายในโรงงานของผู้ประกอบการ
- ทำการทดสอบภาคสนามภายในโรงงานของผู้ประกอบการ

☐ **อยู่ระหว่างการเจรจาความร่วมมือกับภาคอุตสาหกรรม**
(กรุณาระบุแนวทางและรูปแบบการเจรจาพร้อมประมาณการระยะเวลาที่คาดว่าจะเริ่มความร่วมมือได้)

☐ **อื่น ๆ โปรดระบุ**

8.3 สรุปรูปแบบของผลผลิตหรือการนำผลงานไปใช้ประโยชน์

- ได้ระบบต้นแบบที่สามารถนำไปประโยชน์ได้จริงในอุตสาหกรรม
- ในส่วนของตัวเทคโนโลยีการออกแบบสามารถปรับเปลี่ยน Sizing และปริมาณการผลิตตามความต้องการลูกค้าได้ (made to order)

9. ความเชื่อมโยงกับนักวิจัยที่เป็นผู้เชี่ยวชาญในสาขาและ/หรืออุตสาหกรรมที่ทำการวิจัย

- ทำวิจัยร่วมกับ Prof. Kazuo Aoki แห่งมหาวิทยาลัยเทคโนโลยีนากาโอกะ ประเทศญี่ปุ่น ในโครงการ “Microwave Heating of Dielectric Materials”

- ทำวิจัยร่วมกับ Prof. Dr. K. Vafai แห่งมหาวิทยาลัย California ประเทศสหรัฐอเมริกา ในหัวข้อ “Heat and Mass Transfer in Porous Media Under Microwave Energy.

- ทำวิจัยร่วมกับ ดร. ดวงเดือน อาจองค์ ศูนย์เทคโนโลยีโลหะและวัสดุแห่งชาติ (MTEC) ในหัวข้อ “Analysis of Heating Process in Dielectric Materials Using a Continuous Microwave Belt Furnace”

- ทำวิจัยร่วมกับ รศ. ดร. สักกมล เทพหัสดิน ณ อยุธยา แห่งมหาวิทยาลัยเทคโนโลยีพระจอมเกล้าธนบุรี ในโครงการ “Research and Development of Heat and Mass Transfer in Porous Media”

10. ปัญหาที่ทำการวิจัยและความสำคัญของปัญหา

ไม้ยางพาราเป็นวัตถุดิบที่มีปริมาณมากในประเทศไทย ซึ่งเป็นผลพลอยได้ในการผลิตยางพาราและมีความสำคัญในฐานะเป็นพืชเศรษฐกิจที่สามารถนำไปแปรรูปเป็นผลิตภัณฑ์เช่นเฟอร์นิเจอร์ ทำรายได้ให้กับอุตสาหกรรมไม้เป็นอย่างมาก

ในกระบวนการแปรรูปไม้ยางพาราเป็นกระบวนการที่สำคัญอย่างหนึ่งในการผลิตไม้ยางที่ป้อนให้กับโรงงานอุตสาหกรรมที่มีต้นทุนในการผลิตสูง เพราะต้องใช้เครื่องจักรและกระบวนการที่มีความซับซ้อนในการผลิต โดยปกติหลักการของกระบวนการอบแห้งไม้ยางพารานั้นคือ การป้อนพลังงานความร้อนเพื่อทำให้ ความชื้นเคลื่อนตัวออกจากเนื้อไม้ และการเคลื่อนที่ของลมร้อนภายในเตา การใช้พลังงานในกระบวนการอบแห้งดังกล่าวมีต้นทุนสูงเป็นอย่างมาก และส่งผลต่อมลภาวะแก่สิ่งแวดล้อม ในทางเทคนิคในกระบวนการอบแห้งไม้นั้นจะดำเนินการจนให้มีปริมาณความชื้นของไม้ (Moisture Content) ต่ำกว่าจุดหมาด (Fiber Saturation Point) หรือเข้าสู่สภาวะสมดุลกับความชื้นของบรรยากาศ อย่างไรก็ตามกระบวนการอบไม้แบบดั้งเดิม(ดังรูปที่ อ (1) ในเอกสารแนบ) ในกระบวนการผลิตโดยภาพรวมนั้นเริ่มต้นจากทางผู้ผลิตจะรับซื้อไม้ท่อนจากลูกค้าทั่วไปและจากผู้รับเหมาทำแปลงไม้ ที่มีขนาดความยาวโดยประมาณ 1.00 เมตร. 1.10 เมตร.และ 1.25 เมตร. จากนั้นจะมาผ่านกระบวนการแปรรูปตามขนาดความหนาและหน้าไม้ตาม คำสั่งซื้อของลูกค้าแล้วนำ

ไม้ผ่านการแปรรูปแล้วเข้าสู่กระบวนการอัดน้ำยาเข้าเนื้อไม้ เพื่อกันมอดและรา โดยใช้แรงดันสูง ปริมาณในการอัดน้ำยาแต่ละครั้งประมาณ 350 ลูกบาศก์ฟุต จากนั้นนำมาจัดเรียงไม้หลังอัดน้ำยา โดยใช้ไม้ระแนงขนาด 3/4 นิ้ว คั่นกลางแต่ละชั้นตามขนาดความกว้างและความหนา เพื่อให้ระยะห่างของช่องลมร้อนระหว่างชั้นที่คั่นด้วยไม้ระแนงและเพื่อให้มีน้ำหนักกดทับทั้งนี้เพื่อลดการโค้งงอของไม้หลังการอบแห้ง จากนั้นจะลำเลียงไปวางในพื้นที่พักไม้เข้าเตาเพื่อรอการเข้าเตาต่อไป โดยการเข้าเตานั้นจะทำการเข้าเตาทำการอบตามกลุ่มการอบ (โดยใช้ความหนาเป็นตัวแบ่งกลุ่มไม้) ซึ่งสามารถแบ่งกลุ่มการอบตามความหนาโดยมีระยะเวลาการอบ, แบ่งตามกลุ่มและเปอร์เซ็นต์ความชื้นที่ต้องการตามตารางที่ อ (1) ในเอกสารแนบ

ซึ่งเตาอบที่ใช้ในปัจจุบันซึ่งอ้างตามข้อมูลของบริษัทผู้ผลิตคือกลุ่มบริษัท กลุ่มบริษัท วู้ดเวอร์ค มีขนาด ความกว้าง 5.90 เมตร. ความลึก 7.25 เมตร. และความสูง 4.75 เมตร. มอเตอร์ซึ่งใช้เป็นพัดลมขนาด 5.5 แรงม้า(HP) เตาละ 3 ตัว มีการใช้กระแสไฟฟ้ารวม เตาละ18 แอมแปร์ มีปริมาณการใช้ไอน้ำเตาละ 3.83 ลูกบาศก์เมตร/วัน ระดับแรงดันที่ใช้อบประมาณ 3 – 5 บาร์ ขนาดคอยล์ลมร้อน 940 x 560 x 73 มิลลิเมตร. ชุดละ 8 เส้น จำนวน 2 ชุด ประมาณค่าใช้จ่ายด้านพลังงานในการอบไม้เฉลี่ยวันละ 1,300 บาท ต้นทุนในการอบโดยเฉลี่ย 9 บาท/ลูกบาศก์ฟุต

อย่างไรก็ตาม จากการวิจัยเชิงสำรวจ พบว่ากระบวนการอบแห้งไม้แบบดั้งเดิม เป็นกระบวนการที่สิ้นเปลืองพลังงาน และยังมีปัญหาในการควบคุมคุณภาพของเนื้อไม้ และปัญหาสิ่งแวดล้อม จึงเป็นที่มาของการแสวงหาเทคโนโลยีอันใหม่ที่สามารถทดแทนเทคโนโลยีดั้งเดิม

ที่ผ่านมา ผู้วิจัย (รศ .ดร.ผดุงศักดิ์ รัตนเดโช) ได้ให้ความสำคัญกับการใช้เทคโนโลยีไมโครเวฟเป็นแหล่งพลังงานความร้อนเพื่อประยุกต์ใช้กับกระบวนการในอุตสาหกรรมในหลายรูปแบบ (ดูข้อมูลเพิ่มเติมได้ใน http://www.rcme-tu.org/) และได้พัฒนาเครื่องต้นแบบระบบอบแห้งอเนกประสงค์เชิงพาณิชย์โดยใช้ไมโครเวฟชนิดป้อนคลื่นหลายตำแหน่งร่วมกับระบบสายพานลำเลียงอย่างต่อเนื่องดังรูปที่ 1 ระบบนี้ถือได้ว่าเป็นระบบต้นแบบ อันแรกของเมืองไทย ซึ่งจากการทดสอบการทำงานในเบื้องต้น พบว่า ระบบทำงานได้อย่างมีประสิทธิภาพโดยเฉพาะในกระบวนการอบแห้ง ไม้ เซรามิค และคอนกรีต และมีความเหมาะสมเป็นอย่างยิ่งที่สามารถประยุกต์ใช้งานได้อย่างหลากหลายอย่างอเนกประสงค์ ในภาคอุตสาหกรรม (ดังรายละเอียดของผลงานวิจัยตีพิมพ์เผยแพร่ในวารสารนานาชาติ 3 ฉบับ (ดูเอกสารแนบ 1) **โดยเฉพาะในกระบวนการอบแห้งไม้ยางพาราตามที่เสนอในโครงการวิจัยนี้**

อย่างไรก็ตาม เพื่อให้ระบบสามารถทำงานได้อย่างมีประสิทธิภาพมากยิ่งขึ้นจึงมีความจำเป็นต้องทำการวิจัยและพัฒนาเพิ่มเติมอีกขั้นหนึ่ง ก่อนที่จะนำไปใช้งานในเชิงพาณิชย์อย่างสมบูรณ์แบบ ซึ่งโครงการวิจัยนี้ผู้ใช้งานจริงในภาคอุตสาหกรรม จะเข้ามาร่วมดำเนินการเพื่อจะได้มาซึ่งข้อมูลจากภาคสนามจริง รวมทั้งการแก้ไขปัญหาและอุปสรรค์ในหน้างาน เพื่อนำมาสู่การได้เครื่องจักรแบบเชิงพาณิชย์ที่สมบูรณ์ก่อนนำไปใช้งานจริงในภาคอุตสาหกรรม โดยที่โครงการวิจัยนี้จะมุ่งเน้นพัฒนาตัวระบบเพื่อทำการ**อบแห้งไม้ยางพารา ซึ่งถือเป็นไม้เศรษฐกิจและเป็นสินค้าส่งออกที่สำคัญของประเทศ** ตามที่กล่าวข้างต้น

รูปที่ 1 ระบบอบแห้งอเนกประสงค์โดยใช้ไมโครเวฟร่วมกับระบบสายพานลำเลียงอย่างต่อเนื่อง
(ปัจจุบันตัวระบบนี้ได้ทำการยื่นจดสิทธิบัตรเรียบร้อยแล้ว)

ระบบที่นำเสนอในโครงการวิจัยนี้ จะทำการพัฒนาปรับปรุงจากระบบดั้งเดิม (รูปที่ 1) ที่สามารถทำงานได้อย่างมีประสิทธิภาพยิ่งขึ้น (แนวคิดการออกแบบระบบใหม่ดังแสดงในรูปที่ 2) โดยทำการวิจัยพัฒนาร่วมกับ บริษัทศรีพิพัฒน์ เอนจิเนียริ่ง เพื่อนำไปใช้งานจริงในอุตสาหกรรมอบแห้งไม้ยางพาราในจังหวัดทางภาคใต้ของประเทศ

จากงานวิจัยและพัฒนาในระบบเดิมนั้นจะมีเฉพาะพลังงานหลักจากไมโครเวฟ และแหล่งป้อนกำลังคลื่นคือแมกนีตรอน แต่ละตัวไม่สามารถปรับกำลังคลื่นได้ อีกทั้งระบบสายพานลำเลียงยัง

ทำงานได้ไม่เต็มประสิทธิภาพเท่าที่ควร สำหรับระบบใหม่ที่จะวิจัยพัฒนาต่อเนื่องนี้จะทำการกำจัดปัญหาที่เกิดขึ้นทั้งหมด โดยจะทำการพัฒนาปรับปรุงเปลี่ยนแปลงในส่วนต่างๆ ที่สำคัญ ดังนี้

1) วิจัยและพัฒนาระบบแหล่งป้อนกำลังคลื่น (แมกนีตรอน) ใหม่ กล่าวคือ สามารถควบคุมระดับกำลังไมโครเวฟของแต่ละตัวได้อย่างอิสระ ทั้งนี้เพื่อให้ระบบสามารถทำงานได้อย่างยืดหยุ่นและสามารถใช้งานได้กับวัสดุที่นำมาผ่านกระบวนการได้หลากหลายยิ่งขึ้น นอกจากนี้จะทำการพัฒนาปรับปรุงวงจรควบคุมการป้อนคลื่นให้สามารถเลือกตำแหน่งการป้อนคลื่นให้เหมาะสมกับชนิดวัสดุ ที่นำมาผ่านกระบวนการ (Optimum Condition) โดยเน้นถึงแง่ของการประหยัดพลังงานและการควบคุมคุณภาพของวัสดุ

2) วิจัยพัฒนาตัวอุโมงค์ไมโครเวฟ (Microwave Tunnel) ใหม่เพื่อเพิ่มประสิทธิภาพในการกระจายตัวของคลื่นภายในระบบ

3) พัฒนาปรับปรุงระบบสายพานลำเลียงใหม่ เพื่อให้สามารถใช้งานกับวัสดุที่นำมาผ่านกระบวนการได้หลากหลายมากยิ่งขึ้น โดยสามารถปรับความเร็วของสายพานลำเลียงได้ในช่วงที่กว้างขึ้น และสามารถทนสภาพอุณหภูมิที่สูงได้

4) เพิ่มระบบลมร้อนที่สามารถทำงานควบคู่กับระบบไมโครเวฟได้อย่างมีประสิทธิภาพ โดยลมร้อนสามารถปรับอุณหภูมิได้ตั้งแต่อุณหภูมิบรรยากาศ จนถึง 200 ^{o}C

5) วิจัยและพัฒนาระบบป้องกันคลื่นโดยเทคนิคใหม่ที่มีประสิทธิภาพมากกว่าเดิมหลายเท่าเพื่อเพิ่มความมั่นใจแก่ผู้ใช้งานในแง่ของความปลอดภัยอันเกิดจากไมโครเวฟซึ่งในบางสภาวะ (ซึ่งผู้วิจัยให้ความสำคัญกับเรื่องนี้สูงสุด) โดยทำการสร้างระบบป้องกันคลื่นแบบผสม (Hybrid Chokes) กล่าวคือ เป็นลักษณะผสม ของโครงสร้างที่เป็น Reactive และ Resistive

6) วิจัยและพัฒนาวงจรควบคุมใหม่ที่มีประสิทธิภาพสูง โดยสามารถควบคุมและ แสดงผลผ่านหน้าจอคอมพิวเตอร์จึงสะดวกต่อผู้ควบคุมระบบ

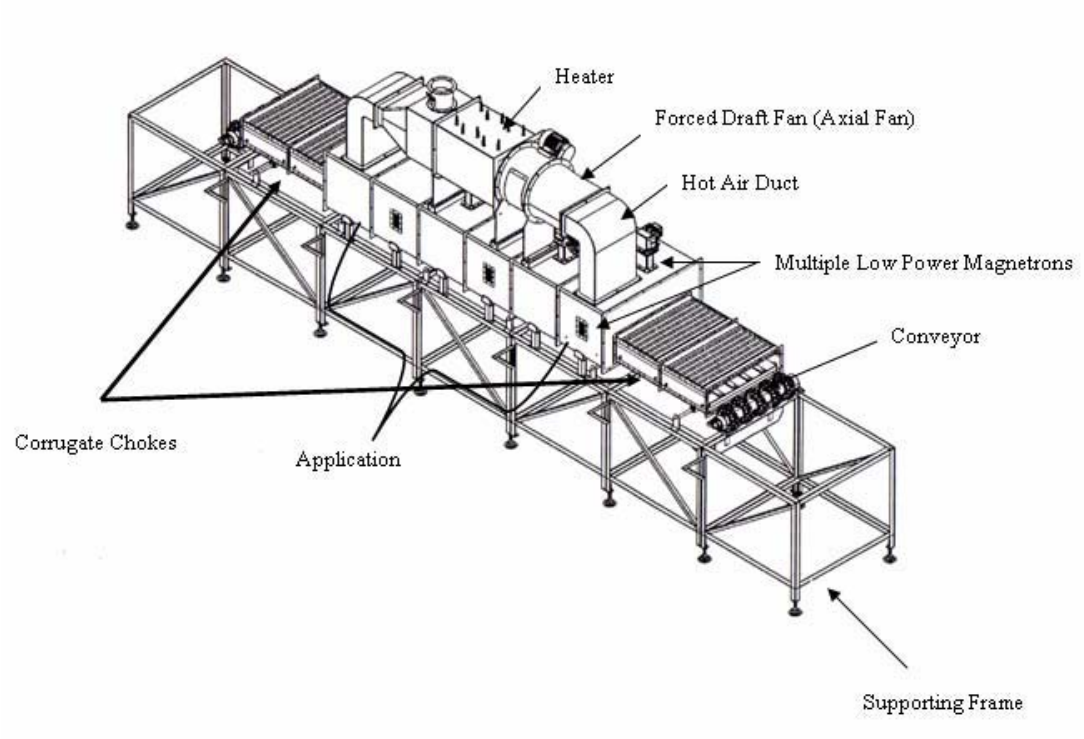

(a)

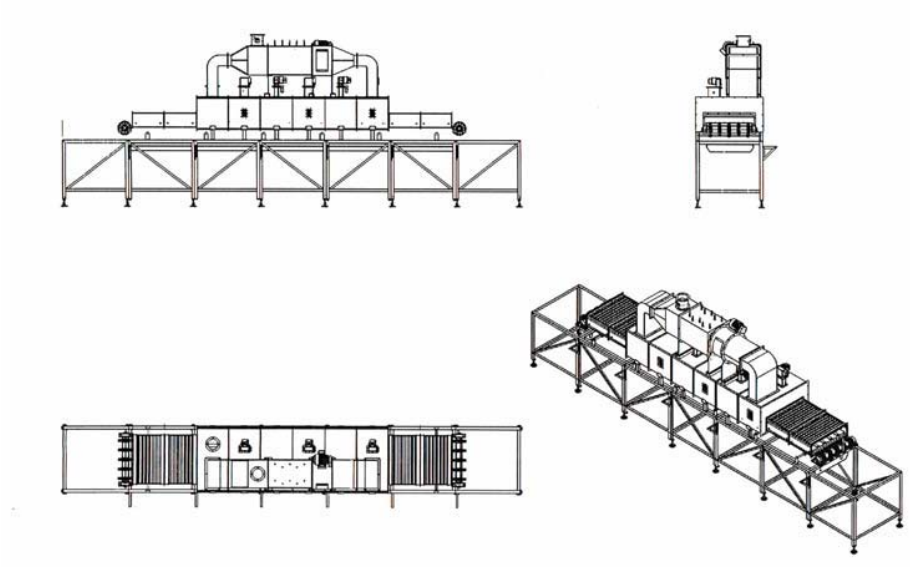

(b)

รูปที่ 2 แนวคิดการออกแบบระบบอบแห้งไม้ยางพาราเชิงพาณิชย์โดยใช้ไมโครเวฟชนิดป้อนคลื่นหลายตำแหน่งที่ไม่สมมาตรร่วมกับระบบลมร้อนและสายพานลำเลียงอย่างต่อเนื่อง

จะเห็นได้ว่าการวิจัยพัฒนาเทคโนโลยีไมโครเวฟฯจะต้องอาศัยองค์ความรู้ในลักษณะเชิงสหวิทยาการ (Multi-disciplinary knowledge) ซึ่งจะนำสู่ความสำเร็จในการสร้างเทคโนโลยีดังกล่าว ซึ่งพบว่าในปัจจุบันกลุ่มนักวิจัยในโลกที่สนใจวิจัยพัฒนาในเทคโนโลยีในระดับเป็นที่ยอมรับและต่อยอดพัฒนาเข้าสู่ระดับอุตสาหกรรมมีเพียงไม่กี่กลุ่ม ผลงานวิจัยของผู้วิจัยเองในศูนย์ก็ถือว่าเป็นกลุ่มหนึ่งที่ได้สร้างผลงานวิจัยเป็นที่ยอมรับในระดับนานาชาติทุกมิติ(ดูเอกสารแนบ 2 และ 3) โดยเนื้อหาที่ศึกษาประกอบด้วยมิติของงานวิจัยพื้นฐาน (Basic Research) งานวิจัยประยุกต์ (Applied Research) และการทำวิจัยพัฒนาออกมาในระดับ Pilot scale จนถึงระดับ Commercial scale ที่สามารถนำไปประยุกต์ใช้ในงานอุตสาหกรรมได้อย่างแท้จริงในปัจจุบัน ซึ่งผลงานวิจัยในมิติต่างๆนี้มีประโยชน์อย่างสูงต่อการพัฒนาวงการอุตสาหกรรมของไทยในเชิงแข่งขันกับตลาดโลก

สรุปข้อได้เปรียบของระบบที่จะพัฒนาในโครงการวิจัยและพัฒนานี้ เมื่อเทียบกับระบบการอบแห้งแบบธรรมดาทั่วไป (Conventional drying) ก็คือ

1) เนื่องจากคลื่นไมโครเวฟสามารถส่งผ่านทะลุเข้าไปในวัสดุที่นำมาผ่านกระบวนการ ดังนั้นความร้อนที่เกิดขึ้นในวัสดุที่จะกระจายสม่ำเสมอทำให้ความแห้งเป็นไปอย่างสม่ำเสมอ ในทุกตำแหน่ง ด้วยเหตุนี้ทำให้การควบคุมคุณภาพทำได้ง่าย

2) เวลาที่ใช้ในกระบวนการมีระยะเวลาสั้น คือประมาน หนึ่งในสิบของกระบวนการให้ความร้อนโดยวิธีดั้งเดิม ทำให้ประหยัดพลังงานกว่าวิธีดั้งเดิมหลายเท่า

3) รักษาคุณภาพดั้งเดิมของวัสดุที่นำมาผ่านกระบวนการ เปลี่ยนแปลงไว้ อาทิเช่น รูปทรง สี และไม่มีปฏิกิริยา oxidization ภายในเนื้อวัสดุ

4) มีประสิทธิภาพเชิงความร้อนสูง กล่าวคือประมาณ 60% - 70% ในขณะที่ใช้กระบวนการให้ความร้อนแบบวิธีธรรมดามี ประสิทธิภาพเชิงความร้อนสูง แค่ประมาณ 20% - 30%

5) เนื่องจากไม่มีการปล่อยควันไอเสียออกมาในระหว่างกระบวนการ ทำให้ไม่มีปัญหากับสิ่งแวดล้อม

6) เนื่องจากในกระบวนการมีชิ้นส่วนทำงานที่มีลักษณะเคลื่อนไหวมีน้อย ทำให้ลดค่าใช้จ่ายในการซ่อมบำรุง

7) เนื่องจากในกระบวนการมีชิ้นส่วนประกอบที่มีขนาดเล็ก ทำให้ใช้พื้นที่ในการติดตั้งน้อย

ผลงานวิจัยพัฒนาเครื่องต้นแบบนี้จะเน้นการใช้วัสดุที่มีอยู่ภายในประเทศและใช้งบประมาณในการสร้างที่ไม่สูงเกินไป แต่สามารถทำงานได้อย่างมีประสิทธิภาพ และสามารถตอบสนองความต้องการของภาคอุตสาหกรรมภายในประเทศได้เป็นอย่างดี

11. วัตถุประสงค์

- วิจัยและพัฒนาเพื่อให้ได้เครื่องต้นแบบในระดับอุตสาหกรรมที่สมบูรณ์และสามารถจดสิทธิบัตรเป็นของคนไทยได้
- ส่งเสริมความร่วมมือกับภาคเอกชน และทำการถ่ายทอดเทคโนโลยีสู่ภาคอุตสาหกรรม
- เสริมสร้างความเข้มแข็งของอุตสาหกรรมไทยและศักยภาพในการแข่งขันในเวทีโลก
- โครงการวิจัยนี้ จะเป็นประโยชน์อย่างสูงโปรแกรมการพัฒนาการเรียนการสอน ทั้งในระดับปริญญาตรี โท และเอก

12. ระเบียบวิธีวิจัย

งานวิจัยนี้ได้เน้นวิจัยเชิงสหวิทยาการ (Multi-disciplinary) และบูรณาการ กล่าวคือได้ผลลัพธ์ในหลายมิติ มิติแรกคือองค์
ความรู้เชิงลึก (งานวิจัยภาคทฤษฎี) ที่สามารถนำไปตอบปัญหาในเชิงปฏิบัติได้ รวมทั้งตีพิมพ์ในวารสารนานาชาติได้ มิติที่สองคือการประดิษฐ์คิดค้นนวัตรกรรมใหม่ที่สามารถตอบสนองภาคการผลิตภายในประเทศและสามารถจดสิทธิบัตรเป็นของคนไทยได้

ในปัจจุบันแม้จะมีนักวิจัยบางกลุ่มพยายามพัฒนาใช้เทคโนโลยีไมโครเวฟมาใช้ในอุตสาหกรรม แต่ก็เป็นเพียงแค่ดัดแปลงไมโครเวฟบ้าน (Domestic microwave oven) และติดตั้งอุปกรณ์บางตัวเข้าไป ซึ่งพบว่ายังไม่สามารถนำไปใช้ในเชิงพาณิชย์ได้อย่างมีประสิทธิภาพ เพราะมีข้อจำกัดเรื่องเทคโนโลยีที่ใช้และมีปัญหาเกี่ยวกับความปลอดภัยโดยเฉพาะการรั่วของรังสี และยังไม่สามารถออกแบบตัวระบบที่มีขนาดใหญ่ได้ นอกจากนี้ระบบไมโครเวฟสำหรับการให้ความร้อนทั่วไปยังจำกัดอยู่ในประเภทที่วัสดุที่นำมาผ่านกระบวนการจะต้องอยู่นิ่ง (Fixed materials) และมีปริมาณที่ไม่มากนัก ข้อด้อยของระบบไมโครเวฟที่วัสดุอยู่นิ่งคือ ทำให้การกระจายตัวของคลื่นหรือความร้อนภายในวัสดุจะไม่สม่ำเสมอ ทำให้เกิดโซนความร้อน (Hot spot zone) และโซนเย็น (Cold zone) ซึ่งไม่มีอันตรกริยากับคลื่น ส่งผลต่อคุณภาพของผลิตภัณฑ์ การวิจัยและพัฒนาเพื่อให้เกิดการกระจายตัว

ของคลื่นไมโครเวฟเป็นลักษณะหลายโหมด (Multi-mode) ด้วยเหตุผลของการกระจายตัวของคลื่น รวมถึงความร้อนในวัสดุที่นำมาผ่านกระบวนการที่ดี ตลอดจนถึงการควบคุมตำแหน่งของการกระจายตัวที่ดีของความร้อนภายในวัสดุ จึงเป็นที่มาของโครงการวิจัยครั้งนี้

ตัวอย่างอุตสาหกรรมที่สามารถนำเอาเทคโนโลยีไมโครเวฟนำไปใช้อย่างแพร่หลาย เช่น การอบแห้งอาหาร อบแห้งสิ่งทอ อบแห้งไม้และกระดาษ อุตสาหกรรมพลาสติก การบ่มคอนกรีต การ Vulcanize ยางพารา การทำ Pasteurization และ Sterilization และอื่นๆอีกมากมาย กระบวนทางไมโครเวฟยังได้ถูกนำไปใช้งานทางการแพทย์ เช่น การคลายเนื้อเยื่อที่แข็งตัว การอุ่นเลือด และ กำจัดเนื้องอก นอกจากนี้ ไมโครเวฟยังสามารถนำไปใช้ในงานแยกส่วนประกอบที่เป็นสารระเหยจากวัสดุ เช่น การแยกกำมะถันออกจากถ่านหินโดยการ Pre-combustion treatment และการแยกสารสกปรกออกจากดิน เป็นต้น

งานวิจัยและพัฒนาระบบอบแห้งไม้ยางพาราเชิงพาณิชย์โดยใช้ไมโครเวฟชนิดป้อนคลื่นหลายตำแหน่งที่ไม่สมมาตรร่วมกับระบบลมร้อนและสายพานลำเลียงอย่างต่อเนื่อง นี้ถือว่าเป็นนวัตกรรมใหม่ที่ต้องใช้เทคโนโลยีออกแบบชั้นสูงที่ต้องคาบเกี่ยวกับศาสตร์ทาง คลื่นแม่เหล็กไฟฟ้า ด้านวัสดุศาสตร์ การถ่ายเทความร้อนและมวล คณิตศาสตร์ชั้นสูง ระเบียบวิธีเชิงตัวเลข และอิเลคทรอนิค-ไฟฟ้าควบคุม และเป็นงานวิจัยเชิงสหวิทยาการที่ครอบคลุมถึงงานวิจัยเชิงทฤษฎีตลอดจนถึงงานวิจัยเชิงประยุกต์ที่สามารถพัฒนาต่อยอดเป็นนวัตกรรมหรือสิ่งประดิษฐ์ใหม่ใหม่ที่สามารถตอบสนองภาคการผลิต

13. จำนวนโครงการที่คณะผู้วิจัยกำลังดำเนินการอยู่ โดยขอให้ระบุระยะเวลาเริ่มต้นและสิ้นสุดของแต่ละโครงการแหล่งทุนและงบประมาณสนับสนุนที่ได้รับ เวลาที่ใช้ทำโครงการวิจัยในแต่ละโครงการเป็นกี่ชั่วโมงต่อสัปดาห์ ทั้งในฐานะหัวหน้าโครงการ ผู้ร่วมโครงการของแต่ละโครงการที่กำลังดำเนินการอยู่

13.1 สำหรับหัวหน้าโครงการโปรดระบุรายละเอียดแต่ละโครงการที่ดำเนินการอยู่ต่อไปนี้

ชื่อโครงการ: งานวิจัยและพัฒนาระบบอบแห้งอเนกประสงค์เชิงพาณิชย์โดยใช้ไมโครเวฟร่วมระบบสุญญากาศ; กรณีศึกษา: ผลิตภัณฑ์ที่มีคุณภาพสูง

ระยะเวลาโครงการ 2 ปี ตั้งแต่ ปี 2550 ถึง 2552

งบประมาณที่ได้รับ 3 ล้านบาท

สถานะของหัวหน้าโครงการ หัวหน้าโครงการ

เวลาที่ใช้ทำวิจัยในโครงการนี้กี่ชั่วโมงต่อสัปดาห์ 14 ชั่วโมงต่อสัปดาห์

13.2 สำหรับหัวหน้าโครงการโปรดระบุรายละเอียดแต่ละโครงการที่ดำเนินการอยู่ต่อไปนี้

ชื่อโครงการ: การจำลองการกระจายของคลื่นแม่เหล็กไฟฟ้าและอุณหภูมิในสมองมนุษย์

ระยะเวลาโครงการ 2 ปี ตั้งแต่ ปี 2551 ถึง 2553

งบประมาณที่ได้รับ ไม่มี

สถานะของหัวหน้าโครงการ หัวหน้าโครงการ

เวลาที่ใช้ทำวิจัยในโครงการนี้กี่ชั่วโมงต่อสัปดาห์ 7 ชั่วโมงต่อสัปดาห์

เอกสารแนบประกอบ 1

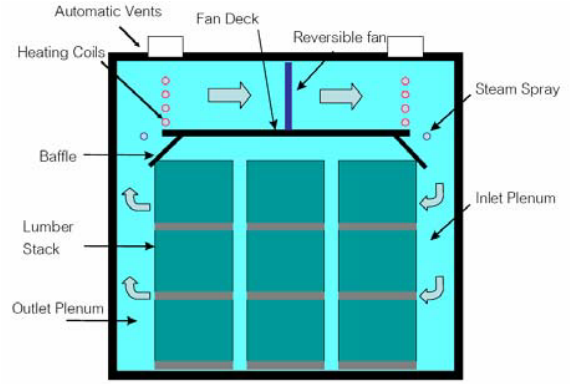

(a)

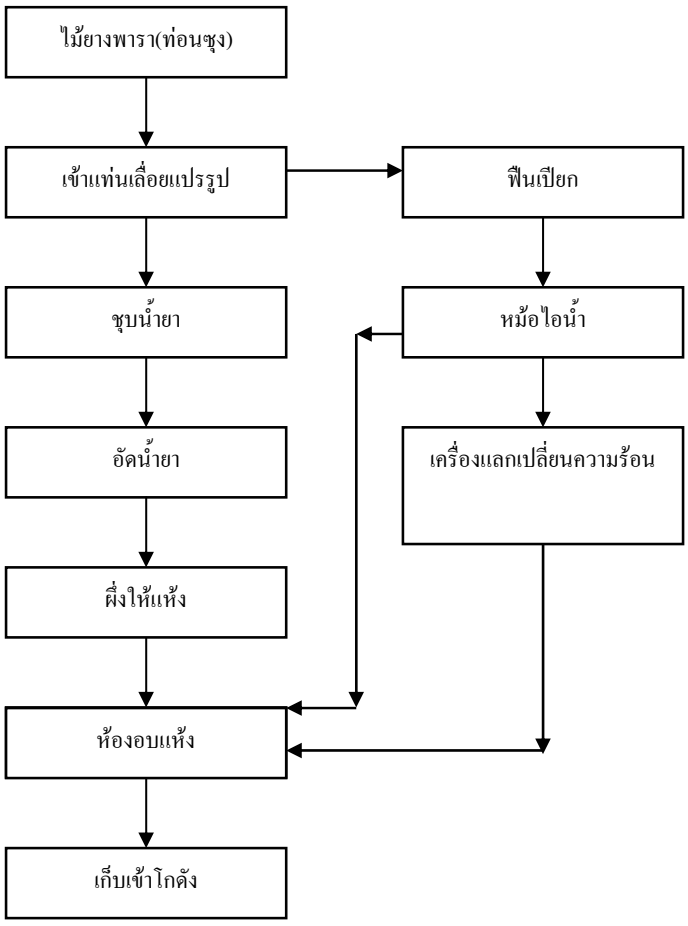

(b)

รูปที่ อ(1) กระบวนการอบแห้งไม้แบบดั้งเดิม (เตาอบแบบ Conventional Kiln) [4]

(O)

ตารางที่ อ(1) ความหนา ปริมาณการอบ และความชื้นของไม้ยางพาราแปรรูปที่ต้องการ***

กลุ่มการอบ (วัน/ซม.)	ขนาดความหนาไม้แปรรูป	ปริมาณการอบแต่ละครั้ง (ลบ.ฟุต/เตา)	ความชื้นไม้แปรรูปที่ต้องการ (%)	
			ไม้แปรรูปเกรด AB	ไม้แปรรูปเกรด C
8 วัน/192 ซม.	4/8" – 1"	800 – 1,000	8	10
10 วัน/240 ซม.	1 1/8" – 1 ½"	1,200	8	10
14 วัน/336 ซม.	1 5/8" – 2"	1,400	8	15
18 วัน/432 ซม.	2 1/8"	1,500	8	20 - 25

*** ข้อมูลจากกลุ่มบริษัท วู้ดเวอร์ค

สำหรับกลุ่มอุตสาหกรรมไม้ยางพาราที่จะเข้าร่วมโครงการวิจัย โดยเฉพาะการทดสอบจริงภาคสนามมีดังนี้

กลุ่มบริษัท วู้ดเวอร์ค ประกอบธุรกิจไม้ยาพารา แปรรูป อัดน้ำยา อบแห้ง มีบริษัทในเครือทั้งหมด 5 บริษัท ดังนี้

1. บริษัท วู้ดเวอร์คกรุ๊ป จำกัด (สำนักงานขาย จ.ตรัง)
2. บริษัท วู้ดเวอร์คครีเอชั่น จำกัด โรงงานผลิต อ.คลองท่อม จ.กระบี่ กำลังการผลิต 100,000 ลบ.ฟุต/เดือน จำนวนเตาอบ 50 เตา (ขนาดหม้อต้มไอน้ำ 10 ตัน)
3. บริษัท วู้ดเวอร์คยูไนเต็ด จำกัด โรงงานผลิต อ.ห้วยยอด จ.ตรัง กำลังการผลิต 100,000 ลบ.ฟุต/เดือน จำนวนเตาอบ 56 เตา (ขนาดหม้อต้มไอน้ำ 10 ตัน)
4. บริษัท วู้ดเวอร์คแอดวานซ์ จำกัด โรงงานผลิต อ.สะเดา จ.สงขลากำลังการผลิต 100,000 ลบ.ฟุต/เดือน จำนวนเตาอบ 60 เตา (ขนาดหม้อต้มไอน้ำ 10 ตัน)
5. บริษัท วู้ดเวอร์คอังสุธน จำกัด โรงงานผลิต อ.ละงู จ.สตูลกำลังการผลิต 80,000 ลบ.ฟุต/เดือน จำนวนเตาอบ 40 เตา (ขนาดหม้อต้มไอน้ำ 8 ตัน)

เอกสารอ้างอิง

(1) Rattanadecho, P. , Suwannapum, N., Watanasungsuit, A. and Duangduen, A., “Drying of Dielectric Materials Using Microwave-Continuous Belt Furnace.”, ASME J. Manufacturing Sciences and Engineering, Volume 129 (1), Feb, 2007, pp. 157-163, : Impact factor 0.532

(2) Rattanadecho, P., Chatveera, B., Atong, D., Makul, N., and Suwannapum, N. “Development of Compressive Strength of Cement Paste under Accelerated Curing by Using A Continuous Microwave Belt Drier”, Material Science and Engineering A Vol. 472, pp. 299-307, 2008 : Impact factor 1.4

(3) S. Vongpradubchai and P.Rattanadecho ,"The Microwave Processing of Wood Using a Continuous Microwave Belt Drier" Chemical Engineering and Processing:Process Intensification : Impact factor 1.159 (Article in Press)

(4) ณัฐพล วิทยานุภากร.(2550).การปรับปรุงประสิทธิภาพการไหลของอากาศในเตาอบไม้ยางพาราด้วย แบบจำลองพลศาสตร์ของของไหล.วิทยานิพนธ์วิทยาศาสตรมหาบัณฑิต สาขาวิทยาศาสตร์และวิศวกรรมวัสดุ มหาวิทยาลัยวลัยลักษณ์ นครศรีธรรมราช

CONTENTS

PAGE

CHAPTER 1

INTRODUCTION AND RELATED THEORY

1.1 Introduction to microwave engineering

The term microwaves refers to alternating current signals with frequencies between 300 MHz (3 x 10^8 Hz) and 300 GHz (3 x 10^{11} Hz), with a corresponding electrical wavelength between $\lambda = c/f$ =1m and λ = 1mm, respectively. Signals with wavelengths on the order of millimeters are called millimeter waves. Figure 1.1 shows the location of the microwave frequency band in the electromagnetic spectrum. Because of the high frequencies (short wavelengths), standard circuit theory generally cannot be used directly to solve microwave network problems. In a sense, standard circuit theory is an approximation or special use of the broader theory of electromagnetic as described by Maxwell's equations. This is due to the fact that, in general, the lumped circuit element approximations of circuit theory are not valid at microwave frequencies. Microwave components are often distributed elements, where the phase of a voltage or current changes significantly over the physical extent of the device, because the device dimensions are on the order of the microwave wavelength. At much lower frequencies, the wavelength is large enough that there is insignificant phase variation across the dimensions of a component. The other extreme of frequency can be identified as optical engineering, in which the wavelength is much shorter than the dimensions of the component. In this case, Maxwell's equations can be simplified to the geometrical optics regime, and optical systems can be designed with the theory of geometrical optics. Such techniques are sometimes applicable to millimeter wave systems, where they are referred to as quasioptical.

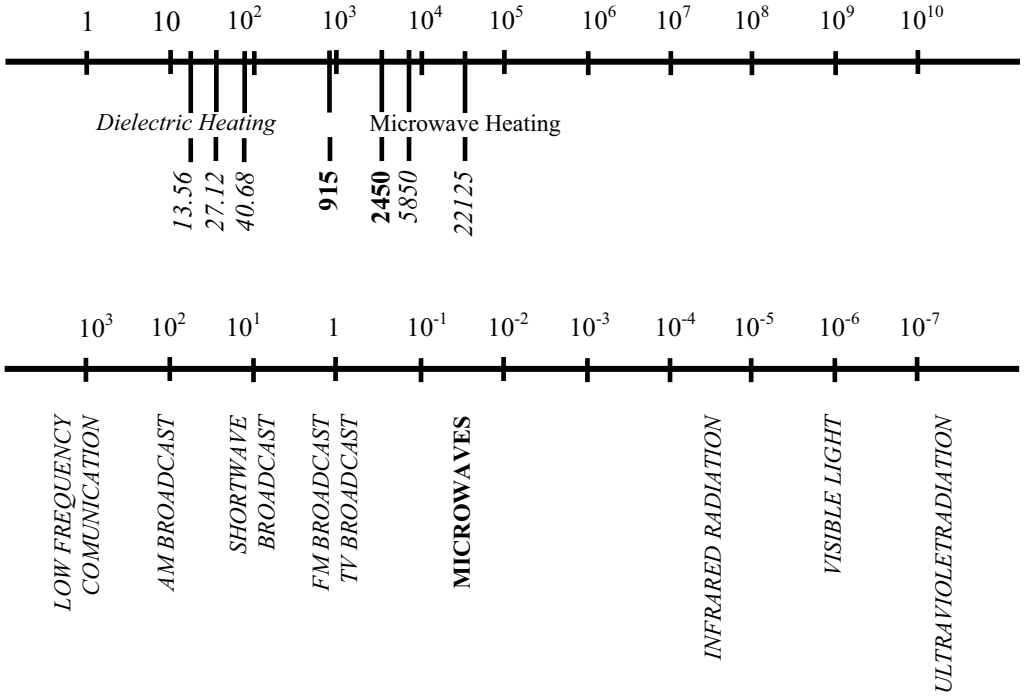

Figure 1.1 The electromagnetic spectrum

In microwave engineering, then, one must often begin with Maxwell's equations and their solutions. It is in the nature of these equations that mathematical complexity arises since Maxwell's equations involved vector differential or integral operations on vector field quantities, and these fields are functions of spatial coordinates. One of the goals of this book, however, is to try to reduce the complexity of a field theory solution to a result that can be expressed in terms of simpler circuit theory. A field theory solution generally provides a complete description of the electromagnetic field at every point in space, which is usually much more information than we really need for most practical purposes. We are typically more interested in terminal quantities such as power, impedance, voltage, and current, which can often be expressed in terms of circuit theory concepts. It is this complexity that adds to the challenge, as well as the rewards, of microwave engineering.

1.2 Applications of microwave engineering

The microwave energy offers so many advantages over conventional heating, why it has not been used more widely in commercial processing over the past 50 years. Perhaps it is being used more than we realize today. Successful processes are rarely disclosed by industry. In any event, with public awareness and the science community's interest on the increase, and with better equipment and electronics for monitoring and controlling processes, the increased use of microwave energy in appropriate niches is a certainty.

Microwave processing is not as simple as putting a material into a home microwave oven for some designated period of time. The chance of failure by this approach far outweighs the probability of success. The size, frequency, and power of these ovens are designed primarily to couple with water and conveniently heat a variety of foods. Although other materials such as ceramics, semiconductors, and polymers may be able to be heated in them, the results will most likely not be sufficient for the quality, scale, and economics required in manufacturing. However, there have been significant advances in equipment design (variable frequency and high temperature capabilities and better control) and the trend is towards microwave systems that have more intelligent processing capabilities and are more user friendly. What would not have been possible 10 years ago in microwave processing of a variety of materials is now feasible because of these advances.

The most successful demonstrations and scale-ups of microwave energy for processing have involved an integrated/interdisciplinary approach where the product manufacturers work in concert with the equipment manufacturers (microwave, mechanical, and electrical engineers) to design the equipment and material systems that will not only work, but will result in a profitable product. A savings in energy is not always sufficient, or even necessary, in order to make the product competitive. Other factors such as a better or unique product, floor space savings, reduction in process time, process flexibility, or a reduction in labor may far outweigh any energy savings.

One of the essential ingredients for future successes in commercialization of microwave processing is closed to working relationship between the potential users,

equipment manufacturers, and research institutions such as universities and federal laboratories, as illustrated in Figure 1.2

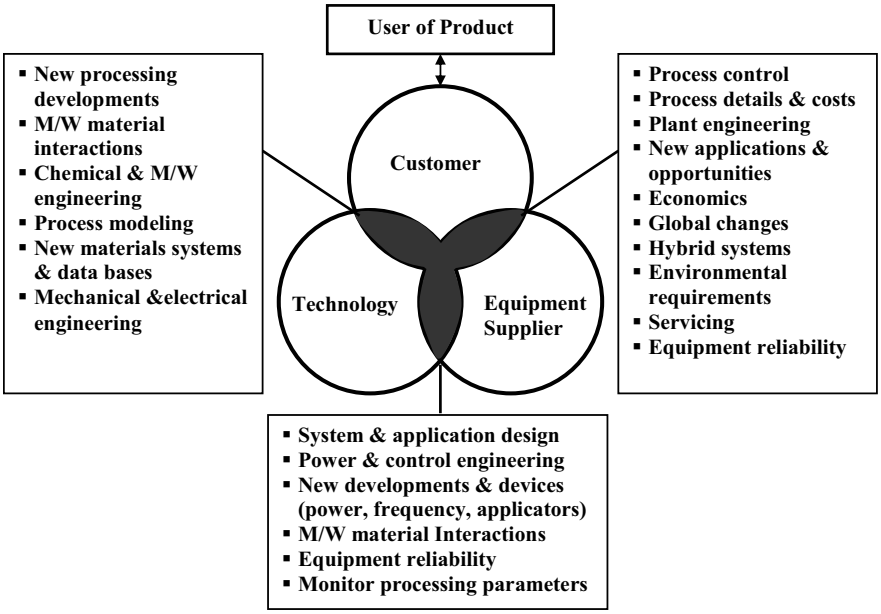

Figure 1.2 Microwave processing-interacting steps to successful applications (Clark, 1996)

Where the communication gaps are closing (overlapping circles), where the needs and requirements of all the groups involved are better and mutually understood, and where the future focus will be on developing a market "pull" for the technology and applications, that shown in table 1.1.

Table.1.1 Application of microwave processing

Material	**Process**
Ceramics / Refractories	- Dry powders, filters, catalytic converters, insulating boards and fiber shapes - Dry slip casting
Chemicals	- Accelerate Reactions - Process Catalysis

Material	Process
Concrete	- Accelerated curing - Assisted Heating - Curing at early-stage
Environmental	- Soil Remediation
Fiber Glass	- Dry yarn, strands, mats and webs
Foam	- Dry - Cure - Expand
Foods	- Precooking - Pasteurisation - Tempering-Thawing - Baking - Freeze drying
Foundries Foundries	- Cure cores and core washes - Lost foam process - Investment casting
Medical	- Medical Waste sterilization
Paper & paper converting	- Dry and profile - Set adhesives - Dry coating
Plastics	- Preheating - Cure thermo sets - Dry polymer forms - Pultrusion
Rubber	- Preheating, drying and expansion - Valcanization - pre-curing
Textiles	- Dry yarn packages, strands, webs - Dry carpet backing

Material	Process
	- Set dyes
Woods	- Veneer dry, redry - Preheat for fiberboard - Dimension lumber drying

1.3 Microwave/Material interactions

1.3.1 Phenomenological Aspects

Microwaves (0.3 to 300 GHz) lie between radiowave frequencies (RF) and infrared (IR) frequencies in the electromagnetic radiation spectrum. Microwaves can be reflected, absorbed and/or transmitted by materials. Reflection and absorption require interaction of the microwaves with the material; transmission is the result of partial reflection and incomplete absorption. During interaction, energy in the form of heat is generated in the material primarily through absorption. Gases, liquids, and solids can interact with microwaves and be heated. Under certain conditions, gases can be excited by microwaves to form plasmas that are also useful for processing. Metals, at least in bulk form, are excellent reflectors of microwave energy and in general are not heated significantly by microwaves. Other materials reflect and absorb heat to various degrees depending on their composition, structure, temperature, and the frequency of the microwaves. To illustrate, pure water at room temperature is a broad-band absorber and absorbs well over a wide microwave frequency range, including 2.45 GHz. However, absorption is sensitive to frequency, and peak absorption for water at 20°C occurs at about 18 GHz. Its absorption improves as ionic salts are added (i.e. composition change) due to increased ionic conduction losses. When water is heated, its absorption decreases at 2.45 GHz. Structural changes also affect its absorption. For example, when water is frozen, its absorption is negligible.

At room temperature, many ceramics and polymers do not absorb appreciably at 2.45 GHz. However, their absorption can be increased by increasing the temperature (in contrast to water), adding absorbing constituents (e.g. Sic, carbon, binders), altering their microstructure and defect structure, by changing their form (e.g. bulk vs powder), or by changing the frequency of the incident radiation. The

wide range of interactions that occur between microwaves and various materials provides many challenges to the processor. On the other hand, it is because of these different interactions that microwaves can be transported, contained, and used at room temperatures as well as at elevated temperatures.

Increasing the temperature (with radiant heat) is a common method used by many researchers to couple microwaves with poorly absorbing (low loss) materials. Once a material is heated to its critical temperature; T_c microwave absorption becomes sufficient to cause self-heating. This hybrid method can result in more uniform temperature gradients because the microwaves heat volumetrically, and the external heat source minimizes surface heat losses. Hybrid heating can be achieved either by using an independent heat source such as a gas or electric furnace in combination with microwaves, or through the use of an external susceptor that couples with the microwaves . In the latter, the material is exposed simultaneously to radiant heat produced by the susceptor and to microwaves.

Another means of heating a no coupling material is to incorporate absorbing additions. Reinforcements, binders, fillers, plasticizers, and dispersants are often added to polymers and ceramics as processing aids or to improve their properties. Proper selection of these additives can improve absorption and make them more favorable for microwave processing. The trend here should be to tailor parameters such as composition and additives specifically to facilitate microwave processing rather than to try to use microwave processing with established parameters. This latter scenario is most likely to fail and cause the processor to miss the real benefits of microwave processing.

1.3.2 Mechanisms of Interaction

Microwaves can interact with materials through either polarization or conduction processes. Polarization involves the short-range displacement of charge through the formation and rotation of electric dipoles (or magnetic dipoles if present). Conduction requires the long-range (compared to rotation) transport of charge. Both processes give rise to losses in certain frequency ranges as illustrated by Figure 1.3. In this figure, the dielectric losses, ε'', are due to ionic conduction, which are dominant at low frequencies, and rotation of permanent dipoles at higher frequencies. The ionic

conduction losses are due to the well-known ohmic losses that occur when ions move through the material and collide with other species. Ionic conduction decreases with increasing frequency because the time allowed for transport in the direction of the field decreases with increasing frequency. Both processes contribute to the losses, and it is not always easy to experimentally differentiate between the two loss mechanisms. Consequently, losses are typically reported as effective losses, when the loss mechanisms are unknown or cannot be clearly separated.

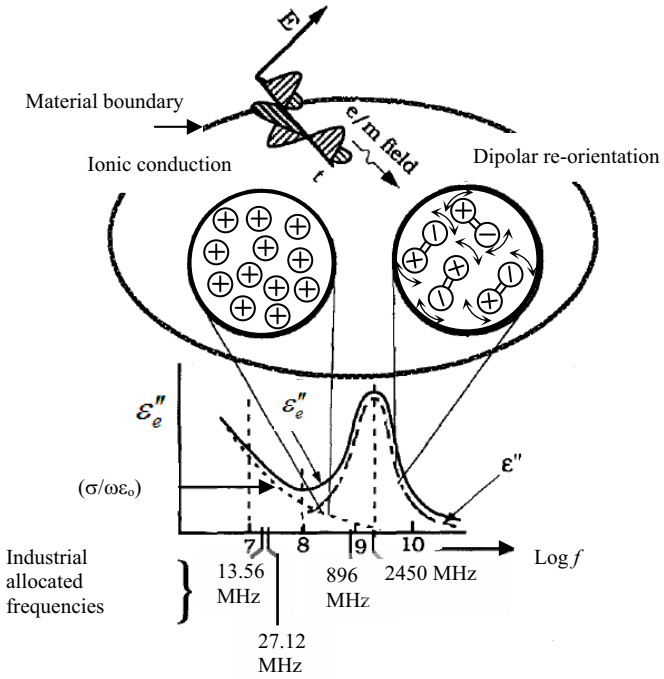

Figure.1.3 Effective loss factor due to dipolar ionic conduction

1.4 The advantage of microwave heating

Corresponding to the simple schematic diagram as shown in Figure1.4, electromagnetic or microwave energy penetrates the dielectric material and heat is generated rapidly throughout it (Figure1.4(a)). Convective heat processing is accomplished by heating the outside of the process material, and the heat travels in wards by conduction (Figure1.4(b)). The speed of conductive heating is controlled by many parameters, most notably by the difference between the surface temperature and internal temperature of the material and the ability of the material to conduct heat. The usual way to speed up the rate of convection heating is to increase surface

temperature. Problems of damaged material caused by surface overheating and temperature variation within the material can be avoided through the use of microwave heating, because energy is delivered instantaneously throughout the mass of the material. By achieving controlled heating rates, accurate process temperature control becomes easier in the microwave heating process. Microwave heating has the ability to maintain better process uniformity, which leads to better quality. The simple schematic diagram of microwave and conventional heating process is shown in Figure1.4.

Figure.1.4 The schematic diagram of (a) microwave and
(b) conventional heating processes

The following paragraph summarizes the advantages of microwave heating in comparison with conventional heating process:

High speed: Short start up time and rapid heating.

Energy penetration: Microwave energy penetration generates heat internally as well as at the surface of the dielectric material. Other methods apply heat only to the surface and temperature must be limited in order to avoid burning. Processing time is long due to thermal conductivity. Microwave energy reduces the heating time and temperature gradient and produces a very high quality product. (more uniform and volumetric heating)

Selective energy absorption: Some material absorbs microwave readily, whereas others do not. Pharmaceuticals, for example, can be pasteurized within their packages without burning the packaging material.

Instantaneous electronic control: Most conventional heating systems (e.g., hot air ovens), require appreciable amounts of time to effect temperature changes. Microwave power levels can be adjusted electronically in a fraction of a second, a characteristic that marks microwave equipment readily adaptable to automated systems and to data logging programs.

High efficiency & speed: Microwave processing requires lower energy for the same or better results than conventional equipment (high energy efficiency 60% to 70% compared with 10% to 30% for conventional units)

Microwave processing is clean: Microwave processing is an inherently dry and fumeless process, which is environmentally clean compared with a process that requires additional media for heat transfer.

1.5 The disadvantage of microwave heating

As illustration many advantages of microwave heating when compared to the convectional heating; however, microwave heating has many disadvantages, too. They can be shown as below:

1.5.1 Constraint with metal container

1.5.2 Heat force control is difficult

1.5.3 Closed container is dangerous because it could be burst

1.5.4 Limited on size of sample

1.5.5 Complexity of operation technique

1.5.6 Limited on type of material, only dielectric materials can be heat with microwave

1.6 Attentions in using microwave

To applied microwave for heating or drying process needs more technical skill from the specialist, so

1.6.1 If the container is metal, spark is generated and no foods heat up.

1.6.2 If food is different in ingredients heating velocity could be different. For instance the food contained more fat will be heat up fastly.

1.6.3 Bad influence to human body of microwave in microwave oven is nearly only the thermal effect. And safe level of microwave is $10mW/cm^2$. Leakage of microwave is mostly occurred in the gap of oven and door. Therefore it is important to pay attentions that gap length is not differed.

1.7 Microwave in thermally drying process

Nowadays, the most important thing in industries, except for producing the high quality products to the markets, is to increase productivity and to reduce production cost. In general, several production processes of agricultural and industrial products are related to drying either by a natural method or using energy from other sources resulting in a low production rate or a high cost products. Microwave drying is one of the most interesting methods in term of mechanisms and economics for heating and drying in various kinds of product.

Microwave (MW) drying is a novel alternative method of drying, allowing to obtain products of acceptable quality. It permits a shorter drying time and a substantial improvement in the quality of dried materials, in relation to those dried with hot air and microwave drying methods. Furthermore, other advantages including environmental friendliness at low temperature, which not only over-comes the limitation of low thermal conductivity of the material under dried condition due to the volumetric heating, but also avoids the defect of shrinkage caused by excessive heating at sample surface, and acquires a wide range of application on the pharmaceutical and food industries. Microwave drying has been investigated as a potential method for obtaining high-quality dried foodstuffs, including fruits, vegetables and grains.

Although combined MW-Conventional heat source for drying process has found some application in many years ago, more research and development is needed before the process is used in large commercial scale. In particular, the effect of thermal condition and MW power on the drying kinetics should be known quantitatively, so that the drying system can be optimized from the cost and quality standpoints. The analyzing on energy consumption as well as exergy demand in microwave drying process and human safety guidance is need to be clarified in details.

The main objective of this research project is to develop the commercialized microwave–convective air drying (Combined unsymmetrical multi-feed microwave and hot air-continuous belt system (CMCB)) and examine the feasibility of using MW-Hot air drier to dry porous materials, i.e., wood and experimentally explore drying characteristics of porous sample in different drying conditions, including microwave radiation time, microwave power level, hot air temperature level and typical microwave feeding process. At the same time, the research results would be beneficial to present a theory basis for further study and industrial application of a combined microwave drying technology in biomaterials in the future.

1.8 The related theory

1.8.1 Theory and energy of heat generation

Microwave heating involves heat dissipation and microwaves propagation which causes the dipoles to vibrate and rotate. When the microwave energy emits from a microwave oscillator (P_{in}) is irradiated inside the microwave applicator, the dielectric materials which has a dielectric loss factor absorbs the energy and are heated up. Then the internal heat generation takes place. The basic equation calculates the density of microwave power absorbed by dielectric material (P_1) is given by (Rattanadecho (2006)):

$$P_1 = \omega \varepsilon_0 \varepsilon_r'' E^2 = 2\pi \cdot f \cdot \varepsilon_0 \cdot \varepsilon_r' (\tan\delta) E^2 \qquad (1\text{-}1)$$

where E is electromagnetic field intensity; f is microwave frequency; ω is angular velocity of microwave; ε_r' is relative dielectric constant; ε_0 is dielectric constant of air and $\tan\delta$ is loss tangent coefficient.

Mathematically, the electric field intensity, E in Eq. (1-1) is related to the equations of electromagnetic wave propagation, i.e., Maxwell's equation which mathematically describe the interdependence of the electromagnetic waves. The general form of Maxwell's equations is expressed as:

$$\nabla\times\left(\frac{1}{\mu_r}\nabla\times E\right)-k_0{}^2\left(\varepsilon_r-\frac{j\sigma}{\omega\varepsilon_0}\right)E=0 \tag{1-2}$$

From Eq.(1-1), P_1 is directly proportional to the frequency of the applied electric field, loss tangent coefficient and root-mean-square value of the electric field. It means that during an increasing of $\tan\delta$ of specimen, energy absorption and heat generation are also increased. While $\tan\delta$ is small, microwave will penetrate into specimen without heat generation. However, the temperature increase depends on other factors such as specific heat, size and characteristic of specimen.

When the material is heated unilaterally, it is found that as the dielectric constant and loss tangent coefficient vary, the penetration depth will be changed and the electric field within the dielectric material is altered. The penetration depth is used to denote the depth at which the power density has decreased to 37 % of its initial value at the surface (Cha-um et al. (2009)):

$$D_p=\frac{1}{\frac{2\pi f}{\upsilon}\sqrt{\frac{\varepsilon_r'\left(\sqrt{1+\left(\frac{\varepsilon_r''}{\varepsilon_r'}\right)^2}-1\right)}{2}}}=\frac{1}{\frac{2\pi f}{\upsilon}\sqrt{\frac{\varepsilon_r'\left(\sqrt{1+(\tan\delta)^2}-1\right)}{2}}} \tag{1-3}$$

where D_P is penetration depth ε_r'' is relative dielectric loss factor and υ is microwave speed. The penetration depth of the microwave power is calculated according to Eq. (3-2), which shows how it depends on the dielectric properties of the

material. It is noted that products with huge dimensions and high loss factors, may occasionally be overheated to a considerably thick layer on the outer layer. To prevent such phenomenon, the power density must be chosen so that enough time is provided for the essential heat exchange between boundary and core. If the thickness of the material is less than the penetration depth, only a fraction of the supplied energy will become absorbed. Furthermore, the dielectric properties of porous material specimens typically show moderate lossiness depending on the actual composition of the material. With large amount of moisture content, it reveals a greater potential for absorbing microwaves. For typical porous material specimens, a decrease in the moisture content typically decreases ε_r'', accompanied by a slight increment in D_p.

In the analysis, energy P_2 is required to heat up the dielectric material which is placed in a microwave applicator. The temperature of material initially (T_1) is raised to T_2. The energy (P_2) can be estimated by the following calorific equation (Vongpradubchai and Rattanadecho (2009)):

$$P_2 = \frac{4.18 \cdot W \cdot C_p \cdot \Delta T}{t} \tag{1-4}$$

where W is weight of the dielectric material; C_p is specific heat of the dielectric material; ΔT is the increment of temperature $(T_2 - T_1)$ and t is heating time.

Assuming an ideal condition, all of the oscillated microwave energy (P_{in}) is absorbed into the dielectric material; such internal heat generation as Eq. (1-1) shows takes place. In this case, the relation between P_{in} and P_2 is shown below:

$$P_{in} = P_2 \tag{1-5}$$

In a practical point of view, however, the transformation energy in applicator exists due to Eq. (1-1) the rate of microwave energy absorbed by means of the dielectric loss factor of the sample and Eq.(1-2) the energy loss in the microwave devices. Accordingly, by taking into account this transformation efficiency, the microwave oscillation output can be calculated by the following equations:

$$P_{in} = \frac{P_2}{\eta} \tag{1-6}$$

$$\eta = \frac{P_2}{P_{in}} \tag{1-7}$$

1.8.2 Incident, reflection, transmission and absorbed wave

In fig.3.1, microwave can be incidental into the packed bed, they can transmit through the hollow the packed bed, and they can be reflected and absorbed by the porous packed bed. By power balance on control volume as shown in fig.3.1, the incident wave can be expressed as:

Incident Wave (A) = Reflected Wave (B) + Transmitted Wave (C)
+ Absorbed Wave (D) (1-8)

where P_{in} is microwave power incident or microwave energy emitted from a microwave oscillator (Incident Wave (A)); P_{ref} is microwave power reflected (Reflected Wave(B)); P_{tran} is microwave power transmitted(Transmitted Wave(C)) and P_{abs} is microwave power absorbed (Absorbed Wave(D)).

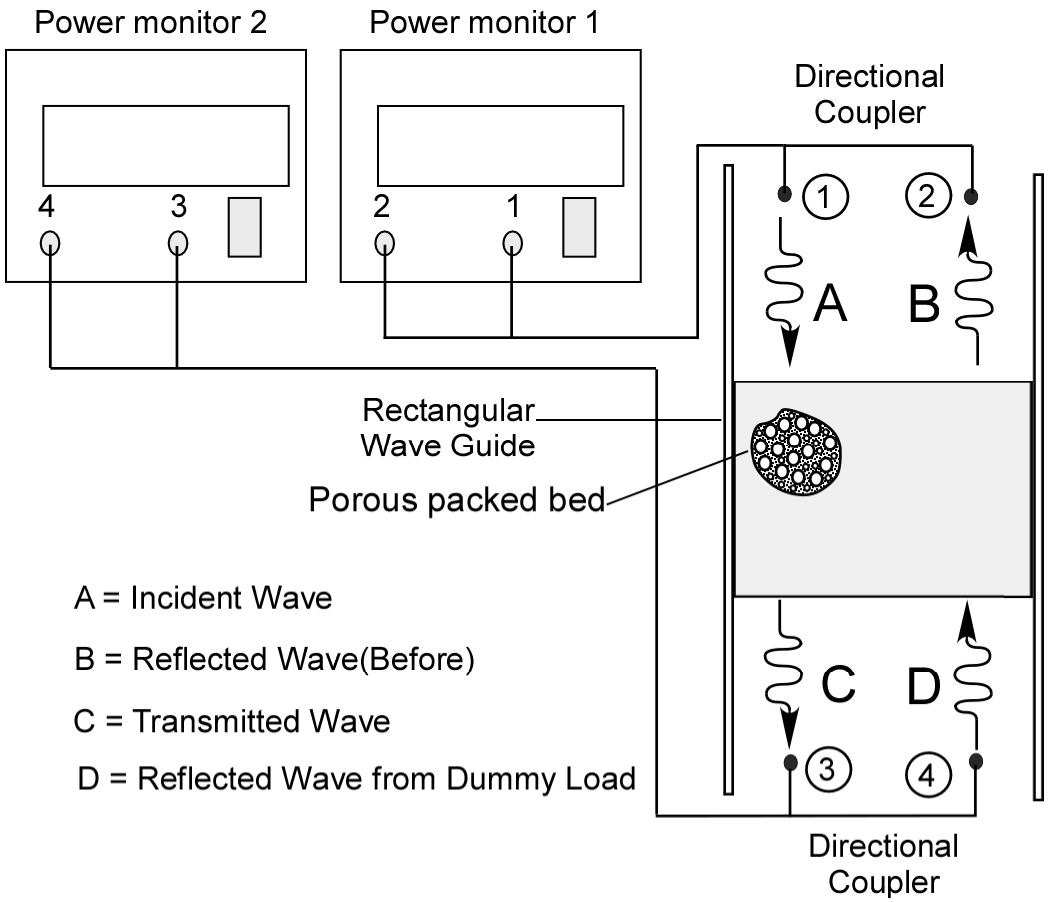

Figure 1.5 Microwave power measuring

In order to calculate the microwave power absorbed, Eq. 1-7 can be rearranged as:

$$P_{abs} = P_{in} - P_{tran} - P_{ref} \tag{1-9}$$

Next, P_{abs} refers to $\dot{Q}_{abs}$ throughout this study, as shown in equations below:

$$P_{abs} = \dot{Q}_{abs} \tag{1-10}$$

The microwave power absorbed efficiency during microwave drying of the porous packed bed provides a true measure of the performance of the drying system which can be expressed as:

$$\eta_{abs} = \left[\frac{Aborbed \quad Wave(D)}{Incident \quad Wave(A)} \right] \times 100 \tag{1-11}$$

$$\eta_{abs} = \left[\frac{P_{abs}}{P_{in}} \right] \times 100 \tag{1-12}$$

Thus, from Eq. (3-9):

$$\eta_{abs} = \left[\frac{\dot{Q}_{abs}}{P_{in}} \right] \times 100 \tag{1-13}$$

1.9 Mass and energy balance equation for the drying process

The conservation of mass for the control volume of drying porous packed bed is shown in figure 1.2. The mass balance equation can be written as (Syahrul et al. (2002)):

$$\frac{dm_{cv}}{dt} = \dot{m}_{g1} - \dot{m}_{g2} \tag{1-14}$$

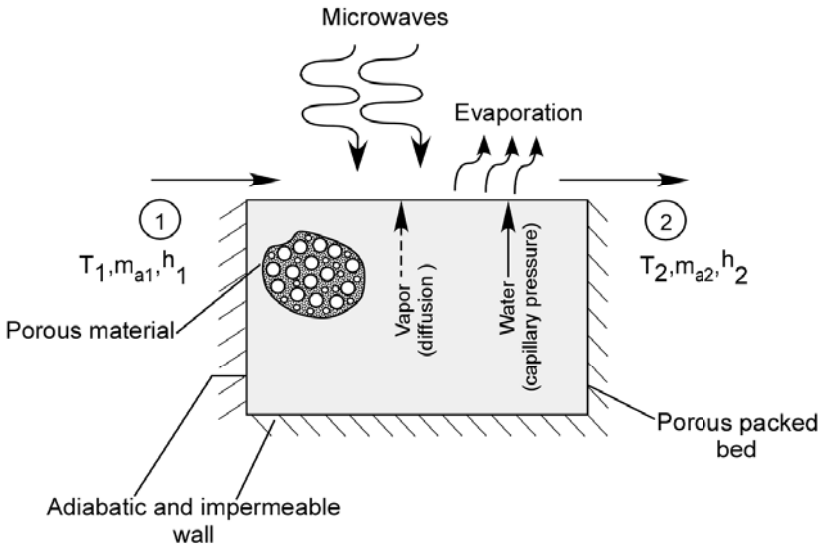

Figure 1.6 Microwave and convective drying process.

Here, Eq.(1-13) is the mass flow rate balance for the control volume where $\dot{m}_{g1}$ and $\dot{m}_{g2}$ denote ,respectively, the mass flow rate at inlet (1) and exit at (2). Similarly, a balance of water in air flowing through the porous packed bed leads to (Syahrul et al. (2002)):

$$W_d \frac{dM_p}{dt} = \dot{m}_a (X_1 - X_2) \tag{1-15}$$

where W_d is weight of dry material and M_p is particle moisture content dry basis. It can be expressed as (Syahrul, et al. (2002)):

$$M_p = \frac{W_b - W_d}{W_d} \tag{1-16}$$

where W_b is weight of material before drying, $\dot{m}_a$ is the mass flow rate of dry air, X_1 and X_2 denote absolute humidity of inlet and exit air, respectively. The left-hand side of the mass balance equation, Eq. (3-14), is the mass flow rate of water in the air flowing on porous packed bed surface. It can be written as: (Syahrul et al. (2002)):

$$\dot{m}_w = \dot{m}_a (X_2 - X_1) \tag{1-17}$$

In the drying processes, we apply the First Law of Thermodynamics (the conservation of energy) for the control volume shown in Figure 3.2. The significant heat transfer is due to the heat of evaporation between the solid and the drying air, and there is also heat rejection to the surroundings. The energy rate balance is simplified by ignoring kinetic and potential energies. Since the mass flow rate of the dry air and the mass of dry material, within the control volume remain constant with time, the energy rate balance can be expressed as:

$$\frac{W_d (h_{m2} - h_{m1})}{\Delta t} = \dot{Q}_{evap} + \dot{m}_a (h_1 - h_2) + \dot{Q}_{abs} - \dot{Q}_{loss} \tag{1-18}$$

where $\dot{Q}_{evap}$ is heat transfer rate due to water evaporation , $\dot{Q}_{abs}$ is microwave energy required for heating up dielectric material, h_m is enthalpy of material, t is time, $\dot{m}_a$ is mass flow rate of dry air , h is enthalpy of dry air and $\dot{Q}_{loss}$ is heat transfer rate to the environment.

Assuming air as an ideal gas, thus the different in specific enthalpy are as follows (Cengel and Boles (2002)):

$$h_{m1} - h_o = c_m(T_{m1} - T_o) \tag{1-19}$$

$$h_{m2} - h_o = c_m(T_{m2} - T_o) \tag{1-20}$$

The enthalpy term of material in Eq.(3-17) can be written as (Cengel and Boles (2002)):

$$h_{m2} - h_{m1} = c_m(T_{m2} - T_{m1}) \tag{1-21}$$

where c_m represents the specific heat of the material. The enthalpy of moist air can be calculated by adding the contribution of each component as it exits in the mixture; thus the enthalpy of moist air is (Cengel and Boles (2002)):

$$h = h_a + Xh_v \tag{1-22}$$

The heat transfer rate due to phase change is (Incropera et al. (2007)):

$$\dot{Q}_{evap} = \dot{m}_w h_{fg} \tag{1-23}$$

where h_{fg} is latent heat of vaporization.

1.10 Specific energy consumption and energy efficiency in drying process

The specific energy consumption (SEC) was estimated in a combined convective - microwave drying processes. The specific energy consumption (SEC) is defined as follows:

$$SEC = \frac{\text{Total energy supplied in drying process}}{\text{Amount of water removed during drying}}, \frac{kJ}{kg} \tag{1-24}$$

$$SEC = \frac{(P_{\text{in}} + Q_{convec})\Delta t}{\text{Amount of water removed during drying}}, \frac{kJ}{kg} \tag{1-25}$$

where Q_{convec} is a convective heat transfer which can be calculated from (Incropera et al.(2007)):

$$Q_{convec} = \overline{h} A(T_{\infty} - T_{surf}) \tag{1-26}$$

and

$$\overline{h} = \frac{\overline{N}_u k}{L} \tag{1-27}$$

where $\overline{h}$ is convection heat transfer coefficient, A is surface area of the packed bed, T_{surf} is temperature at surface of the packed bed, T_{∞} is ambient temperature, $\overline{N}_u$ is Nusselt number, k is thermal conductivity , and L is length of surface of porous packed bed in direction of flow.

From ref. (Dincer et al. (2002)), the energy efficiency (η_e) for drying process is defined as:

$$\eta_e = \frac{W_d[h_{fg}(M_{p1} - M_{p2}) + c_m(T_{m2} - T_{m1})]}{\dot{m}_{da}(h_1 - h_o)\Delta t + \Delta t \dot{Q}_{abs}} \tag{1-28}$$

CHAPTER 2

LITERATURE REVIEW

A general review of the historical development, how microwaves drying and conventional drying with dielectric material, its advantages and limitations, and technological development and applications in drying processing, etc will be presented in this chapter.

2.1 Conventional drying

The most common method of drying process is by using air as the heating medium. A fan is usually used to force heated air through a fixed bed of dielectric material, producing a moisture diffusion process which results in drying. Convection drying is a relatively inefficient process since the air will reach saturation before using all its sensible heat for moisture removal. Using higher air temperatures may increase the drying rate, but also results in damage the dielectric material bed.

Rogers, J.A. and Kaviany, M., 1992 have been investigated the convective heating of an initially partially saturated packed bed and the consequent surface and internal evaporation of the liquid is considered for cases where the temperature everywhere in the bed is below the saturation temperature at the local total pressure. In the first period where the liquid phase is continuous (funicular regime), the effect of surface tension non-uniformity on the liquid and gas phase flows is examined. The critical time (the time at which the surface saturation becomes equal to the immobile saturation) is found from the integration of the conservation equations. The effect of the absolute permeability heterogeneities on this critical time is examined, and it is shown that for normal distributions in porosity, the critical time increases over that for homogeneous permeability. The mass transfer rate during the evaporative front regime is also predicted by treating both the dry and the wet regions and the moving interface. An experiment is performed in which a 0.10 mm glass spheres-ethanol bed is convectively dried, and good agreement is found between the predicted and measured mass transfer rates, critical times, and surface temperatures.

Ratti, C., Araya-Farias, M., Mendez-Lagunas, L. and Makhlouf, J., 2007, have been investigated the convective hot air-drying and freeze-drying in garlic sample where the potential processes to preserve and concentrate allicin in garlic was performed. Both temperature and air velocity had an important effect on hot air drying kinetics. Sample size and temperature significantly affected the duration of freeze-drying, and thus the remaining moisture content of the garlic samples. It is also found that Allicin content decreased with an increase of drying temperature in both convective hot air-drying or freeze-drying. Moderate air temperatures (40 and 50°C) allowed a better allicin retention than higher temperatures (60°C). However, retention of allicin was more important in garlic samples freeze dried at a temperature of 20 °C. The drying method did not show a significant impact on glass transition temperature values, indicating that garlic composition is a more important factor than internal structure. The predictions of the Gordon and Taylor model are in good agreement with the experimental data.

In the work of Sousa, L.H.C.D., Lima., O.C.M. and Pereira, N.C., 2006, the drying process of crude cotton fabric is analyzed under two main aspects: analysis of moisture distribution inside the textile sheet, and analysis of certain operational convective drying process variables. Experimental apparatus consisted of a drying chamber in which samples of pure cotton textile were suspended inside the drying chamber and exposed to a convective hot air flow. The influence of the operational variables on the drying process behavior was studied by two different ways with generalized drying curves. The behavior of moisture distribution profiles was compared to average moisture content of the textile fabric verifying whether average values were able to represent the textile moisture content during the drying process.

Guranunal, H. and Sacilik, K., 2009, in this study, the drying characteristics of hawthorn fruits were examined in a laboratory scale hot air dryer at an air velocity of 0.8 m/s and air temperature in the range of 50–70 °C. Moisture transfer from the test samples was described by applying The Fick's diffusion model, and the effective diffusivity was calculated. The temperature dependence of the effective diffusivity was described by the Arrhenius type relationship. The experimental drying data of hawthorn fruits were used to fit Page, Logarithmic, Approximation of diffusion, Two-term and Midilli et al. models, and the statistical validity of models tested were

determined by nonlinear regression analysis. Estimations by the Midilli et al. model were in good agreement with the experimental result obtained.

In the work of Mwithiga, G. and Olwal, J.O., 2004, the effect of air temperature and sample thickness on the drying kinetics of kale was investigated using a convective air dryer at a fixed airflow rate of 1 m/s and drying air temperatures of 30, 40, 50 and 60 °C. The sliced kale leaves were dried in wire trays in 10,20, 40 and 50 mm thick layers. The drying rate increased with drying air temperature but decreased with layer thickness. The effective diffusivity for 10 mm thick layers was found to increase with the drying air temperature and ranged between 14.9 and 55.9 x 10^{-10} m^2/s. The effect of temperature on diffusivity could be expressed by an Arrhenius type relationship with a high R^2 of 0.9989. The activation energy of kale was found to be 36.115 kJ/mol. When four drying models were developed using the experimental data the Modified Page model was found to be marginally better than the other models in estimating the drying curve over the experimental temperature range.

2.2 Microwave drying

Rattanadecho, P., 2002, the drying of capillary porous materials by microwave with rectangular waveguide has been investigated numerically and experimentally. Most importantly, it focuses on the investigation of the distributions of electric field, temperature and moisture profiles within the capillary porous materials. The measurements of temperature and moisture distributions within the capillary porous materials provide a good basis for understanding of the microwave drying process. The mathematical model gives qualitatively comparable trends to experimental data. The calculations of electromagnetic fields inside the rectangular waveguide and the capillary porous materials show that the variation of particle sizes and initial moisture content changes the degree of penetration and rate of microwave power absorbed within the sample. Further, the small particle size leads to much higher capillary pressure resulting in a faster drying time.

Ratanadecho, P., Aoki, K. and Akahori, M., 2001, the drying of unsaturated porous material due to microwave drying (2.45 GHz) has been investigated numerically and experimentally. Most importantly, this work focuses on the influence

of moisture content on each mechanism (vapor diffusion and capillary flow) during microwave drying process. Based on a model combining the electric field and heat-mass transport equations, it is shown that the variation of initial moisture content and particle size changes the degree of penetration and rate of absorbed energy within the material. The small bead size leads to much higher capillary forces resulting in a faster drying time.

Ratanadecho, P., Aoki, K. and Akahori, M., 2001, the drying of a capillary porous packed bed of glass beads by microwave energy using a rectangular wave-guide was investigated numerically and experimentally. The effects of moisture content, particle size and microwave power level on the drying kinetics were examined. Most importantly, this work focuses on the prediction of the distribution of the electromagnetic field as well as the temperature and moisture distribution within the capillary porous medium. The model, which combines the electromagnetic, temperature, and moisture fields, predicted results that were in good agreement with the experimental data.

Turner, I.W. and Jolly, P.G., 1991, a model is formulated to describe the drying of a slab of porous material in a combined microwave and convective environment. The model describes the evolution of temperature, pressure, moisture and power distributions that occur during the drying process. The microwave internal heat source is calculated from electromagnetic theory with varying dielectric properties. The inclusion of pressure in the model allows the physical phenomena of 'water pumping', often observed in microwave drying systems, to be accounted for. The influence of sample size on the drying kinetics is examined and found to be an important parameter during the drying process. In particular, the effect of resonance on the moisture and temperature profiles and the need for careful consideration of surface mass transfer coefficients are investigated. Simulation results are presented for the combined microwave and convective drying of a homogeneous, isotropic porous material.

Perré, P. and Turner, I.W., 1997, a comparison between experimental and theoretical results for the combined microwave and connective drying of softwood is presented. The microwave applicator used for the experiments is an oversized waveguide, and the results for both sapwood and heartwood are analyzed. To

elucidate on the physics of the process at a fundamental level, a complete model is proposed, which considers the intricate link that transpires between the heat and mass-transfer phenomena and the power distribution throughout the sample during drying. The resulting model, which uses a comprehensive 2-D set of equations to describe the drying process, together with a complete 3-D solution of the Maxwell equations within the waveguide in the time domain, can be used to investigate many aspects of dielectric drying. This research deals with the spatial variation of the power density within the material at various drying times and the effect of the anisotropy of the transfer properties on the shape and evolution of the power distribution. Most importantly, it focuses on the prediction of the location of hot spots and thermal runaway within the sample from the viewpoint of product quality. Strengths and weaknesses of the model are highlighted.

Ratanadecho, P., Aoki, K. and Akahori, M., 2002, the melting of frozen packed beds by a microwave with a rectangular waveguide has been investigated numerically and experimentally. It was performed for the two different layers, which consist of frozen and unfrozen layers. This paper focuses on the prediction of the temperature field, as well as the microwave energy absorbed, and the melting front within the layered packed beds. Based on the combined model of the Maxwell and heat transport equations, the results show that the direction of melting against the incident microwave strongly depends on the structural layered packed beds because of the difference in the dielectric properties between water and ice.

Rattanadecho, P., 2006, microwave heating-drying of wood using a wave guide is a relatively new area of research. In order to gain insight into the phenomena that occur within the wave guide together with the temperature distribution in the wood, a detailed knowledge of absorbed power distribution is necessary. In this paper, a two dimensional numerical model is developed to predicted the distribution of electromagnetic fields (TE_{10}-mode), power and temperatures distributions within wood located in rectangular wave guide. A three dimensional finite difference time domain (FDTD) scheme is used to determine electromagnetic fields and absorbed power by solving the transient Maxwell's equations, and finite difference method is used to obtain unsteady temperature profiles. Temperature dependence of wood dielectric properties is simulated through an iterative process. The simulations are

performed illustrating the influence of irradiation times, working frequencies and sample size. The presented modeling is used to identify the fundamental parameters and provides guidance for microwave drying of wood.

Rattanadecho, P., Suwannapum, N., Watanasungsuit, A. and Duanduen, A., 2007, the drying of dielectric materials by a continuous microwave belt drier has been investigated experimentally. Most importantly, it focuses on the investigation of drying phenomena under microwave environment. In this analysis, the effect of the irradiation time, sample sizes, and microwave power level (number of magnetrons (800W/1 magnetron)) on overall drying kinetics and mechanical properties are studied. The dielectric materials studied are classified into two types including ceramics (microwave demolding of tableware product) and natural rubber. The results showed that using the continuous microwave applicators technique has several advantages over the conventional method such as shorter processing times, volumetric dissipation of energy throughout a product, and high energy efficiency compared with other process, and it offers improvements in product quality. The results presented here provide a basis for fundamental understanding of microwave-heating of various kinds of dielectric materials. Further quantitative validation of experimental data could be very useful, especially in providing information for processing high performance microwave drying for developing the ceramics and rubber industries in Thailand.

Rattanadecho, P., Suwannapum, N., Chatveera, B., Atong, D. and Makul, N., 2008, a high rate of strength development in mortar and concrete can benefit a number of important operations in the construction industry, such as concrete precasting, pavement repair and concrete decontamination. In this study, the acceleration of cement paste curing with microwave energy by using continuous belt drier is investigated. The microwave power was generated by means of 14 compressed air-cooled magnetrons of 800 W each for a maximum of 11.2 kW. The power setting could be adjusted individually in 800 W steps. This study included the heat transfer analysis taking place during the curing of cement paste with microwave energy and the compressive strength development of cement paste. The tested results were compared with those of the conventional cement paste that were cured in water and air. Internal structures of cement paste were investigated for analyzing the

mechanical properties after curing. The variables emphasized on the thermal influences from using microwave energy, properties of cement paste, and time of curing. The test results showed that microwave energy accelerated the early-aged compressive strength of cement paste and did not affect upon later-aged strength; for instance, the growth rate of compressive strength of 30 min-cured and water-to-cement ratio of 0.4 microwave-cured mortar after 3 days was 103% while 101 and 95% for specimens at the ages of 7 and 28 days, respectively. Furthermore, microwave curing can reduce energy consumption and time of curing.

Rattanadecho, P., Duangduen, A. and Vongpradubchai, S., 2006, to demonstrate the potential of microwave drying in the ceramic industry, microwave demolding of tableware product by a continuous microwave belt drier has been investigated. This study focuses on the investigation of the effects of the irradiation time, sample size, microwave power and location of magnetron on overall drying kinetics. The results show that microwave drying has several advantages over the conventional method such as shorter processing time, volumetric dissipation of energy throughout a product, high energy efficiency, reduced amount of mold usage, and offering product quality. Further quantitative validation of experimental data could be very useful, especially in providing information for processing high-performance microwave drying for developing the ceramic industry in Thailand.

Vongpradubchai, S. and Rattanadecho, P.,2009, the drying of wood by microwave energy using a continuous microwave belt drier compared to conventional method has been carried out in this research. In a continuous microwave belt drier, the microwave power is generated by means of 14 compressed air-cooled magnetrons of 800W each for a maximum of 11.2 kW. The power setting could be adjusted individually in 800W steps. Most importantly, it focuses on the investigation of drying phenomena under microwave environment. In this analysis, the effect of the irradiation time and microwave power level on overall drying kinetics and mechanical properties are studied. The results showed that using the continuous microwave applicators technique has several advantages over the conventional method such as shorter processing times, volumetric dissipation of energy throughout a product, high energy efficiency and it offers improvements in product quality. The results presented

here provide a basis for fundamental understanding of microwave-heating of various kinds of dielectric materials.

Jeni, K., Yapa, M. and Rattanadecho, P., 2010, combined microwave (MW) and vacuum drying of biomaterials has a promising potential for high quality dehydrated products. A better knowledge of the drying kinetics of biomaterial products could improve the design and operation of efficient dehydration systems. The experiments were carried out on commercialized biomaterials drier using a combined unsymmetrical double-feed microwave and vacuum system. Three kilograms of tea leaves were applied with the microwave power of 800 (single-feed magnetron) and 1600W (unsymmetrical double-feed magnetrons) operating at 2450MHz frequency. Rotation rates of the rotary drum were held constant at 10 rpm. Vacuum pressure was controlled at the constant pressure of 385 Torr and 535 Torr, respectively. In this study, the system can be operated either in continuous or pulse mode in each experiments. Experiments show that in the case of high power level and continuous operating mode causes greater damage to the structure of tea leaves sample. Microwave drying with pulse operating mode at 385 Torr ensured the shortest drying time and the best overall quality of dried tea leaves, and thus was chosen as the most appropriate technique for tea leaves drying.

2.3 Analysis of energy in drying system

Ogura, H., Hamaguchi, N., Kage, H., and Mujumdar, A.S., 2004. presented Energy and Cost Estimation for Application of Chemical Heat Pump Dryer to Industrial Ceramics Drying. In this article they estimate the potential of a new chemical heat pump dryer (CHPD) application to an industrial ceramics drying process from the viewpoints of energy and cost saving. A $CaSO_4/H_2O/CaSO_4.1/2H_2O$ hydration/dehydration CHPD system and a $CaO/ H_2O/Ca(OH)_2$ hydration/dehydration CHPD system were examined.

Men'shutina, N.V., Gordienko,M.G., Voinovskii, A.A. and Kudra,T.,2005. studied the dynamic criteria for evaluating the energy consumption efficiency of drying equipment. A new approach to the evaluation of the efficiency of drying equipment is considered. The approach employs dynamic efficiency criteria that are calculated from time-distributed parameters (for batch drying) or space-distributed

parameters (for continuous drying) rather than average or input–output data. This approach, in addition to comparing the operation efficiencies of various dryers, allows one to analyze how the efficiency changes during the drying. Sample efficiency evaluations using the dynamic criteria are performed on the basis of experimental data for various types of dryers (fluidized-bed, freeze, and microwave vacuum dryers) and various materials

Prommas, R., Rattanadecho, P. and CholaseukIn, D.,2011, studied the energy and exergy analyses in drying process of porous media using hot air was investigated. Drying experiments were conducted to find the effects of particle size and thermodynamic conditions on energy and exergy profiles. An energy analyses was performed to estimate the energy utilization by applying the first law of thermodynamics. An exergy analyses was performed to determine the exergy inlet, exergy outlet, exergy losses and efficiency during the drying process by applying the second law of thermodynamics. The results show that energy utilization ratio(EUR)and exergy efficiency depend on the particle size as well as hydrodynamic properties. Furthermore, the results of energy and exergy presented here can be applied to other porous drying processes which concern effect of porosity as well as grain size

Syahrul, S., Hamdullahpur, F. and Dincer, I., 2003, this paper deals with thermal modeling of the fluidized bed drying of wet particles to study heat and mass transfer aspects and drying thermal efficiencies. The model is then validated with the literature experimental data obtained for corn. A parametric investigation is undertaken to study the effects of the inlet air temperature, the air velocity and the initial moisture content of the material (i.e. corn) on the process thermal efficiency. The results show that the thermal efficiencies of the fluidized bed drying decrease sharply with decreasing moisture content of corn and hence increasing drying time, and apparently become the lowest at the end of the drying process. This clearly indicates that the moisture transfer from the material depends strongly on the air temperature, air velocity and the moisture content of material. A good agreement is obtained between the model predictions and the available experimental results.

Dincer, I. and Sahin, A.Z., 2004, presented a new model for thermodynamic analysis, in terms of exergy, of a drying process. Exergy efficiencies are derived as

functions of heat and mass transfer parameters. An illustrative example is considered to verify the present model and to illustrate the applicability of the model to actual drying processes at different drying air temperatures, specific exergies of drying air, exergy differences of inlet and outlet products, product weights, moisture contents of drying air, and humidity ratios of drying air. As a result, this work is intended not only to demonstrate the usefulness of exergy analysis in thermodynamic assessments of drying processes, but also to provide insights into their performances and efficiencies.

Akpinar, E.K., Midilli, A. and Bicer,Y., 2005, This paper is concerned with the energy and exergy analyses of the single layer drying process of potato slices via a cyclone type dryer. Using the first law of thermodynamics, an energy analysis was performed to estimate the ratios of energy utilization. An exergy analysis was accomplished to determine the location, type and magnitude of the exergy losses during the drying process by applying the second law of thermo-dynamics. It was concluded that the exergy losses took place mostly in the 1st tray where the available energy was less utilized during the single layer drying process of potato slices. It is emphasized that the potato slices are sufficiently dried in the ranges between 60 and 80 °C and 20–10% relative humidity at 1 and 1.5 ms^{-1} of drying air velocity during 10–12 h despite the exergy losses of 0–1.796 kJ s^{-1}

Waje, S.S., Thorat, B.N. and Mujumdar. A. S., 2007, studied the effects of various process variables and equipment components(geometry) on the performance of a screw conveyor dryer (SCD) were studied in terms of the material throughput and its uniformity, dryer load, specific consumption of mechanical energy, and heat transfer rate. The experimental results for drying of fine crystalline solids (50–100 mm particle size and 550 kg/m^3 bulk density) in a 3-meter-long uninsulated jacketed screw conveyer dryer with a 0.072-m screw diameter have been used. The hydrodynamic performance of the SCD was also studied using sand particles of 350 mm size and 1500 kg/m3 bulk density (tapped). The maximum specific consumption of mechanical energy for conveying was found to be 1 kJ/kg. Moreover, the flow behavior of the material at the dryer discharge was found to depend strongly on the screw speed and the material feed rate.

Sharma, G.P., and Prasad, S., 2006, studied the specific energy consumption in microwave drying of garlic cloves. The convective and microwave-convective drying of garlic cloves was carried out in a laboratory scale microwave dryer, which was developed for this purpose. The specific energy consumption involved in the two drying processes was estimated from the energy supplied to the various components of the dryer during the drying period. The specific energy consumption was computed by dividing the total energy supplied by amount of water removed during the drying process. The specific energy consumption in convective drying of garlic cloves at 70 ^{o}C temperature and 1.0 m/s air velocity was estimated as 85.45 MJ/kg of water evaporated. The increase in air velocity increased the energy consumption. The specific energy consumption at 40W of microwave power output, 70^{o}C air temperature and 1.0 m/s air velocity was 26.32 MJ/kg of water removed, resulting in about a 70% energy saving as compared to convective drying processes. The drying time increased with increase in air velocity in microwave-convective drying process; a trend reverse to what was observed in convective drying process of garlic cloves.

Lakshmi, S., Chakkaravarthi, A., Subramanian, R. and Singh, V.,2005, studied the energy consumption in microwave cooking of rice and its comparison with other domestic appliances. Microwave oven is a multi-utility kitchen appliance that can be used for cooking rice. An energy assessment was carried out under normal and controlled methods of cooking, with unsoaked and presoaked rice, in a microwave oven at various power levels. In controlled cooking, the energy consumption substantially reduced, in both unsoaked (14–24%) and presoaked (12–33%) rice, whereas cooking time marginally increased (up to 2 min) compared to normal cooking. Presoaking rice resulted in energy savings in normal (5–11%) as well as controlled (3–18%) cooking. Although the absorption of microwave energy in water was 86–89%, the conversion efficiency of electrical to microwave energy was only ~50%. Performance of microwave oven was also compared with our earlier studies on electric rice-cooker (ERC) and pressure cooker. Among the cooking appliances assessed, ERC was the most energy-efficient while microwave cooking offered the least cooking time (15–22 min). Microwave cooking was on par with pressure cooking, the most commonly followed method of cooking rice, in terms of energy consumption, besides, it offered shorter cooking time.

Varith, J., Dijkanarukkul, P., Achariyaviriya, A. and Achariyaviriya, S.,2007, Combined microwave-hot air drying of peeled longan. Objectives of this research were to develop and evaluate a drying process for peeled longan using combined microwave-hot air(MWHA). Each experiment employed the peeled 'Dor' longan to be dried to final moisture content of 18% (dry basis). Hot air temperature was regulated for three levels: 40, 50, and 60 ^{o}C, coupled with MW regulated for four levels: 100, 180, 300 and 450 W. Results show that MWHA drying process yielded a unique convex-shaped drying rate period, followed by a falling rate period. A step-wised drying process using 40 ^{o}C hot air with 450 W-MW power for 1.7 hr, followed by 60 ^{o}C hot air with 300 W-MW power for 3.3 hr provided the maximum drying efficiency. Compared to the 65 ^{o}C hot air drying to obtain the golden brown flesh, combined MWHA process reduced drying time by 64.3% and specific energy consumption by 48.2%.

Das, T., Subramanian, R., Chakkaravarthi, A., Singh, V., Ali, S.Z. and Bordoloi, P.K., 2006, energy conservation in cooking rice is an important area for scientific investigation. Experiments were conducted to measure the energy consumption during normal and controlled cooking of both unsoaked and presoaked rice using two types of domestic cooking appliance, namely, an electric rice cooker and a pressure cooker. Cooking rice with controlled energy input, under pressure and with presoaking were the three approaches, which resulted in saving of energy. Electric rice cooker was found to be the most energy efficient among the different combinations of cooking appliance and the types of heat source used in the study. The energy consumption was much less (23–57%) compared to other methods. Prior soaking of rice generally reduced energy consumption as well as cooking time, more prominently during normal cooking. Controlled cooking offered more savings in energy compared to presoaking rice. Considering the energy consumption and cooking time, controlled cooking of presoaked rice was found to be the best among the several approaches investigated. Measurement of water evaporation loss appears to be a good indirect method of assessing the efficiency of heat utilization. Controlled energy input is another useful method that optimizes the energy utilization for cooking, besides presoaking and pressure cooking. Controlled cooking is desirable in all types of rice cooking.

Alibas, I., 2007, studied the energy consumption and colour characteristics of nettle leaves during microwave, vacuum and convective drying Nettle leaves were dried from an initial moisture content of 4.41 to 0.1 (dry basis) by involving microwave, convective and vacuum drying, respectively. Energy consumption and colour parameters for the nettle leaves were compared at these different drying conditions. In particular, the experiments were carried out at four different microwave power levels (500, 650, 750 and 850 W) and air temperatures (50, 75, 100 and 125 ^{o}C) to investigate the effect of these factors on the microwave and convective drying, respectively. Instead, under vacuum drying conditions both the influence of vacuum (20 and 50mm [Hg]) and drying temperature (50 and 75 ^{o}C) were considered. Drying periods ranged from 4 to 6, 30 to 120 and 35 to 65 min for microwave, convective and vacuum drying, respectively. The semi-empirical Page's equation was able to reproduce the experimental drying curves at all operating conditions under microwave, convective and vacuum drying. The optimum method with respect to the drying period, colour and energy consumption was the microwave drying at 850 W.

Alibas, I., 2006, studied the microwave, air and combined microwave–air-drying parameters of pumpkin slices. Pumpkin slices which weighs 50g with moisture of 9.31 g water/g dry solids, were dried using three drying methods, microwave, air and combined microwave–air. Drying continued until slice moisture reduced to 0.1 g water/g dry solids. Two different microwave output powers 160 and 350W were used in the microwave drying. Drying treatments in air-drying were 50 and 75 ^{o}C and 1 m/s fan speed. The combination drying in which microwave and air-drying were applied together was four different combination levels. Drying periods lasted 125–195, 45–90 and 31–51 min for microwave, air and combined microwave–air-drying, respectively, depending on the drying level. Energy consumption was 0.23–0.34, 0.61–0.78 and 0.29–0.42 kWh, respectively. In this study, measured values were compared with predicted values obtained from Page's semi-empirical equation. Optimum drying period, colour and energy consumption was obtained when microwave and air-drying was applied simultaneously and the optimum combination level was 350W microwave applications at 50 ^{o}C.

Aghbashlo, M., Kianmehr, M.H and Arabhosseini, A., 2008, this paper is concerned with the energy and exergy analyses of the continuous-convection drying

of potato slices. The first and second laws of thermodynamics were used to calculate the energy and exergy. A semi-industrial continuous-band dryer has been designed and used for drying experiments. The equipment has a drying chamber of 2m length and the inlet air used for drying is heated by gas power. The experiments were conducted on potato slices with thickness of 5mm at three different air temperatures of 50, 60 and 70^{o}C, drying air mass flow rates of 0.61, 1.22, and 1.83 kg/s and feeding rates of 2.31 x 10^{-4}, 2.78 x 10^{-4}, and 3.48 x 10^{-4} kg/s. The energy utilization and energy utilization ratio were found to vary between 3.75 and 24.04 kJ/s and 0.1513 and 0.3700, respectively. These values show that only a small proportion of the supplied energy by the heater was used for drying. The exergy loss and exergy efficiency were found to be in the range of 0.5987 to 13.71 kJ/s and 0.5713 to 0.9405, respectively, indicating that the drying process was thermodynamically inefficient and much energy was vented in the exhaust air. In addition, the results showed that the feeding rate and the temperature and flow rate of the drying air had an important effect on energy and exergy use. This knowledge will provide insights into the optimization of a continuous dryer and the operating parameters that causes reduction of energy consumption and losses in continuous drying.

Soysal, Y., Öztekin, S. and Eren, Ö., 2006, studied the microwave drying of parsley: modelling, kinetics, and energy aspects. Parsley leaves were dried in a 900W 2450MHz domestic microwave oven to assess the effects of material load on drying time, drying rate, drying efficiency, and specific energy consumption. Microwave drying experiments with different material loads ranging from 64.30 to 128.57 g were performed at microwave power cycle of 9 s on/9 s off at 900 W microwave output power. Drying took place mainly in constant rate and falling rate periods. A relatively long constant rate period was observed after a short heating period. Among the 11 mathematical models tested to fit the drying rates of parsley leaves, the Midilli et al. model with drying rate as a log–log and linear function of time gave the best fit for all the data points. The value of the drying coefficient k decreased with the increase in the dried material load. The multiple regression on the coefficients of the Midilli et al. model for the effects of material load being dried gave the successful results and showed to satisfactorily represent microwave drying kinetics of parsley leaves for the material loads between 64.30 g and 128.57 g. Increasing the material load resulted in

a considerable increase in drying efficiency and a significant decrease in specific energy consumption. About 9.5% increase in drying efficiency and about 18% ($0.92 MJkg^{-1}$ [H_2O]) decrease in specific energy consumption could be obtainable by increasing the material load from 64.30 to 128.57 g.

An excellent review of the drying techniques in dielectric materials using microwave energy has been presented by Mujumdar (1995), Metaxas and Meridith (1983) and Datta and Anantheswaran (2001).

2.3 Final remarks

Microwave drying technique is gaining a renewed interest in both academia and industry. The unique volumetric heat generation and accompanied advantages pave the road for its application in enhancing drying rate and improving product quality. Progress has been made in prolonging the life-span of magnetrons and lowering the capital investment. Techniques to overcome the heating nonuniformity problem have also been developed or are under investigation. The techniques and instrumentation for the measurement of dielectric properties have been fully developed and more and more dielectric properties have been measured and reported. The introduction of fiber optic techniques into microwave drying research has provided means to measure both the temperature and pressure changes during drying, a revolutionary technique that has not been available until the last decade. The heat and mass transfer mechanisms in microwave drying have been and are still being investigated to provide insight into the underlying physics in this unique drying process. With all of the progress, an increase in the application of microwave energy in industrial drying can certainly be foreseen. The next chapters will be presented the application of microwave energy for drying of porous materials where in case of non-hygroscopic porous material (unsaturated glass beads packed bed) and in case of hygroscopic porous material (wood) were performed in a combined multi-feed microwave-convective air and continuous belt system (CMCB) with different drying conditions. The analyzing based on drying kinetics and energy consumption and human safety will be completely explained in each sub-chapter.

CHAPTER 3

ANALYSIS OF ENERGY CONSUMPTION IN DRYING PROCESS OF NON-HYGROSCOPIC POROUS PACKED BED USING A COMBINED MULTI-FEED MICROWAVE - CONVECTIVE AIR AND CONTINUOUS BELT SYSTEM (CMCB)

3.1 Introduction

During the past decade, there are many successful examples of microwave application including the heating and drying of foods, heating and drying of ceramics, heating and curing of concrete, etc. The microwave heating process takes place inside the material, the penetrated depth of which governs how strongly the microwaves are absorbed. It is known that heat dissipated from the microwave energy depends on many parameters such as configuration and structure of porous packed bed samples, microwave power level, microwave field distribution the location of feed ports and dielectric properties of porous packed bed samples. A number of analyses of the microwave heating process have appeared in the recent literatures. An excellent review of the drying techniques in porous material using microwave energy has been presented by Mujumdar (1995), Metaxas (1983) Datta and Anantheswaran(2001) and Schubert and Regier (2005).

The objective of drying is simply to remove water from the dried sample, i.e., porous packed bed without causing any damage. The process must be done both efficiently and economically. Water can leave the surface of the porous packed bed at a given rate depending on many parameters, such as microwave power level and air temperature, etc. In order to accomplish good drying of product, it requires a method that removes the water from the inside of the dried sample to the outside surface at the same rate as the evaporation of surface water.

The reasons for the interest in the interaction of microwaves with porous materials are reported by several investigators in the recent literatures. The microwave energy can lower the drying temperature in several porous materials by several hundred degrees; shorten drying times; reduce drying defects; provide greater throughput; increase energy efficient because the microwave source named “magnetron”, which is capable of very high power output; moreover, it has an

efficiency to convert from electricity to microwave energy of 80% (Pozar (2005)) and lessen floor-space requirements in comparison with conventional drying methods. It is also environmentally friendly and easily integrates into flexible, automated manufacturing systems. It appears that microwaves increase the heating efficiency by concentrating the heating process within porous material rather than in the cavity in which the porous material is placed.

Nowadays, the major concern of drying process is increasing productivity while reducing energy cost. Conventional drying processes of porous material usually take a long time (1–6 hr).The major problem of conventional drying processes is long drying time, which resulted in increased energy consumption. Thus, there have been many attempts to enhance the rate of drying of porous material in order to decrease drying time as well as energy consumption.

For an analysis of microwave energy consumption in heating and drying processes, referred to Sharma and Prasad (2005), this study examined specific energy consumption in microwave drying of garlic cloves. The comparative study of specific energy consumption with two difference drying methods, namely microwave-hot air and hot air drying, was carried out. Other related papers present microwave energy and hot air heating processes. Varith et al. (2007) studied the combined microwave and hot air drying of peeled longan. The influence of moisture content on specific energy consumption (SEC) was examined. The other important paper, written by Lakshmi et al.(2005), presented a comparison of SEC in cooking rice among the microwave oven, electric rice cooker and pressure cooker.

Investigations of energy efficiency of microwave drying of porous material have been performed since the late fifties. Many authors Alibas (2007), Poli et al.(2006), Cheng et al.(2008), Holtz et al.(2009), Soysol et al.(2006), Leiker and Adamska(2004) and Prommas et al.(2010)) emphasis on the advantages of microwave drying over convective drying. Varith et al.(2007) points out the suitability of combined microwave and hot drying of peeled longan. However, there still remain obstacles to be overcome in applying microwave drying technology to drying industry.One of the difficulties is that the microwave power absorbed by moist porous material depends mainly on the moisture content and it is required to move the porous

material for uniform power distribution with on-off type microwave system at fixed power output.

Although a number of studies have been conducted to investigate a microwave heating process, most of them were carried out using a domestic or housing microwave oven and a single or multimode cavity with a non-movable material. Those studies showed that the result may be dependent on the method used to carry out the curing or heating process. The objective of this study is to demonstrate the applicability of microwave energy, as an energy-saving when compared between drying process and electrical consumption and production-cost-reducing technology. The microwave drying of non-hygroscopic porous packed bed in a combined multi-feed microwave-convective air and continuous belt system where a series of 12 magnetrons, 800W each with total power of 9.6 kW were installed, was developed. The experimental results from this study could help to identify some of the potential problems during the practical design stage. This study was of great importance from the practical point of view because it showed the possibility of application of microwave heating-drying of porous materials in industrial scale, especially in a continuous system.

3.2 Experimental procedure

Microwave - convective air drying was carried out using a combined multi-feed microwave-convective air and continuous belt system (CMCB) (Figure 3.1 (a)). The shape of microwave cavity is rectangular with a cross sectional area of 90cm × 45cm × 270cm. The drier was operated at a frequency of 2.45 GHz with maximum working temperature of 180 °C. The microwave power was generated by means of 12 compressed air-cooled magnetrons. The maximum microwave capacity was 9.6 kW with a frequency of 2.45 GHz. The power setting could be adjusted individually in 800W steps. In the continuous processing equipment, two open ends are essential, in which the material to be heated up on the belt conveyer where it was put in and taken out. In this equipment, leakage of microwaves was prevented by the countermeasure in double with a combination of mechanical blocking filter (corrugate choke) and microwave absorber zone filter was provided at each of the open ends. The microwave leakage was controlled under the DHHS (US Department of Health and

Human Services) standard of 5 mW/cm^2. The multiple magnetrons (12 units) were installed in an asymmetrical position on the rectangular cavity (Figure 3.1 (b)). The microwave power was then directly supplied into the drier by using waveguides. An infrared thermometer (located at the opening ends) was used to measure the temperature of the specimens (accurate to ± 0.5 °C).

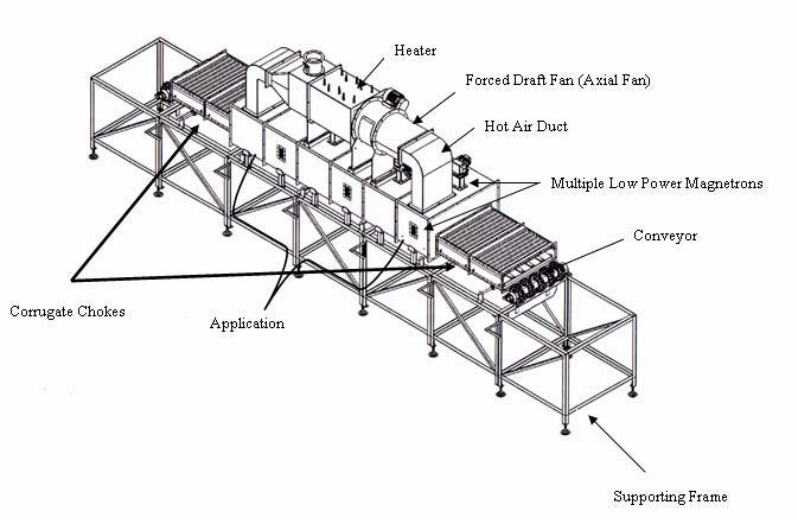

(a)

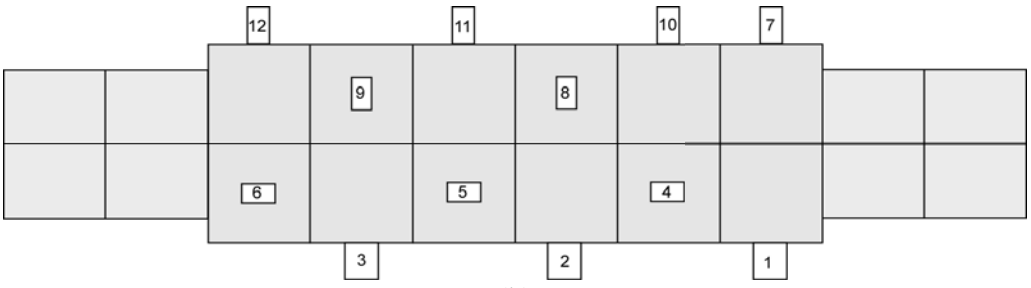

(b)

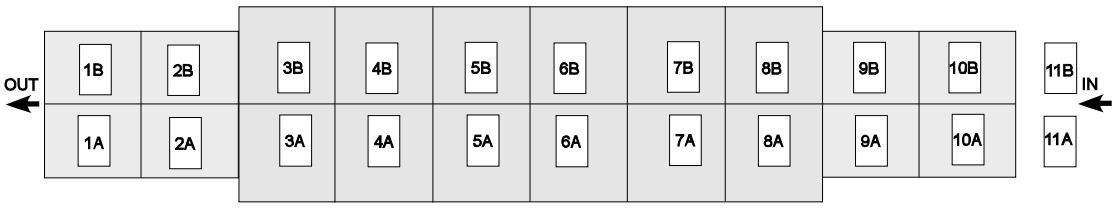

(c)

Figure 3.1 Schematic diagram of experimental set up

(a) A combined multi-feed microwave-convective air and continuous belt system

(b) Feeds magnetrons positioned of 12 units

(c) Feeds samples positioned of 22 packed beds

The magnetrons and transformers used in this system were cooled down by fan. In the continuous heating/drying equipment, two open ends were essential to feed in and feed out the product, through which the material to be heated up on the belt conveyer arranged in certain position, as shown, as in Figure 3.1(c). The belt conveyor system consisted of a drive motor, a tension roller and a belt conveyor. During the drying process, the conveyor speed was adjusted to 0.54 m/min (at the frequency 40 Hz) and the motor speed was controlled by the VSD control unit. Hot air was generated using the 24 unit of electric heaters with the maximum capacity of 10.8 kW and the maximum working temperature of 240°C. The hot air was provided by blower fan with 0.4 kW power through the air duct into the cavity. The hot air temperature was measured by using thermocouple.

As shown in Figure 3.2, the drying samples were non-hygroscopic porous packed bed, which composed of glass beads and water ($S_0 = 1$). A sample container was made from polypropylene with a thickness of 2 mm (with dimension of 14.5cm × 21cm × 5cm). The polypropylene did not absorb microwave energy. In this study, the voids occupied from a fraction up to 38 percent of the whole volume of packed beds. The samples were prepared in two configurations: a single-layered packed bed (d = 0.15 mm, d = 0.40 mm, and d_P =11.5 mm). The sample selected for drying test was a non-hygroscopic porous packed bed with dimensions of 14.5cm × 21cm × 1.15cm.

The 22 porous packed beds had total weight of 11 kg which had the initial water saturation (S_0) of 1.0 and the initial temperature was equal to the ambient temperature

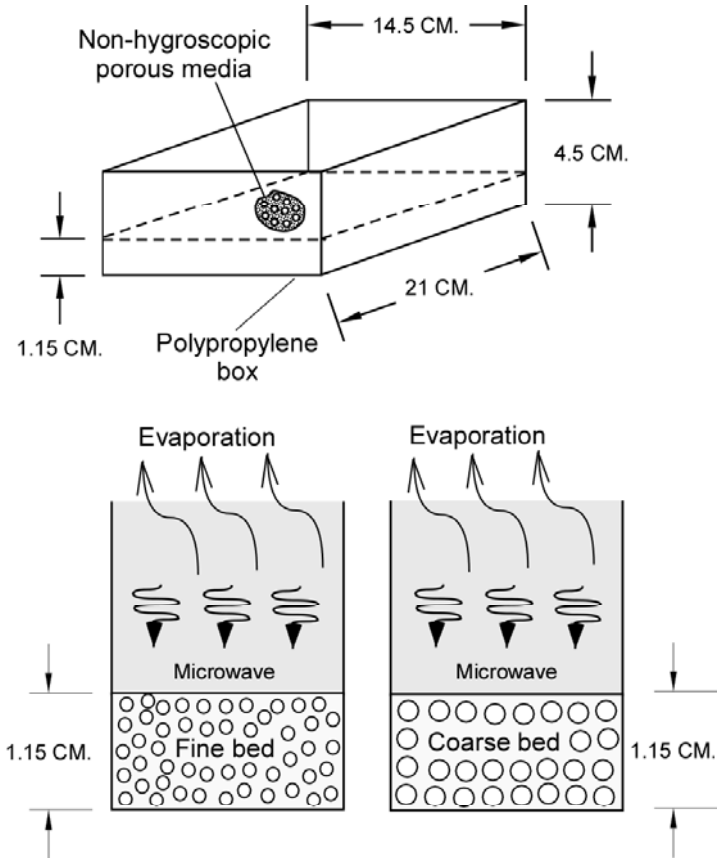

Figure 3.2 Schematic of drying sample (Porous packed bed)

The water saturation in the non-hygroscopic porous packed bed was defined as the fraction of the volume occupied by water to volume of the pores. They were obtained by weighing dry and wet mass of the sample .The water saturation formula can be described in the following from (Ratanadecho (2002)):

$$S = \frac{M_p \cdot \rho_S \cdot (1-\phi)}{\rho_W \cdot \phi \cdot 100} \tag{3-1}$$

where S is water saturation, ρ_s is density of solid, ρ_w is density of water, ϕ is porosity and M_p is particle moisture content dry basis. During the experimental microwave drying processes, the uncertainty of our data might come from the variations in humidity and room temperature. The uncertainty in drying kinetics was

assumed to result from errors in the measured weight of the sample. The calculated drying kinetic uncertainties in all tests were less than 3 %. The uncertainly in temperature was assumed to result of errors in measured input power, ambient temperature and ambient humidity. The calculated uncertainty associated with temperature was less than 2.85%.The different drying cases were then carried out in each test run (see details in tables (3.1) and (3.2)).

3.3 Related theories

3.3.1 Microwave heat generation

Microwave heating involves heat dissipation and microwaves propagation which causes the dipoles to vibrate and rotate. When the microwave energy emits from a microwave oscillator (P_{in}) is irradiated inside the microwave applicator, the dielectric material which has a dielectric loss factor absorbs the energy and are heated up. Then the internal heat generation takes place. The basic equation calculates the density of microwave power absorbed by dielectric material (P_1) is given by (Vongpradubchai and Rattanadecho (2009)) :

$$P_1 = \omega \varepsilon_0 \varepsilon_r'' E^2 = 2\pi \cdot f \cdot \varepsilon_0 \cdot \varepsilon_r' (\tan\delta) E^2 \qquad (3\text{-}2)$$

where E is electromagnetic field intensity, f is microwave frequency, ω is angular velocity of microwave, ε_r' is relative dielectric constant, ε_0 is dielectric constant of air and $tan\delta$ is loss tangent coefficient.

From equation (3-2), P_1 is directly proportional to the frequency of the applied electric field, loss tangent coefficient and root-mean-square value of the electric field. It means that an increasing of $tan\delta$ of specimen, energy absorption and heat generation are also increased. While $tan\delta$ is smaller, microwave will penetrate into specimen without heat generation. However, the temperature increase depends on other factors, such as specific heat, size and characteristic of specimen.

When the material is heated unilaterally, it is found that as the dielectric constant and loss tangent coefficient vary, the penetration depth will be changed and the electric field within the dielectric material is altered. The penetration depth is used

to denote the depth at which the power density has decreased to 37 % of its initial value at the surface (Vongpradubchai and Rattanadecho (2009)):

$$D_p = \frac{1}{\frac{2\pi f}{\upsilon}\sqrt{\frac{\varepsilon_r'\left(\sqrt{1+\left(\frac{\varepsilon_r''}{\varepsilon_r'}\right)^2}-1\right)}{2}}} = \frac{1}{\frac{2\pi f}{\upsilon}\sqrt{\frac{\varepsilon_r'\left(\sqrt{1+(tan\,\delta)^2}-1\right)}{2}}} \tag{3-3}$$

where D_P is penetration depth, ε_r'' is relative dielectric loss factor and υ is microwave speed. The penetration depth of the microwave power is calculated according to Eq. (3-3), which shows how it depends on the dielectric properties of the material. It is noted that products with huge dimensions and high loss factors, may occasionally be overheated to a considerably thick layer on the outer layer. To prevent such phenomenon, the power density must be chosen so that enough time is provided for the essential heat exchange between boundary and core. If the thickness of the material is less than the penetration depth, only a fraction of the supplied energy will become absorbed. Furthermore, the dielectric properties of porous material specimens typically show moderate lossiness depending on the actual composition of the material. With large amount of moisture content, it reveals a greater potential for absorbing microwaves. For typical porous packed bed specimens, a decrease in the moisture content typically decreases ε_r'', accompanied by a slight increment in D_p.

In the analysis, energy P_2 is required to heat up the dielectric material which is placed in a microwave applicator. The temperature of material initially (T_1) is raised to T_2. The energy (P_2) can be estimated by the following calorific equation(Vongpradubchai and Rattanadecho (2009)):

$$P_2 = \frac{4.18 \cdot W \cdot C_p \cdot \Delta T}{t} \tag{3-4}$$

where W is weight of the dielectric material, C_p is specific heat of the dielectric material, ΔT is the increment of temperature $(T_2 - T_1)$ and t is heating time.

Assuming an ideal condition, all of the oscillated microwave energy (P_{in}) is absorbed into the dielectric material; so internal heat generation as Eq. (3-2) takes place. In this case, the relation between P_{in} and P_2 is shown below(Vongpradubchai and Rattanadecho (2009)):

$$P_{in} = P_2 \tag{3-5}$$

In a practical point of view, the transformation energy in applicator exists due to Eq. (3-2) the rate of microwave energy absorbed by means of the dielectric loss factor of the sample and Eq. (3-3) the energy loss in the microwave devices. Accordingly, by taking into account this transformation efficiency, the microwave oscillation output can be calculated by the following equations (Vongpradubchai and Rattanadecho (2009)):

$$P_{in} = \frac{P_2}{\eta_m} \tag{3-6}$$

$$\eta_m = \frac{P_2}{P_{in}} \tag{3-7}$$

where

$$P_2 = \frac{Q \cdot S_p \cdot C_P \cdot \Delta T \cdot 4.18}{60 \cdot \eta_m \cdot 10^3} \tag{3-8}$$

where η_m is efficiency of microwave devices, Q is weight per meter of dielectric material (porous packed bed), S_p is a rate at which the dielectric material is put on the belt conveyer, C_P is specific heat of dielectric material and ΔT is heat-up range of $T_1 - T_0$.

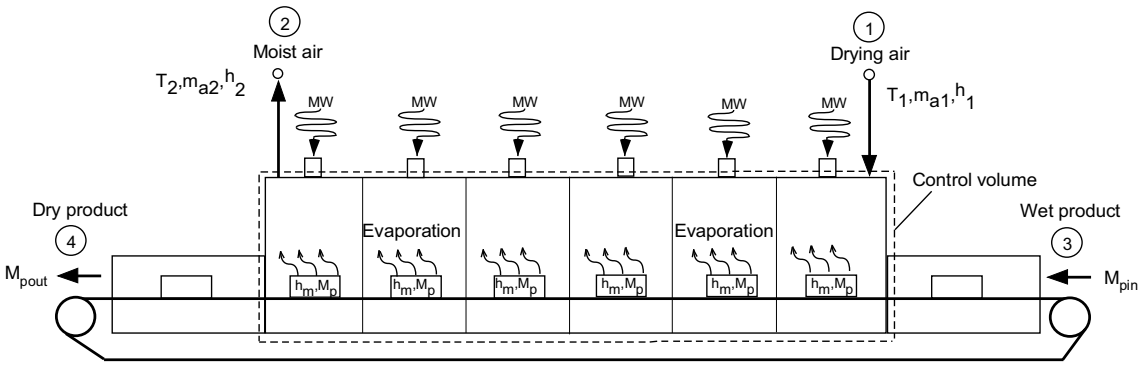

Figure 3.3 Schematic of control volume representing drying process using a combined multi-feed microwave-convective air and continuous belt system (CMCB)

3.3.2 Mass and energy balance equation for the drying process

The conservation of mass for the control volume of cavity is shown in Figure 3.3. The mass balance equation can be written as (Jindarat et al. (2011)):

$$\frac{dm_{cv}}{dt} = \dot{m}_{g1} - \dot{m}_{g2} \tag{3-9}$$

Here, Eq. (3-9) is the mass rate balance for the control volume where $\dot{m}_{g1}$ and $\dot{m}_{g2}$ denote the mass flow rate at inlet (1) and at exit (2), respectively. Similarly, a balance of water in air flowing through the drying cavity leads to (Jindarat et al. (2011)):

$$W_d \frac{dM_p}{dt} = \dot{m}_a (X_1 - X_2) \text{ (3-10)} \tag{3-10}$$

where W_d is weight of dry material and M_p is particle moisture content in dry basis. this can be expressed as (Jindarat et al. (2011)):

$$M_p = \frac{W_b - W_d}{W_d} \tag{3-11}$$

where W_b is weight of material before drying, $\dot{m}_a$ is the mass flow rate of dry air, X_1 and X_2 denote absolute humidity of inlet and exit air, respectively. The left-hand side of the mass balance equation, Eq. (3-10), is the mass flow rate of water in the air flowing from cavity. It can be written as (Jindarat et al. (2011)):

$$\dot{m}_w = \dot{m}_a(X_2 - X_1) \tag{3-12}$$

In the drying process, we apply the first law of thermodynamics (the conservation of energy) for the control volume as shown in Figure 5.3. The significant heat transfer is due to the heat of evaporation between the solid and the drying air, and there is also heat rejection to the surrounding. The energy rate balance is simplified by ignoring kinetic and potential energies. Since the mass flow rate of the dry air and the mass of dry material within the control volume remain constant with time, the energy rate balance can be expressed as:

$$\frac{W_d(h_{m2} - h_{m1})}{\Delta t} = \dot{Q}_{evap} + \dot{m}_a(h_1 - h_2) + \dot{Q}_{MW} - \dot{Q}_{loss} \tag{3-13}$$

where $\dot{Q}_{evap}$ is heat transfer rate due to water evaporation, $\dot{Q}_{MW} = P_{in}$ is microwave energy, h_m is enthalpy of material, t is time, $\dot{m}_a$ is mass flow rate of dry air, h is enthalpy of dry air, and $\dot{Q}_{loss}$ is heat transfer rate to the environment.

Assuming air as an ideal gas, thus the differences in specific enthalpy are as follows (Jindarat et al. (2011)):

$$h_{m1} - h_o = c_m(T_{m1} - T_o) \tag{3-14}$$

$$h_{m2} - h_o = c_m(T_{m2} - T_o) \tag{3-15}$$

The enthalpy term of material in Eq.(3-13) can be written as(Jindarat et al. (2011)):

$$h_{m2} - h_{m1} = c_m(T_{m2} - T_{m1}) \tag{3-16}$$

where c_m represents the specific heat of the material. The enthalpy of moist air can be calculated by adding the contribution of each component as it exits in the mixture; thus the enthalpy of moist air is (Jindarat et al. (2011)):

$$h = h_a + Xh_v \tag{3-17}$$

The heat transfer rate due to phase change is (Jindarat et al. (2011))

$$\dot{Q}_{evap} = \dot{m}_w h_{fg} \tag{3-18}$$

where h_{fg} is latent heat of vaporization.

5.3.3 Specific energy consumption and energy efficiency in drying process

The drying of non-hygroscopic porous packed bed is a process of simultaneous heat and mass transfer. The specific energy consumption during drying process using a combined multi-feed microwave-convective air and continuous belt system and convective drying processes was estimated. The drying conditions are total electrical power supplied in drying process; convective air temperature of 30, 50 and 70 °C, convective air velocity of 0.5 m/s, total microwave power of 4.8 kW. The specific energy consumption (SEC) equation is represented by:

$$SEC = \frac{\text{Total electrical power supplied in drying process}}{\text{Amount of water removed during drying}}, \left[\frac{kW-hr}{kg}\right] \tag{3-19}$$

$$SEC = \frac{P_{total}}{\text{Amount of water removed during drying}}, \left[\frac{kJ}{kg}\right] \tag{3-20}$$

where P_{total} is a total electrical power supplied in drying process; this term can be calculated from:

$$P_{total} = P_{mg} + P_{heater} + P_{exfan} + P_{blfan} + P_{cofan} + P_{con}, \left[kW \times 3600s\right] \tag{3-21}$$

Where P_{mg} is the electrical power supplied in magnetron, P_{heater} is the electrical power supplied in heater, P_{exfan} is the electrical power supplied in exhaust fan, P_{blfan} is the electrical power supplied in blower fan, P_{cofan} is the electrical power supplied in cooling fans and P_{con} is the electrical power supplied in conveyor.

From ref. (Jindarat et al. (2011)), the energy efficiency (η_e) for drying process is defined as:

$$\eta_e = \frac{W_d[h_{fg}(M_{p1} - M_{p2}) + c_m(T_{m2} - T_{m1})]}{\dot{m}_{da}(h_1 - h_o)\Delta t + \Delta t\dot{Q}_{MW}} \tag{3-22}$$

3.4 Results and Discussions

Experimental data are analyzed to obtain the drying kinetics for different drying cases and conditions as listed in Table 3.1 and 3.2.The details of the analysis are as below.

Table 3.1 Drying time and electrical power under various drying conditions (C-Bed)

Testing Condition	Power of Magnetrons (W)	Position of Magnetrons	Air Temperature (°C)	Drying Time (min)	Electrical Power (Kw-hr)	Cost (US$)*
Case 1	800x6	Side (1-10-2-11-3-12)	Ambient Air,30	80	10.5	1.1
Case 2	800x6	Top (7-4-8-5-9-6)	Ambient Air,30	70	8.9	0.91
Case 3	800x6	Side (1-10-2-11-3-12)	Hot Air 70	70	16	1.65
Case 4	800x6	Top (7-4-8-5-9-6)	Hot Air 70	70	13.5	1.39
Case 5	800x6	Side (1-10-2-	Hot Air 50	70	11.9	1.23

		11-3-12)				
Case 6	800x6	Top (7-4-8-5-9-6)	Hot Air 50	70	11.8	1.22
Case 7	800x6	Screw (7-4-2-5-9-12)	Hot Air 50	70	12.2	1.26
Case 8	-	-	Hot Air 70	360	33	3.41

*Remark: Baht foreign exchange reference rates as at 15-27 January 2011 (Unit: Baht per 1 unit of U.S. dollar).

Table 3.2 Drying time and electrical power under various drying conditions (F-Bed)

Testing Condition	Power of Magnetrons (W)	Position of Magnetrons	Air Temperature (°C)	Drying Time (min)	Electrical Power (Kw-hr)	Cost (US$)*
Case 1	800x6	Side (1-10-2-11-3-12)	Ambient Air,30	90	11.4	1.17
Case 2	800x6	Top (7-4-8-5-9-6)	Ambient Air,30	80	9.9	1.02
Case 3	800x6	Side (1-10-2-11-3-12)	Hot Air 70	80	15.7	1.64
Case 4	800x6	Top (7-4-8-5-9-6)	Hot Air 70	80	16	1.65
Case 5	800x6	Side (1-10-2-11-3-12)	Hot Air 50	80	12.6	1.3
Case 6	800x6	Top (7-4-8-5-9-6)	Hot Air 50	80	11.1	1.18
Case 7	800x6	Screw (7-4-2-5-9-12)	Hot Air 50	80	12.7	1.31
Case 8	-	-	Hot Air 70	420	35.5	3.67

*Remark: Baht foreign exchange reference rates as at 15-27 January 2011 (Unit: Baht per 1 unit of U.S. dollar).

3.4.1 Drying kinetics

Figures 3.4-3.7 show the temperature and moisture variations versus elapsed times for C-bed and F-bed with constant initial moisture content of 25% (dry basis). It is found that in the case of microwave – convective air drying (30 and 70°C); the moisture profile of the sample continuously decreases faster than the case of convective drying as show in Figures 5.8 and 5.9. This phenomenon occurred in the case of convective drying (30 and 70°C) combined with microwave energy, thus the bulk of this sample absorbs the largest amount of microwave energy, which corresponds to the level of absorbed energy in samples as described in Eq. (3-2). Furthermore, when the process nearly reaches the end stage of drying, the moisture content inside the sample reduces and the absorption of microwave energy decreases (Ratanadecho (2002)). This period microwave power should be optimized to control in order to reduce power consumption in the drying systems.

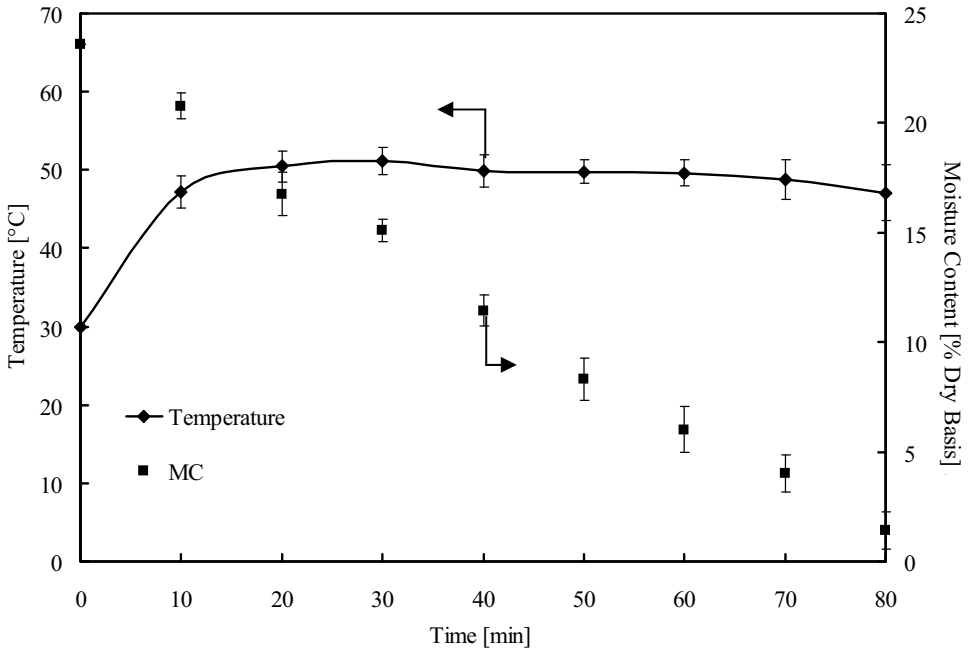

Figure 3.4 Temperature and moisture variations versus elapsed times in case drying using CMCB (T_1= 30 °C)(case 1,C-bed)

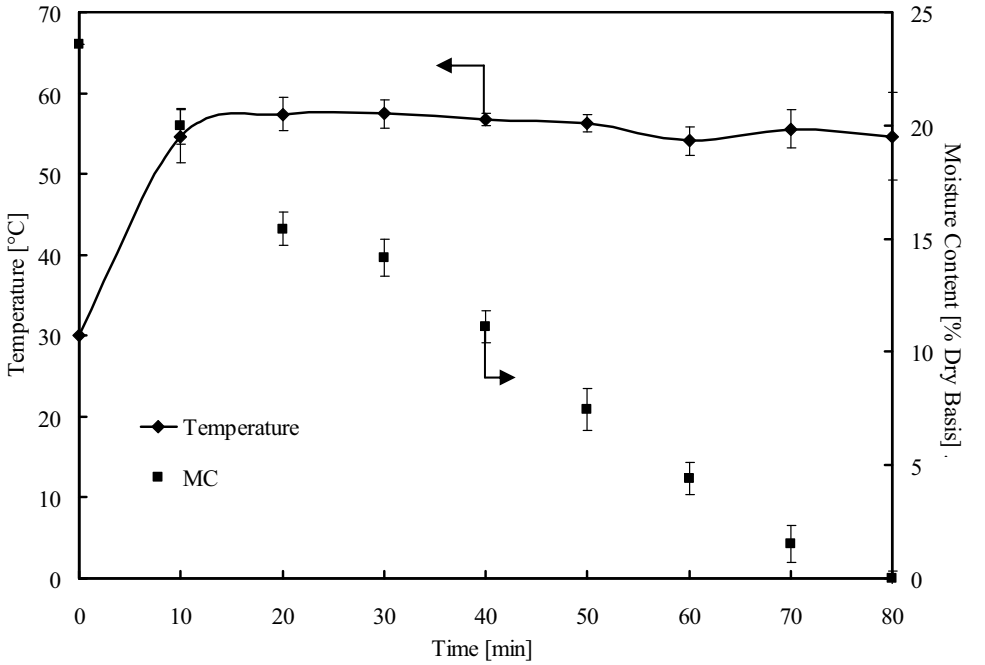

Figure 3.5 Temperature and moisture variations versus elapsed times in case drying using CMCB (T_1= 30 °C)(case 2,C-bed)

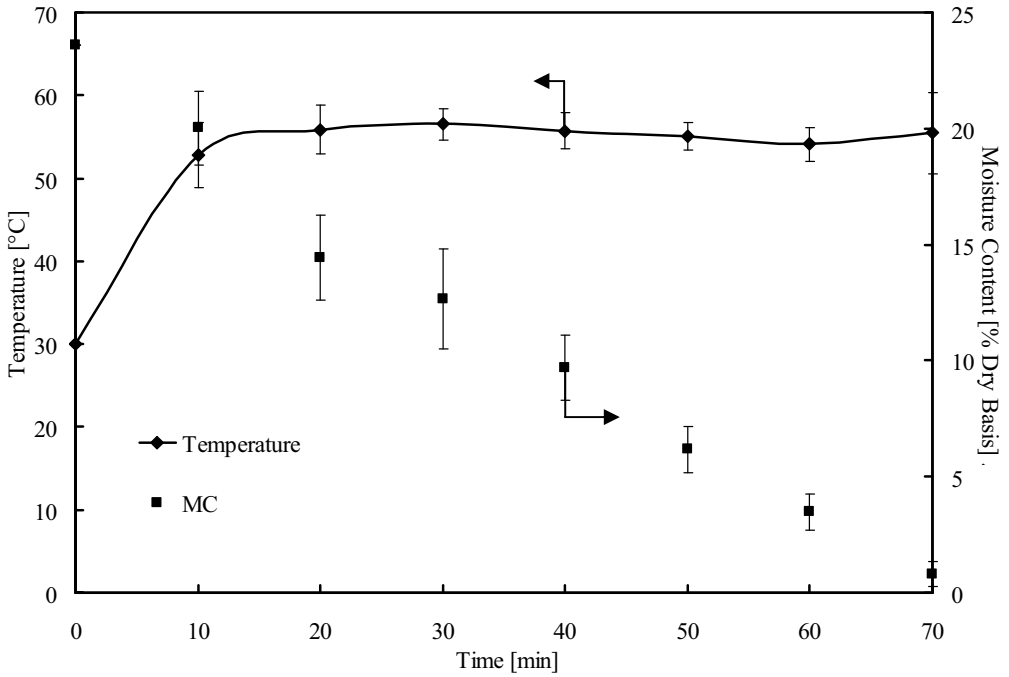

Figure 3.6 Temperature and moisture variations versus elapsed times in case drying using CMCB (T_1= 70 °C)(case 4,C-bed)

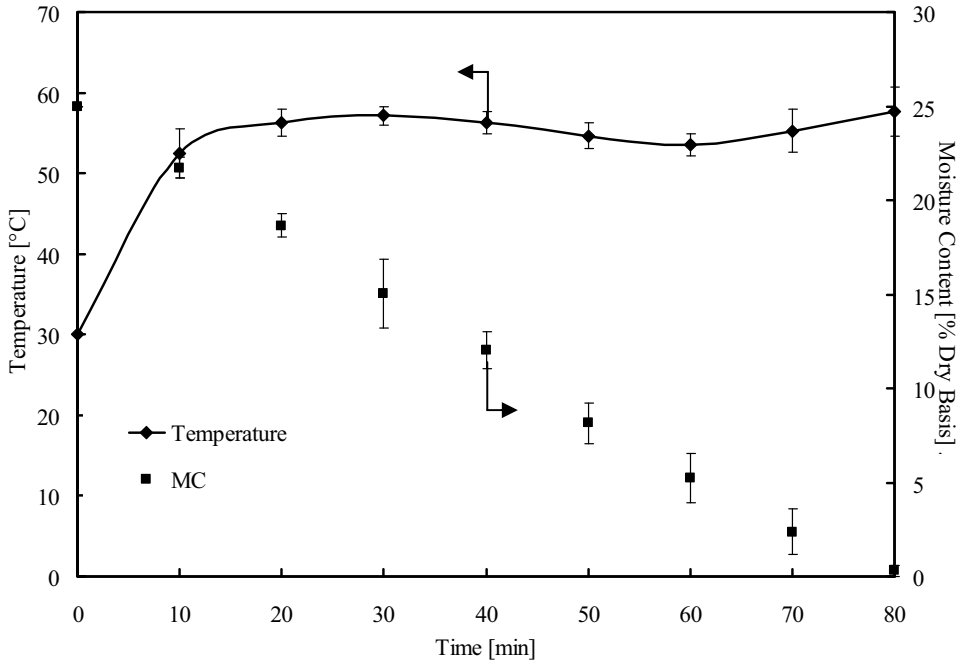

Figure 3.7 Temperature and moisture variations versus elapsed times in case drying using CMCB (T_1= 70 °C)(case 4,F-bed)

Figures 3.4-3.9 show the temperature and moisture variations versus elapsed times with respect to different drying methods. It can be observed from these figures that a combined multi-feed microwave-convective air and continuous belt system drying, the sample is dried quickly without the residual moisture content in the sample due to the uniform heating. It is clear that the drying of microwave-convective air drying times is drastically reduced compared to convective drying, from 420 min to less than 80 min. This investigation combined that microwave drying, i.e., microwave continuous belt drying can yield a considerable gain in drying time by a factor of ten or more. In case of convective drying (Figures 3.8 and 3.9), as the surface is dried while the interior is still wet, the dry layer offers a resistance to the heat transport resulting in a reduction of the evaporation rate as well as drying rate, causing non-uniform heating.

As shown in Figure 3.1(b) microwave oscillated from the magnetron are fed into the cavity. The transmitted wave passes wave guide (the unit number 1-12) to heat up the non-hygroscopic porous packed bed. It is found in Figures 3.5-3.7 that the feed magnetrons positioned on the top of the cavity show the influence of microwave

power absorbed within the sample, and the temperature relation. Within the sample, the electric field attenuates owing to energy absorption, which is converted to the thermal energy, thus the sample temperature increases. However, the feed magnetrons positioned on the side of the cavity shows a lower absorbed microwave power as shown in Figure 3.4. This is because of no direct wave irradiated on the sample; therefore, the influence of the absorbed energy converted to the sample temperature is lower. This phenomenon corresponds to the level of absorbed energy in samples as explained above.

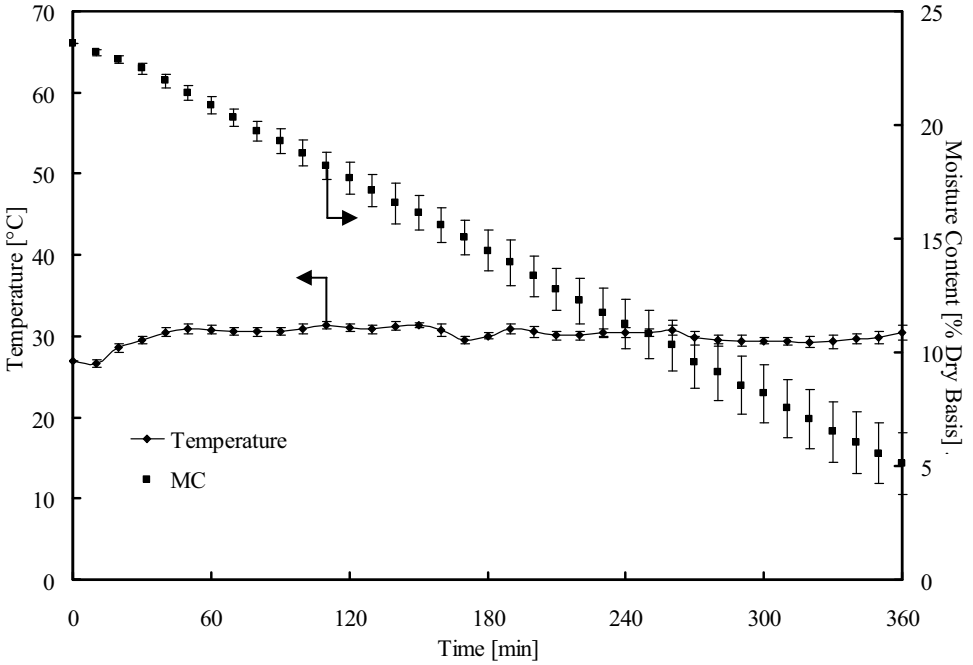

Figure 3.8 Temperature and moisture variations versus elapsed times in case using a convective drying (T_1= 70 °C)(case 8,C-bed)

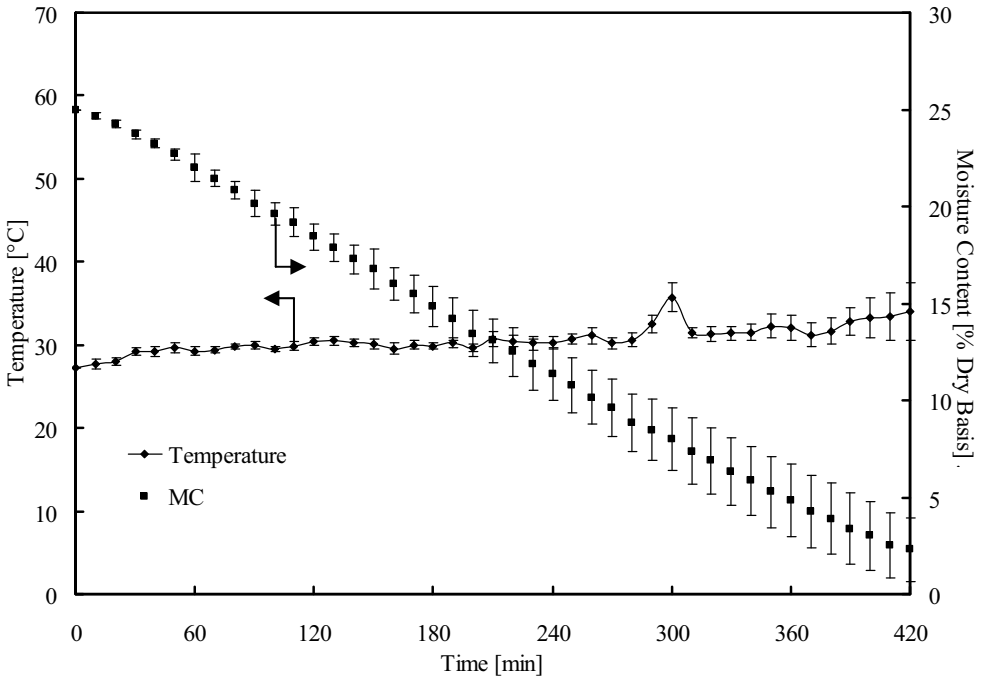

Figure 3.9 Temperature and moisture variations versus elapsed times in case using a convective drying (T_1= 70 °C)(case 8,F-bed)

Figures 3.6 and 3.7 show the temperature variations and moisture content with respect to elapsed times at different testing conditions. It is found that at a microwave - convective air drying (30 and 70°C); the temperature profile of the sample continuously rises while the moisture content profile rapidly decreases. The electric field distribution in cavity is uniform. The temperature and moisture content profiles are also depicted in Figures 3.6 and 3.7. It is observed that the increase of temperature and the decrease of moisture content between packed bed A and B are uniform.

3.4.2 Electrical energy consumption and drying time

The electrical energy consumption during microwave- convective air drying and convective drying of a combined multi-feed microwave-convective air and continuous belt system are given in Figures 3.10 and 3.11. When the two drying methods are compared in term of electrical energy consumption, it is noted that the lowest electrical energy consumption is observed from microwave - convective air drying method and this is followed by convective drying methods. The best result with regard to electrical energy consumption is obtained from microwave power level

of 4.8 kW among all drying methods. Electrical energy consumption at this microwave power level is 8.9 kW-hr (case 2; C-bed) and 9.9 kW-hr (case 2;F-bed). The highest value in all drying methods regarding electrical energy consumption is noted in convective drying process at temperature 70 °C with of 33 kW-hr (case 8;C-bed) and 35.5 kW-hr (case 8;F-bed).

The drying time of the convective drying along the drying process is given in Figures 3.10 and 3.11. The highest value in all drying methods regarding the drying time is noted in the convective drying process operating at the temperature of 70 °C with 360 minutes (case 8;C-bed) and 420 minutes (case 8;F-bed).

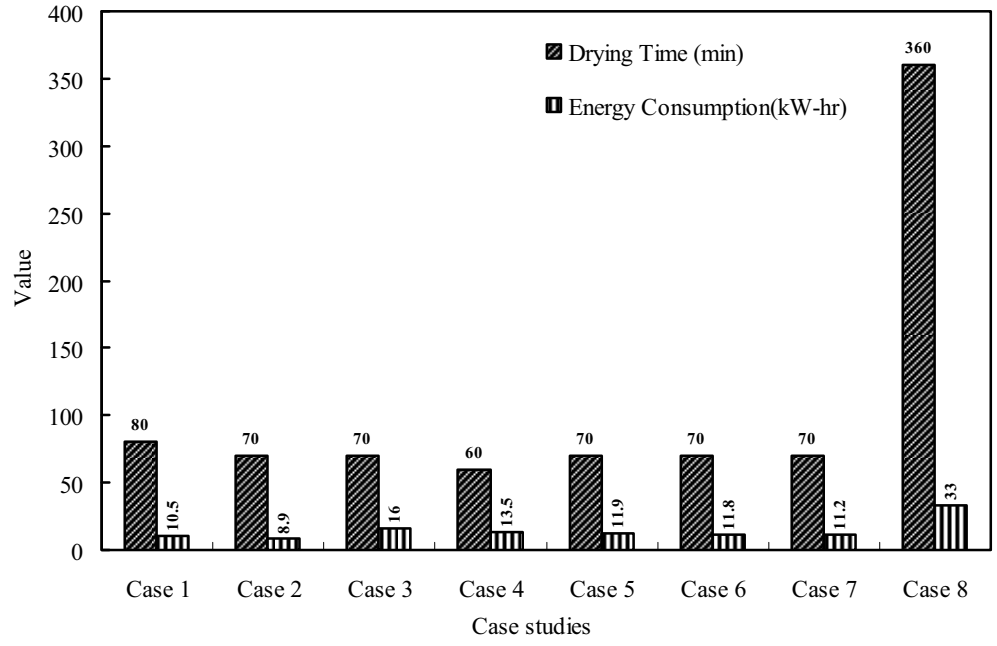

Figure 3.10 Variations in drying time and electrical energy consumption in different case (C-bed)

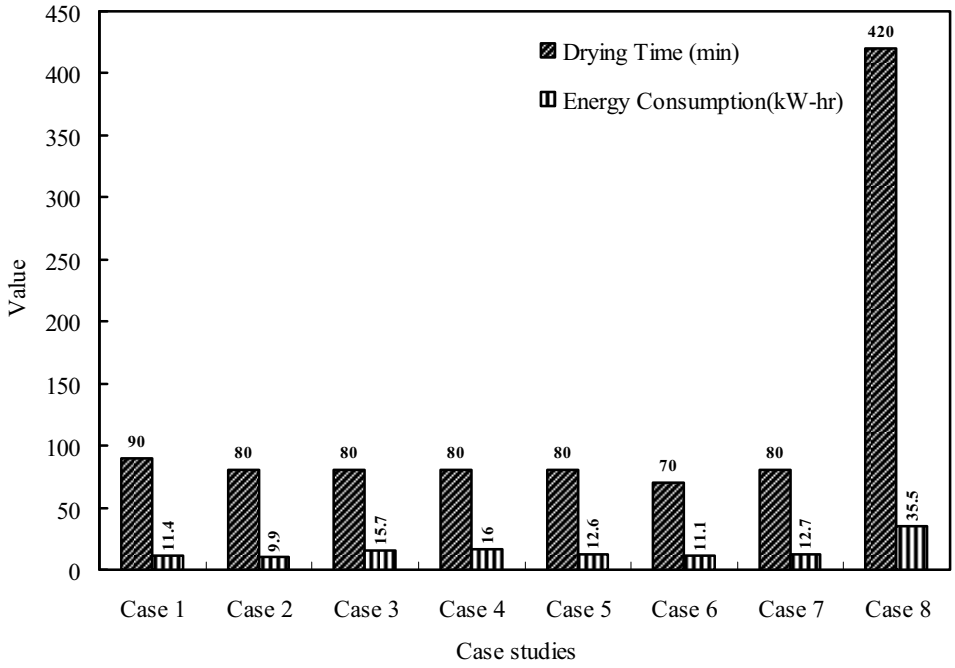

Figure 3.11 Variations in drying time and electrical energy consumption in different case (F-bed)

3.4.3 Analysis of specific energy consumption (SEC)

Figures 3.12 and 3.13 show the specific energy consumption with the variation of the sample particles.

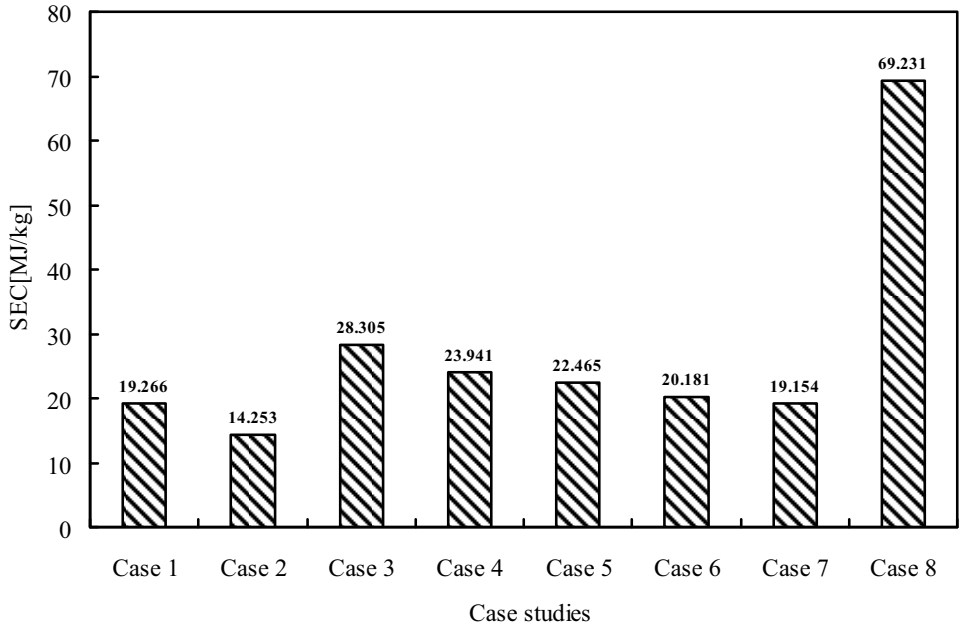

Figure 3.12 Variations in specific energy consumption in different case (C-bed)

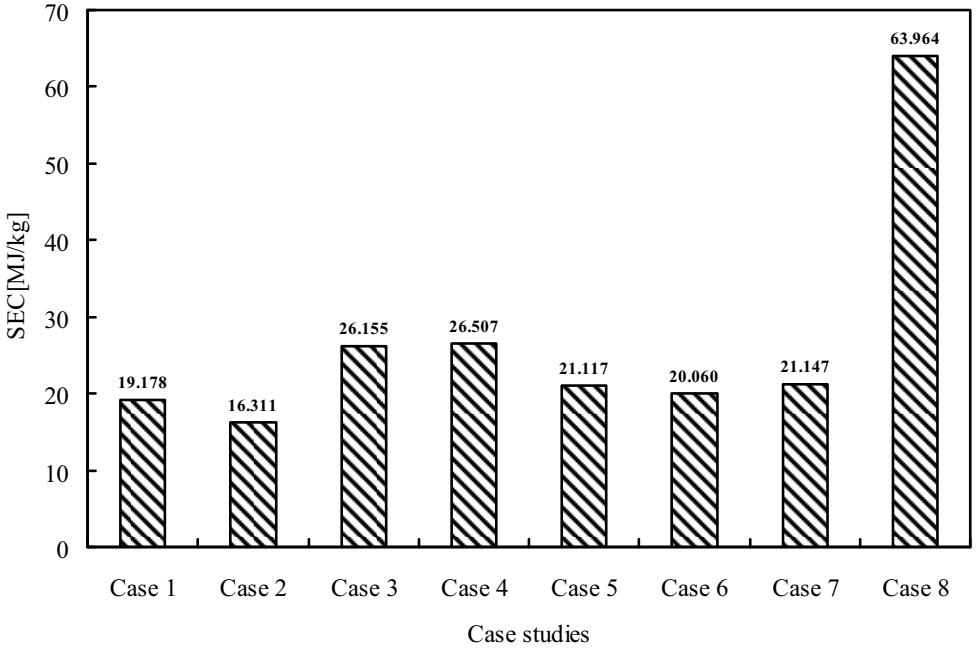

Figure 3.13 Variations in specific energy consumption in different case (F-bed)

To obtain the experimental results, the microwave power level is set at 4.8 kW, and the thickness of the layers with C particles and F particles are fixed. Figures 3.12 and 3.13 show the specific energy consumption with the variation of the sample thickness. It can be seen in the first period of drying (around 0-120 min), the packed

bed can absorb a lot of microwave power due to the high moisture content and thus the specific energy consumption is low in this period.

Microwave-convective air drying can be used to efficiently dry the sample. Non-hygroscopic porous packed bed dried using microwave energy required 5 times less specific energy consumption than the bed dried by a convective drying method at 70 °C. The similar result are also observed in Figures 3.12 and 3.13, the non-hygroscopic porous packed bed dried by microwave-convective air drying can be rapidly dried due to the uniform heating of the drying system as described in the previous section. The drying times of the microwave-convective air drying is less than 80 min which is drastically reduced from the convective drying time of 420 min (Figure 5.13). The results show that microwave drying can yield a considerable gain in drying time, by a factor of two or more. In the case of convective drying, the surface is dried while the interior is still wet, the dry layer offers resistance to the heat transport, resulting in a reduction of the evaporation rate as well as drying rate and also causing high specific energy consumption.

The drying time of the drying trials is carried out by two different drying methods. No marked difference is found between with and without hot air supplied in the cavity. Specific energy consumption depends on the power absorbed by the cavity and the drying time. In this study, the specific energy consumptions at microwave power levels of 4.8 kW are investigated. These short drying times may be due to a result of microwave power levels. However, for convective drying, the drying times are long because the convective heat transfer coefficient of the non-hygroscopic porous packed bed is low. The reduction of specific energy consumption observed during drying and the reduction of drying time are caused by the decrease in convective air levels. The specific energy consumption of microwave-convective air drying at ambient temperature are 14.253 MJ/kg (case 2; C-bed) and 16.311 MJ/kg (case 2; F-bed), whereas the specific energy consumption of convective drying at 70°C are 69.231MJ/kg (case 2; C-bed) and 63.964 MJ/kg (case 2; F-bed). The specific energy consumptions of the combination drying (microwave-convective air drying) give similar trends at all drying processes. The reduction of specific energy consumption is achieved by decreasing the hot air temperature level supplied to

cavity. Figures 3.12 and 3.13 respectively show the comparison of specific energy consumption of different drying cases for C-bed and F-bed. The results show that the lowest specific energy consumption is found from microwave-convective air drying method (ambient air) and followed by convective drying methods (Figures. 3.12 and 3.13).

5.4.4 Energy efficiency

Figures 3.14 and 3.15 show the energy efficiency with respect to the drying time in different cases. It is found that the energy efficiency during drying of C-bed and F-bed at the starting period (0-15 min) is height due to the high quantity of moisture content in the non-hygroscopic porous packed bed which leads to high value of dielectric loss factor, thus the wave absorption is more converted by non-hygroscopic porous packed bed. The results are high energy efficiency after the vapor is moving from the surface of the non-hygroscopic porous packed bed. These causes the moisture content to decrease quickly and the low quantity of absorbed waves because of the decrease energy consumption and decrease the efficiency of absorbed microwave power, therefore the energy efficiency depends on the level of absorbed microwave power.

In Figure 3.14, the energy efficiency profile for the sample in case of C- bed rises up quickly in the early stages of drying (between 10–15 min). However, the efficiency rises slowly after this stage (between 45–70 min). It is evident from the figure that the moisture content inside the sample reducing at the final stages of drying causes the decreases in the absorbed microwave power. Consequently, the energy efficiency profiles decreases in this stage of drying.

Figures 3.14 and 3.15 show the energy efficiency values during microwave - convective air drying of a combined multi-feed microwave-convective air and continuous belt system in case 1 and case 2 (C-bed and F-bed). It can be observed that when the drying methods are compared in term of energy efficiency, it is noted that the highest energy efficiency is presented in case1 and case2 (Table 3.1 and Table 3.2: C-bed and F-bed).No marked difference is found between the supplied hot air in to cavity, since the drying time values obtained in the drying are also not difference. The

result shows that the microwave – convective air drying is not significant to decrease the drying time and to waste more energy consumption.

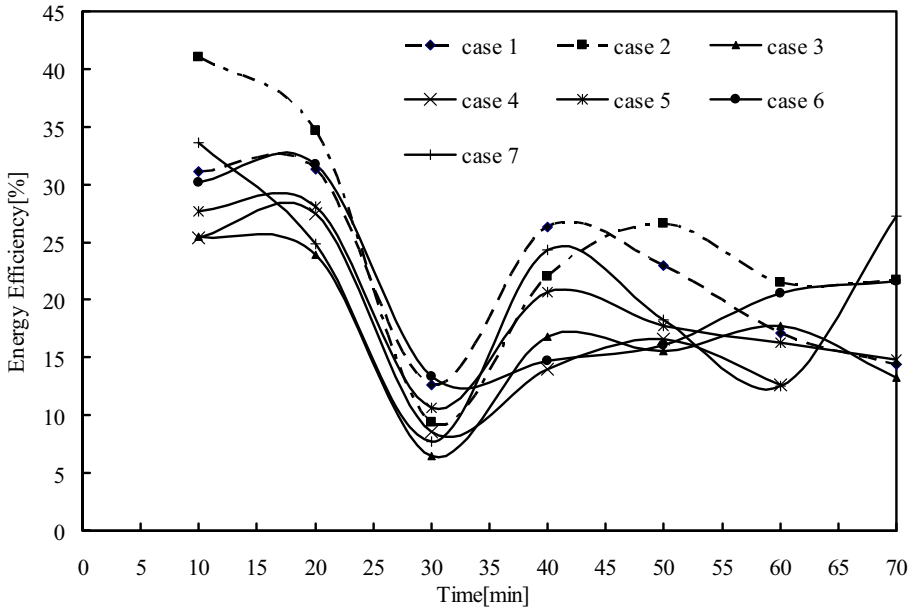

Figure 3.14 Energy efficiency profiles with respect to elapsed time in different case (C-bed)

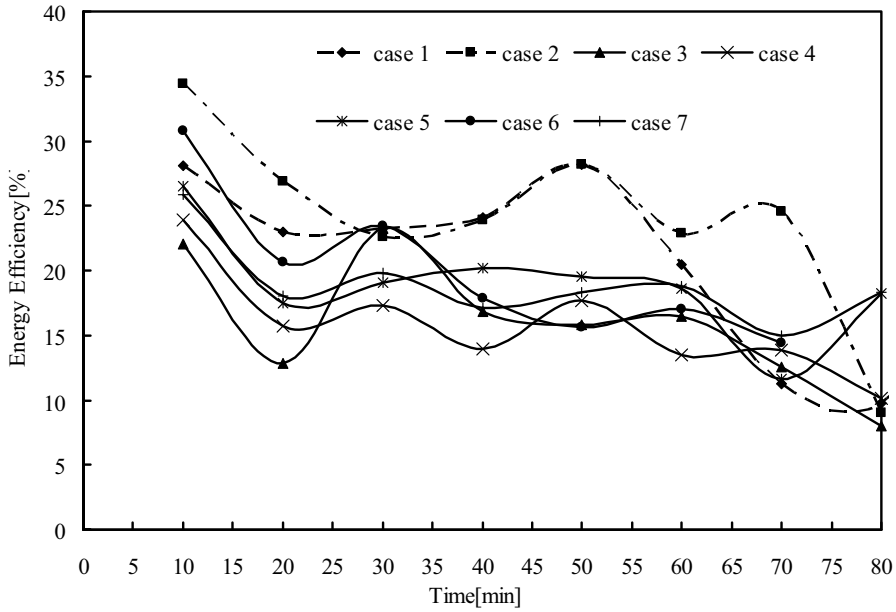

Figure 3.15 Energy efficiency profiles with respect to elapsed time in different case (F-bed)

Figure 3.16 shows the energy efficiency with respect to the drying time. The low energy efficiency of convective drying is presented (case 8; C-bed and F-bed). Energy efficiency depends on the temperature in the cavity and the drying time.

However, the drying times of convective drying so long, due to the convective heat transfer of the non-hygroscopic porous packed bed, is low.

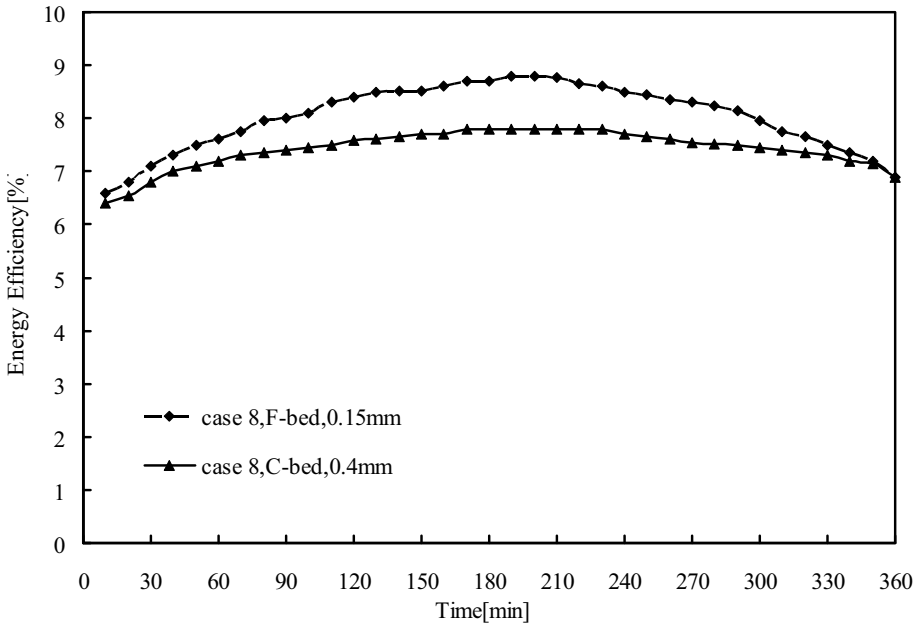

Figure 3.16 Energy efficiency profiles with respect to elapsed time in case 8 (C-bed and F-bed)

3.5 Conclusions

A combined multi-feed microwave-convective air and continuous belt system permits quicker drying at lower temperature, resulting in a 30% reduction in energy consumption for what is normally an energy-intensive process. Non-hygroscopic porous packed bed dried using microwave energy required 5 times less specific energy consumption than the packed bed which dried by a convective drying method at 70°C in a convective cavity due to the microwave influence, uniform heating pattern, and moving belt inside the cavity.

In overall, when handling a combined multi-feed microwave-convective air and continuous belt system correctly, we can conclude that it will realize the following advantages over other drying systems. Moreover, this work depicts the technique that combined the conventional heating with the microwave heating and the continuous belt system together. It shows the potential and the efficient to reduce the electrical energy consumption. If this technology is implemented to the industry, it will decrease the production costs due to the lower electrical energy consumption.

(1) Better heat distribution,
(2) Faster product heating because the multiple magnetrons are placed around the rectangular cavity; this advantage corresponds to the better microwave power distribution, with can penetrate further into the multi-plane of material,
(3) Immediately ready for operation and control of heat capacity without delay,
(4) Continuously supply the material into the system,
(5) The cavity is design to prevent magnetron damage,
(6) No heat storage losses,
(7) Low specific energy consumption and high energy efficiency.

The next steps of the research related to this problem will be done to develop the control system and optimal drying schedules for a combined multi-feed microwave-convective air and continuous belt system of hygroscopic porous material especially biomaterial.

CHAPTER 4

ANALYSIS OF ENERGY CONSUMPTION IN DRYING PROCESS OF PARAWOOD PAKE (HEVEA BRASILIENSIS) USING A COMBINED UNSYMMETRICAL MULTI-FEED MICROWAVE AND HOT AIR-CONTINUOUS BELT SYSTEM (CMCB)

4.1 Introduction

The parawood tree (Hevea brasiliensis) is one of the most important commercial timbers in Thailand because of its application in the furniture industries. Conventional kiln drying is time-consuming and takes 6 to 26 days (Yamsaengsung and Tabtiang (2011)), depending on the thickness of the wood. Hence, manufacturers have become interested in ways to reduce the drying time, decrease wood discoloration due to waiting, and increase productivity. Still, if wood is dried too slow, it will damage the wood and the color change, crack, or check due to residual stresses. One alternative that has received much attention is the use of microwave because of its higher drying rates, better quality products due to the absence of oxidative reactions, and energy savings due to shorter drying time. low temperature drying also has been shown to contribute to improvements in dimensional stability and lowering of the equilibrium moisture content in woods

The drying of wood is the most energy-intensive and costly process in the forest products industry. Conventional wood dryers function under the basis of convective heat transfer from circulating hot air to the surface of wood followed by subsequent conductive heat transfer from the surface to the canter of wood. These dryers require considerable amount of energy and long drying times in order to obtain high quality woods. Therefore, innovative wood drying methods have been searched and studied. Unlike the conventional heating, where heat is applied externally to the surface of the material, microwave irradiation penetrates and simultaneously heats the bulk of the material. When properly designed, microwave drying systems have several advantages over conventional mechanical methods including, reduction of the drying time, high energy efficiency, and improvements in product quality for various industrial applications (Perre and Turner (1994)). Microwave drying of wood

products, however, has not been used to a larger extent in wood industries mainly due to the insufficient knowledge of the complex interaction between wood and process parameters during drying as well as the higher investment expenses. Recently the development of inexpensive and reliable microwave sources has been increasing attracted to applications in wood industry.

Investigations on microwave drying of wood have been performed since the late fifties. Many authors (Antti (1992), Masakasu Miura et al.(2003), Oloyede and Groombridge (2000), Lehne et al.(1999), Turner and Lee (1994) and Vonpradubchai and Rattanadecho (2005)) emphasize in the advantages of microwave drying over convective drying. Turner (1994), points out the suitability of combined microwave and convective drying. However, there still remain obstacles to be overcome in applying microwave drying technology to wood industry. One of the difficulties is that the microwave power absorbed by moist wood depends mainly on the moisture content and it is required to move the wood for uniform power distribution with on-off type microwave system at fixed power output.

For an analysis of microwave energy consumption in heating and drying processes, referred to Sharma and Prasad (2005), this study examined specific energy consumption in microwave drying of garlic cloves. The comparative study of specific energy consumption with two difference drying methods, namely microwave-hot air and hot air drying, was carried out. Other related papers present microwave energy and hot air heating processes. Varith et al.(2007), studied the combined microwave and hot air drying of peeled longan. The influence of moisture content on specific energy consumption (SEC) was examined. The other important paper, written by Lakshmi et al.(2005), presented a comparison of SEC in cooking rice among the microwave oven, electric rice cooker and pressure cooker.

Investigations of energy efficiency of microwave drying of porous material have been performed since the late fifties. Many authors (Alibas (2007), Poli et al. (2006), Cheng et al. (2008), Holtz et al. (2009), Soysol et al. (2006), Leiker and Adamska (2006) and Prommas et al. (2010)) emphasis on the advantages of microwave drying over convective drying. Varith et al. (2007), points out the suitability of combined microwave and hot drying of peeled longan. However, there still remain obstacles to be overcome in applying microwave drying technology to

drying industry. One of the difficulties is that the microwave power absorbed by moist porous material depends mainly on the moisture content and it is required to move the porous material for uniform power distribution with on-off type microwave system at fixed power output.

4.2 Experimental procedure

Microwave - convective air drying was carried out using a Combined unsymmetrical multi-feed microwave and hot air-continuous belt system (CMCB) (Figure 4.1 (a)). The shape of microwave cavity is rectangular with a cross sectional area of 90cm × 45cm × 270cm. The drier was operated at a frequency of 2.45 GHz with maximum working temperature of 180°C. The microwave power was generated by means of 12 compressed air-cooled magnetrons. The maximum microwave capacity was 9.6 kW with a frequency of 2.45 GHz. The power setting could be adjusted individually in 800W steps. In the continuous processing equipment, two open ends are essential, in which the material to be heated up on the belt conveyer where it was put in and taken out. In this equipment, leakage of microwaves was prevented by the countermeasure in double with a combination of mechanical blocking filter (corrugate choke) and microwave absorber zone filter was provided at each of the open ends. The microwave leakage was controlled under the DHHS (US Department of Health and Human Services) standard of 5 mW/cm^2. The multiple magnetrons (12 units) were installed in an asymmetrical position on the rectangular cavity (Figure 4.1 (b)). The microwave power was then directly supplied into the drier by using waveguides. An infrared thermometer (located at the opening ends) was used to measure the temperature of the specimens (accurate to ± 0.5 °C).

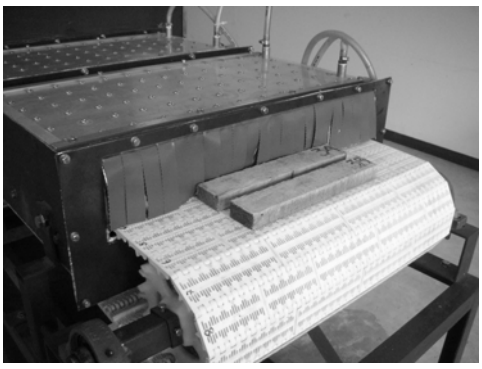

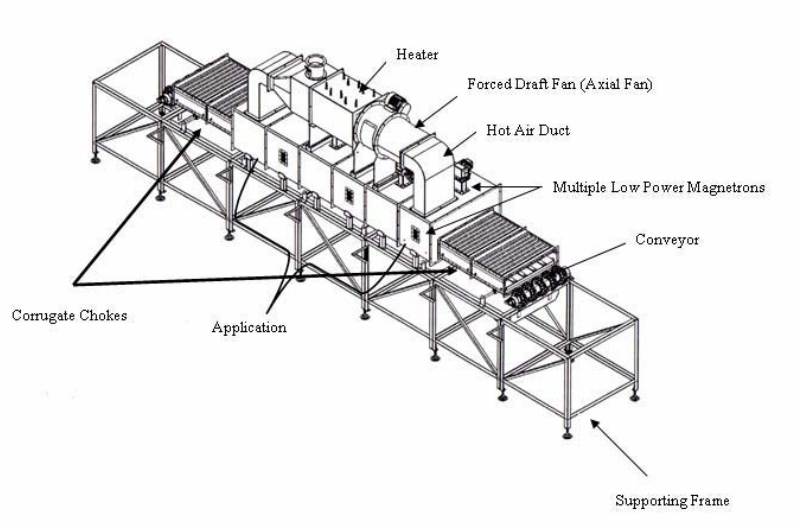

(a)

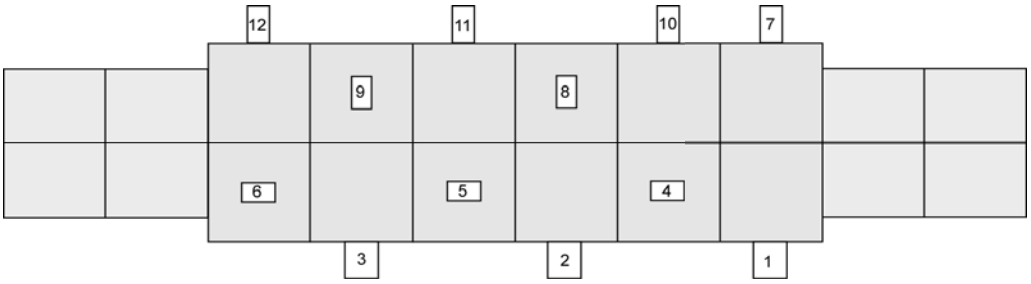

(b)

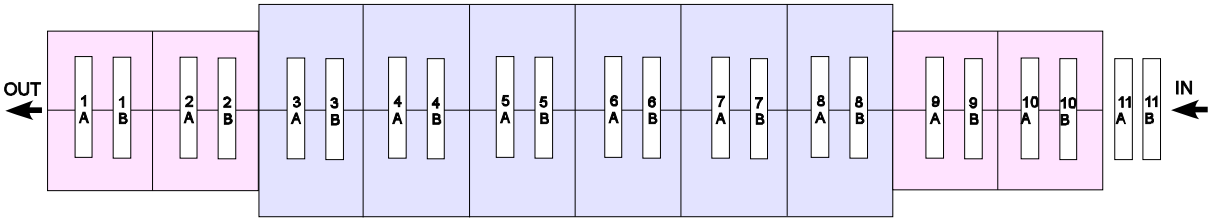

(c)

Figure 4.1 Schematic diagram of experimental set up

(a) A combined multi-feed microwave-convective air and continuous belt system

(b) Feeds magnetrons positioned of 12 units

(c) Feeds samples positioned of 22 packed beds

The magnetrons and transformers used in this system were cooled down by fan. In the continuous heating/drying equipment, two open ends were essential to feed in and feed out the product, through which the material to be heated up on the belt conveyer arranged in certain position, as shown, as in Figure 4.1(c). The belt conveyor system consisted of a drive motor, a tension roller and a belt conveyor. During the drying process, the conveyor speed was adjusted to 0.54 m/min (at the frequency 40 Hz) and the motor speed was controlled by the VSD control unit. Hot air was generated using the 24 unit of electric heaters with the maximum capacity of 10.8 kW and the maximum working temperature of 240°C. The hot air was provided by blower fan with 0.4 kW power through the air duct into the cavity. The hot air temperature was measured by using thermocouple.

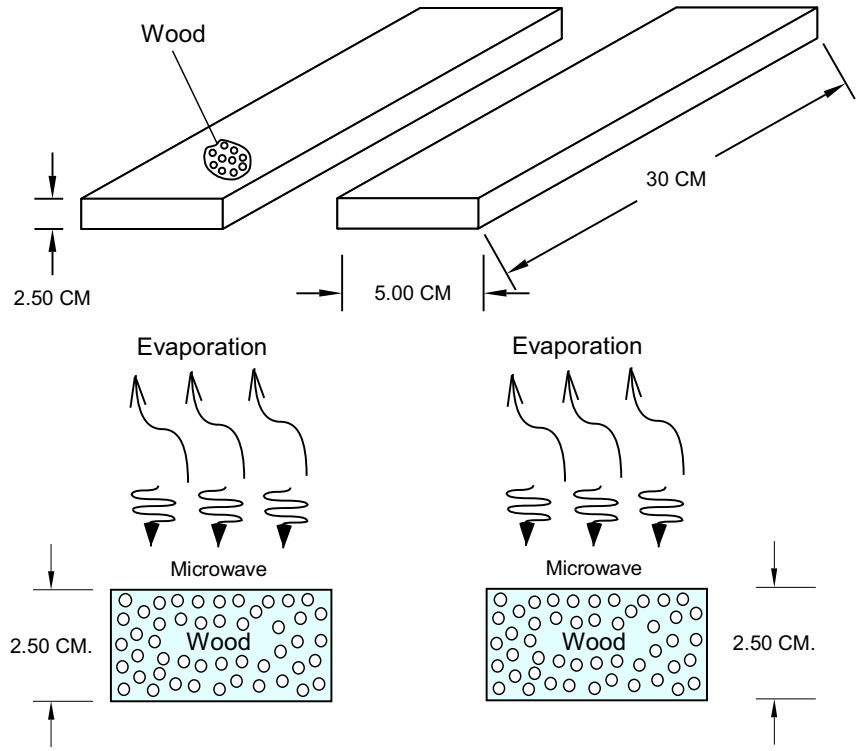

Figure 4.2 Schematic of drying sample (Parawood pake)

As shown in Figure 7.2, the specimen selected for drying test was a parawood with dimensions of 5cm X 2.5cm x 30cm which had the initial moisture content of 70%(dry basis) and the initial temperature of 30°C.

4.3 Related theories

4.3.1 Microwave heat generation

Microwave heating involves heat dissipation and microwaves propagation which causes the dipoles to vibrate and rotate. When the microwave energy emits from a microwave oscillator (P_{in}) is irradiated inside the microwave applicator, the dielectric material which has a dielectric loss factor absorbs the energy and are heated up. Then the internal heat generation takes place. The basic equation calculates the density of microwave power absorbed by dielectric material (P_1) is given by (Jindarat et al. (2011)):

$$P_1 = \omega \varepsilon_0 \varepsilon_r'' E^2 = 2\pi \cdot f \cdot \varepsilon_0 \cdot \varepsilon_r' (tan\delta) E^2 \tag{4.1}$$

where E is electromagnetic field intensity, f is microwave frequency, ω is angular velocity of microwave, ε_r' is relative dielectric constant, ε_0 is dielectric constant of air and $tan\delta$ is loss tangent coefficient.

From equation (4.1), P_1 is directly proportional to the frequency of the applied electric field, loss tangent coefficient and root-mean-square value of the electric field. It means that an increasing of $tan\delta$ of specimen, energy absorption and heat generation are also increased. While $tan\delta$ is smaller, microwave will penetrate into specimen without heat generation. However, the temperature increase depends on other factors, such as specific heat, size and characteristic of specimen.

When the material is heated unilaterally, it is found that as the dielectric constant and loss tangent coefficient vary, the penetration depth will be changed and the electric field within the dielectric material is altered. The penetration depth is used to denote the depth at which the power density has decreased to 37 % of its initial value at the surface (Jindarat et al. (2011)) :

$$D_p = \frac{1}{\frac{2\pi f}{\upsilon}\sqrt{\frac{\varepsilon_r'\left(\sqrt{1+\left(\frac{\varepsilon_r''}{\varepsilon_r'}\right)^2}-1\right)}{2}}} = \frac{1}{\frac{2\pi f}{\upsilon}\sqrt{\frac{\varepsilon_r'\left(\sqrt{1+(tan\delta)^2}-1\right)}{2}}} \tag{4.2}$$

where D_P is penetration depth, ε_r'' is relative dielectric loss factor and υ is microwave speed. The penetration depth of the microwave power is calculated according to Eq. (4.2), which shows how it depends on the dielectric properties of the material. It is noted that products with huge dimensions and high loss factors, may occasionally be overheated to a considerably thick layer on the outer layer. To prevent such phenomenon, the power density must be chosen so that enough time is provided for the essential heat exchange between boundary and core. If the thickness of the material is less than the penetration depth, only a fraction of the supplied energy will become absorbed. Furthermore, the dielectric properties of porous material specimens typically show moderate lossiness depending on the actual composition of the material. With large amount of moisture content, it reveals a greater potential for absorbing microwaves. For typical porous packed bed specimens, a decrease in the moisture content typically decreases ε_r'', accompanied by a slight increment in D_p.

In the analysis, energy P_2 is required to heat up the dielectric material which is placed in a microwave applicator. The temperature of material initially (T_1) is raised to T_2. The energy (P_2) can be estimated by the following calorific equation (Jindarat et al. (2011)):

$$P_2 = \frac{4.18 \cdot W \cdot C_p \cdot \Delta T}{t} \tag{4.3}$$

where W is weight of the dielectric material, C_p is specific heat of the dielectric material, ΔT is the increment of temperature $(T_2 - T_1)$ and t is heating time.

Assuming an ideal condition, all of the oscillated microwave energy (P_{in}) is absorbed into the dielectric material; so internal heat generation as Eq. (4.2) takes place. In this case, the relation between P_{in} and P_2 is shown below (Jindarat et al. (2011)):

$$P_{in} = P_2 \tag{4.4}$$

In a practical point of view, the transformation energy in applicator exists due to Eq. (4.1) the rate of microwave energy absorbed by means of the dielectric loss factor of the sample and Eq.(4.2) the energy loss in the microwave devices. Accordingly, by taking into account this transformation efficiency, the microwave oscillation output can be calculated by the following equations (Jindarat et al. (2011)):

$$P_{in} = \frac{P_2}{\eta_m} \tag{4-5}$$

$$\eta_m = \frac{P_2}{P_{in}} \tag{4-6}$$

where

$$P_2 = \frac{Q \cdot S_p \cdot C_P \cdot \Delta T \cdot 4.18}{60 \cdot \eta_m \cdot 10^3} \tag{4-7}$$

where η_m is efficiency of microwave devices, Q is weight per meter of dielectric material (parawood), S_p is a rate at which the dielectric material is put on the belt conveyer, C_P is specific heat of dielectric material and ΔT is heat-up range of $T_1 - T_0$.

4.3.2 Mass and energy balance equation for the drying process

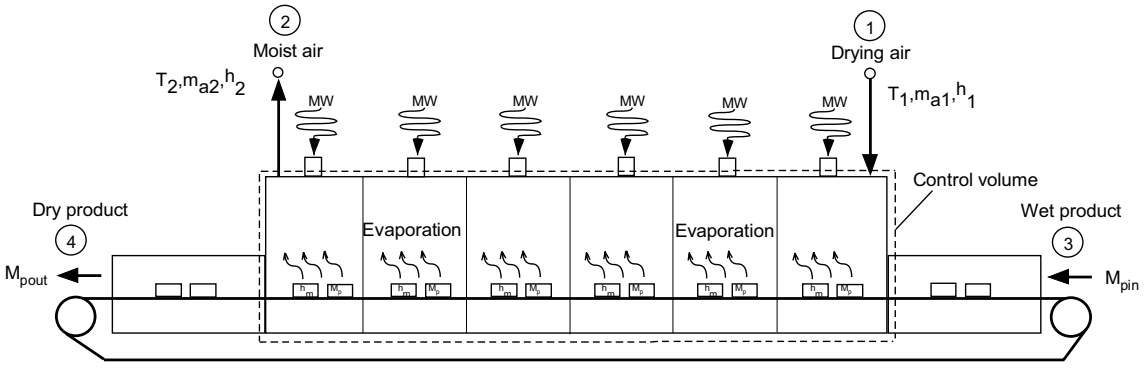

Figure 4.3 Schematic of control volume representing drying process using Combined unsymmetrical multi-feed microwave and hot air-continuous belt system (CMCB)

The conservation of mass for the control volume of cavity is shown in Figure 4.3. The mass balance equation can be written as (Jindarat et al. (2011)):

$$\frac{dm_{cv}}{dt} = \dot{m}_{g1} - \dot{m}_{g2} \tag{4.8}$$

Here, Eq. (4.8) is the mass rate balance for the control volume where $\dot{m}_{g1}$ and $\dot{m}_{g2}$ denote the mass flow rate at inlet (1) and at exit (2), respectively. Similarly, a balance of water in air flowing through the drying cavity leads to (Jindarat et al. (2011)):

$$W_d \frac{dM_p}{dt} = \dot{m}_a (X_1 - X_2) \tag{4.9}$$

where W_d is weight of dry material and M_p is particle moisture content in dry basis. this can be expressed as(Jindarat et al. (2011)):

$$M_p = \frac{W_b - W_d}{W_d} \tag{4.10}$$

where W_b is weight of material before drying, $\dot{m}_a$ is the mass flow rate of dry air, X_1 and X_2 denote absolute humidity of inlet and exit air, respectively. The left-hand side of the mass balance equation, Eq. (4.9), is the mass flow rate of water in the air flowing from cavity. It can be written as (Jindarat et al. (2011)):

$$\dot{m}_w = \dot{m}_a (X_2 - X_1) \tag{4.11}$$

In the drying process, we apply the first law of thermodynamics (the conservation of energy) for the control volume as shown in Figure 4.3. The significant heat transfer is due to the heat of evaporation between the solid and the drying air, and there is also heat rejection to the surrounding. The energy rate balance is simplified by ignoring kinetic and potential energies. Since the mass flow rate of the dry air and the

mass of dry material within the control volume remain constant with time, the energy rate balance can be expressed as:

$$\frac{W_d(h_{m2}-h_{m1})}{\Delta t}=\dot{Q}_{evap}+\dot{m}_a(h_1-h_2)+\dot{Q}_{MW}-\dot{Q}_{loss} \tag{4.12}$$

where $\dot{Q}_{evap}$ is heat transfer rate due to water evaporation, $\dot{Q}_{MW}=P_{in}$ is microwave energy, h_m is enthalpy of material, t is time, $\dot{m}_a$ is mass flow rate of dry air, h is enthalpy of dry air, and $\dot{Q}_{loss}$ is heat transfer rate to the environment.

Assuming air as an ideal gas, thus the differences in specific enthalpy are as follows (Jindarat et al. (2011)):

$$h_{m1}-h_o=c_m(T_{m1}-T_o) \tag{4-13}$$

$$h_{m2}-h_o=c_m(T_{m2}-T_o) \tag{4-14}$$

The enthalpy term of material in Eq.(4-13) can be written as(Jindarat et al. (2011)):

$$h_{m2}-h_{m1}=c_m(T_{m2}-T_{m1}) \tag{4-15}$$

where c_m represents the specific heat of the material. The enthalpy of moist air can be calculated by adding the contribution of each component as it exits in the mixture; thus the enthalpy of moist air is (Jindarat et al. (2011)):

$$h=h_a+Xh_v \tag{4.16}$$

The heat transfer rate due to phase change is (Jindarat et al. (2011)):

$$\dot{Q}_{evap}=\dot{m}_w h_{fg} \tag{4.17}$$

where h_{fg} is latent heat of vaporization.

7.3.3 Specific energy consumption and energy efficiency in drying process

The drying of parawood is a process of simultaneous heat and mass transfer. The specific energy consumption during drying process using Combined unsymmetrical multi-feed microwave and hot air-continuous belt system and convective drying processes was estimated. The drying conditions are total electrical power supplied in drying process; convective air temperature of 30, 50 and 70°C, convective air velocity of 0.5 m/s, total microwave power of 4.8 kW. The specific energy consumption (SEC) equation is represented by:

$$SEC = \frac{\text{Total electrical power supplied in drying process}}{\text{Amount of water removed during drying}}, \left[\frac{kW-hr}{kg}\right] \tag{4.18}$$

$$SEC = \frac{P_{total}}{\text{Amount of water removed during drying}}, \left[\frac{kJ}{kg}\right] \tag{4.19}$$

where P_{total} is a total electrical power supplied in drying process; this term can be calculated from:

$$P_{total} = P_{mg} + P_{heater} + P_{exfan} + P_{blfan} + P_{cofan} + P_{con}, \left[kW \times 3600s\right] \tag{4.20}$$

Where P_{mg} is the electrical power supplied in magnetron, P_{heater} is the electrical power supplied in heater, P_{exfan} is the electrical power supplied in exhaust fan, P_{blfan} is the electrical power supplied in blower fan, P_{cofan} is the electrical power supplied in cooling fans and P_{con} is the electrical power supplied in conveyor.

From ref. (Jindarat et al. (2011)), the energy efficiency (η_e) for drying process is defined as:

$$\eta_e = \frac{W_d[h_{fg}(M_{p1} - M_{p2}) + c_m(T_{m2} - T_{m1})]}{\dot{m}_{da}(h_1 - h_o)\Delta t + \Delta t \dot{Q}_{MW}} \tag{4.21}$$

4.4 Result and discussions

Experimental data are analyzed to obtain the drying kinetics for different drying cases and conditions as listed in Table 4.1. The details of the analysis are as below.

Table 4.1 Drying time and electrical power under various drying conditions

Testing Condition	Power of Magnetrons (W)	Position of Magnetrons	Air Temperature (°C)	Hybrid Drying (min ⎮ min)	Drying Time (min)	ElectricalPower (Kw-hr)
Case 1	800x6	Top (7-4-8-5-9-6)	Hot Air 70	MW+HA:80	80	15.3
Case 2	800x6	Screw (7-4-2-5-9-12)	Hot Air 70	MW+HA:90	90	16.5
Case 3	800x6	Top (7-4-8-5-9-6)	Ambient Air 30	MW+AA:80	80	10.4
Case 4	800x6	Screw (7-4-2-5-9-12)	Ambient Air 30	MW+AA:90	90	11.4
Case 5	800x6	Top (7-4-8-5-9-6)	Hot Air 70	HA:30 ⎮ MW+HA:90	120	18.5
Case 6	800x6	Top (7-4-8-5-9-6)	Amb. Air 30**:** Hot Air 70	AA:30 ⎮ MW+HA:100	130	8.6
Case 7	800x6	Top (7-4-8-5-9-6)	Amb.Air 30**:** Amb. Air 30	AA:30 ⎮ MW+AA:90	120	12.1
Case 8	800x6	Top (7-4-8-5-9-6)	Hot Air 70: Hot Air 70	MW+HA:30 ⎮ HA:150	180	18.7
Case 9	800x6	Top (7-4-8-5-9-6)	Hot Air 70: Hot	HA:20 ⎮ MW+HA:80	100	10.9

			Air 70			
Case 8	-	-	Hot Air 70	HA:480	480	42.8

Remark : (MW+HA:30 | HA:150) MW+HA:30 is supplied microwave-hot air 30 minutes at first period | HA:150 is supplied hot air 150 minutes at last period; Amb.: Ambient

Figure 4.4 show the temperature and moisture variations versus elapsed times for parwood pake with constant initial moisture content of 70% (dry basis). It is found that in the case of microwave – convective air drying (top feed microwave 4.8 kW microwave power level and 70°C hot air); the moisture profile of the sample continuously, thus the bulk of this sample absorbs the largest amount of microwave energy, which corresponds to the level of absorbed energy in samples as described in Eq. (4.2).The discussion on averaged temperatures of bulk load (cavity temperature) with respect to elapsed times with various testing conditions. In Figure 4.4, the averaged temperature of bulk load (parawood pake) is influenced by applied position feed microwave power level and microwave operating modes. Position feed Magnetron on top as well as microwave operating mode are strongly effects on the internal heat generation and drying rate of dried samples. Furthermore, the higher microwave power level as well as continuous microwave operating mode can increase the temperature and drying rate by providing more energy for vaporizing water thus accelerating moisture removal at greater temperature while the convective hot air on parawood pake serface allows water to evaporate at lower temperature.

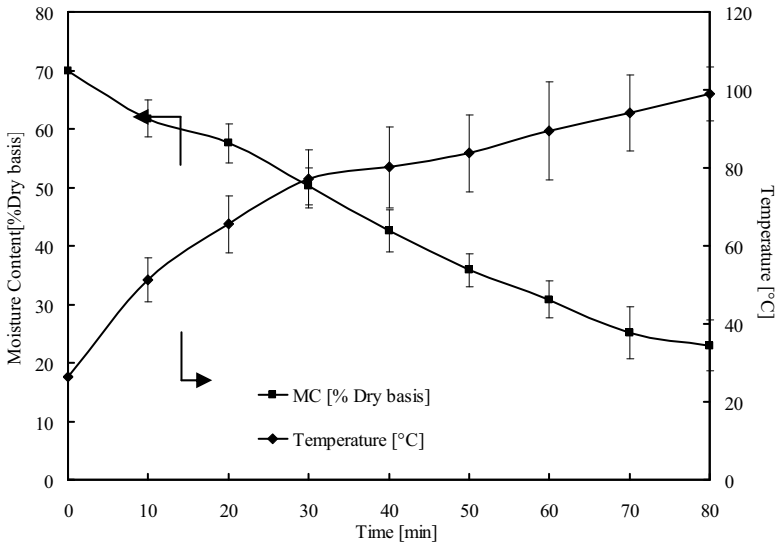

Figure 4.4 Temperature and moisture variations versus elapsed times in case drying using CMCB (T_1= 70 °C) (case 1:Top feed)

Figure 4.5 show the temperature and moisture variations versus elapsed times for parawood pake with constant initial moisture content of 70% (dry basis). It is found that in the case of a combined multi-feed microwave-convective air and continuous belt system (screw feed microwave 4.8 kW microwave power level and 70°C hot air). The temperature and moisture variations versus elapsed times are known as a parameter of the microwave power level (4.8 kW). During the very first period of heating, most of the microwave energy supplied is used to heat the sample. The temperature of sample is raised rapidly up to 45 °C in a few minutes. It is found that only minor temperature differences are observed when convective air is applied. This is because of an undesired non-uniform heating pattern which can be prevented either by changing the field configuration or by moving the product on a conveyer belt through the cavity where microwave could be fed at several positions. Besides, considering the multiple magnetron system, the different directions of transmitted wave from different magnetron make the uniformity of temperature inside the samples. This is because of its wave interference and the influence of the wave penetration capability as shown in Eq. (4.2).

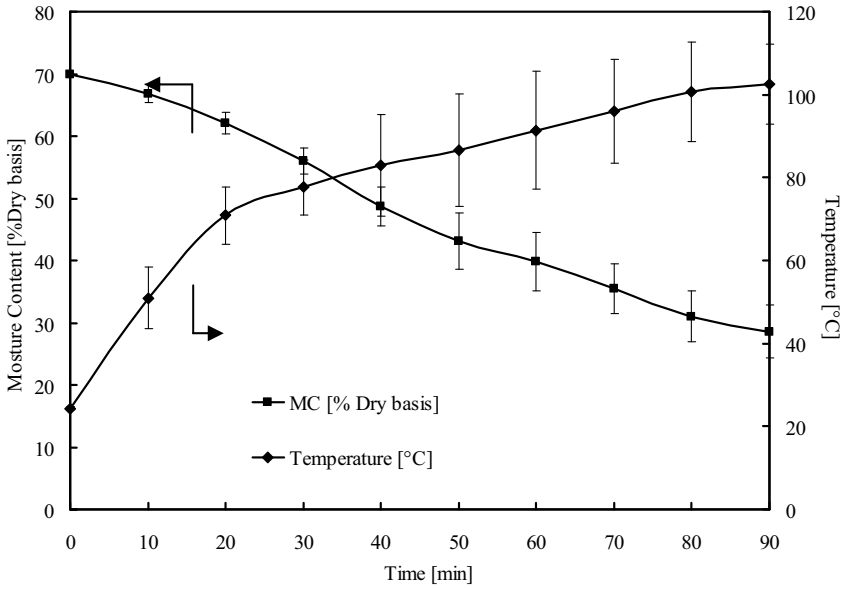

Figure 4.5 Temperature and moisture variations versus elapsed times in case drying using CMCB (T_1= 70 °C)(case 2 : Screw feed)

Figures 4.6-4.7 shows the temperature and moisture content profile with respect to elapsed times as a parameter of applied unsymmetrical position feed magnetron(screw and top feed magnetron) with fixed the microwave power level. During the very first period of heating, most of the microwave energy supplied is used to heat the specimen. Parawood specimen temperature is raised rapidly up to 45 °C in a few minutes. It is found that only minor temperature differences are observed when microwave energy is supplied to specimen. This is because an desired uniform heating pattern can be prevented by changing the field configuration either by moving the product on a conveyer belt through the cavity where microwave could be fed at several positions. Besides, considering the multiple magnetron system, the different directions of transmitted wave(screw feed magnetron) from different magnetron make the uniformity of temperature inside the specimens. This is because of its wave interference and the influence of the wave penetration capability shown in Eq. (4.2).

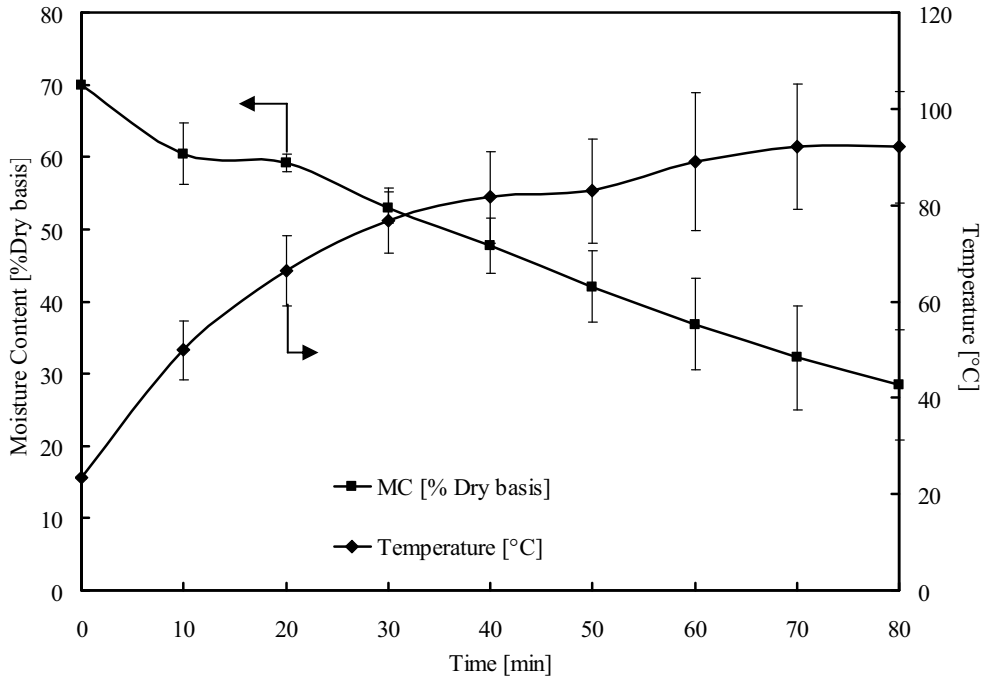

Figure 4.6 Temperature and moisture variations versus elapsed times in case drying using CMCB (T_1= Ambient 30 °C)(case 3:Top feed)

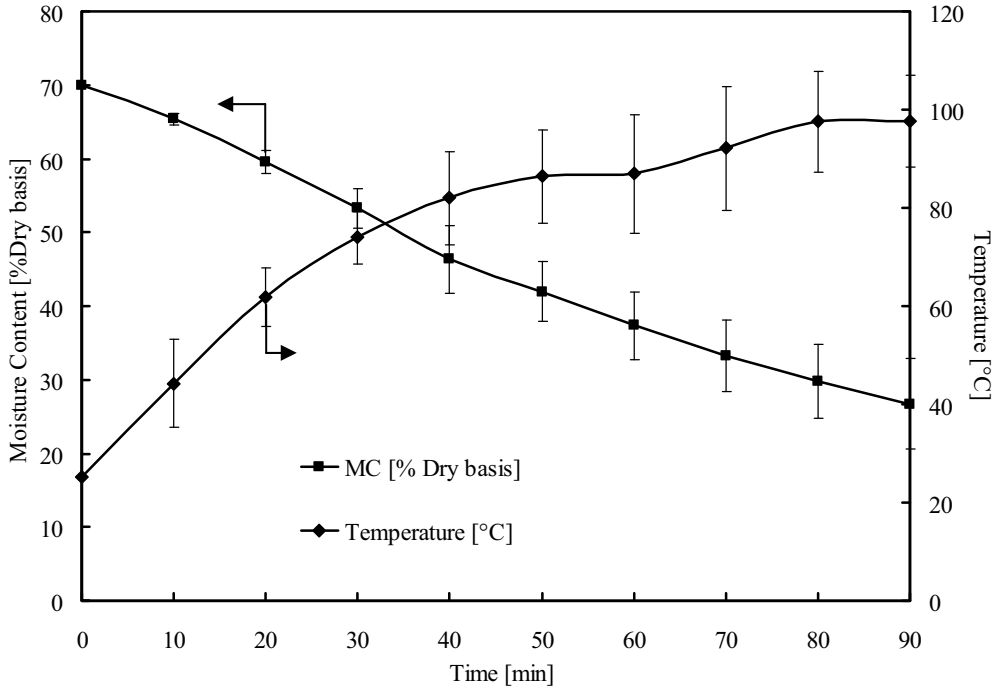

Figure 4.7 Temperature and moisture variations versus elapsed times in case drying using CMCB (T_1= Ambient 30 °C)(case 4 : Screw feed)

Figures 4.8-4.10 the temperature and moisture variations versus elapsed times are known as the parameters of the convective air first period (0-30 minutes: case 5 supplied hot air 70°C, case 6 and 7 supplied ambient air). During the first period of heating, most of the hot air energy supplied is used to heat the sample. The temperature of the sample is raised slowly during the first 30 minutes and the moisture content will gradually slow down as well. It is found that the temperature increases after the supplied microwave energy is applied since at this period, complete the drying process, the sample is filled with the moisture content, which rapidly responses to the microwave energy at this frequency. Therefore, the major increasing of temperature comes from the microwave energy. On the other hand, at a high temperature and high microwave power level , the moisture content of the wood continuously decreases faster than that in the case of convective hot air drying(first period:0-30 minutes). Since the movement of the wood inside the cavity to get the microwave energy in a many of positions.

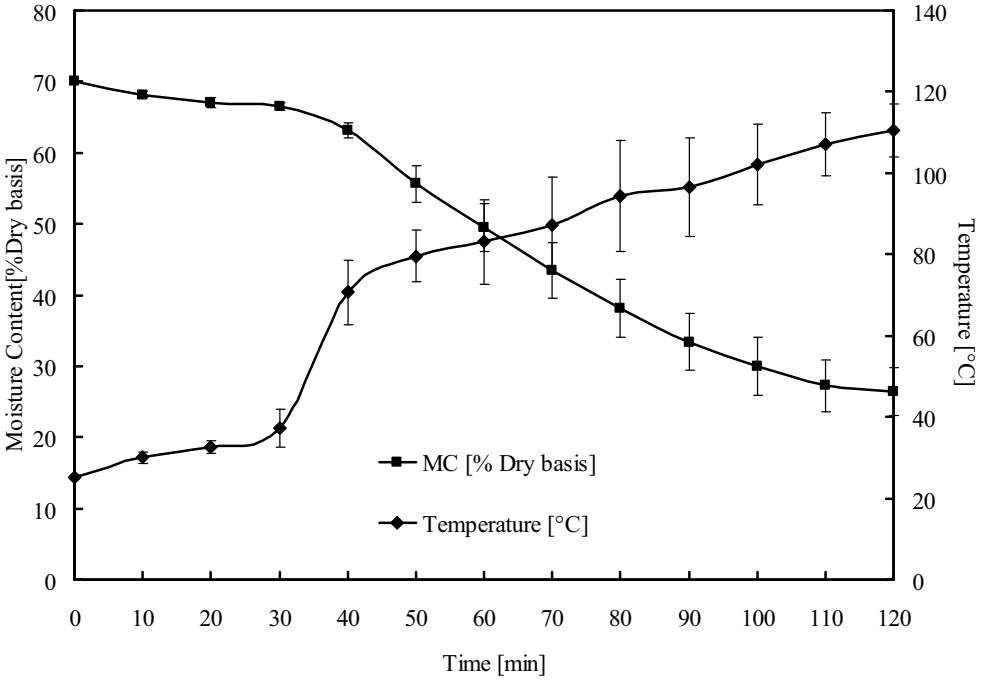

Figure 4.8 Temperature and moisture variations versus elapsed times in case drying using CMCB (T_1= hot air 70 °C)(case 5:Top feed)

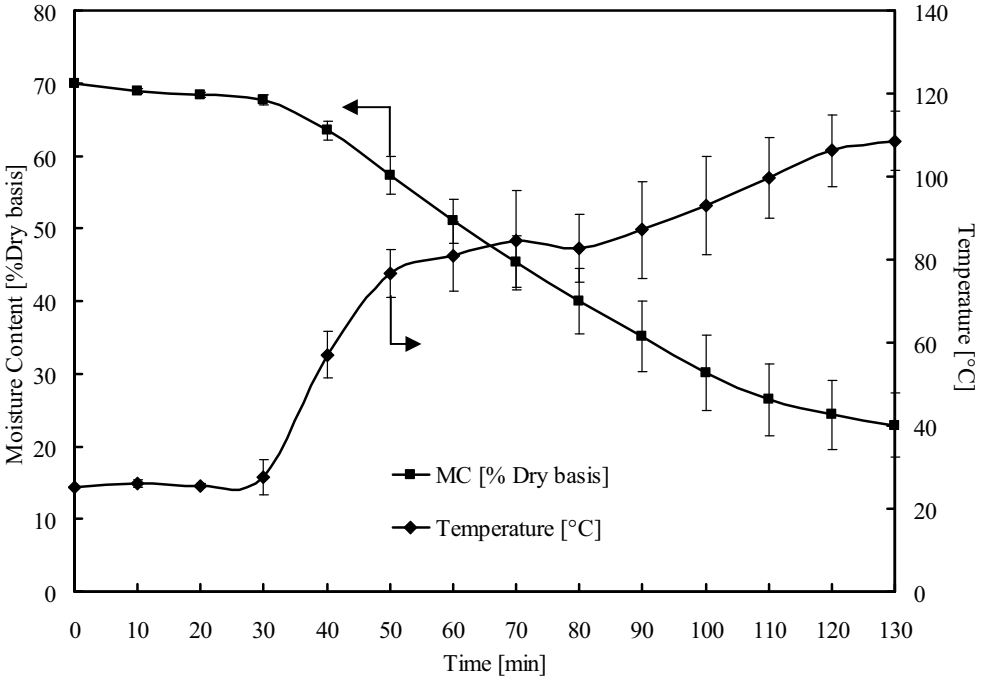

Figure 4.9 Temperature and moisture variations versus elapsed times in case drying using CMCB (T_1= hot air 70 °C)(case 6:Top feed)

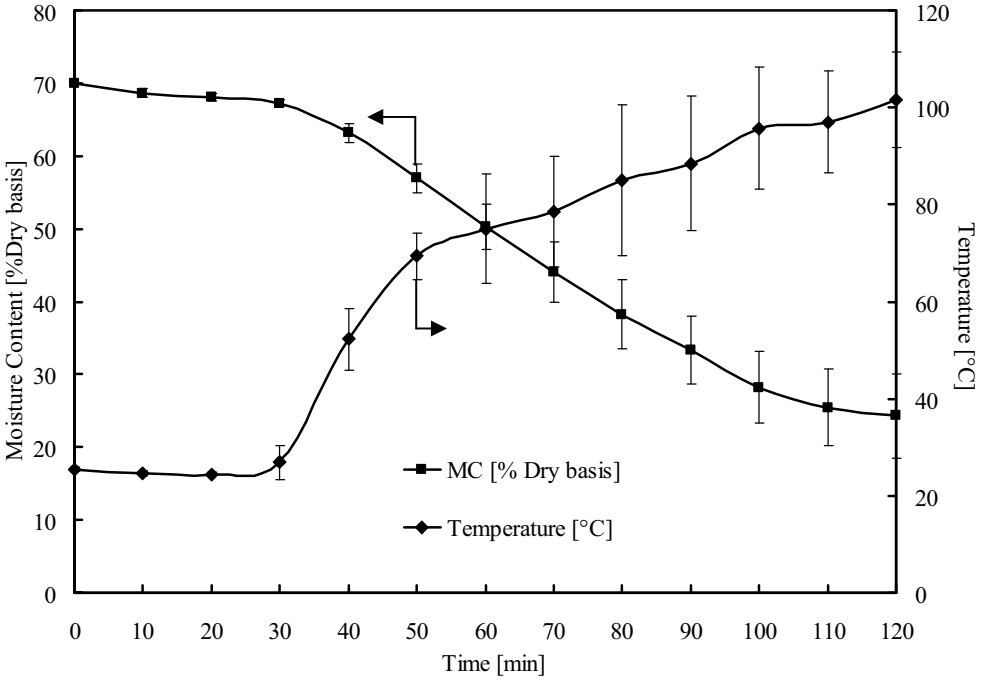

Figure 4.10 Temperature and moisture variations versus elapsed times in case drying using CMCB (T_1= hot air 70 °C)(case 7:Top feed)

Figure 4.11 the temperature and moisture variations versus elapsed times are known as the parameters of the microwave - convective air first period (0-30 minutes: case 8 supplied microwave 4.8 kW and hot air 70°C). During the first period of heating, most of the microwave-hot air energy supplied is used to heat the sample. The temperature of the specimen is raised rapidly during the first 30 minutes and the moisture content will drop dramatically as well. During the later period of heating, most of the hot air energy supplied is used to heat the specimen. The temperature of the sample is decrease slowly during the 30-180 minutes and the moisture content in the specimen is not decreases and constant until the end of the drying process.

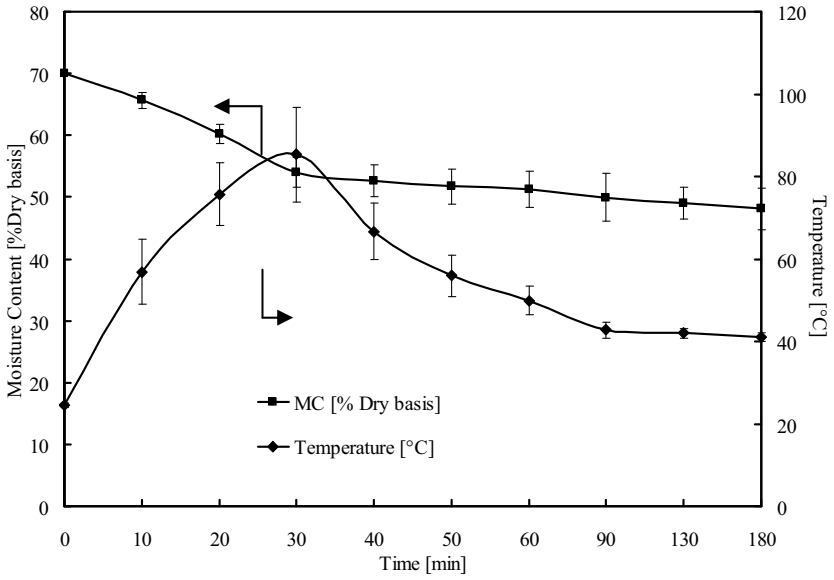

Figure 4.11 Temperature and moisture variations versus elapsed times in case drying using CMCB (T_1= hot air 70 °C)(case 8:Top feed)

Figure 4.12, the temperature and moisture variations versus elapsed times are known as the parameters of the convective air first period (0-20 minutes: case 5 supplied hot air 70°C). During the first period of heating, most of the hot air energy supplied is used to heat the sample. The temperature of the sample is raised slowly during the first 20 minutes and the moisture content will gradually slow down as well. It is found that the temperature increases after the supplied microwave energy is applied since at this period, complete the drying process, the sample is filled with the moisture content, which rapidly responses to the microwave energy at this frequency. Therefore, the major increasing of temperature comes from the microwave energy. On

the other hand, at a high temperature and high microwave power level , the moisture content of the wood continuously decreases faster than that in the case of convective hot air drying(first period: 0-20 minutes).

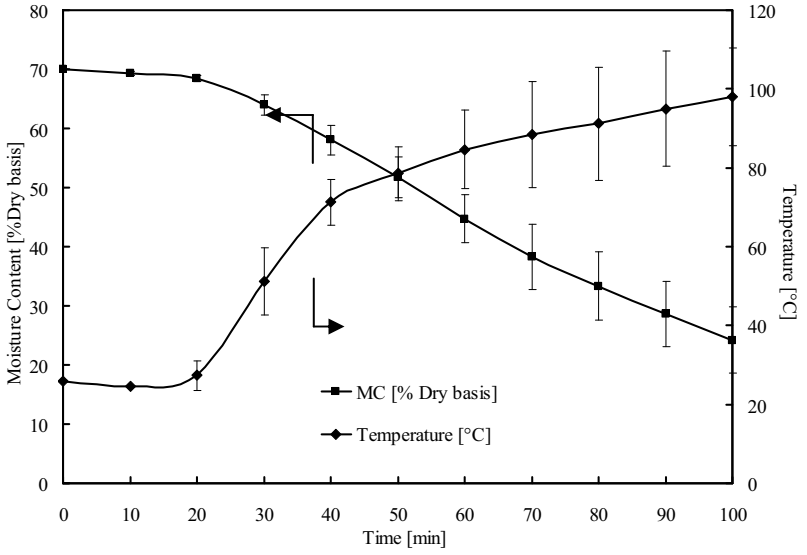

Figure 4.12 Temperature and moisture variations versus elapsed times in case drying using CMCB (T_1= hot air 70 °C)(case 9:Top feed)

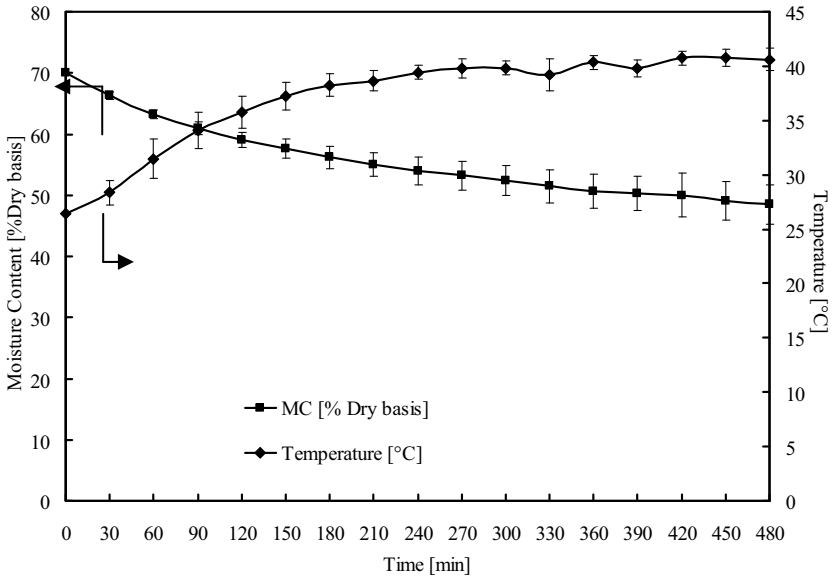

Figure 4.13 Temperature and moisture variations versus elapsed times in case using convective drying (T_1= hot air 70 °C)(case 10)

Figure 4.13, presents temperature and moisture variations versus elapsed times in case using convective drying using hot air. From the figure, the overall drying time required to reduce the moisture content of all the boards within the stack below 28% (dry basis) using the hot air 70 °C was 8 hours. In the case of convective drying (Figure 4.13: case 10), as the surface is dried while the interior is still wet, the dry layer offers a resistance to the heat transport, resulting in a reduction of the evaporation rate as well as drying rate, causing uniform heating.

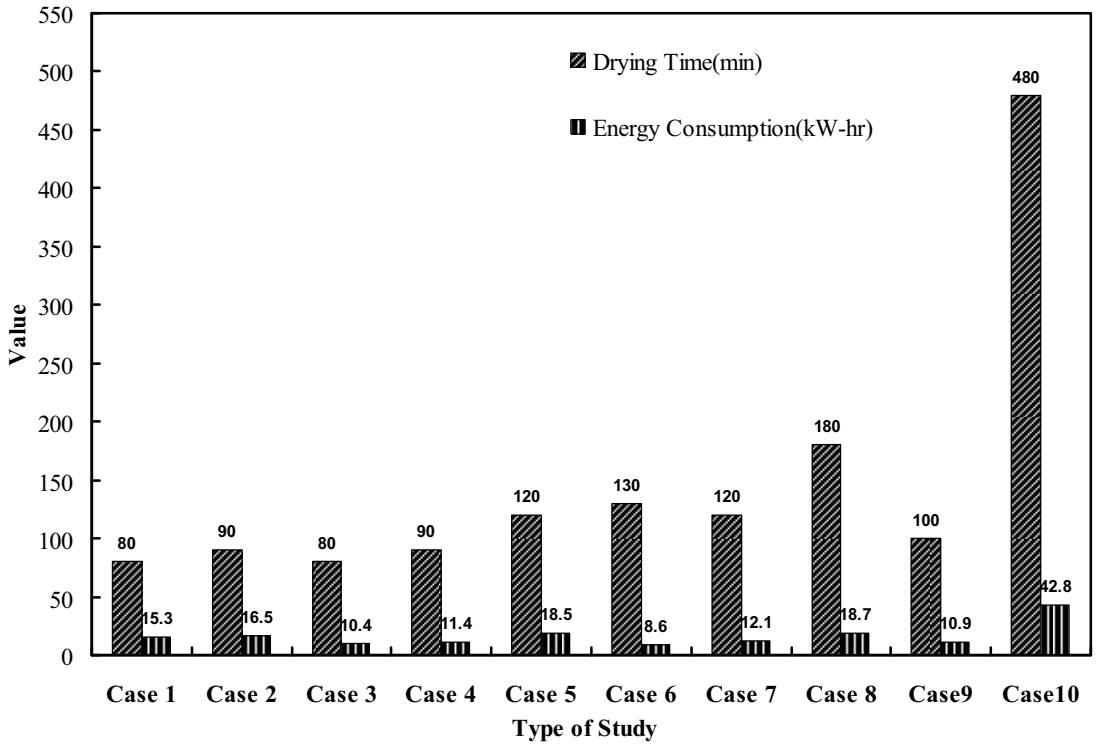

Figure 4.14 Variations in drying time and electrical energy consumption in different case

The electrical energy consumption during microwave- convective air drying and convective drying of a combined multi-feed microwave-convective air and continuous belt system are given in Figure 4.14. When the drying methods are compared in term of electrical energy consumption, it is noted that the lowest electrical energy consumption is observed from microwave - convective air drying method and this is followed by convective drying methods. The best result with regard to electrical energy consumption is obtained from microwave power level of 4.8 kW among all drying methods. Electrical energy consumption at this microwave

power level is 10.4 kW-hr (case 3) and 8.6 kW-hr (case 6). The highest value in all drying methods regarding electrical energy consumption is noted in convective drying process at temperature 70 °C with of 42.8 kW-hr(case 10). The drying time of the convective drying along the drying process is given in Figure 4.14. The highest value in all drying methods regarding the drying time is noted in the convective drying process operating at the temperature of 70 °C with 480 minutes.

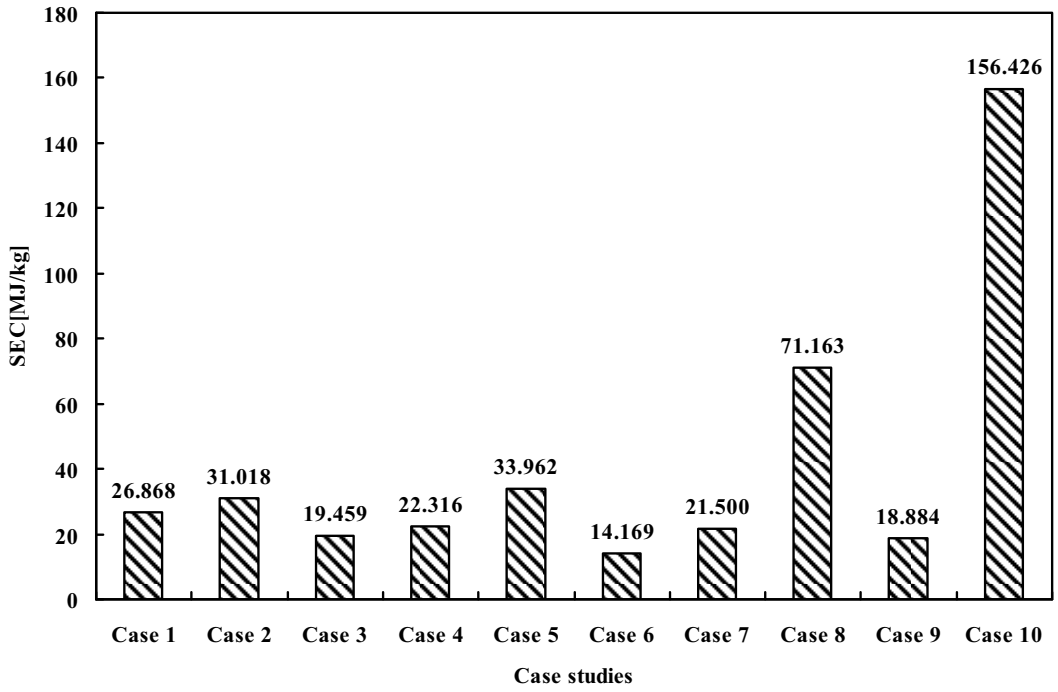

Figure 4.15 Variations in drying time and specific energy consumption in different case

Figure 4.15 show the specific energy consumption with the variation of the parawood specimen. To obtain the experimental results, the microwave power level is set at 4.8 kW and hot air 70 °C, and the specimen are shown Figure 4.2. Figure 4.15 show the specific energy consumption with the variation of difference case.

The specific energy consumption of the drying trials is carried out by two different drying methods. No marked difference is found between with and without hot air supplied in the cavity. Specific energy consumption depends on the electrical power supplied in drying process and amount of water removed during drying. In this study, the specific energy consumptions at microwave power levels of 4.8 kW and hot air 70°C are investigated. These short drying times may be due to a result of

microwave power levels. However, for convective drying, the drying times are long because the convective heat transfer coefficient of the parawood pake is low. The reduction of specific energy consumption observed during drying and the reduction of specific energy consumption are caused by supplied convective air during the first 30 minutes (case 6). The specific energy consumption of microwave-convective air drying at ambient temperature are 14.169 MJ/kg The reduction of specific energy consumption observed during drying and the reduction of specific energy consumption are caused by supplied convective air during the first 30 minutes(case 6). The specific energy consumption of microwave-convective air drying at ambient temperature are 14.1. MJ/kg (case 6), whereas the specific energy consumption of convective drying at 70°C are 156.426MJ/kg (case 10). The specific energy consumptions of the combination drying (microwave – convective air drying) give similar trends at all drying processes. The reduction of specific energy consumption is achieved by decreasing the hot air temperature level supplied to cavity. Figure 4.15, respectively show the comparison of specific energy consumption of different drying cases for position feed magnetron and entering the hot air during drying(first period or late period). The results show that the lowest specific energy consumption is found from microwave – convective air drying method (ambient air), and entering the ambient air during drying (first period: case 6).

Figure 4.16 shows the energy efficiency with respect to the drying time. It seem that the high energy efficiency near the starting period about 0-30 minutes(case 1 and 3 feed magnetron on top) Since the supplied the microwave directly onto the specimen. The results are high energy efficiency after the vapour has moving from the surface of the specimen. This causes the moisture content to quickly decrease and the low quantity of absorbed waves causes the decrease energy consumption. The energy efficiency profiles at various times and locations for four cases are shown in Figure 4.16 The energy efficiency profile within the specimen rises up quickly in the early stages of drying process (about 0–10 min) However, its rise slows down after this stage(about 10–90 min). It is evident from the figure that near the end stages of drying as the moisture content inside the sample is reduced, this decreases the microwave power absorbed. Consequently, the energy efficiency profiles are decreased in this stage of drying process.

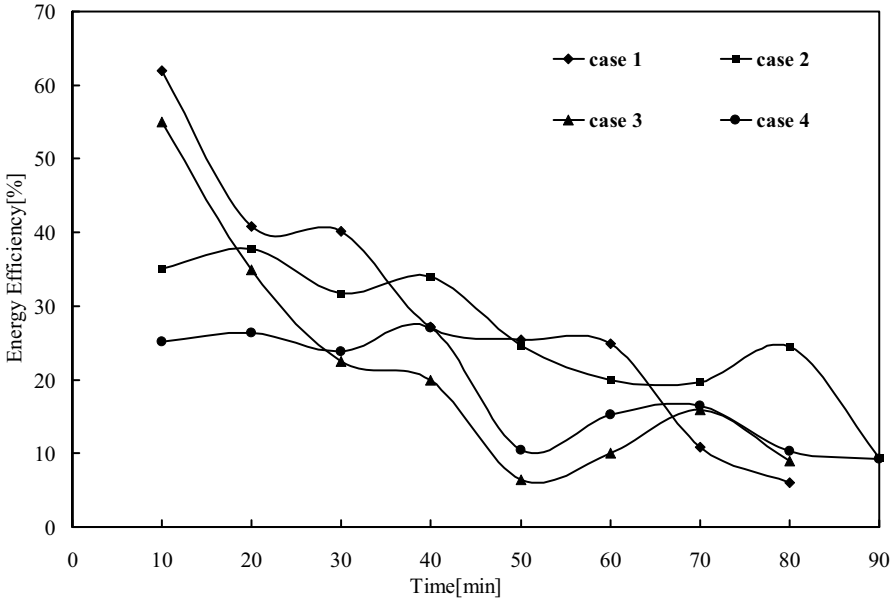

Figure 4.16 Energy efficiency profiles with respect to elapsed time in different case (case 1-4)

Figure 4.17, the efficiency profiles with respect to elapsed time in different case are known as the parameters of the microwave power level 4.8 kW. During the first period of heating, most of the hot air supplied is used to heat the sample (case 5-6-7-9). Figure 4.17, the supplied convective air first period (0-30 and 0-20 minutes: case 5-6-7-9 supplied ambient air 30 °C and hot air 70°C). During the first period of heating, most of the hot air energy supplied is used to heat the sample. The energy efficiency of the sample is raised slowly during the first 30 minutes. It is found that the energy efficiency increases after the supplied microwave energy is applied since at this period, complete the drying process, the sample is filled with the moisture content, which rapidly responses to the microwave energy at this frequency. Therefore, the major increasing of energy efficiency comes from the microwave energy. The moisture content of wood decreases the absorbed microwave power decreases as well. So the energy efficiency will be reduced accordingly.

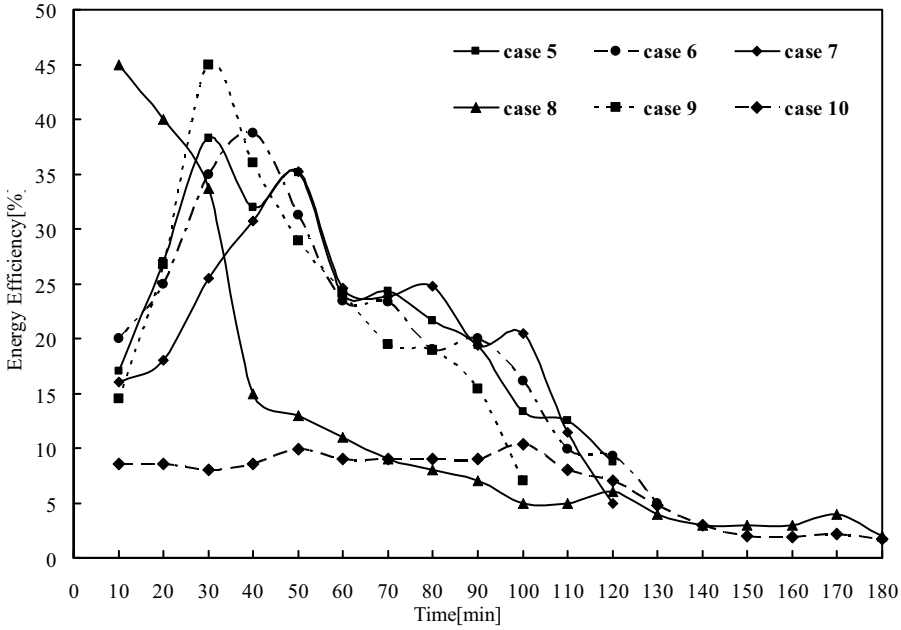

Figure 4.17 Energy efficiency profiles with respect to elapsed time in different case (case 6-10)

Figure 4.17, the supplied microwave energy first period (0-30minutes: case 8 supplied ambient air 30 °C and microwave power level 4.8 kW). During the first period of heating, most of the microwave energy supplied is used to heat the sample. The energy efficiency of the sample is Increasing rapidly. Therefore, the major increasing of energy efficiency comes from the microwave energy. The moisture content of wood decreases the absorbed microwave power decreases as well. So the energy efficiency will be reduced accordingly.

Figure 4.17 case 10 shows the energy efficiency with respect to the drying time. The low energy efficiency of convective drying is presented (case 10). Energy efficiency depends on the temperature in the cavity and the drying time. However, the drying times of convective drying so long, due to the convective heat transfer of the parawood pake, is low.

(a) (b)

Figure 4.18 (a) Parawood pake before drying (b) Parawood pake after drying (CMCB)

Figure 4.18 shows the roughly color shades for parawood pake which were dried with CMCB operating modes. It is observed that the drying with CMHS gives better product quality in physical appearance. It should be summarized again that the drying conditions at high initial weight of parawood pake are increased the drying rate and decreased averaged temperature of bulk load.

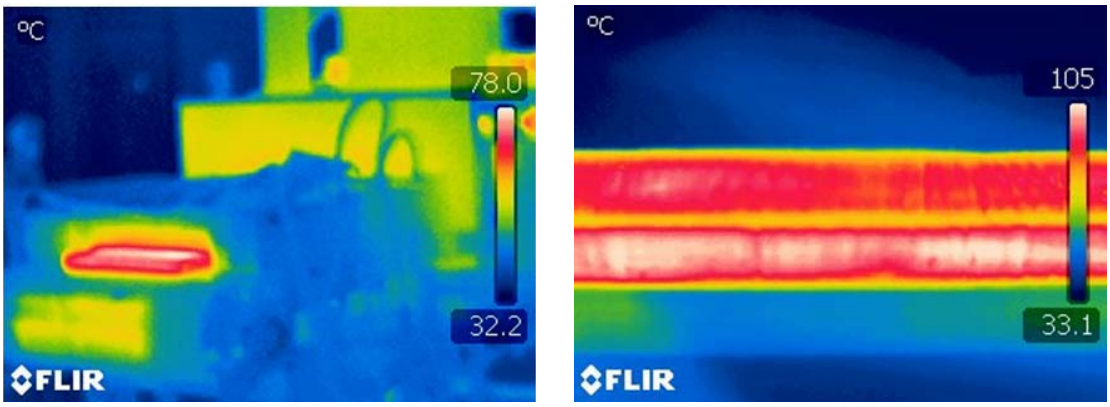

Figure 4.19 Thermally Imaged depicted by FLIR Thermography - Infrared Cameras & Thermal Imagers (Parawood pake sample at the outlet of)

Figure 4.19 shows the temperature distribution in Parawood pake depicted by FLIR Thermography - Infrared Cameras & Thermal Imagers. From this figure illustrates that the uniformity of temperature pattern in the sample was effectively achieved. This result is corresponded with the expecting designed where the idea of using unsymmetrical multi-feed microwave for enhancing the uniformity of electromagnetic wave inside multi-mode cavity (Figure 4.20) is proposed. Figures

4.19 and 4.20 can confirm the Excellency performance of using a Combined unsymmetrical multi-feed microwave and hot air-continuous belt system (CMCB) developed by Prof. Phadungsak Rattanadecho-RCME for industrialized drying process in agricultural products in Thailand.

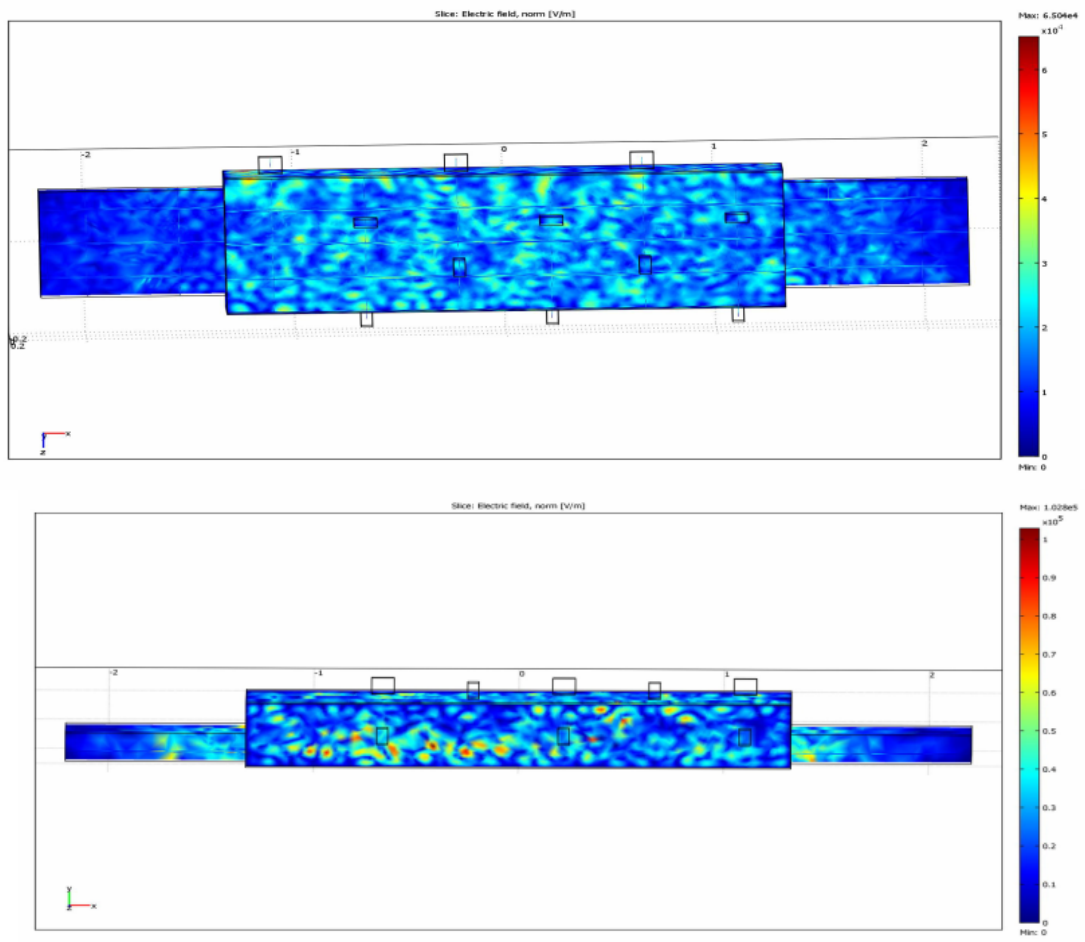

Figure 4.20 Computer simulation of electromagnetic field inside multi-mode cavity based on the concept of using the unsymmetrical multi-feed microwave

4.5 Conclusions

A combined unsymmetrical multi-feed microwave and hot air-continuous belt system permits quicker drying at lower temperature, resulting in a 30% reduction in energy consumption for what is normally an energy-intensive process. Parawood pake

dried using microwave energy required 8 times less specific energy consumption than the Parawood pake which dried by a convective drying method at 70°C in a convective cavity. Moreover, this work depicts the technique that combined the conventional heating with the microwave heating and the continuous belt system together. It shows the potential and the efficient to reduce the electrical energy consumption. If this technology is implemented to the industry, it will decrease the production costs due to the lower electrical energy consumption.

In overall, when handling a combined unsymmetrical multi-feed microwave and hot air-continuous belt system correctly, we can conclude that it will realize the following advantages over other drying systems.

(1) Better heat distribution,
(2) Faster product heating because the multiple magnetrons are placed around the rectangular cavity; this advantage corresponds to the better microwave power distribution, with can penetrate further into the multi-plane of material,
(3) Immediately ready for operation and control of heat capacity without delay,
(4) Continuously supply the material into the system,
(5) The cavity is design to prevent magnetron damage,
(6) No heat storage losses,
(7) Low specific energy consumption and high energy efficiency.

CHAPTER 5

NUMERICAL ANALYSIS OF SPECIFIC ABSORPTION RATE AND HEAT TRANSFER IN THE HUMAN BODY EXPOSED TO LEAKAGE ELECTROMAGNETIC FIELD AT 915 MHZ AND 2,450 MHZ

5.1 Introduction

Electromagnetic energy is a heat source that has an advantage over conventional heating methods because an electromagnetic wave that penetrates the surface is converted into thermal energy within the material volumetrically. High speed startup, selective energy absorption, instantaneous electric control, non-pollution, high energy efficiency, and high product quality are several advantages of microwave heating. Therefore, this technology is used in many industrial and household applications such as heating process (Rattanadecho et al., 2009) and drying process (Rattanadecho et al., 2002). Rapid development of electromagnetic energy applications causes an increase in public concern about health risks from electromagnetic energy emitted from various sources (Ziegelberger, 2009).

Increasing use of high power electromagnetic energy results in the necessity to identify the limits of safe exposure with respect to thermal hazards. The amount of energy absorbed by tissue depends on many factors including frequency, dielectric property of the tissue, irradiating time exposure, intensity of electromagnetic radiation, and water content of the tissue. For this reason, public organizations throughout the world have established safety guidelines for electromagnetic wave absorption values (Ziegelberger, 2009). For human exposure to electromagnetic fields, these guidelines are based on peak spatial-average specific absorption rate (SAR) for human body tissues.

The power absorption in human tissues induces temperature increase inside tissues. The severity of the physiological effect produced by small temperature increases can be expected to worsen in sensitive organs. An increase of approximate1-5°C in human body temperature can cause numerous malformations, temporary infertility in males, brain lesions, and blood chemistry changes. Even a small

temperature increase in human body (approximately 1°C) can lead to altered production of hormones and suppressed immune response (Stuchly, 1995).

In the past, the experimental data on the correlation of SAR levels to the temperature increases in human body are sparse. There is a research on SAR distribution of three-layer human body which simulates three-layer physical models of skin, fat and muscle tissues (Nishizawa and Hashimoto, 1999). There are limited data available on thermal properties and dielectric properties of human tissues, as very few epidemiological studies have been conducted. There have been some experimental studies in animals such as rat (Seufi et al., 2009), cow (Yang et al., 2007) and pig (Kanai et al., 2007). However, the results may not represent behavior of human tissues. Most previous studies of human body exposed to electromagnetic field did not consider heat transfer, resulting in an incomplete analysis to result. Therefore, modeling of heat transport in human tissues is needed in order to obtain complete explanation. The modeling of heat transfer in human tissues has been investigated. Earlier studies of heat transfer in human tissues utilized the general bioheat equation (Pennes, 1948). Thereafter, the coupled model of general bioheat equation and Maxwell's equation were used to model human tissues exposed to electromagnetic field (Spiegel, 1984). Other researches have been done for temperature distribution over the surface, and the various biotissues exposed to an electric field have been studied (Dragun et al., 2005, Ozen et al., 2008). Furthermore, few reports have suggested thermal interactions for microwave frequency fields (Samaras et al., 2007). Researchers also carried out studies on temperature increases in human head exposed to a hand-held cellular phone (Wang and Fujiwara, 1999, Hirata et al., 2005, Garcia et al., 2007).

However, most studies of temperature increases induced by electromagnetic wave have not considered realistic domain of the human body with complicated organs of several types of tissue. There are few studies on the temperature and electromagnetic field interaction in realistic physical model of the human body due to the complexity of the problem, even though it is directly related to the thermal injury of tissues. Therefore, in order to provide information on levels of exposure and health effects from electromagnetic radiation adequately, it is essential to simulate the

coupled electromagnetic field and heat transfer within an anatomically based human body model to represent actual process of heat transfer within the human body.

This research is a pioneer work that simulates the SAR distribution and temperature distribution over an anatomically based human body. In this research, a two-dimensional human cross section model (Shiba and Higaki, 2009) was used to simulate the SAR distribution and temperature distribution over the human body at different frequencies. Electromagnetic wave propagation in tissues was investigated by using Maxwell's equations. An analysis of heat transfer in human tissues exposed to microwaves was investigated by using the bioheat equation. The effects of operating frequency (915 MHz and 2,450 MHz) and the leakage power density (5, 10, 50, and 100mW/cm^2) on distributions of specific absorption rate and temperature profile within the human body are systematically investigated. The 915 MHz and 2,450 MHz frequencies were chosen for simulations in this study because are within in the microwave band and are used most frequently in the application of industrial high power microwave heating. The obtained values provide an indication of limitations that must be considered for temperature increases due to localized electromagnetic energy absorption.

5.2 Formulation of the problem

Electromagnetic fields emitted by high power radiation devices are harmful. Fig. 5.1 shows the leakage of electromagnetic energy from the industrial microwave drying system to a human body. It is known that a human body exposed to intense electromagnetic waves can cause significant thermal damage in sensitive tissues within the human trunk. Therefore, it is necessary to investigate the temperature distributions due to exposure to electromagnetic waves in order to investigate the hot spot zones within the human body especially in abdominal and thoracic cavities.

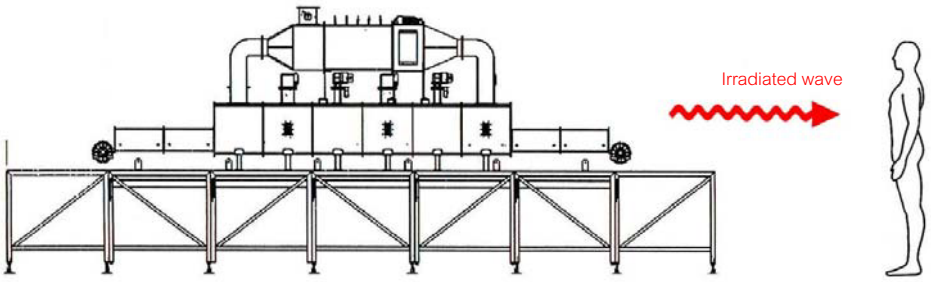

Fig. 5.1 Wave leakage from an electromagnetic radiation device

Due to ethical consideration, exposing a live human body to electromagnetic fields for experimental purposes is difficult. It is more convenient to develop a realistic model through numerical simulation. In the next section, an analysis of specific absorption rate and heat transfer in the human body exposed to electromagnetic field is illustrated. The system of governing equations as well as initial and boundary conditions are solved numerically using the finite element method (FEM).

5.3 Methods and model

The first step in evaluating the effects of a certain exposure to radiation in the human body is the determination of the induced internal electromagnetic field and its spatial distribution. Thereafter, electromagnetic energy absorption which results in temperature increases within particular parts of the human body and other interactions can be considered.

5.3.1 Human model

From Fig. 5.2, a two-dimensional human body model used in this study is obtained by image processing technique from the work of Shiba and Higaki (Shiba and Higaki, 2009). The model has a dimension of 400 mm in width and 525 mm in height. This model comprises 10 types of tissues which are the skin, bone, muscle, fat, nerve, blood, and so forth. These tissues have different dielectric and thermal properties.

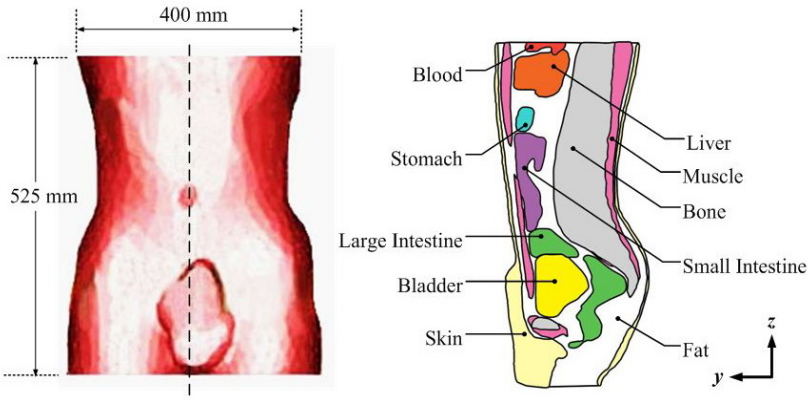

Fig. 5.2 Human body vertical cross section (Shiba and Higaki, 2009)

The thermal properties and dielectric properties of tissues at the frequencies of 915 MHz and 2,450 MHz are given in Table 5.1 and Table 5.2, respectively. As very few studies associated with human tissue properties have been conducted, some of the tissue properties are not quantified. It is also difficult to directly measure tissue properties of a live human. Therefore, we used an assumption of comparing them to animal tissues (It should be noted that the properties based on animal experiments are used for most thermal parameters because no actual data are available for the parameters of the human model). Fig 5.2 shows a vertical cross section through the middle plane of the human trunk model.

5.3.2 Equations for electromagnetic wave propagation analysis

Mathematical models were developed to predict the electric field, SAR and temperature distribution within the human body. To simplify the problem, the following assumptions were made:

1. Electromagnetic wave propagation is modeled in two dimensions over the y-z plane.

2. The human body in which electromagnetic waves and human body interaction proceed in the open region.

3. The computational space is truncated by scattering boundary condition.

4. In the human body, an electromagnetic wave is characterized by transverse electric fields (TE-Mode).

5. The model assumes that dielectric properties of tissues are constant.

The electromagnetic wave propagation in the human body is calculated by Maxwell's equations (Spiegel, 1984), which mathematically describe the interdependence of the electromagnetic waves. The general form of Maxwell's equations is simplified to demonstrate the electromagnetic field of microwave penetrated in the human body as the following equations:

$$\nabla \times \left(\frac{1}{\mu_r} \nabla \times E \right) - k_0^2 \left(\varepsilon_r - \frac{j\sigma}{\omega \varepsilon_0} \right) E = 0 \tag{5-1}$$

$$\varepsilon_r = n^2 \tag{5-2}$$

where E is electric field intensity (V/m), μ_r is relative magnetic permeability, n is refractive index, ε_r is relative dielectric constant, $\varepsilon_0 = 8.8542 \times 10^{-12}$ F/m is permittivity of free space, and σ is electric conductivity (S/m), $j = \sqrt{-1}$.

5.3.2.1 Boundary condition for wave propagation analysis

Microwave energy is emitted by a microwave high power device and strikes the human body with a particular power density. Therefore, boundary condition for electromagnetic wave, as shown in Fig. 5.3, is considered in the following.

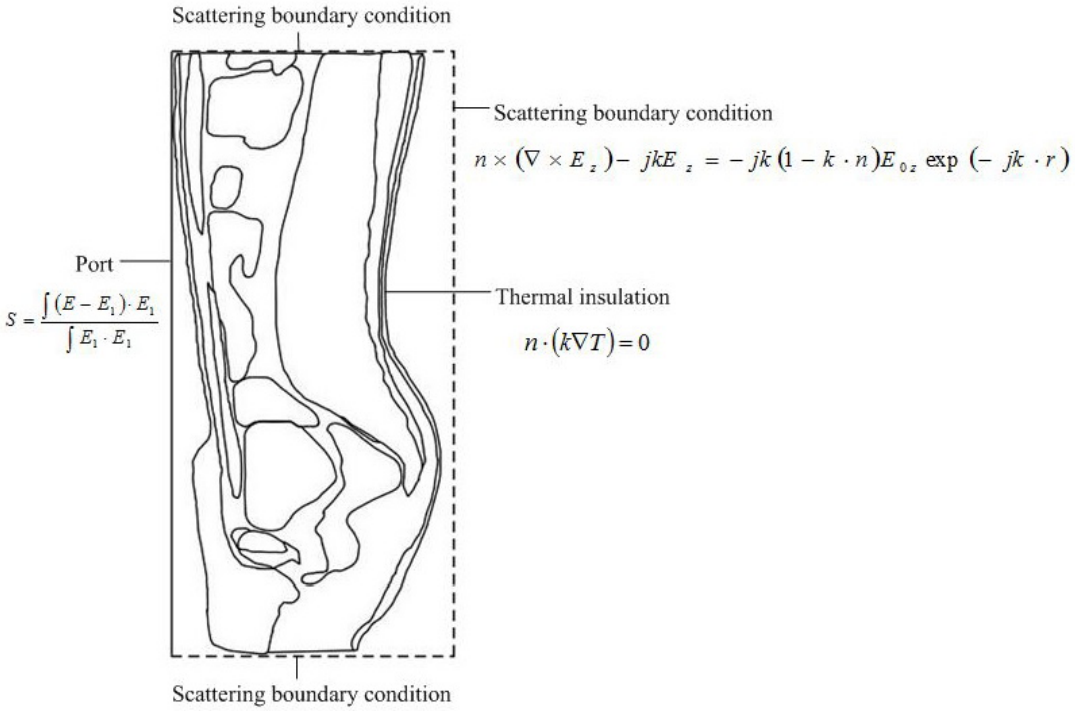

Fig. 5.3 Boundary condition for analysis

It is assumed that the uniform wave flux strikes the left side of the human body. Therefore, at the left boundary of the considered domain, an electromagnetic simulator employs TE wave propagation port with specified power density

$$S = \int (E - E_1) \cdot E_1 / \int E_1 \cdot E_1 \tag{5-3}$$

Boundary conditions along the interfaces between different mediums, for example, between air and tissue or tissue and tissue, are considered as continuity boundary condition

$$n \times (H_1 - H_2) = 0 \tag{5-4}$$

The outer sides of the tissue boundaries are considered as scattering boundary condition

$$n \times \left(\nabla \times E_z\right) - jkE_z = -jk\left(1 - k \cdot n\right)E_{0z}\, exp\left(-jk \cdot r\right) \tag{5-5}$$

5.3.3 Interaction of electromagnetic waves and human tissues

Interaction of electromagnetic fields with biological tissues can be defined in terms of specific absorption rate (SAR). Human tissues are generally lossy mediums for EM waves with finite electric conductivity. They are usually neither good dielectric materials nor good conductors. When EM waves propagate through the human tissues, the energy of EM waves is absorbed by the tissues. The specific absorption rate is defined as power dissipation rate normalized by material density (Kanai et al., 2007). The specific absorption rate is given by

$$SAR = \frac{\sigma}{\rho}|E|^2 \tag{5-6}$$

where E is the root mean square electric-field (V/m), σ is the conductivity (S/m) and ρ is mass density of the tissue (kg/m^3).

5.3.4 Equations for heat transfer analysis

The electric field within the model attenuates due to energy absorption. The absorbed energy is converted to thermal energy, which increases the tissue temperature. To solve the thermal problem, the temperature distribution in the human body has been evaluated by the coupling of bioheat equation and Maxwell's equations. The temperature distribution is corresponded to the specific absorption rate. This is because the specific absorption rate within the human body distributes owing to energy absorption. Thereafter, the absorbed energy is converted to thermal energy, which increases the tissue temperature.

Heat transfer analysis of the human body is modeled in two dimensions over the y-z plane. To simplify the problem, the following assumptions were made:

1. Human tissues are bio-materials with constant thermal properties.
2. There is no phase change of substance occurs within the tissues.
3. There is no energy exchange throughout the human body model.
4. There is no chemical reactions occur within the tissues.

Like electromagnetic field, temperature profiles also can be assumed to be two dimensional in the y-z plane. There is a continuity boundary condition between the organs within the human body. The temperature distribution inside the human model is obtained by using the Pennes' bio-heat equation (Yang et al., 2007). The transient bioheat equation effectively describes how transfer occurs within the human body, and the equation can be written as

$$\rho C \frac{\partial T}{\partial t} = \nabla \cdot (k \nabla T) + \rho_b C_b \omega_b (T_b - T) + Q_{met} + Q_{ext} \tag{5-7}$$

where ρ is the tissue density (kg/m^3), C is the heat capacity of tissue (J/kg K), k is thermal conductivity of tissue (W/m K), T is the temperature ($^\circ$C), T_b is the temperature of blood ($^\circ$C), ρ_b is the density of blood before entering ablation region (kg/m^3), C_b is the specific heat capacity of blood (J/ kg K), ω_b is the blood perfusion rate (1/s), Q_{met} is the metabolism heat source (W/ m^3) and Q_{ext} is the external heat source (microwave heat-source density) (W/ m^3).

In the analysis, heat conduction between tissue and blood flow is approximated by the term $\rho_b C_b \omega_b (T_b - T)$. The metabolism heat source is negligible and therefore $Q_{met} = 0$.

The external heat source is equal to the resistive heat generated by electromagnetic field (microwave power absorbed), which defined as

$$Q_{ext} = \frac{1}{2} \sigma_{tissue} \left| \overline{E} \right|^2 \tag{5-8}$$

where $\sigma_{tissue} = 2\pi f \varepsilon_r' \varepsilon_0$

5.3.4.1 Boundary condition for heat transfer analysis

The heat transfer analysis is considered only in the human body domain, which does not include parts of the surrounding space. As shown in Fig. 5.3, the boundaries of the human body are considered as insulated boundary condition

$$n.(k\nabla T) = 0 \tag{5-9}$$

It is assumed that no contact resistant occurs between the internal organs of the human body. Therefore, the internal boundaries are assumed to be a continuity boundary condition

$$n \cdot (k_u \nabla T_u - k_d \nabla T_d) = 0 \tag{5-10}$$

5.3.4.2 Initial condition for heat transfer analysis

For this analysis, the temperature distribution within the human body is assumed to be uniform. Therefore, the initial temperature of the human body is defined as

$$T(t_0) = 37°C \tag{5-11}$$

The thermoregulation mechanisms and the metabolic heat generation of each tissue have been neglected to illustrate the clear temperature distribution. At the skin–air interface, the insulated boundary condition has been imposed to clearly illustrate the temperature distribution.

5.3.5 Calculation procedure

Up to date there are three principal techniques within computation electromagnetic (CEM); Finite Difference Time Domain Method (FDTD) (Rattanadecho et al., 2009), Method of Moments (MOM) (Spiegel, 1984), and Finite Element Method (FEM). FEM has been extensively used in simulation of electromagnetic field. Moreover, FEM models can provide users with quick and accurate solutions to multiple systems of differential equations.

In this research, finite element method is used to analyze the transient problems. The computational scheme is to assemble finite element model and compute a local heat generation term by performing an electromagnetic calculation using tissue properties. In order to obtain a good approximation, a fine mesh is

specified in the sensitive areas. This study provides a variable mesh method for solving the problem as shown in Fig. 5.4. The model of electromagnetic field and thermal field are solved by FEM model, which was implemented using COMSOL^{TM} Multiphysics 3.4, to demonstrate the phenomenon that occurs within the human body exposed to electromagnetic field. The study employs an implicit time step scheme to solve the electric field and temperature field. In this research, a time step of 10^{-2} s and 10^{-12} s are used to solve Maxwell's equations and Bioheat equation, respectively. These are found practical to achieve each time step convergence. The temperature distribution has been evaluated by taking into account the specific absorption rate due to the electromagnetic field exposure at a particular frequency. Until the steady state is reached, the temperature at each time step is collected.

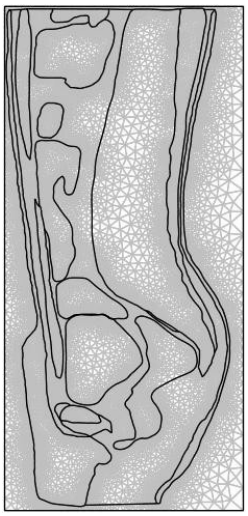

Fig. 5.4 An initial two-dimensional finite element mesh of human cross section model

The 2D model is discretized using triangular elements and the Lagrange quadratic is used to approximate temperature and SAR variation across each element. Convergence test of the frequency of 2,450MHz are carried out to identify the suitable number of elements required. The number of elements where solution is independent of mesh density is found to be 92,469. Higher numbers of elements are not tested due to lack of computational memory and performance. The convergence curve resulting from the convergence test is shown in Fig. 5.5.

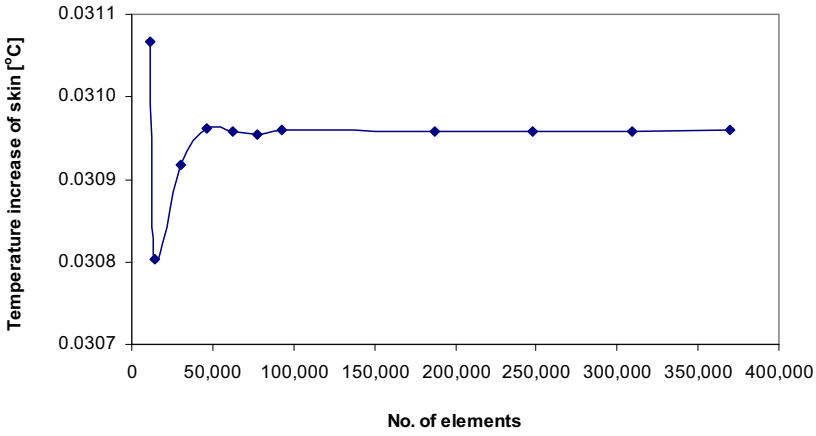

Fig. 5.5 Grid convergence curve of the 2D model

5.4 Results and discussion

In this study, the couple of the mathematical model of bioheat transfer and electromagnetic wave propagation as well as initial temperature of 37°C for all cases are used for the analysis. For the simulation, the thermal properties and dielectric properties are directly taken from Table 5.1 and Table 5.2, respectively. The exposed leakage power density used in this study refers to ICNIRP standard for safety level at the maximum SAR value of 10 W/kg (Ziegelberger, 2009). However, there are frequently exceeded values of leakage power density in the industrial working area due to the leakage of microwave from the microwave high power devices (Ziegelberger, 2009). In the drying industry, only two microwave frequencies of 915 MHz and 2,450 MHz are available. In this analysis, the effects of operating frequency (915 MHz and 2,450 MHz) and leakage power density (5, 10, 50, and 100mW/cm^2) on distributions of specific absorption rate and temperature profile within the human body are systematically investigated. The influences of frequencies and leakage power density on the human body subject to electromagnetic wave are completely discussed in detail.

Table 5.1 Dielectric properties of tissues

Tissue		915 MHz		2,450 MHz	
	ρ (kg/m³)	σ (S/m)	ε_r	σ (S/m)	ε_r
Skin	1,125	0.92	44.86	2.16	41.79
Fat	916	0.09	5.97	0.13	5.51
Muscle	1,047	1.33	50.44	1.60	46.40
Bone	1,038	2.10	44.80	2.10	44.80
Large intestine	1,043	2.04	53.90	2.04	53.90
Small intestine	1,043	3.17	54.40	3.17	54.40
Bladder	1,030	0.69	18.00	0.69	18.00
Blood	1,058	2.54	58.30	2.54	58.30
Stomach	1,050	2.21	62.20	2.21	62.20
Liver	1,030	1.69	43.00	1.69	43.00

Table 5.2 Thermal properties of tissues

Tissue	k (W/m·K)	C_p (J/kg·K)	ω_b	Q_{met} (W/m^3)
Skin	0.35	3,437	0.02	1,620
Fat	0.22	2,300	4.58E-04	300
Muscle	0.6	3,500	8.69E-03	480
Bone	0.436	1,300	4.36E-04	610
Large intestine	0.6	3,500	1.39E-02	9,500
Small intestine	0.6	3,500	1.74E-02	9,500
Bladder	0.561	3,900	0.00E+00	
Blood	0.45	3,960		
Stomach	0.527	3,500	7.00E-03	
Liver	0.497	3,600	0.017201	

5.4.1 Verification of the model

It must be noted in advance that it is not possible to make direct comparison of the model in this study and the experimental results. In order to verify the accuracy of the present numerical model, the simple case of the simulated results is then validated against the numerical results with the same geometric model obtained by Nishizawa et al. (Nishizawa and Hashimoto, 1999). The horizontal cross section of the three layer human tissues as shown in Fig. 5.6 is used in the validation case.

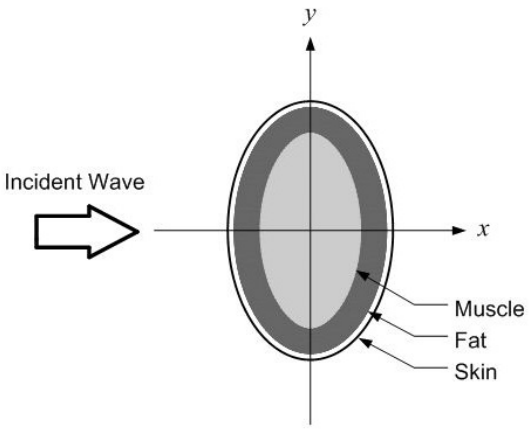

Fig. 5.6 Geometry of the validation model obtained from the previous work (Nishizawa and Hashimoto, 1999)

In the validation case, the leakage power density exposed to the electromagnetic frequency of 1,300 MHz is 1 mW/cm^2. The results of the selected test case are illustrated in Fig. 5.7 for SAR distribution in the human body.

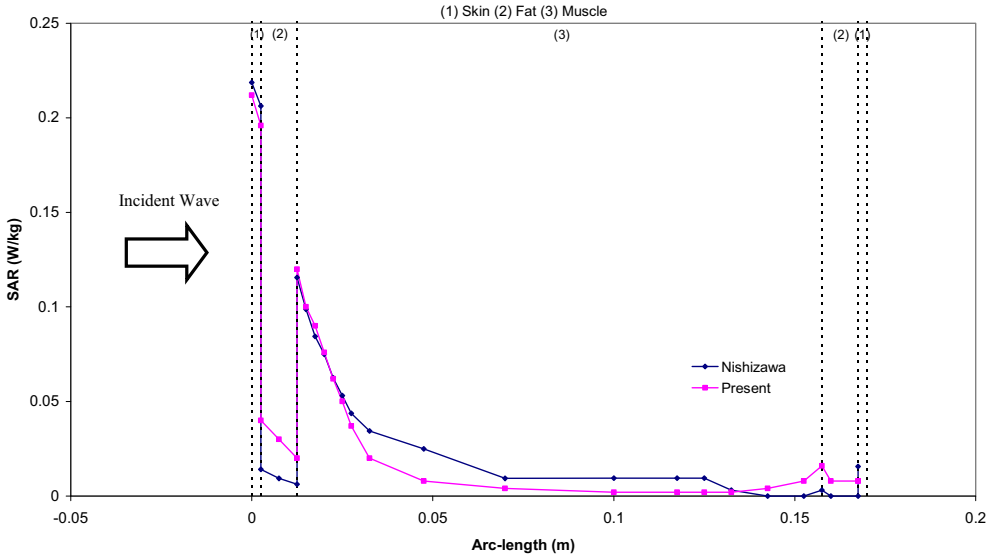

Fig. 5.7 Comparison of the calculated SAR distribution to the SAR distribution obtained by Nishizawa et al. (Nishizawa and Hashimoto, 1999)

Table 5.3 clearly shows a good agreement of the maximum value of the SAR of tissue between the present solution and that of Nishizawa. This favorable comparison lends confidence in the accuracy of the present numerical model. It is important to note that there may be some errors occurring in the simulations which are generated by the input dielectric properties and the numerical scheme.

Table 5.3 Comparison of the results obtained in the present study with those of Nishizawa et al. (Nishizawa and Hashimoto, 1999)

	Present work	Published work (Nishizawa and Hashimoto, 1999)	% Difference
SAR_{max} in skin	0.212	0.220	3.63
SAR_{max} in fat	0.198	0.206	3.88
SAR_{max} in muscle	0.116	0.120	3.33

5.4.2 Distribution of electric field

To illustrate the distribution of penetrated electric field inside each organ of the human body, simulation analysis is required. Fig. 5.8 shows the simulation of electric field pattern inside the human body exposed to electromagnetic field of TE mode propagation along the vertical cross section human body model at the frequencies of 915 MHz and 2,450 MHz.

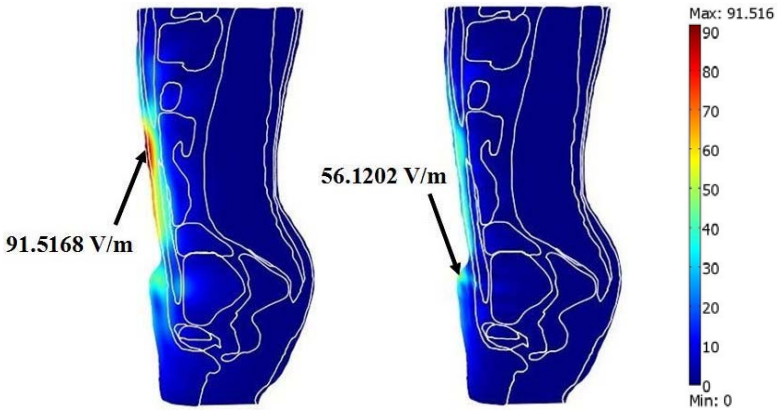

Fig. 5.8 Electric field distribution in human body (V/m) exposed to the leakage power density of 5 mW/cm^2 at the frequencies of (a) 915 MHz (b) 2,450 MHz

Fig. 5.8(a) shows the distribution of electric field at the frequency of 915 MHz. It is found that a large part of electromagnetic wave at 915 MHz can penetrate further into the body. This electric field leads to deeper electromagnetic energy absorbed in the organs of the human body in comparison to the frequency of 2,450 MHz which will be discussed later. With the lower frequency, a large part of electromagnetic wave is able to penetrate into the human body due to its long wavelength which corresponds to a larger penetration depth.

Fig. 5.8(b) shows the distribution of electric field at the frequency of 2,450 MHz. High frequency wave has a short wavelength which corresponds to a small penetration depth of electromagnetic wave. It is found that the electric field diminishes within very small distances, which results in a low specific absorption rate in organs deep inside the human trunk. This phenomenon explains why the electric field and therefore the specific absorption rate are greatest at the skin and decay sharply along the propagation direction for a short wavelength. It can be seen that the distribution of electric field for the higher frequency occurs in the area of outer parts of the body, especially in skin, fat, and muscle. The maximum electric field intensities are 91.51 V/m at the frequency of 915 MHz and 56.12 V/m at the frequency of 2,450 MHz. The electric field within the human body is extinguished where the electric field attenuates due to absorbed electromagnetic energy and is converted to heat.

5.4.3 SAR Distribution in human tissues

Fig. 5.9 shows the SAR distribution evaluated on the vertical section of the human body in which the maximum SAR value occurs. It is evident from the results that the dielectric properties as shown in Table 5.1 can become significant on SAR distribution in human tissues when microwave energy is exposed in these tissues. The magnitude of dielectric properties in each organ will directly affect the amount of SAR within the human body. The highest SAR values are obtained in the region of the skin for the frequency of 915 MHz at 3.43 W/kg and for the frequency of 2,450 MHz at 3.02 W/kg. It is found that the SAR distribution in the human model is different due to the effect of the frequency and the dielectric properties of human tissues. From Fig. 5.9, it appears that for the frequency of 915 MHz, the highest SAR values also occur in the muscle and the small intestine due to the effect of high value

of the dielectric properties. Comparing to ICNIRP limit of SAR value (2W/kg), the resulting SAR values are exceeded in all cases.

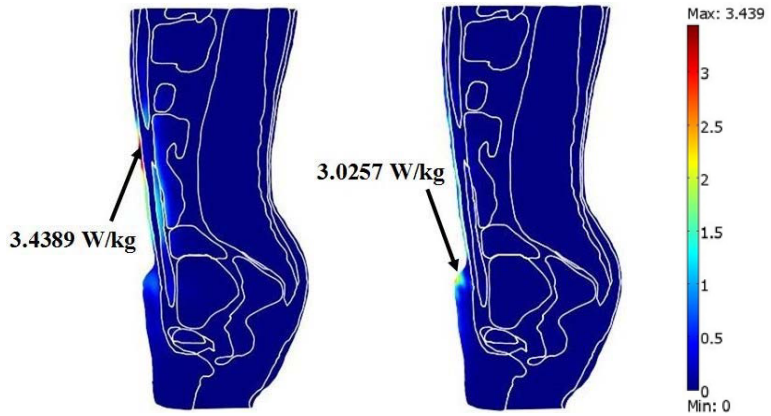

(a) **(b)**

Fig. 5.9 SAR distribution in the human body (W/kg) exposed to the leakage power density of 5 mW/cm^2 at the frequencies of (a) 915 MHz (b) 2,450 MHz

5.4.4 Temperature distribution

Fig. 5.10 shows the temperature increase of the organs in the human body exposed to electromagnetic waves at various times. For the human body exposed to the leakage of electromagnetic wave from a high power microwave heating device at the frequency of 915 MHz or 2,450 MHz for a period of time, the temperature within the human body (Fig. 5.13) is increased corresponding to the specific absorption rate (Fig. 5.12). This is because the electric field within the human body attenuates owing to the energy absorbed and thereafter the absorbed energy is converted to thermal energy, which increases the human body temperature. It is found that at the different frequencies, the distribution patterns of temperature at a particular time are quite different. The hot spot zone is strongly displayed at the 10 minutes for the frequency of 915 MHz, owing to the extensive penetration depth and different properties of tissues. To a lesser extent, at the frequency of 2,450 MHz, the temperature increases in the human body are always found at the periphery of the body correlated with the electric field and SAR (Fig. 5.8-5.9).

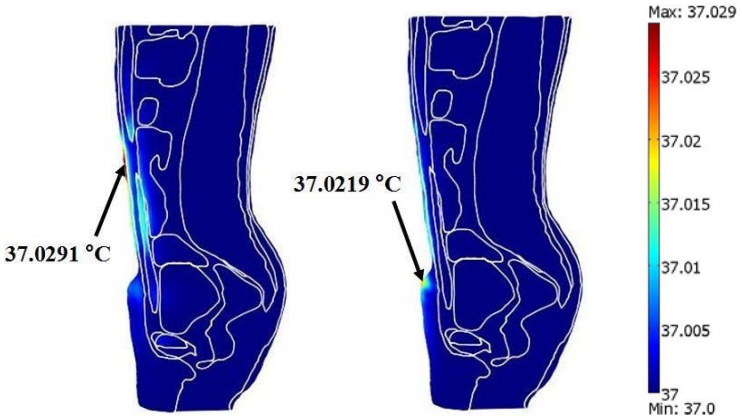

(a)

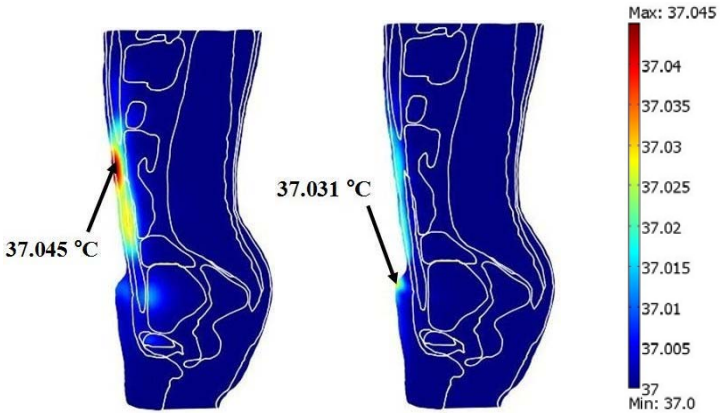

(b)

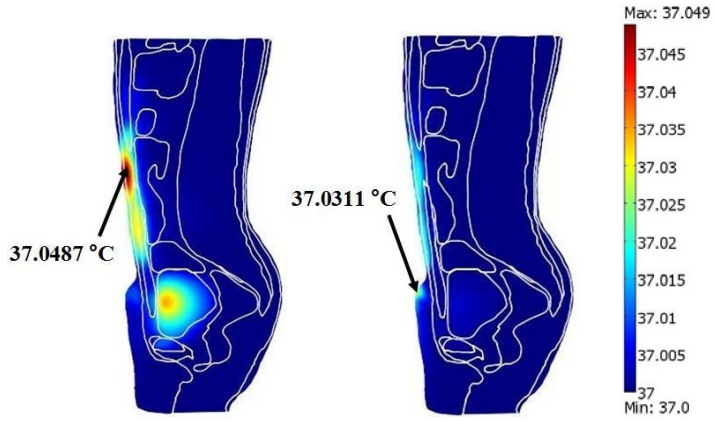

(c)

Fig. 5.10 The temperature distribution of the human body exposed to electromagnetic wave at the frequencies of 915 MHz and 2,450 MHz

(a) 1 minute (b) 10 minutes (c) steady-state

For the case of microwave frequency at 915 MHz, the highest temperature of 37.0487 °C occurs in the fat as shown in Fig. 5.10(a). A different pattern of temperature distribution is obtained at the 2,450 MHz frequency as shown in Fig. 5.10(b), in which the highest temperature of 37.0311 °C is presented in the skin. The maximum temperature increases, with the leakage power density of 5 mW/cm^2, at the 915 MHz and 2,450 MHz frequencies are 0.048 °C and 0.031 °C respectively. There are much lower than the thermal damage temperature within the ranges of 1-5^{o}C.

An electromagnetic wave exposure (for example, the leakage from microwave heating system) usually lasts only a few minutes; hence, the steady-state temperature rise is rarely reached, except for workers who work in the leakage area. Figures 5.11-5.12 show the temperature distributions inside the human body at the 915 MHz and 2,450 MHz frequencies for different exposure times. At 915 MHz, fat tissue temperature increases slower than the other tissues due to its low lossy behavior. Fat tissue also has maximum steady state temperature due to its low blood perfusion rate. It is found that at 915 MHz the internal tissues (fat and bone) reach steady state slower than the external tissues (skin) due to the low thermal conductivity of the fat tissue. However, at 2,450 MHz all of the temperature increases can reach steady state within a short period due to the high thermal conductivity of the skin tissue as well as the low heat capacity of the fat tissue.

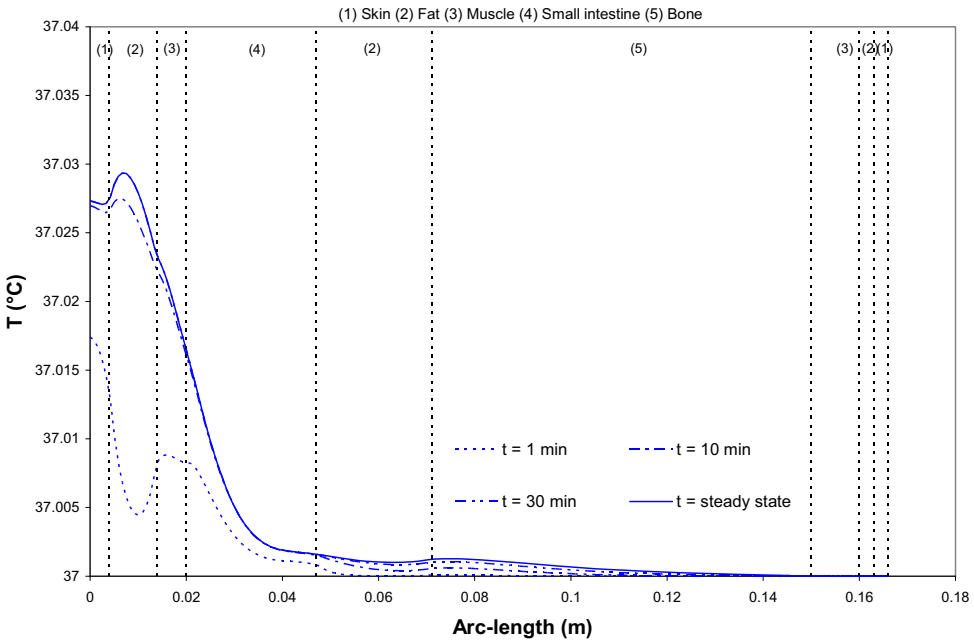

Fig. 5.11 Temperature distribution versus arc-length of the human body at various times exposed to the electromagnetic frequency of 915 MHz at the leakage power density of 5 mW/cm^2

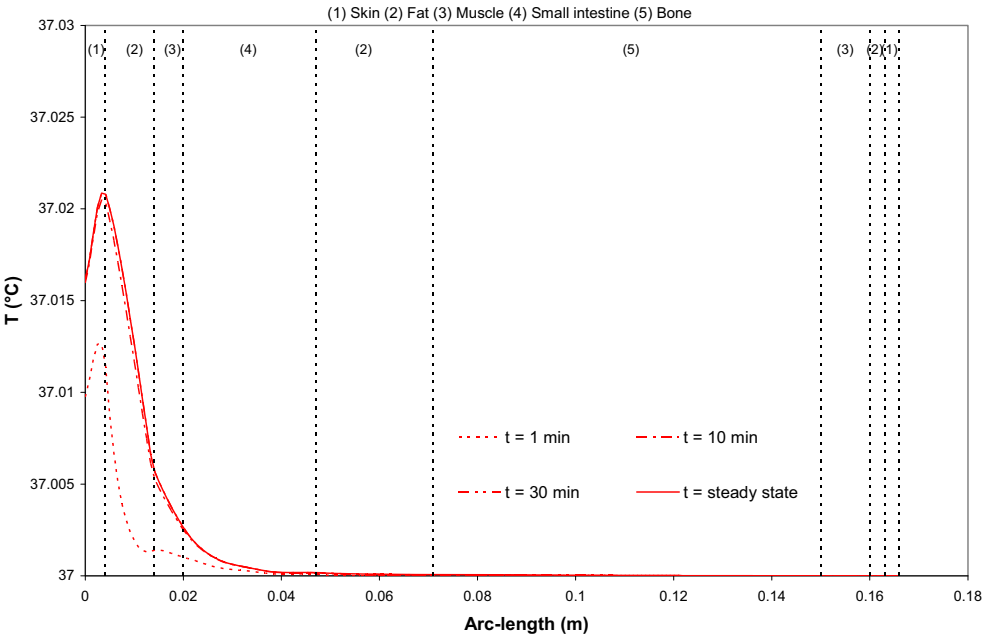

Fig. 5.12 Temperature distribution versus arc-length of the human body at various times exposed to the electromagnetic frequency of 2,450 MHz at the leakage power density of 5 mW/cm^2

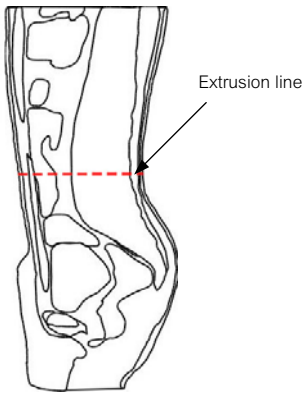

Fig. 5.13 The extrusion line in the human body where the SAR and temperature distribution are considered

5.4.5 Comparison of SAR distribution and temperature distribution in human tissues

Consider the relation of SAR and temperature distribution at the extrusion line (Fig. 5.13), temperature increases of human tissues are induced by local dissipation of SAR. For a human exposed to the leakage power density of 5 mW/cm^2, Fig. 5.14 shows the maximum SAR of the 2,450 MHz frequency (2.0 W/kg) in the skin region. The maximum SAR value of the 2,450 MHz is approximately equal to the maximum SAR value of the 915 MHz frequency (2.0 W/kg) in the skin.

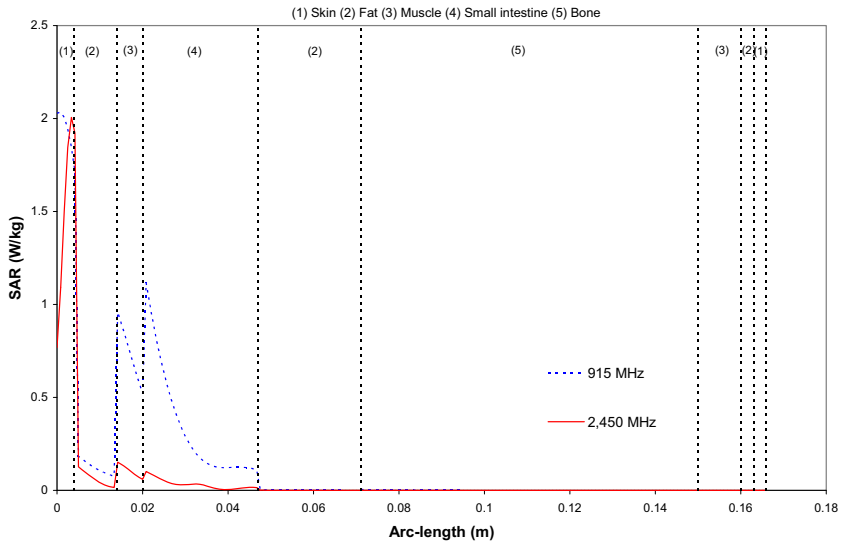

Fig. 5.14 SAR distribution versus arc-length of the human body exposed to the leakage power density of electromagnetic field at the 5 mW/cm^2

However, Fig. 5.15 shows that the maximum temperature increase of the 2,450 MHz frequency in the skin (0.02 °C) is lower than the maximum temperature increase of the 915 MHz frequency in the fat (0.03 °C). This different behavior is due to the fact that for the same SAR value at different frequency, the temperature increase is difference. The maximum SAR of the 2,450 MHz frequency induces the temperature increase in the skin that is lower than the temperature increase in the fat of the 915 MHz frequency. Consequently, since the interior of the fat region has lower blood perfusion rate (4.58×10^{-4} 1/s) than the skin (0.02 1/s) and fat is bounded by low thermal conductivity tissue (skin), the heat transfer of fat from blood perfusion is less effective. At the same time, the high blood perfusion is present in the skin.

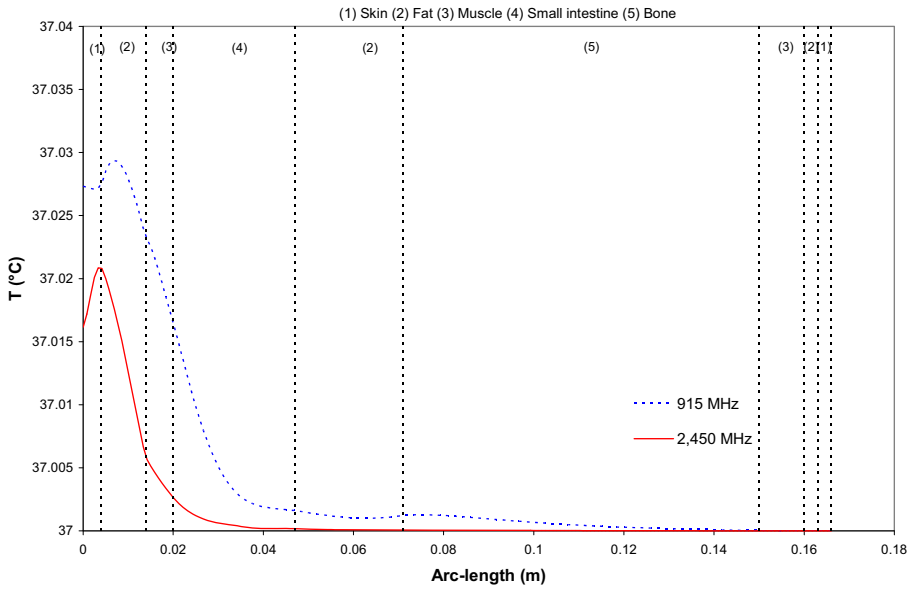

Fig. 5.15 Temperature distribution versus arc-length of the human body exposed to the leakage power density of electromagnetic field at 5 mW/cm^2

The localized maximum SAR for the frequencies of 915 MHz and 2,450 MHz is shown in Fig. 5.16. For the value of localized SAR for each organ, it is found that SAR increases as the frequency decreases. For both frequencies, the three highest SARs are shown for skin, muscle and small intestine. Furthermore, the localized SARs of the 915 MHz frequency are higher than the 2,450 MHz frequency in all organs.

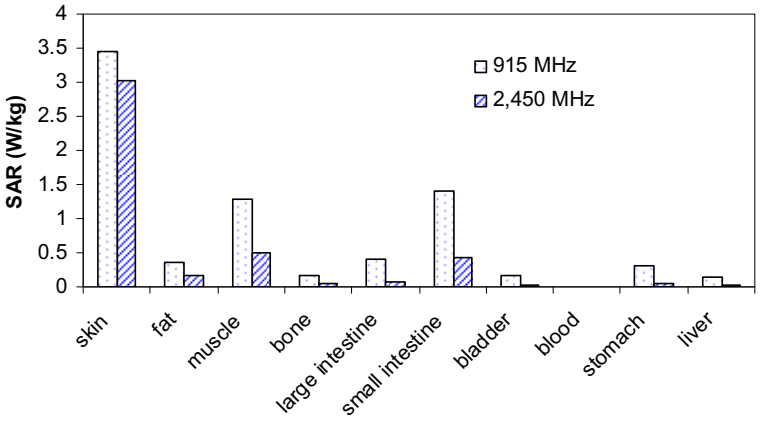

Fig. 5.16 Comparison of the maximum SAR in human tissues at the frequencies of 915 MHz and 2,450 MHz

The maximum localized temperature increases in all tissues for the frequency of 915 MHz and 2,450 MHz are shown in Fig. 5.17. The maximum temperature increase occurs in fat at the 915 MHz frequency, whereas the maximum temperature increase appears in the skin tissues at the 2,450 MHz frequency. Since the penetration depth of the 915 MHz microwave frequency is larger than the 2,450 MHz frequency, and the inner organs have high dielectric properties, the larger temperature increases of the 915 MHz frequency are particularly high in the inner tissues (small intestine and bladder).

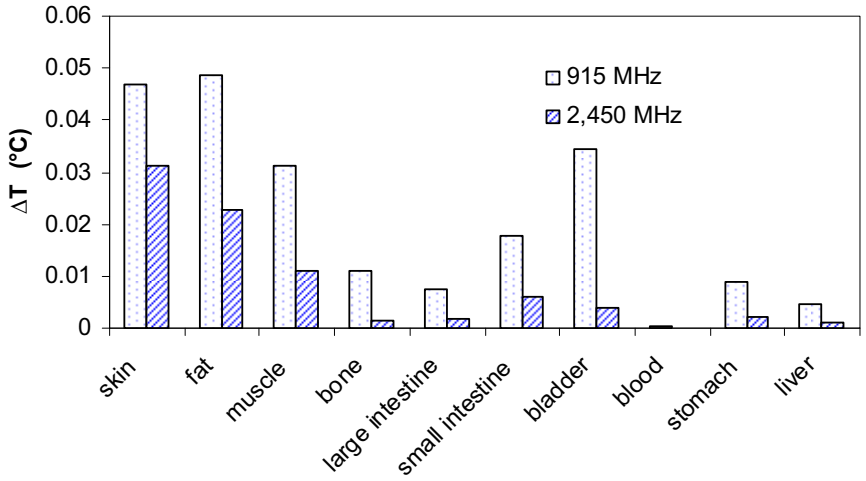

Fig. 5.17 Comparison of the temperature increases in human tissues at the frequencies of 915 MHz and 2,450 MHz.

As a result, the human heterogeneous tissues greatly influence the temperature increases in the skin region exposed to the frequency of 2,450 MHz and in the fat region for the frequency of 915 MHz. It is found that the temperature distributions are not proportional to the local SAR values. Nevertheless, these are also related to the parameters such as thermal conductivity, dielectric properties, blood perfusion rate and etc. It is therefore important to use a thermal model couple with electromagnetic wave propagation model to asses the health risk in term of temperature increase from electromagnetic exposure.

5.4.6 Effect of leakage power density

The effect of leakage power density (the power irradiated on the human surface) has also investigated. The incident power and leakage power density are related as shown in Table 5.4.

Table 5.4 The relationship between the incident power and the leakage power density of microwave

Incident power	Power density
10.5W	5mW/cm^2
21.0W	10mW/cm^2
105W	50mW/cm^2
210W	100mW/cm^2

Fig. 5.18 shows the comparison of the temperature increase distribution within the human body at various incident powers, at t=1min, with the frequency of 915MHz, along the extrusion line (Fig. 5.11). Fig. 5.19 shows the temperature fields of the human body exposed to the electromagnetic frequency of 915 MHz at t=1min corresponding to leakage power densities as shown in Table 5.4. It is found that incident power significantly influences the rate of temperature increase. Greater power provides greater heat generation inside the human body, thereby increasing the rate of temperature rise.

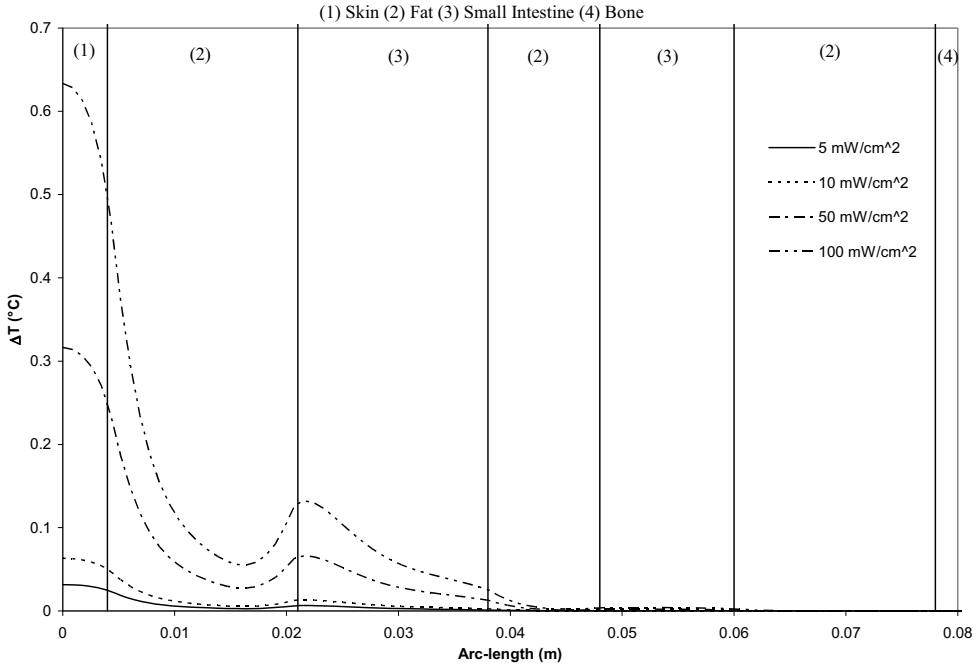

Fig. 5.18 Temperature increase versus arc-length of the human body exposed to the electromagnetic frequency of 915 MHz at various leakage power densities, at t=1min

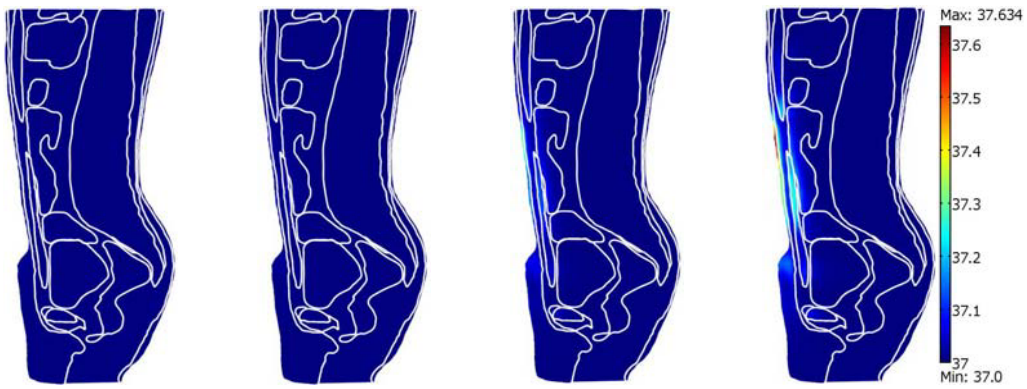

Fig. 5.19 Temperature distribution of the human body exposed to the electromagnetic frequency of 915 MHz at t=1min, at various leakage power densities:
(a) 5mW/cm^2 (b) 10mW/cm^2 (c) 50mW/cm^2 (d) 100mW/cm^2

5.5 Conclusions

This study presents the numerical simulation SAR and temperature distribution in the human body exposed to electromagnetic field at the frequencies of 915 MHz and 2,450 MHz with the power densities of 5, 10, 50, and 100mW/cm^2. The numerical simulations in this study show several important features of the energy absorption in the human body. The results show that the maximum temperatures in various organs are significantly different at different frequencies. The maximum temperature is found at the skin for the frequency of 2,450 MHz and is found at the fat for the frequency of 915 MHz. While the maximum SAR value in both frequencies are found at the skin. It is found that greater leakage power density results in a greater heat generation inside the human body, thereby increasing the rate of temperature increase. Moreover, it is found that the temperature distributions in the human body induced by electromagnetic fields are not directly related to the SAR distribution due to the effect of dielectric properties, thermal properties, blood perfusion, and penetration depth of the microwave power.

Therefore, health effect assessment of electromagnetic wave at various frequencies requires the utilization of the numerical simulation of SAR model along with the thermal model. However, the dielectric properties of some tissues are not indicated as a function of frequency due to the limited number of human tissue dielectric properties in the literature, and this may affect the accuracy of the simulation results. This will allow a better understanding of the realistic situation of the interaction between electromagnetic field and the human tissues.

CHAPTER 6

THE EFFECTS OF DIELECTRIC SHIELD ON SPECIFIC ABSORPTION RATE AND HEAT TRANSFER IN THE HUMAN BODY EXPOSED TO LEAKAGE MICROWAVE ENERGY

6.1 Introduction

Microwave is a form of electromagnetic wave with wavelengths ranging from 1 m down to 1 mm, with frequencies between 0.3 and 300 GHz. Microwave energy has proven to be an efficient and reliable form of heating for a wide range of industrial processes such as heating process (Ratanadecho et al., 2009), curing process (Makul and Ratanadecho, 2010), and melting process (Ratanadecho and Serttikul, 2007). As applications of microwave energy become widespread, adverse effects caused by the leakage microwave energy are increasingly a subject of concern (Stuchly, 1995, Ryan et al., 1995). In many countries, various studies on biological effects have been made and many results have been reported. There has been an intensive model analysis of the SAR of the human body (Spiegel, 1984, Wessapan et al., 2011). The protection is serious for researchers who work with high-power electromagnetic waves. In connection with research on human protection from electromagnetic field exposure, some researches have been carried out on how effectively the human body is protected from unwanted electromagnetic waves (Guy et al., 1987). Furthermore, fundamental analysis of shielding effects of lossy dielectric materials located in front of a human body have also been carried out by some researchers (Nishizawa and Hashimoto, 1999, Hashimoto and Nishizawa and Hashimoto, 1999). However, the heat transfer model has not been included in the modeling analysis.

The computation of the temperature increase is one of the main tasks in the evaluation of the risk related to the exposure of humans to electromagnetic fields (Samaras et al., 2007). Nevertheless, most studies of human protection from electromagnetic field exposure have not been considered the temperature increase within the domain of the human body especially in the human organism. There are

few studies on the temperature and electromagnetic field interaction in a realistic physical model of the human body due to the complexity of the problem, even though it is directly related to the thermal injury of tissues (Wessapan et al., 2011, Shiba and Higaki, 2009, Hirata et al., 2006). Therefore, in order to provide information on protection of the human body against electromagnetic fields adequately, it is essential to simulate the electromagnetic field and heat transfer models to represent an actual process of shield protection from possibly harmful effects of electromagnetic fields. This research is a pioneer work on human protection from electromagnetic field exposure that simulates the SAR distribution and temperature distribution over an anatomically based human body.

This work is extended from the previous chapter in which the human body exposed to leakage electromagnetic field is investigated. This study mainly analyzes the shielding effect of a dielectric shield being placed in front of a human body. Specifically, lossy dielectric media are chosen as the dielectric shield material. The local SARs and temperature increase of human model are calculated for various operating frequencies. Three shield dielectric properties at microwave frequencies of 300, 915, 1300, and 2450 MHz are selected for the shielding investigation. The system of governing equations, as well as initial and boundary conditions are solved numerically, using finite element method (FEM). Moreover, this research is also focusing on the interaction between electromagnetic field and organs in the human trunk.

6.2 Formulation of the Problem

Fig. 6.1 depicts a physical model of the problem. The incident plane wave (TE wave) with a microwave power density of 5 mW/cm^2 is incident on the dielectric shield in front of the human model and penetrated into the human model. A human model including ten kinds of organs is used for our analysis.

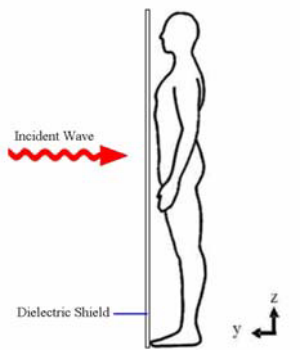

Fig. 6.1 Human model with dielectric shield

6.2.1 Human model

Fig. 6.2 shows a vertical cross section through the middle plane of the human trunk model. A two-dimensional human body model used in this work is obtained by image processing technique from the work of Shiba and Higaki (Shiba and Higaki, 2009). The human model has a dimension of 300 mm in width and 525 mm in height. This human model comprises 10 types of tissues which are the skin, fat, muscle, bone, large intestine, small intestine, bladder, blood, stomach, and liver, respectively. These tissues have different dielectric and thermal properties. The thermal properties and dielectric properties of these tissues at the frequencies of 300, 915, 1300, and 2450 MHz are given in Table 6.1 and Table 6.2, respectively.

Table 6.1 Dielectric properties of tissues

Tissue	300 MHz		915 MHz		1,300 MHz		2,450 MHz	
	σ (S/m)	ε_r	σ (S/m)	ε_r	σ (S/m)	ε_r	σ (S/m)	ε_r
Skin	0.35	48.41	0.92	44.86	1.25	43.56	2.16	41.79
Fat	0.06	6.55	0.09	5.97	0.10	5.80	0.13	5.51
Muscle	1.08	55.45	1.33	50.44	1.42	48.96	1.60	46.40
Bone	2.10	44.80	2.10	44.80	2.10	44.80	2.10	44.80

Large intestine	2.04	53.90	2.04	53.90	2.04	53.90	2.04	53.90
Small intestine	3.17	54.40	3.17	54.40	3.17	54.40	3.17	54.40
Bladder	0.69	18.00	0.69	18.00	0.69	18.00	0.69	18.00
Blood	2.54	58.30	2.54	58.30	2.54	58.30	2.54	58.30
Stomach	2.21	62.20	2.21	62.20	2.21	62.20	2.21	62.20
Liver	1.69	43.00	1.69	43.00	1.69	43.00	1.69	43.00

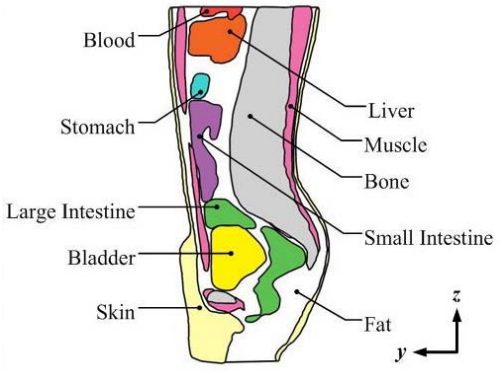

Fig. 6.2 Human body in vertical cross section plane (Shiba and Higaki, 2009)

Table 6.2 Thermal properties of tissues

Tissue	ρ (kg/m³)	k (W/m·K)	C_p (J/kg·K)	ω_b	Q_{met} (W/m^3)
Skin	1,125	0.35	3,437	0.02	1,620
Fat	916	0.22	2,300	4.58E-04	300
Muscle	1,047	0.6	3,500	8.69E-03	480

Bone	1,038	0.436	1,300	4.36E-04	610
Large intestine	1,043	0.6	3,500	1.39E-02	9,500
Small intestine	1,043	0.6	3,500	1.74E-02	9,500
Bladder	1,030	0.561	3,900	0.00E+00	-
Blood	1,058	0.45	3,960	-	-
Stomach	1,050	0.527	3,500	7.00E-03	-
Liver	1,030	0.497	3,600	0.017201	-

6.2.2 Modeling of electromagnetic fields

A mathematical model is developed to calculate the electric field, SAR, and temperature distribution within the human model. To simplify the problem, the following assumptions are made; electromagnetic wave propagation is modeled in two dimensions over the y-z plane, in which waves and object interaction proceed in the open region, and the computational space is truncated by scattering boundary condition. The propagation of an electromagnetic wave is characterized by transverse electric fields (TE-Mode). The dielectric properties of human tissues are frequency dependent as shown in Table 6.1. Since the temperature increase in the human model is slightly changed, the model assumes that the dielectric properties of tissues are independent to temperature change for the specified frequency.

The electromagnetic wave propagation is calculated by Maxwell's equations (Spiegel, 1984), which mathematically describe the interdependence of the electromagnetic waves. The general form of Maxwell's equations is simplified to demonstrate the electromagnetic field of microwave penetrated into the human model as the following equations:

$$\nabla \times \left(\frac{1}{\mu_r} \nabla \times E \right) - k_0^{\,2} \left(\varepsilon_r - \frac{j\sigma}{\omega \varepsilon_0} \right) E = 0 \tag{6-1}$$

$$\varepsilon_r = n^2 \tag{6-2}$$

where E is electric field intensity (V/m), μ_r is relative magnetic permeability (H/m), n is refractive index, ε_r is relative dielectric constant, ε_0=8.8542×10^{-12} (F/m) is permittivity of free space, and σ is electric conductivity (S/m), $j=\sqrt{-1}$.

6.2.2.1 Boundary condition for wave propagation analysis

Microwave energy is emitted by a microwave high power device and strikes the dielectric shield in front of the human model with a microwave power density of 5 mW/cm^2. The microwave power density in terms of mW/cm^2 in 2D model can be presumed by dividing the microwave power (mW) by a frontal area of the incident microwave (cm^2). Therefore, boundary conditions used for electromagnetic wave, as shown in Fig. 6.3, are considered in the following.

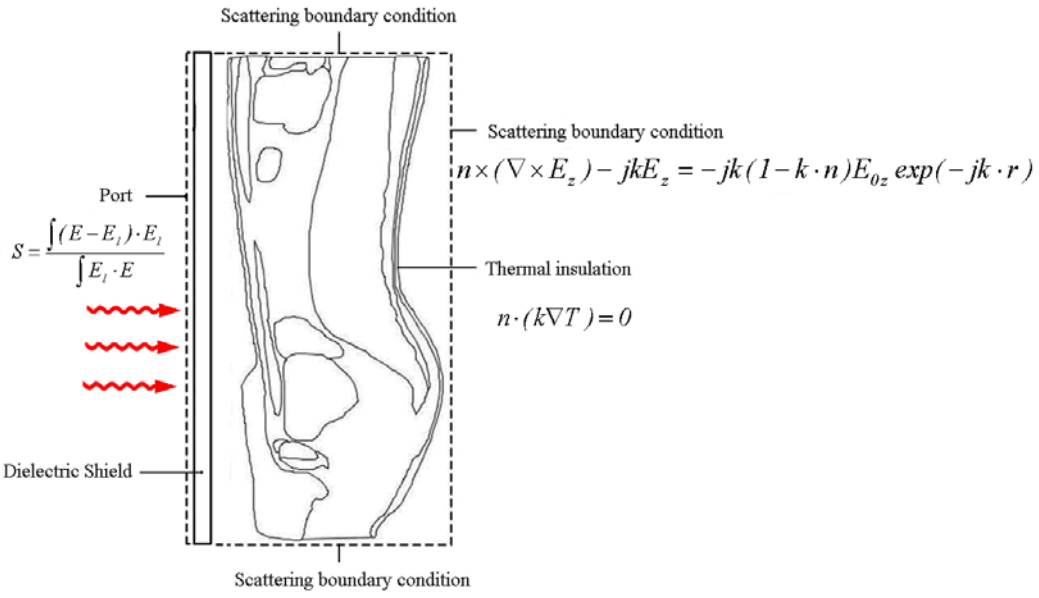

Fig. 6.3 Physical model and boundary condition used for analysis

It is assumed that the uniform wave flux strikes the left side of the human model, where the dielectric shield is located and then penetrates into the human model. From the viewpoint of convergence of the electromagnetic field, only

the TE wave is used as the incident wave. Therefore, at the left boundary of the considered domain, an electromagnetic simulator employs TE wave propagation port with specified power density:

$$S = \int\left(E - E_1\right)\cdot E_1 \Big/ \int E_1 \cdot E_1 \tag{6-3}$$

Boundary conditions along the interfaces between different mediums, for example, between air and tissue or tissue and tissue (with different dielectric properties), are considered as continuity boundary condition:

$$n \times \left(H_1 - H_2\right) = 0 \tag{6-4}$$

The outer sides of the tissue boundaries are considered as scattering boundary condition:

$$n \times \left(\nabla \times E_z\right) - jkE_z = -jk\left(1 - k \cdot n\right)E_{0z} \exp\left(-jk \cdot r\right) \tag{6-5}$$

6.2.3 Interaction of electromagnetic waves and human tissues

Interaction of electromagnetic fields with biological tissues can be defined in terms of the SAR. When EM waves propagate through the dielectric shield and then penetrate into the human tissues, the energy of EM waves is absorbed by the tissues. The SAR is defined as the power dissipation rate normalized by tissue density (Hirata et al., 2006). The SAR is given by:

$$SAR = \frac{\sigma}{\rho}\left|E\right|^2 \tag{6-6}$$

where E is the root mean square electric-field (V/m), σ is the conductivity (S/m) and ρ is mass density of the tissue (kg/m^3).

6.2.4 Modeling of heat transfer

The heat transfer analysis is considered only in the human body domain, which does not include parts of the surrounding space as well as the dielectric shield. To reduce complexity of the problem, the following assumptions have been introduced.

1) There is no phase change and mass transfer in the human model.

2) The human tissues are bio-material with constant thermal properties.

3) There is no chemical reaction occurring within the human model.

4) The initial temperature through the human model is uniform.

The heat transfer analysis of the human model is modeled in two dimensions over the y-z plane. The temperature distribution inside the human model is obtained by using the Pennes' bio-heat equation (Pennes, 1998). The transient bioheat equation effectively describes how heat transfer occurs within the human model, and the equation can be written as:

$$\rho C \frac{\partial T}{\partial t} = \nabla \cdot (k \nabla T) + \rho_b C_b \omega_b (T_b - T) + Q_{met} + Q_{ext} \tag{6-7}$$

where ρ is the tissue density (kg/m^3), C is the heat capacity of tissue (J/kg·K), k is thermal conductivity of tissue (W/m·K), T is the temperature (°C), T_b is the temperature of blood flow (°C), ρ_b is the density of blood before entering ablation region (kg/m^3), C_b is the specific heat capacity of blood (J/ kg·K), ω_b is the blood perfusion rate (1/s), Q_{met} is the metabolism heat source (W/ m^3) and Q_{ext} is the external heat source (microwave heat-source density) (W/ m^3).

In this analysis, heat conduction between tissue and blood flow is approximated by the term $\rho_b C_b \omega_b (T_b - T)$. This analysis, the thermoregulation mechanisms and the metabolic heat generation of each tissue have been neglected to illustrate the clear temperature distribution. The metabolism heat source is negligible and therefore $Q_{met} = 0$.

The external heat source is equal to the resistive heat generated by electromagnetic field (microwave power absorbed):

$$Q_{ext} = \frac{1}{2}\sigma_{tissue}\left|\overline{E}\right|^2 \tag{6-8}$$

where $\sigma_{tissue} = 2\pi f\varepsilon'_r\varepsilon_0$

6.2.4.1 Boundary condition for heat transfer analysis

At the skin–air interface, the insulated boundary condition has been imposed to clearly illustrate the temperature distribution. As shown in Fig. 6.3, the boundaries of human body are considered as insulated boundary condition:

$$n.(k\nabla T) = 0 \tag{6-9}$$

It is assumed that no contact resistant occurs between the internal organs of the human body. Therefore, the internal boundaries are assumed to be a continuity boundary condition between the tissue layers within the human model:

$$n\cdot(k_u\nabla T_u - k_d\nabla T_d) = 0 \tag{6-10}$$

6.2.4.2 Initial condition for heat transfer analysis

For this analysis, the temperature distribution within human body is assumed to be uniform. Therefore, initial temperature of human body is defined as

$$T(t_0) = 37°\text{C} \tag{6-11}$$

6.2.5 Penetration depth

The penetration depth (D_p) is defined as the distance at which the microwave power density has decreased to 37 % of its initial value at the surface (Basak et al., 2006):

$$D_p = \frac{1}{\frac{2\pi f}{\upsilon}\sqrt{\frac{\varepsilon_r'\left(\sqrt{1+\left(\frac{\varepsilon_r''}{\varepsilon_r'}\right)^2}-1\right)}{2}}} = \frac{1}{\frac{2\pi f}{\upsilon}\sqrt{\frac{\varepsilon_r'\left(\sqrt{1+(\tan\delta)^2}-1\right)}{2}}} \quad (6\text{-}12)$$

where ε_r'' is the relative dielectric loss factor and υ is the speed of microwave (m/s).

The penetration depth of the microwave power is calculated using (Eq.(6-4) to (6-12)), which shows how it depends on the dielectric properties of the dielectric material. The shield dielectric properties and the penetration depth of the dielectric shield are summarized in Table 6.3.

Table 6.3 Dielectric properties of shield and penetration depth

Operating frequency (MHz)	D_p (cm)		
	Low lossy 10-*j*5	Medium lossy 10-*j*10	High lossy 20-*j*20
300	10.36	5.53	3.91
915	3.40	1.81	1.28
1,300	2.39	1.28	0.90
2,450	1.27	0.68	0.48

It is shown that the D_P is greatly dependent on the shield dielectric properties as well as the operating frequency. With high lossy of dielectric shield typically shows greater potential for absorbing microwaves in dielectric shield, while an increase in operating frequency typically decreases in D_P.

6.3 Numerical procedure

The model of bioheat equation and Maxwell's equation are used to simulate the SAR and temperature increase in the human model. The computational scheme is to first assemble finite element model and compute a local heat generation

term by performing an electromagnetic calculation using tissue properties. In order to obtain a good approximation, a fine mesh is specified in the sensitive areas. This study provides a variable mesh method for solving the problem as shown in Fig. 6.4.

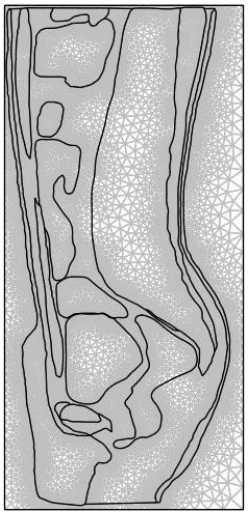

Fig. 6.4 A two-dimensional finite element mesh of human cross section model

The model of electromagnetic field and thermal field are solved by FEM. The model is implemented using COMSOL^{TM} Multiphysics 3.4, to demonstrate the phenomenon that occurs within the human body exposed to leakage microwave energy. The study employs an implicit time step scheme to solve the electric field and temperature field. The 2D model is discretized using triangular elements and the Lagrange quadratic is used to approximate the temperature and SAR variation across each element. Convergence test of the frequency of 2450MHz are carried out to identify the suitable number of elements required. The number of elements where solution is independent of mesh density is found to be 92,469. The convergence curve resulting from the convergence test is shown in Fig. 6.5.

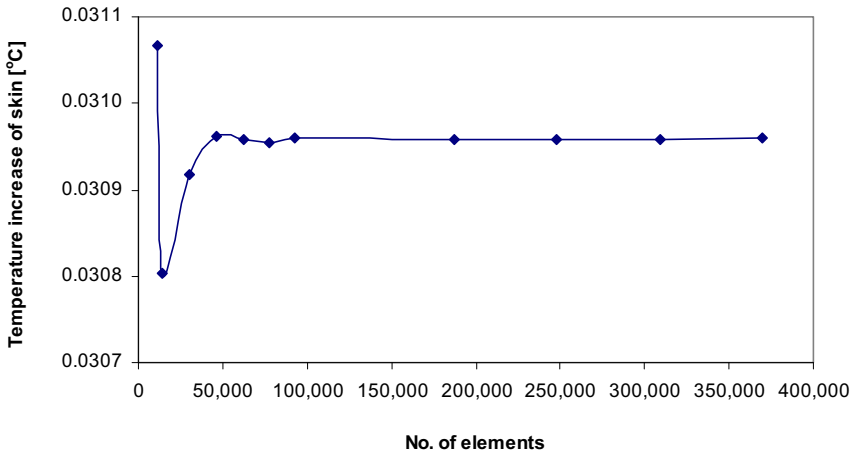

Fig. 6.5 Grid convergence curve of the 2D model

6.4 Results and discussion

In this section, the couple of the mathematical model of bioheat transfer and electromagnetic wave propagation as well as an initial temperature of 37°C for all cases is used for the analysis. For the simulation, the thermal properties and dielectric properties are directly taken from Table 6.1 to Table 6.3, respectively. The influences of shield dielectric properties and operating frequency on SAR and temperature increase within the human model are clearly investigated.

6.4.1 Numerical validations

It must be noted in advance that it is not possible to make a direct comparison of the model in this study and the experimental results due to the medical ethics. In order to verify the accuracy of the present numerical model, the simple case of the simulated results is then validated against the numerical results with the same geometric model presented by Nishizawa and Hashimoto (Nishizawa and Hashimoto, 1999). The horizontal cross section of the three layer human tissues as shown in Fig. 6.6 is used in the validation case.

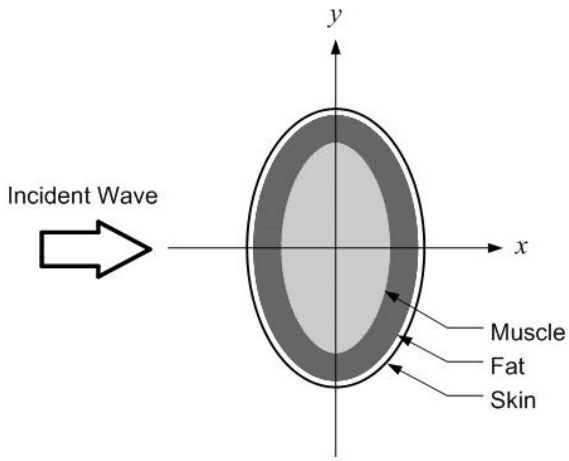

Fig. 6.6 Geometry of the validation model (Nishizawa and Hashimoto, 1999)

In the validation case, the leakage microwave power density of 1 mW/cm^2 at the electromagnetic frequency of 1300 MHz is considered. The results of the selected test case are illustrated in Fig. 6.7 for SAR distribution in the human body.

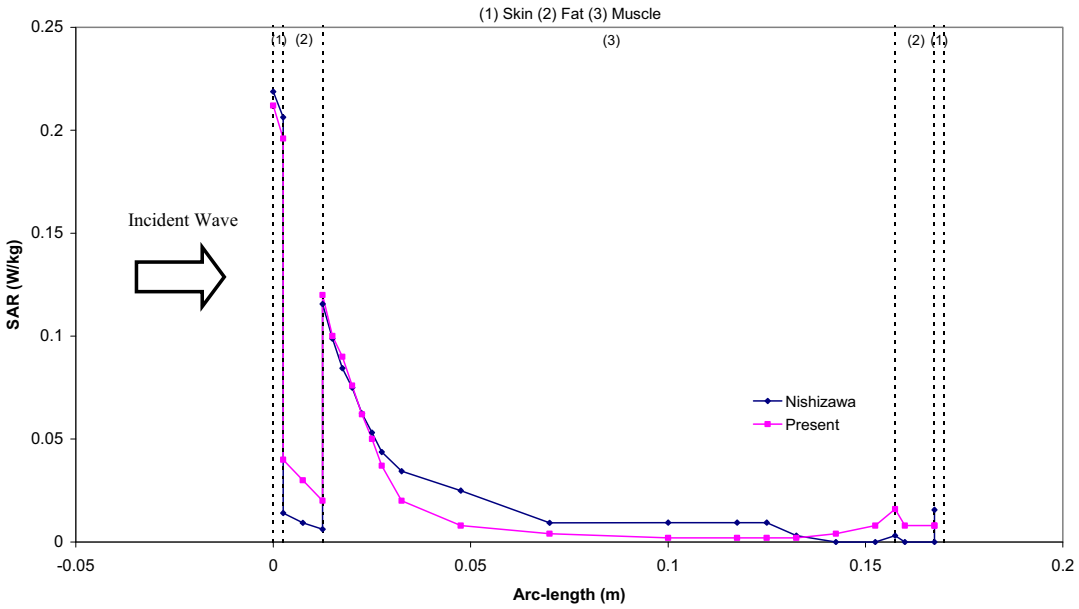

Fig. 6.7 Comparison of the calculated SAR distribution to the SAR distribution obtained by Nishizawa and Hashimoto (Nishizawa and Hashimoto, 1999)

Table 6.4 clearly shows a good agreement of the maximum value of the SAR of tissue between the present solution and that of Nishizawa and Hashimoto (Nishizawa and Hashimoto, 1999). This favorable comparison lends confidence in the accuracy of the present numerical model. It is important to note that there may be some errors occurring in the simulations which are generated by the input dielectric properties data base and the numerical scheme.

Table 6.4 Comparison of the results obtained in the present study with those of Nishizawa and Hashimoto (Nishizawa and Hashimoto, 1999)

	Present work	Published work (Nishizawa and Hashimoto, 1999)	% Difference
SAR_{max} in skin	0.212	0.220	3.63
SAR_{max} in fat	0.198	0.206	3.88
SAR_{max} in muscle	0.116	0.120	3.33

6.4.2 The effects of shield dielectric properties and operating frequency

Fig. 6.8 shows the meshes of the human model as well as the SAR and temperature distribution in the case of unshielded human model exposed to the microwave power density of 5mW/cm^2 at the frequency of 300 MHz. It is found that the temperature distributions are not proportional to the local SAR values. Nevertheless, these are also related to the parameters such as thermal conductivity, dielectric properties, blood perfusion rate and etc.

In the case of using dielectric shield, the dielectric properties for the shield are chosen as (low-loss; 10-*j*5), (medium-loss; 10-*j*10), and (high-loss; 20-*j*20). The shield gap distance and shield thickness are set to 0.5cm and 0.3cm, respectively. Fig. 6.9 and Fig. 6.10 show the maximum SAR and maximum temperature increase, respectively, in the human model with the test frequencies of 300MHz, 915MHz, 1300MHz and 2450MHz.

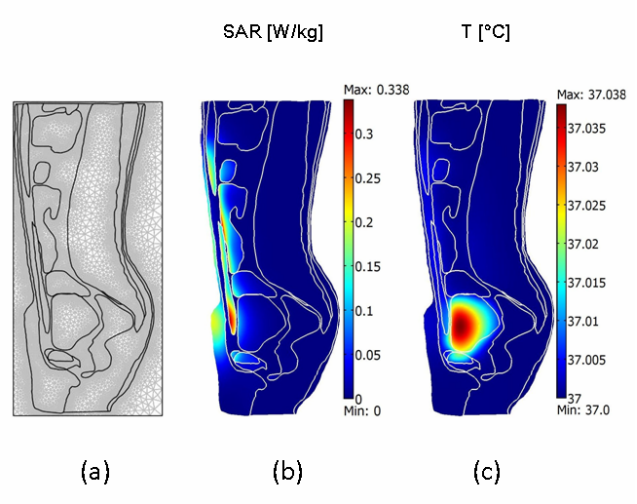

Fig. 6.8 Analysis of SAR and temperature distribution in the human model exposed to the microwave power density of 5mW/cm^2 at the frequency of 300MHz

a. An initial finite element meshes of human cross section model.

b. SAR distribution of the shieldless case.

c. Temperature distribution of the shieldless case

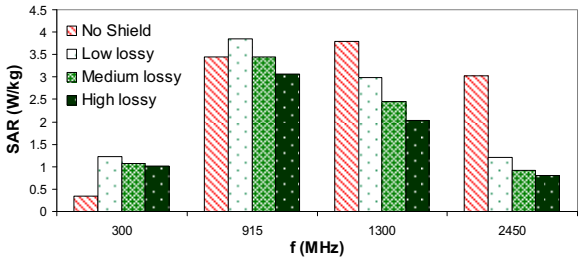

Fig. 6.9 Comparison of the maximum SAR in human model at the frequencies of 300MHz, 915 MHz, 1,300MHz and 2,450 MHz

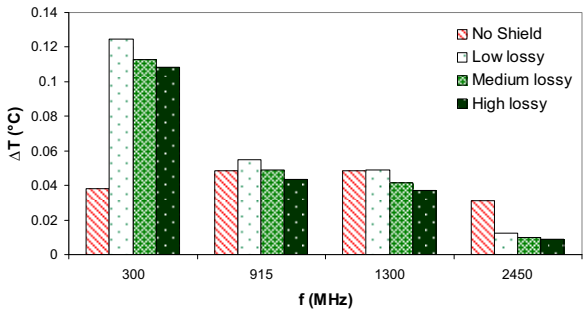

Fig. 6.10 Comparison of the maximum temperature increases in human model at the frequencies of 300MHz, 915 MHz, 1,300MHz and 2,450 MHz

In this section, we illustrate the maximum value of SAR and temperature increase in the human model without attention to the organism. In the unshielded case, the maximum SAR value appeared at 1,300 MHz as shown in Fig. 6.9, while the maximum temperature increase appeared at 915MHz as shown in Fig. 6.10. This is because of the differences of dielectric and thermal properties of tissues cause spatial distortions of the resonance excitation.

Since in this study, the thickness of the dielectric shield is less than the penetration depth, only a part of the supplied microwave energy is absorbed by the dielectric shield and the other parts are allowed to penetrate further through the dielectric shield. This causes the interference of waves penetrate further into the human model and reflected from the human skin travel back to the dielectric shield. Consequently, the reflection and transmission components at each interface contribute to the resonance of standing wave within the gap and the human model.

It is evident from Fig. 6.9 and Fig. 6.10 that in the higher frequency of 1300 and 2450 MHz, when using dielectric shield, a significant reduction of SAR and temperature increase within the human model is achieved because of its smaller penetration depth. However, in the lower frequency of 300MHz corresponding to a long wavelength, the SAR and the temperature increase have higher value than the values of the unshielded case. The reason behind this result is that the penetration depth of the dielectric shield at 300MHz that is much greater than the dielectric shield thickness. This increases a larger part of the incident wave to penetrate further through the dielectric shield and also penetrate into the human model. The great value

of SAR and temperature increase in human model is caused by stronger resonance effects that occur at the low frequencies.

While in the frequency of 915MHz, an insignificant shielding effect of medium lossy dielectric shield is illustrated. It is found that by using low lossy dielectric shield at the frequency of 915MHz, SAR as well as temperature increase is higher compared to values of the unshielded case. This is because the resonance phenomena between the low lossy dielectric shield and human model is displayed stronger. The multiple reflections within the gap and the human model caused the accumulation of microwave energy in the gap which leads to an increase the SAR and temperature in human organism by which the reflection rate of microwave strongly depends on the dielectric properties of the dielectric shield. By using the high lossy dielectric shield, the shielding effect is significant. This is because of a large reduction of microwave power density within the human model due to the weakness of resonance, corresponding to the lowering penetration depth of microwave. It is confirmed that the appropriate dielectric properties of the dielectric shield greatly depend on the operating frequencies.

6.4.3 SAR in organs

As shown in Fig. 6.11, based on the results of the local maximum SAR of the unshielded case, at a low frequency of 300 MHz, peak values of SAR occurred, found both in the small intestine and the muscle. With the use of the low lossy shield, the greater values of SAR occurred as compared to the unshielded case. This is because of a larger part of the incident wave that penetrates further into the gap and human model. This caused the accumulation of microwave energy in the gap and the human model. Fig. 6.12 shows the maximum SAR in organs at a high frequency of 2,450MHz. It is clearly evident from Fig. 6.12 that a peak value of local SAR is found only at the skin due to a smaller penetration depth at high frequency range. However, large reduction of the SAR value is achieved when using the same dielectric shield (low-loss shield) with the case of 300 MHz due to the weakness of resonance.

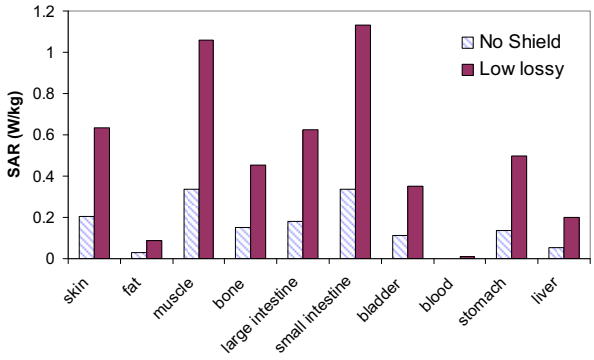

Fig. 6.11 Comparison of the maximum SAR in human organs of the unshielded and shielded human model at the frequency of 300 MHz

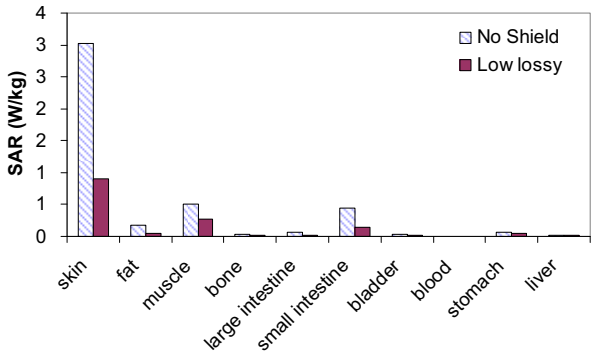

Fig. 6.12 Comparison of the maximum SAR in human organs of the unshielded and shielded human model at the frequency of 2,450 MHz

Fig 6.11 and 6.12 show the maximum SAR and the maximum temperature increase in the human model, with focusing on the human organism. It is found that the SAR and the temperature increase primarily depend on the penetration depth of microwave which corresponds to the operating frequency as well as the dielectric properties of the dielectric shield. As the dielectric properties of a dielectric shield vary, the penetration depth will be changed and the electric field passing through the dielectric shield is altered. If the penetration depth is changing, a fraction of the microwave energy absorbed is also changed which related to the resonance within the model. Consequently, the shielding effect of dielectric shield is changed.

6.5 Conclusions

This work presents the simulations of SAR and heat transfer in the human model, where microwave energy strikes the dielectric shield in front of the human model. The SAR and temperature distributions in the human model are governed by the electric field as well as the dielectric properties of tissue.

The results show an interaction between physical parameters: operating frequencies and shield dielectric properties. For human exposure to microwave energy, the installed dielectric shield strongly affects the SAR and the temperature increase in the human body. Actually, the microwaves can transmit through the dielectric shield, and can penetrate into the human model that contribute to the resonance of standing wave with in the gap and human model.

Since the frequency increases, the penetration depth for microwave gets smaller and resonance effect becomes weakness. Consequently, the shielding effect is significant. Therefore, the appropriate dielectric properties, which can effectively reduce the SAR and the temperature increase in human body of the dielectric shield, are greatly dependent on the operating frequency. Additionally, this work presents an interesting viewpoint on the microwave shielding properties of dielectric shields at various operating frequencies, with focusing on the human organism.

CHAPTER 7

OVERALL CONCLUTIONS

The drying of parawood pake has been interested by many researchers and become complex, coupled, and multiphase processes with a wide range of applications in industry. In addition, as a result of high cost of energy, an operation with a high potential for optimizing with respect to energy savings has been realized. For many years, it has been studied experimentally for measuring drying kinetics on the macro-scale.

The fore mentioned works concerned mainly with, energy analyses of drying process. Normally, most of wood in the drying process are bio materials. In the recent works the authors were mention about bio materials structure, with are concern with energy analysis of drying process. The main purposes of this research are as follows;

1. To develop the mathematical models of calculating for the specific energy consumption(SEC) and energy efficiency in drying process within sample in convection drying and a Combined Unsymmetrical Multi-Feed Microwave and Hot Air-Continuous Belt System (CMCB)

2. To study the influence of operating parameters and drying kinetic on energy analysis in convection drying and a Combined Unsymmetrical Multi-Feed Microwave and Hot Air-Continuous Belt System (CMCB) in order to apply the analysis results to achieve in industrial applications

Through the numerous investigations performed in this work, many valuable conclusions can be drawn. They can be summarized as follows:

1. Energy analysis of the drying process of the parawood pake were carried out in this study. Taking in to considerations the result from these analyses, the following conclusion may be drawn on energy utilization, energy utilization ratio decreased with decreasing drying time.

2. The effects of applied position feed microwave power level configuration on the overall drying kinetics are clarified. The drying rate in the specimen (parawood pake) top feed magnetron is higher than that of the screw feed magnetron . It has a shorter drying time due to the microwave energy on the material directly.

3. Energy of the drying process of the parawood pake are analyzed. It can be

concluded that energy efficiency also depend on location of magnetron position feed magnetron , convective air temperature.

The CMCB technique developed in this study has been proven to be a promising technique for the drying of parawood pake products. Theoretical model developed has been experimentally validated and used to predict CMCB drying behavior. There is vast opportunity for further studies relating to both practical and theoretical aspects of this drying technique. Future studies could be directed to following topics:

A combined electromagnetic field and energy analysis is needed. This is the only way to accurately calculate energy consumption of products during CMCB drying. For bio materials, an assumption of energy efficiency is acceptable. For large objects, however, this assumption will cause not cause a crash.

REFERENCES

Abbasi Souraki, B., Mowla, D.(2007) Experimental and theoretical investigation of drying behaviour of garlic in an inert medium fluidized bed assisted by microwave, *J.Food Engineering.,* 88, pp.438-449.

Abbasi Souraki, B., Mowla, D.(2008) Simulation of drying behaviour of a small spherical foodstuff in a microwave assisted fluidized bed of inert particles, Food Research International., 41, pp.255–265.

Aghbashlo, M., Kianmehr, M.H and Arabhosseini, A., (2008) Energy and Exergy Analyses of Thin-Layer Drying of Potato Slices in a Semi-Industrial Continuous Band Dryer, *Drying Technology*, 26,pp.1501–1508.

Akpinar, E. K. (2004) Exergy and energy analysis of drying of red pepper slices in a convective type dryer, Int.Comm.Heat Mass Transfer., 31,pp.1165-1176.

Akpinar, E.K., Midilli, A., Bicer,Y., (2005) Energy and Exergy of Potato Drying Process Via Cyclone Type Dryer, *Int. Energy Conversion and Management*, 46,pp.2530–2552.

Alibas, I. (2007) Energy Consumption and Colour Characteristics of Nettle Leaves During Microwave, Vacuum and Convective Drying, *Biosystems Engineering*, 96(4), pp. 495–502

Alibas, I. (2006) Microwave, air and combined microwave–air-drying parameters of pumpkin, *Swiss Society of Food Science and Technology*, 40,pp.1445–1451

AOAC (1995) Official methods of analysis of AOAC international (16th ed.), USA.

Atong, D., Clark, D.E. (2003) The Effect of Reaction Parameters on Microwave Induced Combustion Synthesis of AI203TiC Composite Powders, Microwave and Radio Frequency Applications. *American Ceramics Society*, Westerville, OH pp. 207-220

Atong, D., Rattanadecho, P. and Vongpradubchai, S. 2006) Drying of a slip casting for tableware product using microwave continuous belt, Drying Technology, 24, pp.589–594.

Alibas, I., (2007) Energy Consumption and Colour Characteristics of Nettle Leaves during Microwave, Vacuum and Convective Drying, Biosystems Engineering ,96(4),pp.495–502.

Ayappa, K.G., Davis, H.T., Davis, E.A. and Gordon, J.(1991) Analysis of microwave heating of materials with temperature dependent properties, *AIChE J*., 37(3), pp. 313-322.

Boyaci, I.H., Sumnu, G., and Sakiyan, O. (2009) Estimation of dielectric properties of cakes based on porosity, moisture content, and formulations using statistical methods and artificial neural networks. *Food Bioprocess Technology*, doi:10.1007/s11947-008-0064-z.

Buffer, C.R. (1993) Microwave Cooking and Processing, Engineering Fundamentals *for the Food Scientist, AVI book* , Van Nostand Reinhold, New York

Cengel,Y.A. and Boles, M.A.(2002) Thermodynamics:An Engineering Approach, McGraw-Hill Companies, Inc., New York.

Cha-um, W., P. Rattanadecho, P. and Pakdee, W. (2009) Experimental analysis of microwave heating of dielectric materials using a rectangular wave guide (MODE: TE10) (Case study: water layer and saturated porous medium*), Int. J. Experimental Thermal and Fluid Science*,33,pp. 472-481

Cheng, J., Zhou, J., Li, Y., Liu, J. and Cen, K.(2008) Improvement of coal water slurry property through coal physicochemical modifications by microwave irradiation and thermal heat, *Energy & Fuels*, 22, pp.2422–2428.

Chow T.V.and Reader H.C. (2000) Understanding Microwave Heating Cavities, Artech House.

Curet, S., Rouaud, O., Boillereaux, L. (2008) Microwave tempering and heating in a single-mode cavity: Numerical and experimental investigations *Chemical Engineering and Processing: Process Intensification*, 47 (9-10), pp. 1656-1665.

Datta, A.K., Anantheswaran, R.C. (2001). *Handbook of Microwave Technology for Food Applications*. Marcel Dekker, New York

Das, T., Subramanian,R., Chakkaravarthi, A., Singh,V., Ali, S.Z., Bordoloi, P.K., (2006) Energy Conservation in Domestic Rice Cooking, *Journal of Food Engineering*, 75,pp.156–166

Dincer, I. and Sahin, A.Z. (2004) A new model for thermodynamic analysis of a drying process, *International Journal of Heat and Mass Transfer*, 47, pp.645-652.

Dincer, I., Rosen, M. A., (2002) Energy, Environment and Sustainable Development, Elsevier Ltd., Burlington.

Duerr, L.,(1982) Proceedings of the Short Course: Microwave Technology and Applications for Industry (1982), Center for Professional Advancement, East Brunswick, New Jersey.

Decareau R.V. (1985) *Microwave in the food processing industry*, New York: Academic Press.

Feng, H. Tang, J. Cavalieri, R.P. and Plumb, O.A. (2001) Heat and mass transport in microwave drying of porous materials in a spouted bed, *A.I.Ch.E. J.,* 47,pp. 1499-1512.

Feng, H. Tang, J. (1998) Microwave finish drying of diced apple slices in a spouted bed, *Journal of Food Science*, 47, pp.1499-1512.

Goksu, E.I., Sumnu, G. and Esin, A.(2005) Effect of microwave on fluidized bed drying of macaroni beads, *Journal of Food Engineering*, 66, pp. 463-468.

Guranunal.H., Sacilik.K., (2009) Drying Characteristics of Hathorn Fruits in A Convective Hot-Air Dryer, *Journal of Food Processing and Preservation* ,35,.pp.272-279

Holtz, E., Ahrné, L., Karlsson, T. H., Rittenauer, M. and Rasmuson, A.(2009) The role of processing parameters on energy efficiency during microwave convective drying of porous materials, *Drying Technology*, 27, pp. 173–185.

Incropera, F.P., David, P., Dewitt, D.P., Bergmann,T.L. and Lavine, A.(2007) *Fundamental of Heat and Mass Transfer*, John Wiley & Sons(Asia) Pte, Ltd., Danvers.

Jindarat, W., Rattanadecho, P. and Vongpradubchai, S.(2010) Analysis of energy consumption in microwave and convective drying process of multi-layered porous material inside a rectangular wave guide, *Int. J. Exp. Therm. Fluid Sci.,* 35, pp.728-737.

Jeni, K., Yapa, M. and Rattanadecho, P., (2010) Design and Analysis of the Commercialized Drier Processing Using a Combined Unsymmetrical Double-Feed Microwave and Vacuum System(Case Study: Tea Leaves)**,** Chemical Engineering and Processing:Process Intensification, 49, pp.389-395

Kent, M. (1977) Complex Permittivity of Fishmeal: A General Discussion of Temperature Density and Moisture Dependence, *J. Microwave Power,* 12, pp.341-345.

Lakshmi, S., Chakkaravarthi, A., Subramanian, R., Singh, V. (2005) Energy consumption in microwave cooking of rice and its comparison with other domestic appliances, *J.Food Engineering.,* 78, pp.715-722.

Leiker, M. and Adamska, M. A.(2004) Energy efficiency and drying rates during vacuum microwave drying of wood, *Holz Roh Werkst*, 62, pp. 203–208.

Maroulis, Z.B., Saravacos, G.D., and Mujumdar, A.S.(2006) *Handbook of Industrial Drying*, Taylor & Francis Group.,Singapore.

Markowski, M., Bondaruk, J. and Błaszczak, W.(2009) Rehydration behavior of vacuum-microwave-dried potato cubes, *Drying Technology*, 27, pp. 296-305.

Metaxas, A.C., Meridith, R.J. (1983). Industrial Microwave Heating. Peter Peregrinus, Ltd, London

Metaxas, AC., (1974) Design of a TM_{010} Resonant Cavity as a Heating Device at 2.45 GHz. *J. Microwave Power*, 9(2),pp. 123-128.

Men'Shutina, N.V., M.G.Gordienko, M.G., Voinovskii, A.A. and Kudra, T.(2003) Dynamics criteria for evaluating the energy consumption of drying equipment, *Theoretical Foundations of Chemical Engineering*, 39,pp158-162.

Mihoubi, D. and Bellagi, A.(2009) Drying-induced stresses during convective and combined microwave and convective drying of saturated porous media, *Drying Technology*, 27, pp. 851-856.

Midilli. A; Kucuk H; Yapar, Z., (2002). A New Model for Single Layer Drying, *Drying Technology*, 20(7), pp.1503–1513

Mujumdar, A.S. (1995). *Handbook of Industrial Drying*. 2nd ed., Marcel Dekker, New York

Mwithiga, G. and Olwal, J.O. (2005) The drying kinetics of kale (Brassica oleracea) in a convective hot air dryer, *Journal of Food Engineering*, 71, pp.373–378

Guranunal.H., Sacilik.K., (2009) The Drying Kinetics of Kale (Brassica Oleracea) in A Convective Hot Air Dryer, *Journal of Food Engineering*, 71,pp.373–378.

Ogura, H. Hamaguchi, N., Kagea, H. and Mujumdar, A.S. (2004) Energy and cost estimation for application of chemical heat pump dryer to industrial ceramics drying, *J. Drying technology,* 22,pp.307-323.

Ogura, H., Hamaguchi, N., Kage, H., and Mujumdar, A.S.,(2004) Energy and Cost Estimation for Application of Chemical Heat Pump Dryer to Industrial Ceramics Drying, *Drying Technology*, 22 (1&2), pp.307-324.

Ohlsson, T. Bengtsson, N.E. and Risman, P.O. (1974) The Frequency and Temperature Dependence of Dielectric Food Data as Determined by a Cavity Perturbation Technique, *J. Microwave Power*, 9(2), pp. 129.

Perré, P., Turner, I.W. (1997) Microwave Drying of Softwood in an Oversized Waveguide: Theory and Experiment *AIChE Journal*, 43 (10), pp. 2579-2595.

Poli, G., Sola, R. and Veronesi, P.(2006) Microwave-assisted combustion synthesis of NiAl intermetallics in a single mode applicator: Modeling and optimization, *Materials Science and Engineering*, A 441, pp.149–156.

Pozar,D.M. (2005) Microwave engineering, 3rd , Jones Wiley & Sons, USA

Prommas, R., Rattanadecho, P. and Cholaseuk, D.(2010) Energy and exergy analyses in drying process of porous media using hot air, *Int. Commun. Heat Mass Transfer*, 37, pp. 372–378.

Ratanadecho, P., Aoki, K., Akahori, M. (2001) Experimental and numerical study of microwave drying in unsaturated porous material *International Communications in Heat and Mass Transfer*, 28 (5), pp. 605-616.

Ratanadecho, P., Aoki, K., Akahori, M. (2001) A numerical and experimental study of microwave drying using a rectangular wave guide *Drying Technology*, 19 (9), pp. 2209-2234.

Ratanadecho, P., Aoki, K., Akahori, M. (2002) Influence of irradiation time, particle sizes, and initial moisture content during microwave drying of multi-layered capillary porous materials *Journal of Heat Transfer*, 124 (1), pp. 151-161.

Ratanadecho, P., Aoki, K., Akahori, M. (2002) The characteristics of microwave melting of frozen packed beds using a rectangular waveguide *IEEE Transactions on Microwave Theory and Techniques*, 50 (6), pp. 1495-1502.

Rattanadecho, P. (2006) The simulation of microwave heating of wood using a rectangular wave guide: Influence of frequency and sample size *Chemical Engineering Science*, 61 (14), pp. 4798-4811.

Rattanadecho, P., Suwannapum, N., Chatveera, B., Atong, D., Makul, N. (2008) Development of compressive strength of cement paste under accelerated curing by using a continuous microwave thermal processor *Materials Science and Engineering A*, 472 (1-2), pp. 299-307.

Rattanadecho, P., Suwannapum, N., Watanasungsuit, A., Duanduen, A. (2007) Drying of dielectric materials using a continuous microwave belt drier (Case study: Ceramics and natural rubber) *Journal of Manufacturing Science and Engineering, Transactions of the ASME*, 129 (1), pp. 157-163.

Rattanadecho, P , Duangduen, A., Vongpradubchai, S. (2006) Drying of a Slip Casting for Tableware Product Using Microwave-Continuous Belt Furnace.", *Drying Technology An International J.*, Vol. 26, pp. 589-594,

Ratti, C., Araya-Farias, M., Mendez-Lagunas, L., Makhlouf, J.,(2007) Drying of Garlic (Allium sativum) and Its Effect on Allicin Retention, *Drying Technology*, 25,pp.349–356.

Risman P.O., Ohlsson T., Wass B. (1987) Principles and models of power density distribution in microwave oven loads. *J. Microwave Power EE,* pp.193-198.

Rogers J.A., Kaviany M., (1992) Funicular and Evaporative-Front Regimes in Convective Drying of Granular Beds, Int. *J. Heat Mass Transfer*, 35(2), pp.469-480.

Sander, A.(2007) Thin-layer drying of porous materials: Selection of the appropriate mathematical model and relationships between thin-layer models parameters, *Chem. Eng. Process* , 46, pp. 1324-1331.

Salagnac, P., Dutournie´, P. and Glouannec, P.(2008) Optimal operating conditions of microwave-convective drying of a porous medium, *Ind. Eng. Chem. Res*, 47, pp.133-144.

Schiffmann, R.F. (1995) *Microwave and dielectric drying: in handbook of industrial drying*, Marcel Dekker, New York.

Schubert, H., Regier, M. (2005). The Microwave Processing of Foods. Woodhead Publishing Limited and CRC Press, Cambridge

Sharma, G.P.; Prasad, S. (2005) Specific energy consumption in microwave drying of garlic cloves, *J. Food Engineering*. 31, pp.1921-1926.

Sousa,L.H.C.D., Lima, O.C.M, Pereira. N.C,(2006) Analysis of Drying Kinetics and Moisture Distribution in Convective Textile Fabric Drying, *Drying Technology*, 24,pp.485–497.

St-Denis, E., (1998). Performance Optimization of a Multi-slotted Waveguide for Microwave Processing, Unpublished Ph.D. Thesis. McGill University, Montreai, Canada.

Sunjka, P.S., Rennie, T.J., Beaudry, C. and Raghavan, G.S.V.(2004) Microwave-convective and microwave-vacuum drying of cranberries: A comparative study, *Drying Technology*, 22 (5), pp.1217-1231.

Syahrul, S., Hamdullahpur, F. and Dincer, I. (2002) Exergy analysis of fluidized bed drying of moist particles, *Int. J. Energy.* 2, pp.87–98.

Syahrul, S., Hamdullahpur, F. and Dincer, I. (2003) Thermodynamic modeling of fluidized bed drying of moist particles, Int. J. Thermal Sciences, 42 ,pp.691–701.

Syahrul, S., Hamdullahpur, F. and Dincer, I. (2002) Thermal analysis in fluidized bed drying of moist particles, Int. J. Applied Thermal Engineering,22, pp.1763–1775.

Soysal, Y., öztekin, S. and Eren, ö.(2006) Microwave drying of parsley: Modelling, kinetics, and energy aspects, Biosystems Engineering, 93 (4), pp. 403–413.

Turner, I.W., Jolly, P.G. (1991) Combined microwave and convective drying of a porous material *Drying Technology*, 9 (5), pp. 1209-1269.

Varith, J.; Dijkanarukkul, P.; Achariyaviriya, A.; Achariyaviriya, S. (2007) Combined microwave-hot air drying of peeled longon , J. Food Engineering., 31, pp.459-468.

Vadivambal, R. and Jayas, D.S. (2009) Non-uniform temperature distribution during microwave heating of food materials A-review, *Food Bioprocess Technology*, doi:10.1007/s11947-008-0136-0.

Vongpradubchai, S.; Rattanadecho, P. (2009) The microwave processing of wood using a continuous microwave belt drier, Chem. Eng. Process., 33, pp.472-481.

Yamsaengsung, R.; Tabtiang, S.(2011) Hybrid drying of rubberwood using superheated steam and hot air in a pilot-scale, *Drying Technology*, 29,pp. 1170-1178.

Waje, S.S., B. N., Thorat,B.N., Mujumdar. A. S.(2007) Screw Conveyor Dryer: Process and Equipment Design, *Drying Technology*, 25,pp. 241–247.

Zhang, Y., Liu, R., Hu, Y. and Li, G.(2009) Microwave heating in preparation of magnetic molecularly imprinted polymer beads for trace Triazines analysis in complicated samples, *Anal. Chem*., 81, pp. 967–976.

Appendix

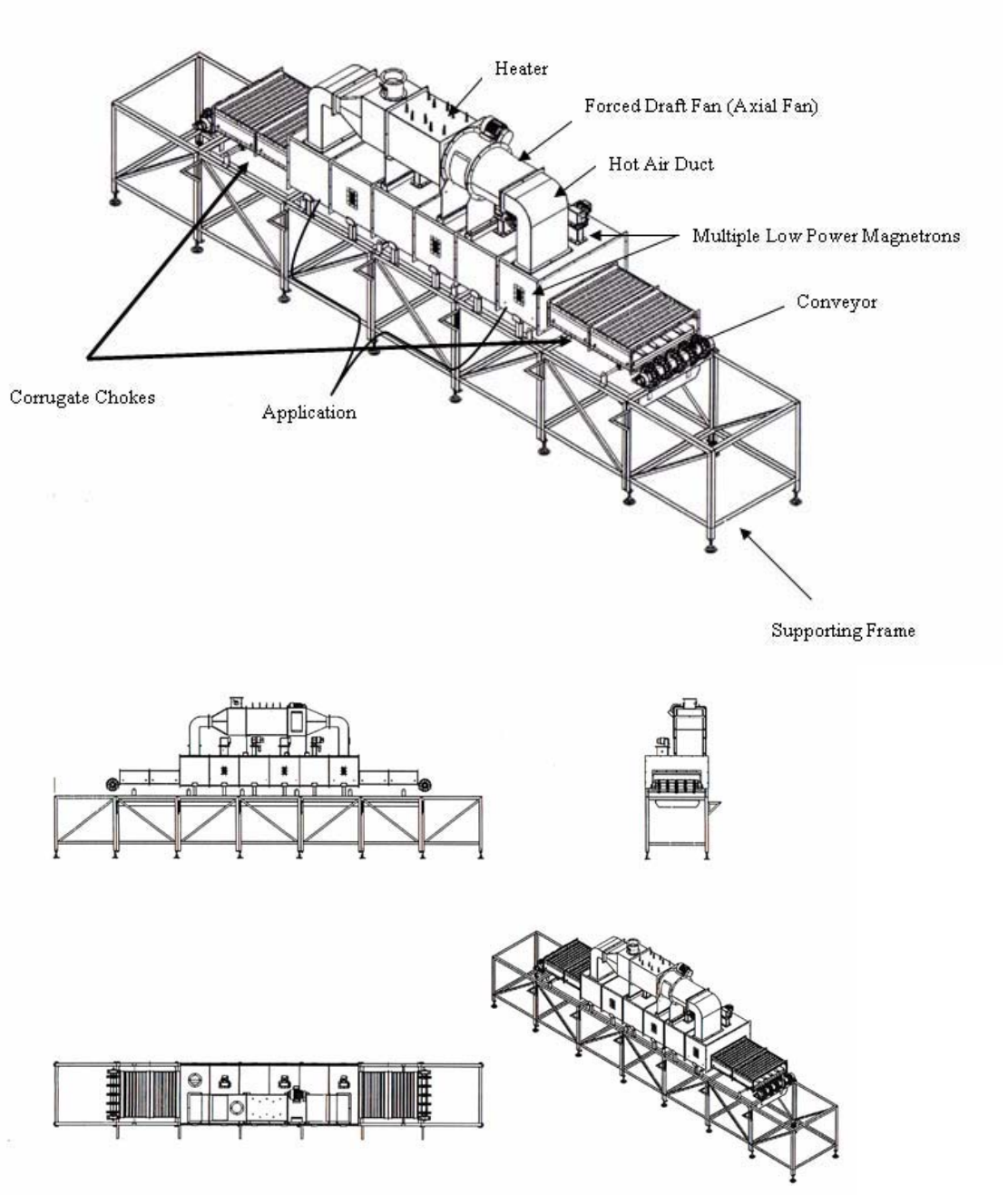
Heater
Forced Draft Fan (Axial Fan)
Hot Air Duct
Multiple Low Power Magnetrons
Conveyor
Corrugate Chokes
Application
Supporting Frame

(a)

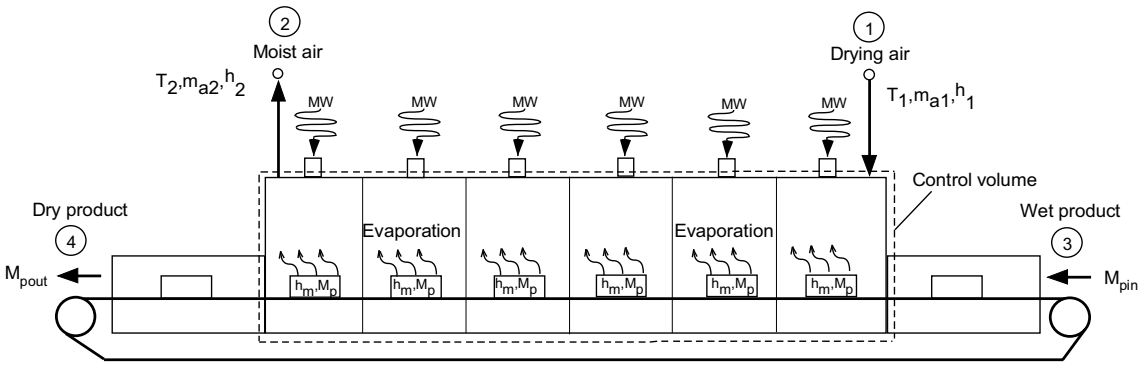

(b)

Schematic Diagram of a Combined Multi-Feed Microwave - Convective Air and Continuous Belt System (CMCB)

First Pilot Plant has been designed

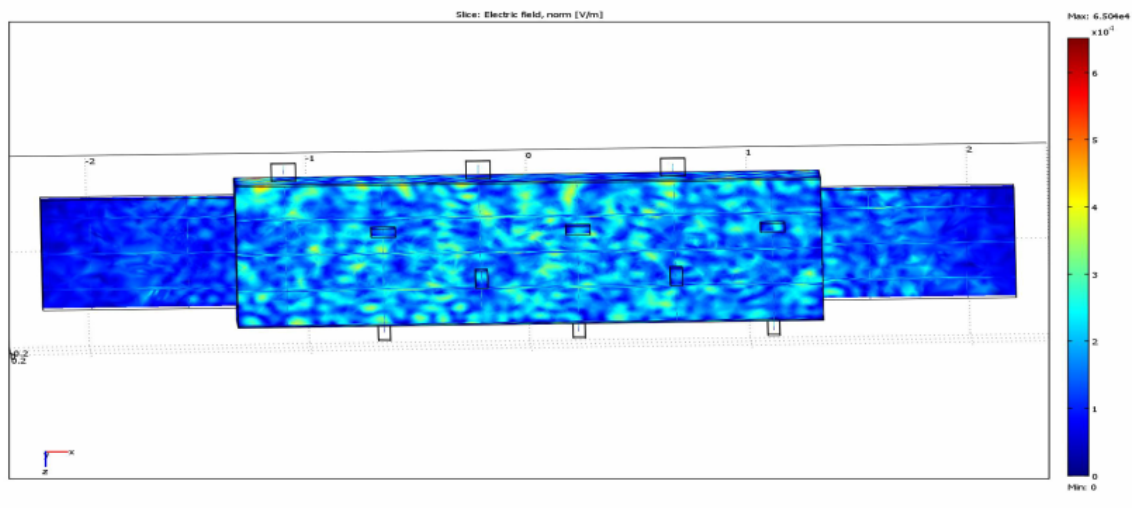

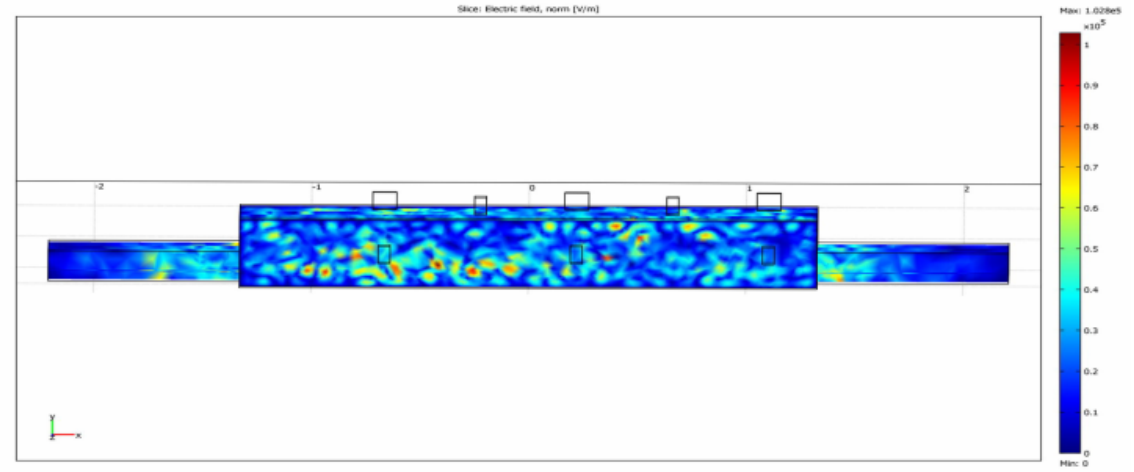

Computer simulation of electromagnetic field inside multi-mode cavity

Hand on for a Combined Multi-Feed Microwave - Convective Air and Continuous Belt System (CMCB)

Ready to Implementation in Drying Process

The Completing CMCB

Experiment

Sample feeding

Sample before dried with Combined Multi-Feed Microwave - Convective Air and Continuous Belt System (CMCB)

Sample after dried with Combined Multi-Feed Microwave - Convective Air and Continuous Belt System (CMCB)

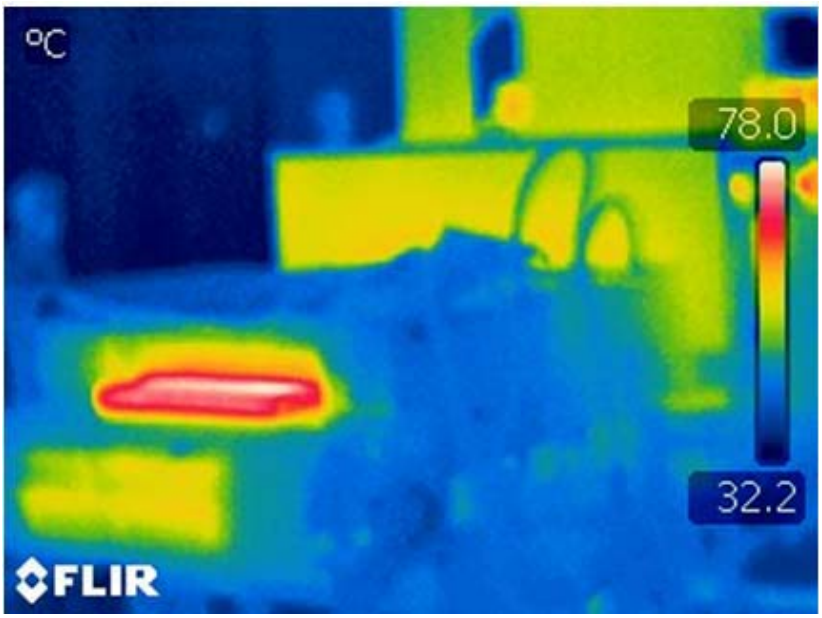

Sample at the outlet of CMCB

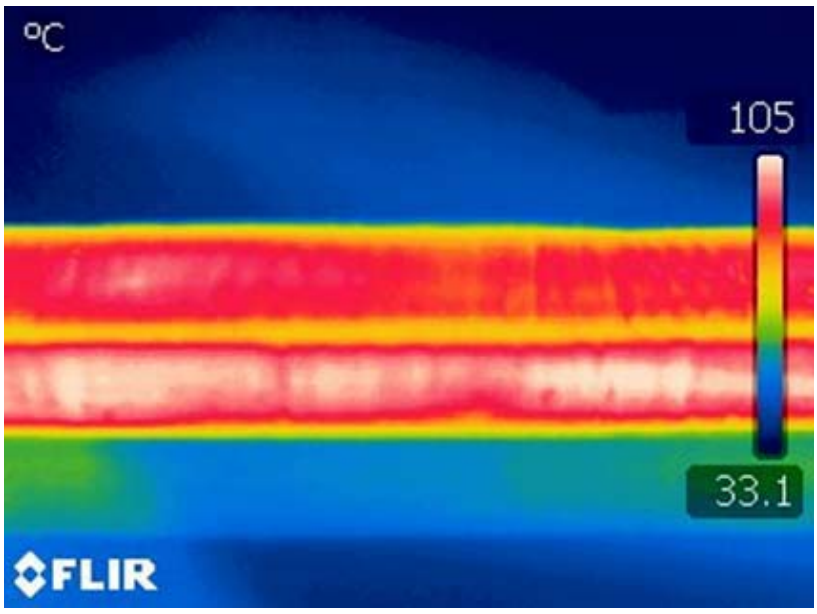

Temperature distribution with uniformity pattern in *Wood Sample* showing the Excellency performance of CMCB developed by Prof. Phadungsak Rattanadecho

Thermally Imaged depicted by **FLIR Thermography - Infrared Cameras & Thermal Imagers**

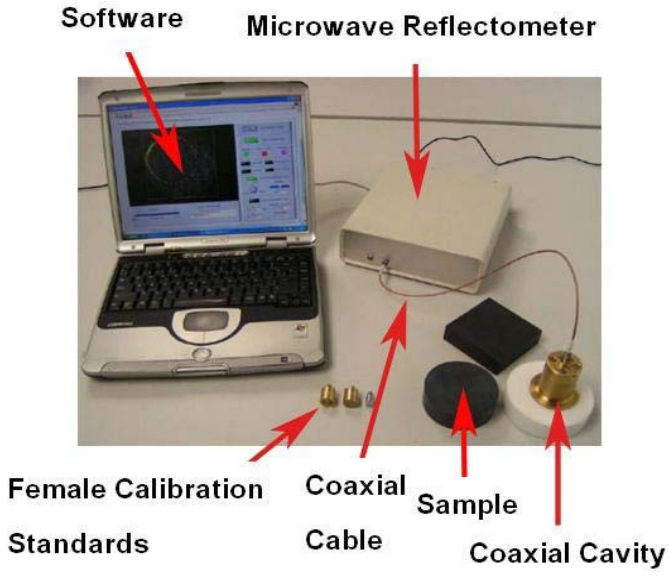
Software
Microwave Reflectometer
Female Calibration Standards
Coaxial Cable
Sample
Coaxial Cavity

(a)


Optical Fiber Optics
Software
Microwave Reflectometer
Female Calibration Standards
Coaxial Cable
Sample
Coaxial Cavity
Network Analyzer System
Microwave-Rectangular Waveguide System
Digital Readout MW leakage Detector
Microwave Spouted Bed Drier
RCME

(b)

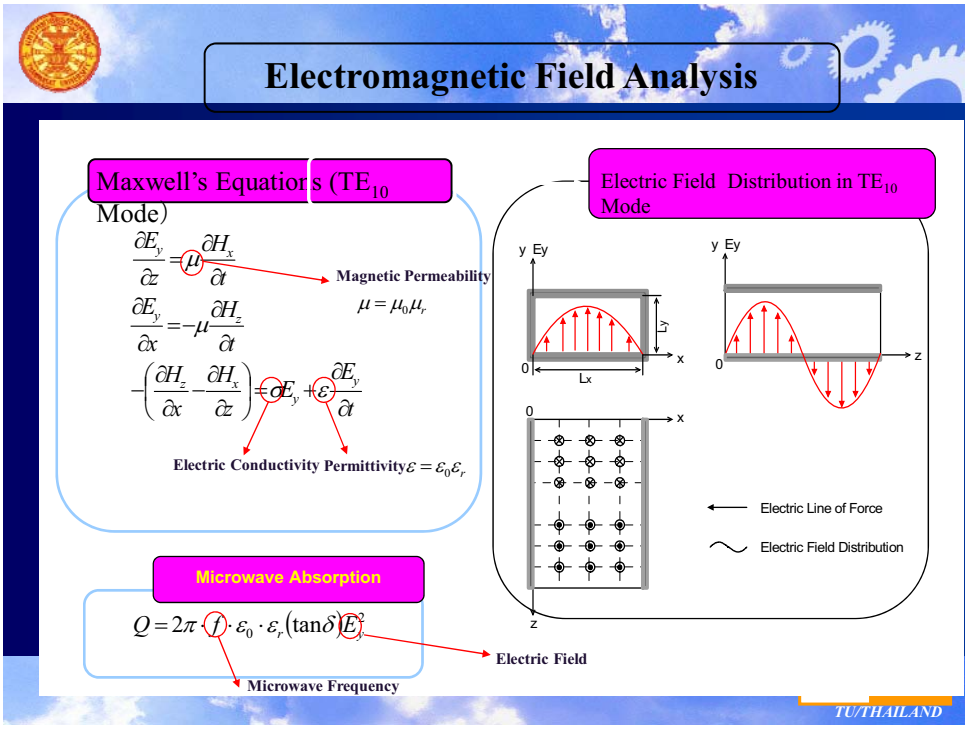

(c)

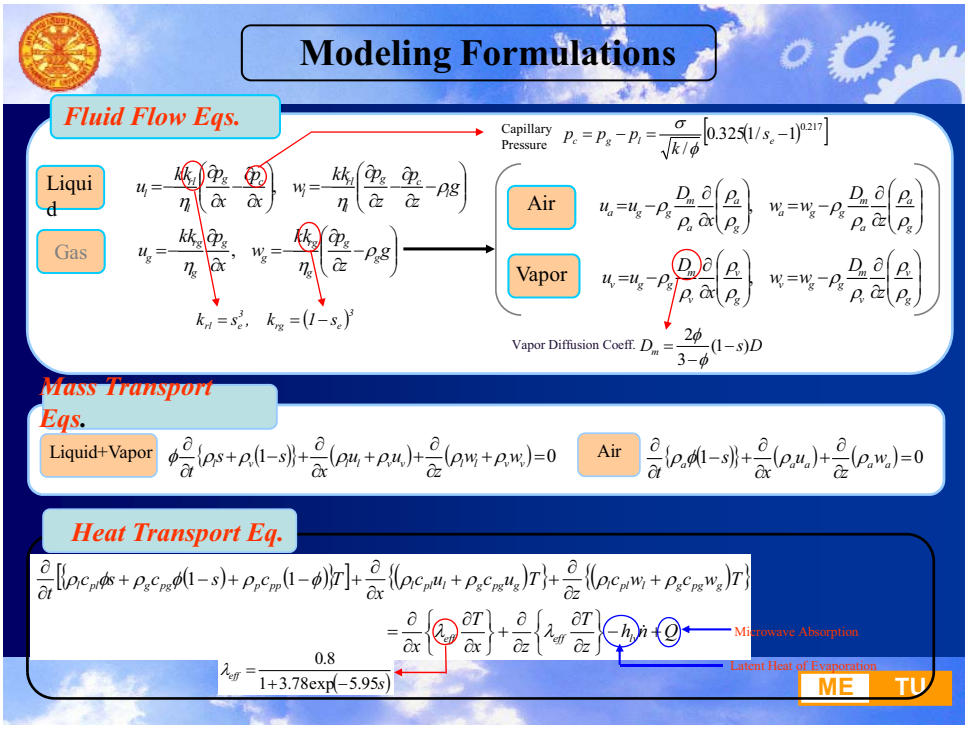

(d)

Facilities used in this research project

PUBLICATIONS

1. Jindarat, W., Rattanadecho, P., Vongpradubchai, S. and Pianroj, Y., **"Analysis of Energy Consumption in Drying Process of Non-Hygroscopic Porous Packed Bed Using a Combined Multi-Feed Microwave - Convective Air and Continuous Belt System"**, Drying Technology An International J., Vol.29(08), pp. 926 - 938, 2011 : Impact factor 1.662

2. Jindarat, W., Rattanadecho, P.and Vongpradubchai, S.**"Analysis of Energy Consumption in Microwave and Convective Drying Process of Multi-Layer Porous Material Inside a Rectangular Wave Guide"**, Experimental Thermal and Fluid Science. 35, pp.728-737,2011: Impact factor 1.234

3. Vongpradubchai, S. and Rattanadecho, P.,**"The Microwave Processing of Wood Using a Continuous Microwave Belt Drier"** Chemical Engineering and Processing:Process Intensification , Vol 48(5), pp 997-1003, 2009 : Impact factor 1.518

4. Wessapan, T, Srisawatdhisukul, S., and Rattanadecho, P**.** "**Numerical Analysis of Specific Absorption Rate and Heat Transfer in the Human Body Exposed to Leakage Microwave Power at 915 MHz and 2,450 MHz**". ASME JOURNAL OF HEAT TRANSFER ,Vol 133(5), pp.051101.1-13, 2011: Impact factor 1.200

5. Wessapan, T, Srisawatdhisukul, S., and Rattanadecho, P**." The effects of dielectric Shield on specific Absorption Rate and Heat Transfer in The Human Body Exposed to Leakage Microwave energy"** International Communications in Heat and Mass Transfer, 38, pp.255-262, 2011 Impact Factor 1.189

Experimental Thermal and Fluid Science 35 (2011) 728–737

Contents lists available at ScienceDirect

Experimental Thermal and Fluid Science

journal homepage: www.elsevier.com/locate/etfs

Analysis of energy consumption in microwave and convective drying process of multi-layered porous material inside a rectangular wave guide

W. Jindarat, P. Rattanadecho *, S. Vongpradubchai

Research Center of Microwave Utilization in Engineering (RCME), Department of Mechanical Engineering, Faculty of Engineering, Thammasat University (Rangsit Campus), Pathumthani 12120, Thailand

ARTICLE INFO

Article history:
Received 30 September 2009
Received in revised form 5 August 2010
Accepted 24 November 2010
Available online 28 November 2010

Keywords:
Microwave energy
Drying process
Multi-layered porous material
Specific energy consumption (*SEC*)
Energy efficiency

ABSTRACT

This work applies the first law of thermodynamics to estimate the ratio of energy utilization in microwave drying process using a rectangular waveguide. Two porous packed bed systems are considered such as attaching fine bed on coarse bed (F–C) and attaching coarse bed on fine bed (C–F). The effects of layered configuration and layered thickness on drying rate, power absorbed efficiency, specific energy consumption (*SEC*), and energy efficiency are studied in detail. The results show that the variations of all parameters have strongly affected on microwave penetration depth and power absorbed within the packed bed. Furthermore, F–C bed with equal layer thickness corresponds to great energy efficiency.

1. Introduction

Energy used in the drying and heating process is important for production processes in the industrial and household sectors. However, the price of energy is extremely expensive; therefore, there are a strong incentive to invent processes that will use energy efficiently. Currently, widely used drying and heating processes are complicated and inefficient; moreover, it is generally damaging to the environment. What is needed is a simplified, lower-cost approach to this process one that will be replicable in a range of situations.

The conventional drying process had been a central subject for research and development was investigated by Maroulis et al. [1] where a study of drying parameter to apply the design for conveyor belt drying has carried out: a study by Men'Shutina et al. [2] focused on thermal efficiency in the conveyor belt dryer process, and Akpinar [3] analyzed the energy and exergy in red of pepper slices drying with a convective-type dryer.

For an analysis of energy consumption during applied microwave energy on heating and drying processes has been investigated by many researches. Sharma and Prasad [4], this study examined the specific energy consumption in microwave drying of garlic cloves. The drying processes used to microwave and hot air drying in accordance with microwave oven for comparing specific energy consumption (*SEC*). Other important papers [1–13] were addressing the combined microwave energy and hot air drying processes for several kinds of dielectric materials. Such as Varith et al. [5], was studying of the combined microwave and hot air drying of peeled longan, which investigated the variation of moisture content and *SEC* in several drying conditions. Another important studied, Lakshmi et al. [6], was comparison the variation of *SEC* in cooking rice among the microwave oven, electric rice cooker and pressure cooker.

For theoretical research, Ratanadecho et al. [7] studied the influence of irradiation time, particle size, and initial moisture content on drying kinetics during microwave drying of multi-layered capillary porous materials in a rectangular waveguide. Feng et al. [8] carried out combined microwave and spouted bed drying process for diced apple. Experimental results of heat and mass transport were the compared to the results from a mathematical model.

From the previous works, the effects of sample structure and the *SEC* were minimal studied in drying processes. The objective of this study is to experimentally analyze the effects of layered configuration and layered thickness on the microwave drying of multi-layered porous packed bed with a rectangular waveguide. An operating frequency is 2.45 GHz. The knowledge gained will provide an understanding in porous media and the parameters which can help to reduce the *SEC*.

* Corresponding author. Tel.: +66 02 564 3001 9, fax: +66 02 564 3010.
E-mail address: ratphadu@engr.tu.ac.th (P. Rattanadecho).

0894-1777/$ - see front matter © 2010 Elsevier Inc. All rights reserved.
doi:10.1016/j.expthermflusci.2010.11.008

Nomenclature

A	porous packed bed surface area (m^2)
C_p	specific heat of the dielectric material (kJ/kg K)
c_m	material specific heat (kJ/kg K)
D_p	penetration depth (m)
d_p	dept of packed bed (mm)
E	electromagnetic field intensity (V/cm)
f	microwave frequency (Hz)
h	enthalpy (kJ/kg)
h_m	enthalpy of material (kJ/kg)
$\bar{h}$	convection heat transfer coefficient (W/m^2 K)
h_{fg}	latent heat of vaporization (kJ/kg_{water})
k	thermal conductivity (W/m K)
M_p	particle moisture content dry basis (kg_{water}/kg_{solid})
$\dot{m}$	mass flow rate (kg/s)
$\dot{m}_a$	mass flow rate of dry air (kg/s)
$\dot{m}_w$	mass flow rate of water from the surface of a porous packed bed (kg/s)
$\overline{N}_u$	Nusselt number
P_{in}	microwave power incident (microwave energy emitted from a microwave oscillator) (kW)
P_1	density of microwave power absorbed by dielectric material (kW/cm^3)
P_2	energy is required to heat up the dielectric material (kW)
P_{abs}	microwave power absorbed (kW)
P_{tran}	microwave power transmitted (kW)
P_{ref}	microwave power reflected (kW)
$\dot{Q}_{evap}$	heat transfer rate due to water evaporation (kW)
$\dot{Q}_{abs}$	microwave energy to be required for heating up dielectric material (kW)
$\dot{Q}_{loss}$	heat transfer rate to the environment (kW)
Q_{convec}	convection heat transfer (kW)
SEC	specific energy consumption (kJ/kg)
S	water saturation
T	temperature (°C)
T_{surf}	temperature at porous packed bed surface (°C)
T_∞	ambient temperature (°C)
t	time (s)
tan δ	loss tangent coefficient (–)
W	weight of the dielectric material (kg)
W_d	weight of dry material (kg)
W_b	weight of material before drying (kg)
W_{in}	total work entering the system (kJ)
W_{out}	total work leaving the system (kJ)
X	absolute humidity (kg_{vapor}/kg_{dryair})

Greek letters

ε''_r	relative dielectric loss factor
ε'_r	relative dielectric constant
ε_0	permittivity of air (F/m)
X	humidity ratio (kg_{vapor}/kg_{dryair})
ΔT	the increment temperature (°C)
η_{abs}	microwave power absorbed efficiency (%)
η_e	energy efficiency (%)
ρ_s	density of solid (glass bead) (kg/m^3)
ρ_w	density of water (kg/m^3)
ϕ	porosity (m^3/m^3)
υ	velocity of propagation (m/s)
ρ	density (kg/m^3)
ω	angular velocity of microwave (rad/s)

Subscripts

o	standard state value
0	free space
1	inlet
2	outlet
a	air
ab	absorb
b	before
$convec$	convection
da	drying air
d	dry material
fg	difference in property between saturated liquid and saturated vapor
g	gas
in	input
l	liquid water
m	material
out	output
ref	reflect
r	relative
s	solid
$surf$	surface
$tran$	transmit
v	vapor
w	water
∞	ambient condition

2. Experimental apparatus

Fig. 1 shows the experimental apparatus of microwave drying of the porous packed bed using a rectangular waveguide. The microwave system was a monochromatic wave of TE_{10} mode operating at a frequency of 2.45 GHz. Microwave energy was generated by magnetron (Micro Denshi Co., model UM-1500, Tokyo, Japan); it was transmitted along the z-direction of the rectangular waveguide with inside dimensions of 110 mm × 55 mm toward a water load situated at the end of the waveguide. The water load (lower absorbing boundary) ensured that only a minimal amount of microwave energy was reflected back to the sample. In addition, an isolator (upper absorbing boundary) was used to trap any microwave energy reflected from the sample to prevent it from damaging the magnetron. The output of the magnetron was adjustable from 0 to 1500 W. The power of incident, reflected and transmitted waves were measured by a wattmeter using a directional coupler (Micro Denshi Co., model DR-5000, Tokyo, Japan). The distributions of temperature within the porous packed bed were measured using fiberoptic (LUXTRON Fluroptic Thermometer, Model 790, Santa Clara, Canada, accurate to ±0.5 °C. The fiberoptic probes were inserted into the sample at the center and at the following depth from the surface of the packed bed: 5, 15, 25, and 35 mm (as seen in Fig. 2).

As seen in Fig. 3, the samples were porous packed bed, which composed of glass beads, water, and air. A sample container was made from polypropylene with a thickness of 1 mm, it did not absorb microwave energy. In this study, the voids occupy from a fraction up to 38 percent of the whole volume of packed beds. The dimensions of packed bed are chosen to be 110 mm × 50 mm. The samples were prepared in two configurations: a single-layered packed bed (fine bed with diameter of 0.15 mm (F–bed) and coarse bed with diameter of 0.40 mm (C–bed)) and two-layered packed bed, respectively. The case of two-layered packed bed was classified in two configurations: F–C bed (attaching fine bed (d = 0.15 mm, d_P = 10, 20, 25, 30, and 40 mm) on coarse bed

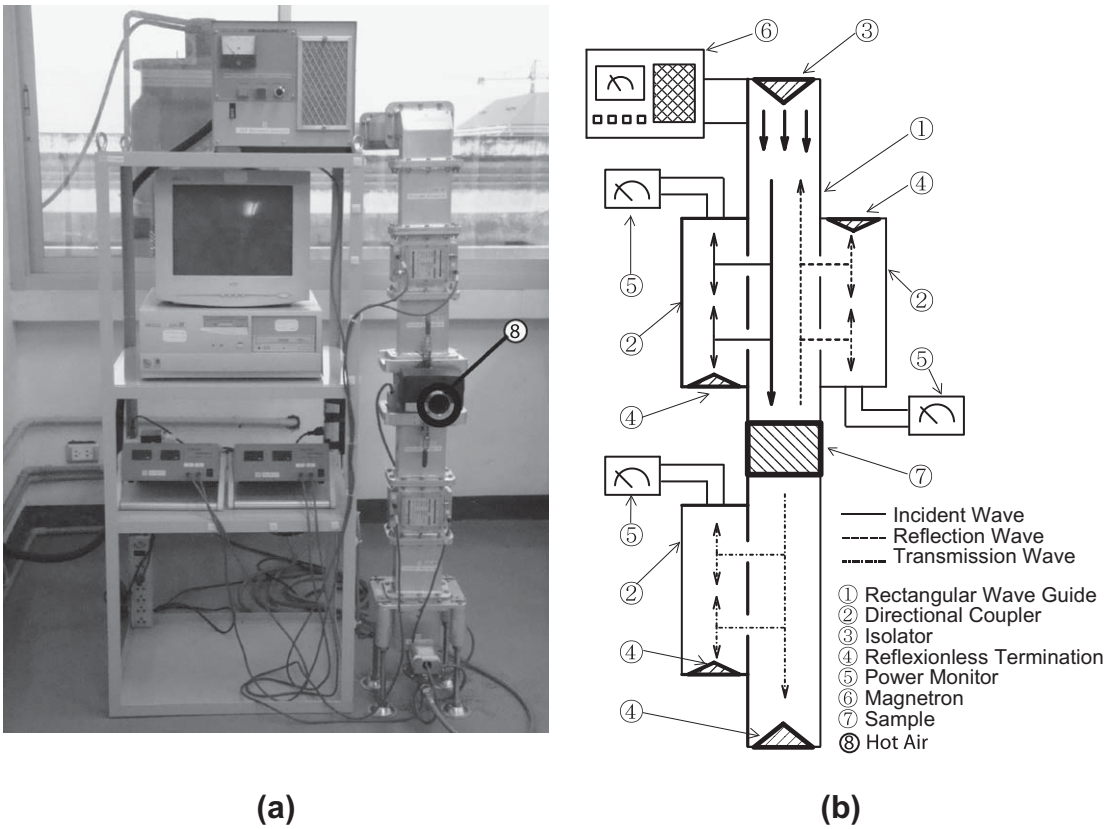

Fig. 1. Schematic of experimental facility: (a) equipment setup; (b) microwave measuring system.

(d = 0.40 mm, d_P = 40, 30, 25, 20, and 10 mm) and C–F bed (attaching coarse bed (d = 0.40 mm, d_P = 10, 20, 25, 30, and 40 mm) on fine bed (d = 0.15 mm, d_P = 40, 30, 25, 20, and 10 mm), respectively. The water saturations in the packed bed were defined as the fraction of the volume occupied by water to volume of the pores. They were obtained by weighing dry and wet mass of the sample which were cut out in volume (four positions) of about 110 mm × 354.61 mm × 312.5 mm at the end of each run. The water saturation formula can be described in the following from [7]:

$$S = \frac{M_p \cdot \rho_s \cdot (1-\phi)}{\rho_w \cdot \phi \cdot 100} \tag{1}$$

where S is water saturation; ρ_s is density of solid; ρ_w is density of water; ϕ is porosity and M_p is particle moisture content dry basis. During the experimental microwave drying processes, the uncertainty of our data might come from the variations in humidity and room temperature. The uncertainty in drying kinetics was assumed to result from errors in the measured weight of the sample. The calculated drying kinetic uncertainties in all tests were less than 3%. The uncertainly in temperature was assumed to result from errors in measured input power, ambient temperature and ambient humidity. The calculated uncertainty associated with temperature was less than 2.85%.

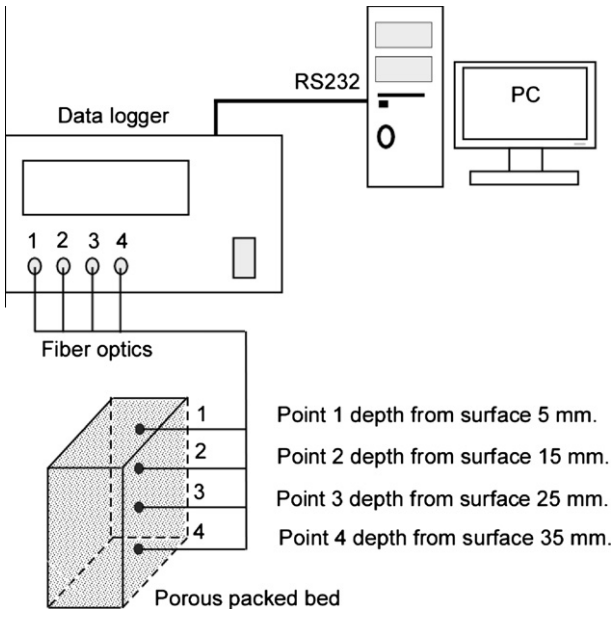

Fig. 2. Temperature measuring.

3. Related theories

3.1. Theory and energy of heat generation

Microwave heating involves heat dissipation and microwaves propagation which causes the dipoles to vibrate and rotate. When the microwave energy emits from a microwave oscillator (P_{in}) is irradiated inside the microwave applicator, the dielectric materials which has a dielectric loss factor absorbs the energy and are heated up. Then the internal heat generation takes place. The basic equation calculates the density of microwave power absorbed by dielectric material (P_1) is given by [14]:

$$P_1 = \omega \varepsilon_0 \varepsilon_r'' E^2 = 2\pi \cdot f \cdot \varepsilon_0 \cdot \varepsilon_r' (\tan\delta) E^2 \tag{2}$$

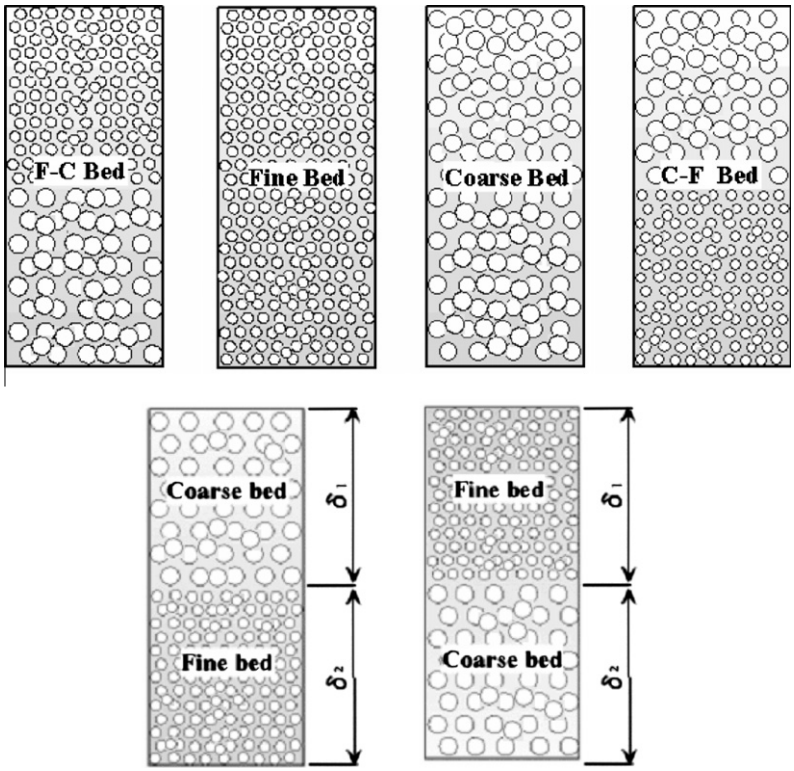

Fig. 3. Multi-layered porous packed bed (sample).

where E is electromagnetic field intensity; f is microwave frequency; ω is angular velocity of microwave; ε'_r is relative dielectric constant; ε_0 is dielectric constant of air and tan δ is dielectric loss tangent coefficient.

From Eq. (2), P_1 is directly proportional to the frequency of the applied electric field and loss tangent coefficient and root-mean-square value of the electric field. It means that during an increasing of tan δ of specimen, energy absorption and heat generation are also increased. While tan δ is small, microwave will penetrate into specimen without heat generation. However, the temperature increase depends on other factors such as specific heat, size and characteristic of specimen.

When the material is heated unilaterally, it is found that as the dielectric constant and loss tangent coefficient vary, the penetration depth will be changed and the electric field within the dielectric material is altered. The penetration depth is used to denote the depth at which the power density has decreased to 37% of its initial value at the surface [16]:

$$D_p = \frac{1}{\frac{2\pi f}{\upsilon}\sqrt{\frac{\varepsilon'_r\left(\sqrt{1+\left(\frac{\varepsilon''_r}{\varepsilon'_r}\right)^2}-1\right)}{2}}} = \frac{1}{\frac{2\pi f}{\upsilon}\sqrt{\frac{\varepsilon'_r\left(\sqrt{1+(\tan\delta)^2}-1\right)}{2}}} \tag{3}$$

where D_P is penetration depth ε''_r is relative dielectric loss factor and υ is microwave speed. The penetration depth of the microwave power is calculated according to Eq. (3), which shows how it depends on the dielectric properties of the material. It is noted that products with huge dimensions and high loss factors, may occasionally be overheated to a considerably thick layer on the outer layer. To prevent such phenomenon, the power density must be chosen so that enough time is provided for the essential heat exchange between boundary and core. If the thickness of the material is less than the penetration depth, only a fraction of the supplied energy will become absorbed. Furthermore, the dielectric properties of porous material specimens typically show moderate lousiness depending on the actual composition of the material. With large amount of moisture content, it reveals a greater potential for absorbing microwaves. For typical porous material specimens, a decrease in the moisture content typically decreases ε''_r, accompanied by a slight increment in D_p.

In the analysis, energy P_2 is required to heat up the dielectric material W(g) which is placed in a microwave applicator. The temperature of material initially T_1, is raised to T_2. The energy P_2 can be estimated by the following calorific equation [17]:

$$P_2 = \frac{4.18 \cdot W \cdot C_p \cdot \Delta T}{t} \tag{4}$$

where W is weight of the dielectric material; C_p is specific heat of the dielectric material; ΔT is the increment of temperature $(T_2 - T_1)$ and t is heating time.

Assuming an ideal condition, all of the oscillated microwave energy (P_{in}) is absorbed into the dielectric material; such internal heat generation as Eq. (2) shows takes place. In this case, the relation between P_{in} and P_2 is shown below:

$$P_{in} = P_2 \tag{5}$$

In a practical point of view, however, the transformation energy in applicator exists due to Eq. (2) the rate of microwave energy absorbed by means of the dielectric loss factor of the sample and Eq. (3) the energy loss in the microwave devices. Accordingly, by taking into account this transformation efficiency, the microwave oscillation output can be calculated by the following equations:

$$P_{in} = \frac{P_2}{\eta} \tag{6}$$

$$\eta = \frac{P_2}{P_{in}} \tag{7}$$

3.2. Incident, reflection, transmission and absorbed wave

In Fig. 4, microwave can be incidental into the packed bed, it can transmit through the packed bed, and it also can be reflected and absorbed by the porous packed bed. By power balance on control volume as shown in Fig. 4, the incident wave can be expressed as:

$$\text{Incident Wave (A)} = \text{Reflected Wave (B)} + \text{Transmitted Wave (C)} + \text{Absorbed Wave (D)} \quad (8)$$

where P_{in} is microwave power incident or microwave energy emitted from a microwave oscillator (Incident Wave (A)); P_{ref} is microwave power reflected (Reflected Wave (B)); P_{tran} is microwave power transmitted (Transmitted Wave (C)) and P_{abs} is microwave power absorbed (Absorbed Wave (D)).

In order to calculate the microwave power absorbed, Eq. (8) can be rearranged as:

$$P_{abs} = P_{in} - P_{tran} - P_{ref} \quad (9)$$

Next, refers to throughout this study, as shown in equations below:

$$P_{abs} = \dot{Q}_{abs} \quad (10)$$

The microwave power absorbed efficiency during microwave drying of the porous packed bed provides a true measure of the performance of the drying system which can be expressed as:

$$\eta_{abs} = \left[\frac{\text{Absorbed Wave (D)}}{\text{Incident Wave(A)}}\right] \times 100 \quad (11)$$

$$\eta_{abs} = \left[\frac{P_{abs}}{P_{in}}\right] \times 100 \quad (12)$$

$$\eta_{abs} = \left[\frac{\dot{Q}_{abs}}{P_{in}}\right] \times 100 \quad (13)$$

3.3. Mass and energy balance equation for the drying process

The conservation of mass for the control volume of drying porous packed bed is shown in Fig. 5. The mass balance equation can be written as [11]:

$$\frac{dm_{cv}}{dt} = \dot{m}_{g1} - \dot{m}_{g2} \quad (14)$$

Here, Eq. (14) is the mass flow rate balance for the control volume where $\dot{m}_{g1}$ and $\dot{m}_{g2}$ denote, respectively, the mass flow rate at inlet (1) and exit at (2). Similarly, a balance of water in air flowing through the porous packed bed leads to [11]:

$$W_d \frac{dM_p}{dt} = \dot{m}_a(X_1 - X_2) \quad (15)$$

where W_d is weight of dry material and M_p is particle moisture content, dry basis; this can be expressed as [11]:

$$M_p = \frac{W_b - W_d}{W_d} \quad (16)$$

where W_b is weight of material before drying; $\dot{m}_a$ is the mass flow rate of dry air; X_1 and X_2 denote, respectively, absolute humidity of inlet and exit air. The left-hand side of the mass balance equation, Eq. (15), is the mass flow rate of water in the air flowing on porous packed bed surface, can be written as [11]:

$$\dot{m}_w = \dot{m}_a(X_2 - X_1) \quad (17)$$

In the drying processes, we apply the first law of thermodynamics (the law of conservation of energy) for the control volume

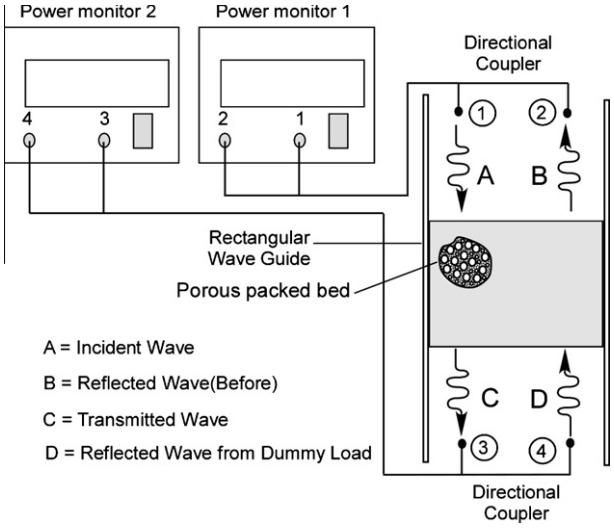

Fig. 4. Microwave power measuring.

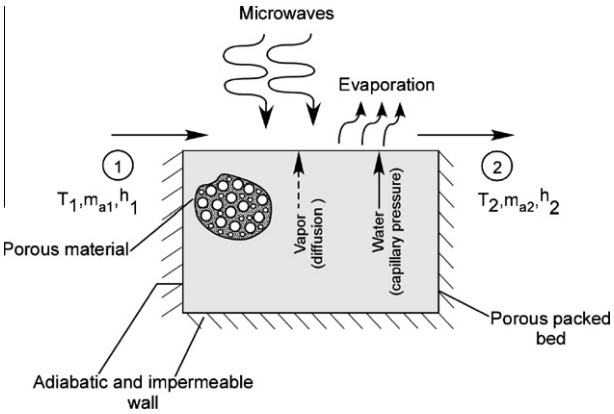

Fig. 5. Microwave and convective drying process.

shown in Fig. 5. The significant heat transfer is due to the heat of evaporation between the solid and the drying air, and there is also heat rejection to the surroundings. The energy rate balance is simplified by ignoring kinetic and potential energies. Since the mass flow rate of the dry air and the mass of dry material, within the control volume remain constant with time, the energy rate balance can be expressed as:

$$\frac{W_d(h_{m2} - h_{m1})}{\Delta t} = \dot{Q}_{evap} + \dot{m}_a(h_1 - h_2) + \dot{Q}_{abs} - \dot{Q}_{loss} \quad (18)$$

where $\dot{Q}_{evap}$ is heat transfer rate due to water evaporation ; $\dot{Q}_{abs}$ is microwave energy required for heating up dielectric material; h_m is enthalpy of material; t is time; $\dot{m}_a$ is mass flow rate of dry air ; h is enthalpy of dry air and $\dot{Q}_{loss}$ is heat transfer rate to the environment.

Assuming air as an ideal gas, thus the different in specific enthalpy are as follows [18]:

$$h_{m1} - h_o = c_m(T_{m1} - T_o) \quad (19)$$

$$h_{m2} - h_o = c_m(T_{m2} - T_o) \quad (20)$$

The enthalpy term of material in Eq. (18) can be written as [18]:

$$h_{m2} - h_{m1} = c_m(T_{m2} - T_{m1}) \quad (21)$$

where c_m represents the specific heat of the material. The enthalpy of moist air can be calculated by adding the contribution of each component as it exits in the mixture; thus the enthalpy of moist air is [18]:

$$h = h_a + Xh_v \tag{22}$$

The heat transfer rate due to phase change is [15]:

$$\dot{Q}_{evap} = \dot{m}_w h_{fg} \tag{23}$$

where h_{fg} is latent heat of vaporization.

3.4. Specific energy consumption and energy efficiency in drying process

The *SEC* was estimated in a combined convective - microwave drying processes. Considering the total energy supplied to dry porous packed bed from initial water saturation of 0.60 ($S_0 = 0.60$) to approximately a desired water saturation of 0.17 ($S_0 = 0.17$). The convective-microwave drying process was conducted in the same conditions with keeping the microwave power incident of 50 W, air temperature of 27.2 °C, and velocity of 3.71 m/s. The *SEC* is defined as follows:

$$SEC = \frac{\text{Total energy supplied in drying process}}{\text{Amount of water removed during drying}}, \frac{kJ}{kg} \tag{24}$$

$$SEC = \frac{(P_{in} + Q_{convec})\Delta t}{\text{Amount of water removed during drying}}, \frac{kJ}{kg} \tag{25}$$

where Q_{convec} is a convective heat transfer which can be calculated from [15]:

$$Q_{convec} = \bar{h}A(T_{surf} - T_{\infty}) \tag{26}$$

$$\bar{h} = \frac{\overline{N}_u k}{L} \tag{27}$$

where $\bar{h}$ is convection heat transfer coefficient; A is porous packed bed surface area ; T_{surf} is temperature at porous packed bed surface; T_{∞} is ambient temperature; $\overline{N}_u$ is Nusselt number; k is thermal conductivity and L is length of surface of porous packed bed in direction of flow.

From Ref. [19], the energy efficiency for drying process is defined as:

$$\eta_e = \frac{W_d[h_{fg}(M_{p1} - M_{p2}) + c_m(T_{m2} - T_{m1})]}{\dot{m}_{da}(h_1 - h_o)\Delta t + \Delta t \dot{Q}_{abs}} \tag{28}$$

where c_m is material specific heat.

4. Results and discussion

The experiments of a combined of convective air and microwave drying process were conducted by varying layered configuration and layered thickness of porous packed bed. For porous packed beds of two different sizes (0.15 mm and 0.40 mm), microwave power incident of 50 W, air velocities of 3.71 m/s, and air temperature of 27.2 °C, the temperature distribution and the *SEC* were carried out.

4.1. Case I. Single layered porous packed bed (F, C bed)

Figs. 6 and 7 illustrate the distributions of temperature and averaged saturation of the F–bed and C–bed during the combined drying process, respectively. The thickness of packed bed is 50 mm ($d_p = 50$ mm). Temperature is measured at four positions of the sample. In Figs. 6 and 7 show the third position, which measured form surface downward to a depth of 25 mm. From

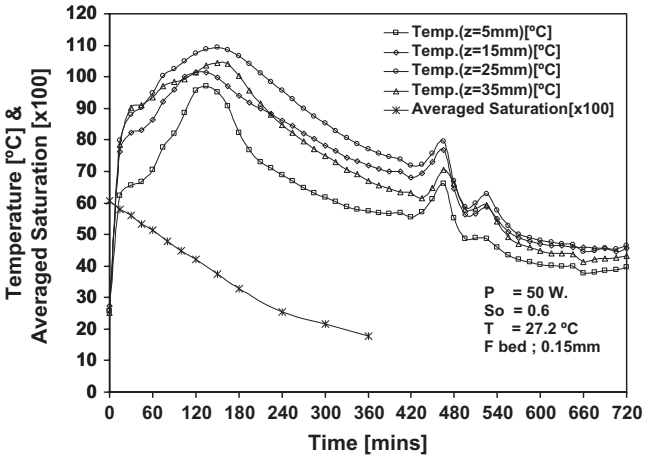

Fig. 6. Temperature and averaged saturation profiles with respect to elapsed time (F-bed, depth 50 mm).

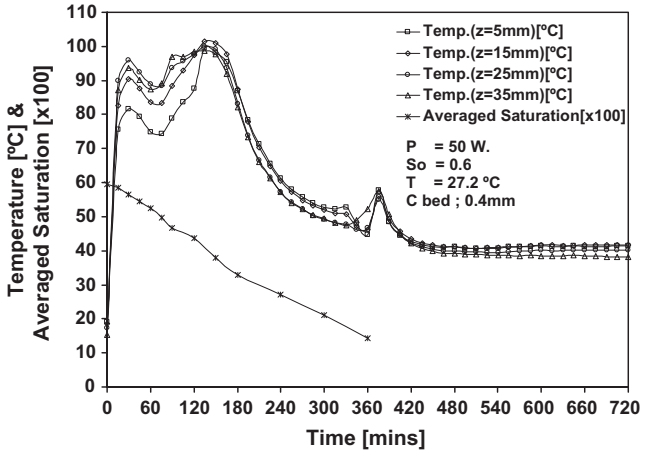

Fig. 7. Temperature and averaged saturation profiles with respect to elapsed time (C-bed, depth 50 mm).

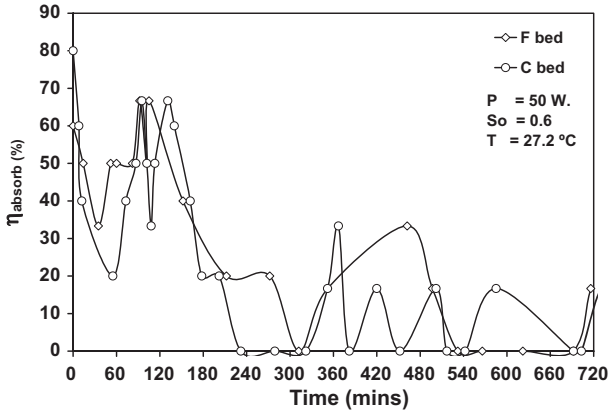

Fig. 8. The variation of microwave power absorbed efficiency with respect to elapsed time (F-bed, C-bed, depth 50 mm).

the starting time until 120 min elapsed, the microwave energy supplied is absorbed by porous packed bed sample, which is shown in Fig. 8 and whose microwave power absorbed efficiency can be calculated with Eq. (13). After that it is converted to heat the

sample temperature from ambient temperature to 109 °C and 95 °C for microwave power 50 Watts. At this point, there is high moisture content. The high moisture content at this period is reflected by the high loss tangent coefficient (tan δ). The next period from 120 to 720 min as shown in Fig. 8 depicts the increase transmitted wave and decrease reflected waves, which implies the microwave power absorption become lower than in the first period. Due to the fact that the moisture content is reduced, the loss tangent coefficient (tan δ) is decreased.

Figs. 6 and 7 show the temperature profiles measured by fiber-optic at various times and locations in the case of $S_0 = 0.6$, $d = 0.15$ mm and $d = 0.40$. The microwave and convective drying gives higher temperatures inside the drying sample while the surface temperature stays colder due to the cooling effect of surrounding air. At the same time the evaporation takes place at the surface of the sample at a lower temperature due to evaporative cooling. It is seen that the temperature profiles within the sample rise up steadily in the early stages of drying (about 60 min). Due to the large initial moisture content, the skin depth heating effect causes the majority of microwave to be reflected from the surface during early irradiation stage resulting in a lower rate of microwave power absorbed in the interior (Fig. 8). As the drying process proceeds (about 60–240 min), after the majority of moisture content is removed from the sample, the microwave can penetrate further into the sample as material dries (as referred to Fig. 8) where the strength of the microwave power absorbed increases (Fig. 8). During this stage of drying, the behavior of dielectric properties is influenced primarily by that of moisture content, and heating becomes more volumetric. In time about 240 min, the temperature starts to drop, this is mainly due to fact that the moisture inside the sample is significantly reduced, reducing dielectric loss factor as well as microwave power absorbed (Fig. 8). However, at long stages of drying (about 480 min: F-bed, 360 min: C-bed), the temperature increases rapidly due to the characteristic of dielectric loss factor, which becomes to dominant microwave drying at low moisture content where the stronger standing wave with a larger amplitude established within the sample. Nevertheless, near the end stages of drying as the majority of moisture content inside the sample is removed, this decreases the microwave power absorbed.

4.2. Case II. Two-layered porous packed bed

Experimental data of a combined drying process of two-layered porous packed bed are shown in Figs. 9–14, which corresponds to that of $S_0 = 0.60$ and $P_{in} = 50$ W. The data is along the center axis ($x = 55$ mm) of rectangular waveguide. Figs. 9 and 12 show the distribution of temperature and averaged saturation within F–C bed with layered thickness of fine bed as 10 and 25 mm, respectively. From a macroscopic point of view for the hydrodynamic characteristic properties within the two-layered porous packed bed, we will consider the liquid water transport at the interface between two beds where the difference of particle size is considered during microwave drying. As referred to Ratanadecho et al. [7], in the case of the same capillary pressure, a smaller particle size corresponds to higher water content. Now, consider the case where two particle sizes having same capillary pressure and different particle sizes at the interface are justified. The capillary pressure has the same value at the interface between two beds, but the water saturation becomes discontinuous at the interface of two beds. This is because of the differences of the water characteristics between the two beds, the liquid water will be moved from the coarse bed to the fine bed (which corresponds to a higher capillary pressure) resulting in a faster drying time.

On the other hand, in the case of C–F bed with layered thickness of coarse bed as 10 and 25 mm are shown in Figs. 10 and 13,

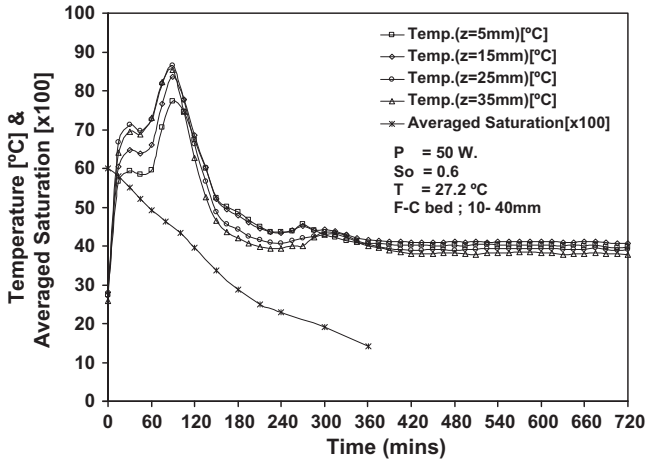

Fig. 9. Temperature and averaged saturation profiles with respect to elapsed time (F–C bed, depth 10–40 mm).

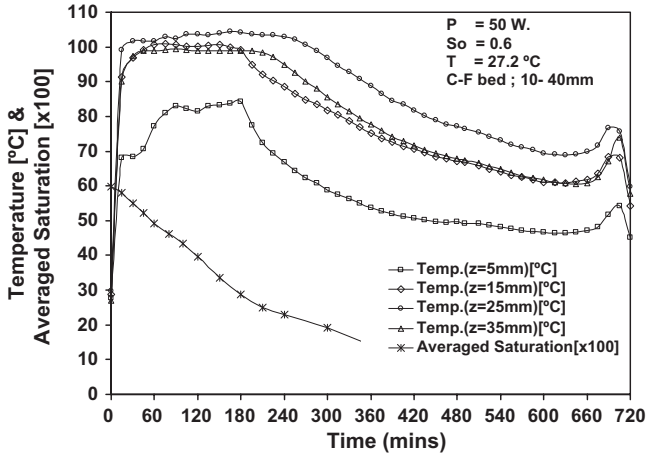

Fig. 10. Temperature and averaged saturation profiles with respect to elapsed time (C–F bed; depth 10–40 mm).

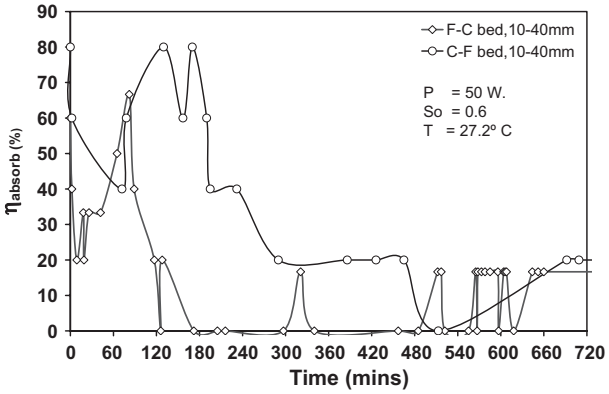

Fig. 11. The variation of microwave power absorbed efficiency with respect to elapsed time (F–C bed, C–F bed, depth 10–40 mm).

respectively. It is seen that the moisture content inside the fine bed is much higher because a coarse bed set on the fine bed retards the upward migration of liquid water at the interface between two beds, while the moisture content inside the coarse bed stays lower due to the lower capillary pressure [7].

The temperature profiles at various times and locations for both cases are shown in Figs. 10 and 13, respectively. Figs. 10 and 13 show that the temperature profile within the C–F bed rises up quickly in the early stages of drying process (about 10–60 min) However, its rise slows down after this stage. It is evident from the figure that near the end stages of drying as the moisture content inside the sample is reduced, the absorbed microwave power decreases (Figs. 11 and 14). Consequently, the temperature profiles are decreased in this stage of drying process. However, the temperature profile within the C–F bed (Figs. 10 and 13), corresponds to the moisture content profile where the temperature continuously rises faster than that in the case of F–C bed (Figs. 9 and 12). Further, the temperature remains high at the end of drying. This is because a stronger standing wave with a larger amplitude is formed inside the C–F bed and having of dry layer-coarse bed (upper layer) protects the reflection of wave from the surface, resulting in a higher rate of microwave power absorbed in the interior (Figs. 11 and 14).

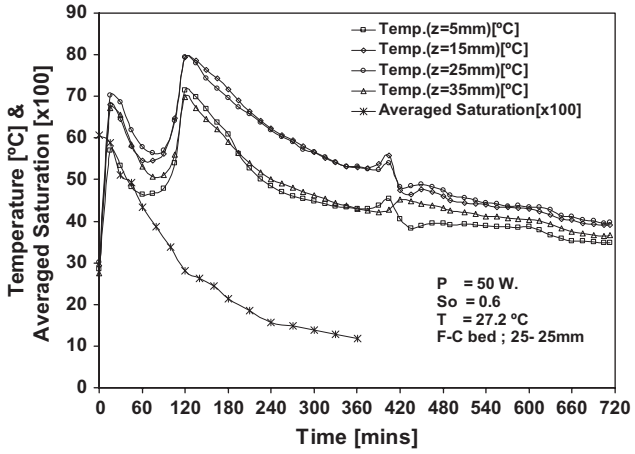

Fig. 12. Temperature and averaged saturation profiles with respect to elapsed time (F–C bed, depth 25–25 mm).

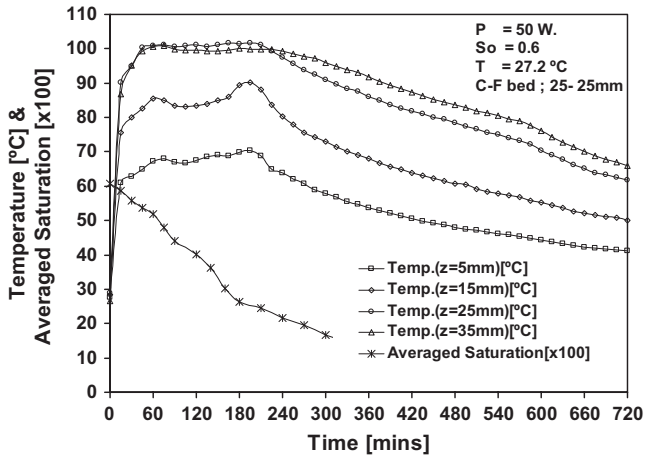

Fig. 13. Temperature and averaged saturation profiles with respect to elapsed time (C–F bed, depth 25–25 mm).

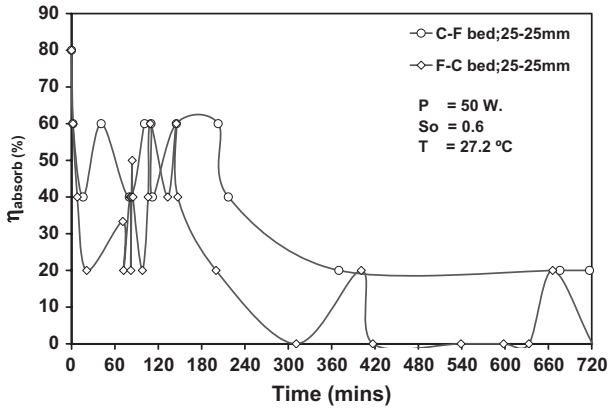

Fig. 14. The variation of microwave power absorbed efficiency with respect to elapsed time (F–C bed, C–F bed, depth 25–25 mm).

4.3. Specific energy consumption (SEC)

This subsection carried out the *SEC* of the porous packed bed with various layered configurations and layered thickness. The microwave power incident (P_{in}) is set at 50 W, air temperature of 27.2 °C with velocities of 3.71 m/s. The *SEC* within the various type of porous packed bed at drying time of 120, 240, and 360 min are shown in Figs. 15–17, respectively. From the Figs, it is shown that the *SEC* will increase with time proceed. This is because total energy supplied is remained while amount of water removed are decreasing during the drying process (ref. from Eq. (24)).

Comparing with the various packed bed configurations in Fig. 15, the *SEC* is lower corresponding to the case of F–C bed with each layered thickness of 25 mm. The *SEC* is 11.62 MJ/kg which means this packed bed type can remove higher amount of water than other types. After time proceed (t = 240 min) as seen in Fig. 16, For the case of F-C bed, it is interesting to observe that the value of the SEC is gradually decreased when the thickness of fine bead increases from 10 mm to 25 mm. After that, the SEC of the layer is gradually increased corresponds to increasing of fine bead thickness (30 mm to 40 mm). Finally, t = 360 min as seen in Fig. 17, the layered thickness of the packed bed was set to 10 and 25 mm with fine bead on top. It depicts that the specific energy consumption of the packed bed was lower than the coarse bead on top due to the capillary pressure [7] that cause moisture content to move to the surface quickly. In turn, these causes are force the moisture content to move out off the packed bed quickly, so the specific energy consumption is reduced, this effect to increase the efficiency of the system. Furthermore, it also observes that the relation between the *SEC* value and layered thickness of two-layered porous packed bed is non-linear. The reasons behind these phenomena need more investigations. Based on these studies, it is shown that the F-C bed with each layered thickness of 25 mm corresponds to the minimum value of SEC throughout drying process due to strongly capillary and osmotic action.

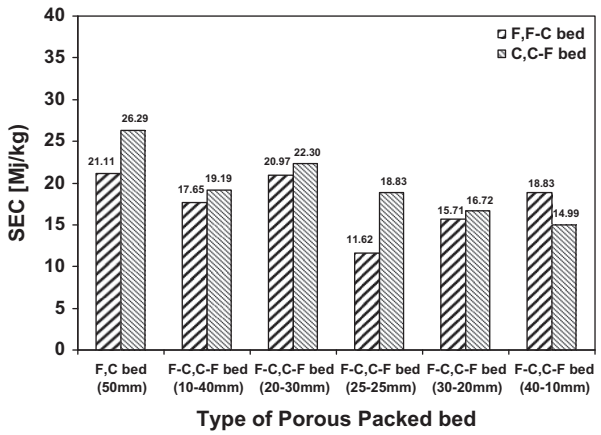

Fig. 15. Variation in specific energy consumption under microwave and convective drying at drying time 120 min.

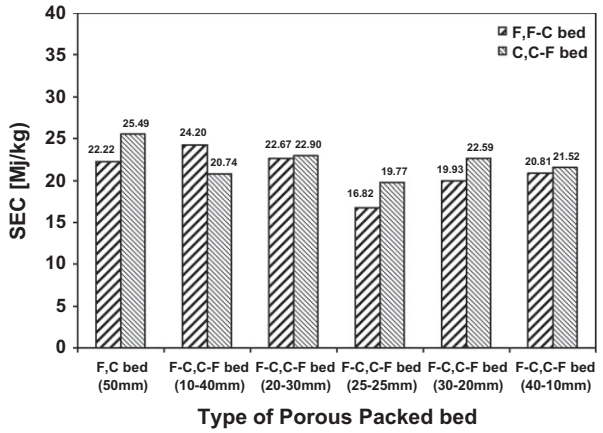

Fig. 16. Variation in specific energy consumption under microwave and convective drying at drying time 240 min.

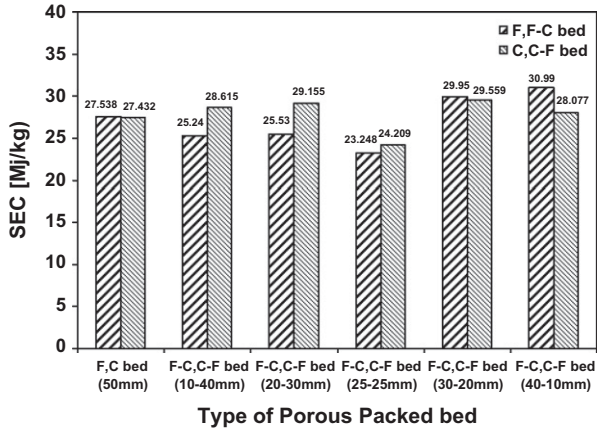

Fig. 17. Variation in specific energy consumption under microwave and convective drying at drying time 360 min.

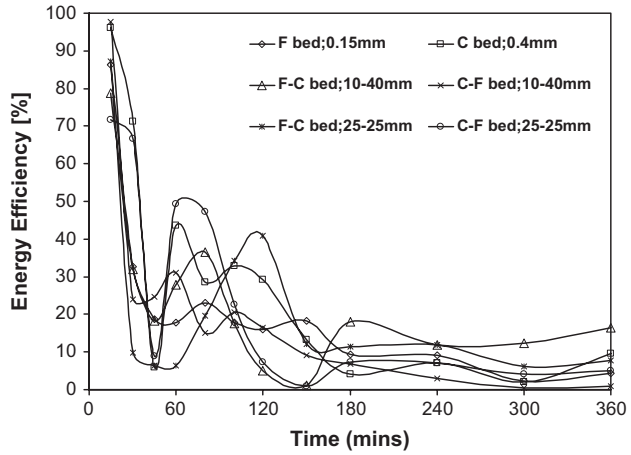

Fig. 18. Energy efficiency profiles with respect to elapsed time.

4.4. Energy efficiency

Fig. 18 shows the energy efficiency with respect to the drying time. It seem that the high energy efficiency near the starting period about 0–60 min due to the high quantity of moisture content in the packed bed, thus the wave absorption is more converted by packed bed. The results are high energy efficiency after the vapor has moving from the surface of the porous packed bed. This causes the moisture content to quickly decrease and the low quantity of absorbed waves causes the decrease energy consumption and decrease microwave power absorbed efficiency (Eq. (13)). This cause is lower thermal efficiency; therefore, energy efficiency depends on the efficiency with which the waves are absorbed.

The energy efficiency profiles at various times and locations for six cases are shown in Fig. 18. The energy efficiency profile within the F–C and C–F bed rises up quickly in the early stages of drying process (about 10–120 min). However, its rise slows down after this stage (about 120–360 min). It is evident from the figure that near the end stages of drying as the moisture content inside the sample is reduced, this decreases the microwave power absorbed. Consequently, the energy efficiency profiles are decreased in this stage of drying process.

5. Conclusion

In this work, the energy efficiency and specific energy consumption of the combined convective-microwave drying process of multi-layered porous packed bed were presented in detail. Taking into considerations the results from these analyses, the following conclusion may be drawn on the *SEC* increased with decreasing energy efficiency during the drying process. Both the *SEC* and energy efficiency depend on the particle size in case of single-layered porous packed bed and layered configurations in case of two-layered porous packed bed.

The effects of layered configurations and layered thicknesses on the overall drying kinetics were clarified. The drying rate and energy efficiency in the case of the F–C bed with equal layered thickness of 25 mm is slightly higher than that other case of porous packed bed. It is also found that the drying rate relates to the moisture content within the packed bed.

This knowledge means that drying and heating processes using microwave energy can be designed to be significantly more efficient, reducing the drying period and so reducing specific energy consumption.

Acknowledgment

The authors are pleased to acknowledge the Thailand Research Fund (TRF) for supporting this research work.

References

[1] Z.B. Maroulis, G.D. Saravacos, A.S. Mujumdar, Handbook of Industrial Drying, Taylor & Francis Group, Singapore, 2006.
[2] N.V. Men'Shutina, M.G. Gordienko, A.A. Voinovskii, T. Kudra, Dynamics criteria for evaluating the energy consumption of drying equipment, Theor. Found. Chem. Eng. 39 (2003) 158–162.
[3] E.K. Akpinar, Exergy and energy analysis of drying of red pepper slices in a convective type dryer, Int. Comm. Heat Mass Transfer 31 (2004) 1165–1176.
[4] G.P. Sharma, S. Prasad, Specific energy consumption in microwave drying of garlic cloves, J. Food Eng. 31 (2005) 1921–1926.
[5] J. Varith, P. Dijkanarukkul, A. Achariyaviriya, S. Achariyaviriya, Combined microwave-hot air drying of peeled longon, J. Food Eng. 31 (2007) 459–468.
[6] S. Lakshmi, A. Chakkaravarthi, R. Subramanian, V. Singh, Energy consumption in microwave cooking of rice and its comparison with other domestic appliances, J. Food Eng. 78 (2005) 715–722.
[7] P. Ratanadecho, K. Aoki, M. Akahori, Influence of irradiation time, particle sizes and initial moisture content during microwave drying of multi-layered capillary porous materials, ASME J. Heat Trans. 124 (2002) 151–161.
[8] H. Feng, J. Tang, R.P. Cavalieri, O.A. Plumb, Heat and mass transport in microwave drying of porous materials in a spouted bed, A.I.Ch.E. J. 47 (2001) 1499–1512.
[9] B. Abbasi Souraki, D. Mowla, Experimental and theoretical investigation of drying behaviour of garlic in an inert medium fluidized bed assisted by microwave, J. Food Eng. 88 (2007) 438–449.
[10] H. Ogura, N. Hamaguchi, H. Kagea, A.S. Mujumdar, Energy and cost estimation for application of chemical heat pump dryer to industrial ceramics drying, J. Drying Technol. 22 (2004) 307–323.

[11] S. Syahrul, F. Hamdullahpur, I. Dincer, Exergy analysis of fluidized bed drying of moist particles, Int. J. Energy 2 (2002) 87–98.
[12] S. Syahrul, I. Dincer, F. Hamdullahpur, Thermodynamic modeling of fluidized bed drying of moist particles, Int. J. Therm. Sci. 42 (2003) 691–701.
[13] S. Syahrul, F. Hamdullahpur, I. Dincer, Thermal analysis in fluidized bed drying of moist particles, Int. J. Appl. Therm. Eng. 22 (2002) 1763–1775.
[14] P. Rattanadecho, The simulation of microwave heating of wood using a rectangular wave guide: influence of frequency and sample size, Int. J. Chem. Eng. Sci. 61 (2006) 4798–4811.
[15] Frank P. Incropera, David P. Dewitt, Theodore L. Bergmann, Adrienne Lavine, Fundamental of Heat and Mass Transfer, John Wiley & Sons (Asia) Pvt., Ltd., Danvers, 2007.
[16] W. Cha-um, P. Rattanadecho, W. Pakdee, Experimental analysis of microwave heating of dielectric materials using a rectangular wave guide (MODE: TE10) (case study: water layer and saturated porous medium), Int. J. Exp. Therm. Fluid Sci. 33 (2009) 472–481.
[17] S. Vongpradubchai, P. Rattanadecho, The microwave processing of wood using a continuous microwave belt drier, Int. J. Chem. Eng. Process. 33 (2009) 472–481.
[18] Y.A. Cengel, M.A. Boles, Thermodynamics: An Engineering Approach, McGraw-Hill Companies, Inc., New York, 2002.
[19] I. Dincer, M.A. Rosen, Energy, Environment and Sustainable Development, Elsevier Ltd., Burlington, 2002.

Chemical Engineering and Processing 48 (2009) 997–1003

Contents lists available at ScienceDirect

Chemical Engineering and Processing: Process Intensification

journal homepage: www.elsevier.com/locate/cep

The microwave processing of wood using a continuous microwave belt drier

S. Vongpradubchai, P. Rattanadecho*

Research Center of Microwave Utilization in Engineering (R.C.M.E.), Department of Mechanical Engineering, Faculty of Engineering, Thammasat University (Rangsit Campus), Pathumthani 12120, Thailand

ARTICLE INFO

Article history:
Received 6 August 2008
Received in revised form 9 December 2008
Accepted 15 January 2009
Available online 24 January 2009

Keywords:
Microwave
Processing
Wood
Drying
Dielectric

ABSTRACT

In this study, the drying of wood by microwave energy using a continuous microwave belt drier was compared to that by conventional method. By using a continuous microwave belt drier, the microwave power was generated by means of 14 compressed air-cooled magnetrons of 800 W each that gives a maximum of 11.2 kW. The power setting could be adjusted individually in 800 W steps. Most importantly, this work focuses on the investigation of drying phenomena under microwave environment. In this analysis, the effects of the irradiation time and microwave power level on overall drying kinetics and mechanical properties were studied. The results showed that using the continuous microwave applicators technique has several advantages over the conventional method such as shorter processing times, volumetric dissipation of energy throughout a product, high energy efficiency as well as improvements in product quality. The results presented here provide a fundamental understanding of microwave-heating of various kinds of dielectric materials.

1. Introduction

Nowadays, the most important thing in industries, except for producing the high quality products to the markets, is to increase productivity and to reduce production cost. In general, several production processes of agricultural and industrial products are related to drying either by a natural method or using energy from other sources resulting in a low production rate or a high cost product. Microwave drying is one of the most interesting methods for drying materials. During the past decade, there are many successful examples of microwave applications including the heating and drying of foods, heating and drying of ceramics, heating and drying of concrete and vulcanizations of rubber and drying of wood. A number of analyses of the microwave heating process have appeared in the recent literature ([1–30] and [32,33]). An excellent review of the drying techniques in dielectric materials using microwave energy has been presented by Mujumdar [1], Metaxas and Meridith [2] and Schubert and Regier [3].

The drying of wood is the most energy-intensive and costly process in the forest products industry. Conventional wood dryers function under the basis of convective heat transfer from circulating hot air to the surface of wood followed by subsequent conductive heat transfer from the surface to the center of wood. These dryers require considerable amount of energy and long drying times in order to obtain high quality woods. Therefore, innovative wood drying methods have been searched and studied. Unlike the conventional heating, where heat is applied externally to the surface of the material, microwave irradiation penetrates and simultaneously heats the bulk of the material. When properly designed, microwave drying systems have several advantages over conventional mechanical methods including, reduction of the drying time, high energy efficiency, and improvements in product quality for various industrial applications [24]. Microwave drying of wood products, however, has not been used to a larger extent in wood industries mainly due to the insufficient knowledge of the complex interaction between wood and process parameters during drying as well as the higher investment expenses. Recently the development of inexpensive and reliable microwave sources has been increasing attracted to applications in wood industry.

Investigations on microwave drying of wood have been performed since the late fifties. Many authors (Antti [25], Masakasu Miura et al. [26], Oloyede and Groombridge [27], Lehne et al. [28], Turner [29] and Lee [30]) emphasize in the advantages of microwave drying over convective drying. Turner [29] points out the suitability of combined microwave and convective drying. However, there still remain obstacles to be overcome in applying microwave drying technology to wood industry. One of the difficulties is that the microwave power absorbed by moist wood depends mainly on the moisture content and it is required to move the wood for uniform power distribution with on-off type microwave system at fixed power output.

Although a number of studies have been conducted to investigate a microwave heating process, most of them were carried out using a domestic or housing microwave oven and a single or mul-

* Corresponding author. Tel.: +66 0 2564 3001 9; fax: +66 0 2564 3010.
E-mail address: ratphadu@engr.tu.ac.th (P. Rattanadecho).

0255-2701/$ – see front matter © 2009 Elsevier B.V. All rights reserved.
doi:10.1016/j.cep.2009.01.008

timode cavity with a non-movable material. Those studies showed that the result may be dependent on the method used to carry out the curing or heating process. The objective of this study is to demonstrate the applicability of microwave energy, as an energy-saving and production-cost-reducing technology. The microwave drying of wood in a continuous microwave belt drier where a series of 14 magnetrons, 800 W each with total power of 11.2 kW were installed. The experimental results from this study could help to identify some of the potential problems during the practical design stage. This study is of great importance from the practical point of view because it shows the possibility of application of microwave heating-drying of dielectric materials on an industrial scale, especially in a continuous system.

2. Related theories

With the basic knowledge of heating by microwave energy, it concerns heat dissipation and typical microwaves propagation in which the dipoles start to vibrate and rotate furiously by mean of the electric field. When the microwave energy emitted from a microwave oscillator (Pin) is irradiated inside the microwave applicator, the dielectric materials which has a dielectric loss factor absorb the energy and are heated up. which has a dielectric loss factor. Then the internal heat generation takes places. The basic equation to calculate the density of microwave power absorbed by dielectric material (P_1) is given by [19]:

$$P_1 = \omega\varepsilon_0\varepsilon_r'' E^2 = 2\pi f\varepsilon_0\varepsilon_r(\tan\,\delta)E^2 \tag{1}$$

where E is electromagnetic field intensity; f is microwave frequency; ω is angular velocity of microwave; ε_r is relative dielectric constant; ε_0 is dielectric constant of air and $\tan\delta$ is dielectric loss tangent coefficient.

From Eq. (1), P_1 is directly proportional to the frequency of the applied electric field and dielectric loss tangent coefficient and root-mean-square value of the electric field. It means that increasing of $\tan\delta$ of specimen, energy absorption and heat generation are also increased. While $\tan\delta$ is small, microwave will penetrate into specimen without heat generation. However, the temperature increase probably depends on other factors such as specific heat, size and characteristic of specimen.

When the material is heated unilaterally, it is found that as the dielectric constant and loss tangent coefficient vary, the penetration depth will be changed and the electric field within the dielectric material is altered. The penetration depth is used to denote the depth at which the power density has decreased to 37% of its initial value at the surface [23].

$$D_P = \frac{1}{(2\pi f/\upsilon)\sqrt{\left[\varepsilon_r'\left(\sqrt{1+(\varepsilon_r''/\varepsilon_r')^2}-1\right)\right]/2}} = \frac{1}{(2\pi f/\upsilon)\sqrt{\left[\varepsilon_r'(\sqrt{1+(\tan\,\delta)^2}-1)\right]/2}} \tag{2}$$

where D_P is penetration depth ε_r'' is relative dielectric loss factor and υ is microwave speed. The penetration depth of the microwave power is calculated according to Eq. (2), which shows how it depends on the dielectric properties of the material. It is noted that products with huge dimensions and high loss factors, may occasionally overheat a considerably thick layer on the outer layer. To prevent such phenomenon, the power density must be chosen so that enough time is provided for the essential heat exchange between boundary and core. If the thickness of the material is less than the penetration depth, only a fraction of the supplied energy will become absorbed. Furthermore, the dielectric properties of wood specimens typically show moderate lossiness depending on the actual composition of the material. With large amount of moisture content, it reveals a greater potential for absorbing microwaves. For all wood specimens, a decrease in the moisture content typically decreases ε'', accompanied by a slight increment in D_P.

In the analysis, energy P_2 is required to heat up the dielectric material W(g) placed in a microwave applicator. The temperature of material is initially T_1 is raised to T_2. The energy P_2 can be estimated by the following calorific equation:

$$P_2\ (\mathrm{W}) = \frac{4.18WC_P\,\Delta T}{t} \tag{3}$$

where W is weight of the dielectric material (g), C_P is specific heat of the dielectric material (Cal/gr °C), ΔT is the increment of temperature ($T_2 - T_1$) (°C), t is heating time (s).

Assuming an ideal condition, all of the oscillated microwave energy (P_{in}) is absorbed into the dielectric material; such internal heat generation as Eq. (1) shows takes place. In this case the relation between P_{in} and P_2 is shown below:

$$P_{in}\ (\mathrm{W}) = P_2 \tag{4}$$

In a practical point of view, however, the transformation energy (η) in applicator is exists due to (1) the rate of microwave energy absorbed by means of the dielectric loss factor of the sample and (2) the energy loss in the microwave devices. Accordingly, by taking into account of this transformation efficiency, the microwave oscillation output can be calculated by the following equation:

$$P_{in}\ (\mathrm{W}) = \frac{P_2}{\eta} \tag{5}$$

Accordingly, in order to determine the efficiency of the applicator during the microwave processing of wood using a continuous microwave belt drier, the Eqs. (3) and (5) can be manipulated as follows:

$$\eta = \frac{P_2}{P_{in}} \tag{6}$$

where

$$P_2 = \frac{QSC_P\,\Delta T 4.18}{60\eta_m \times 10^3} \tag{7}$$

where η_m (%) is efficiency of microwave devices, Q (g/m) is weight per meter of dielectric material (softwood), S (m/min) is a rate at which the dielectric material is put on the belt conveyer, C_P [Cal/gr (°C)] is specific heat of dielectric material, ΔT (°C) is heat-up range of $T_1 - T_0$.

3. Research methodology

From a practical point of view, it is well known that for a given microwave system, a load (specimen) placed in different locations inside the applicator absorbs microwave differently. Furthermore, despite the high number of stimulated modes, often a non-uniform field distribution that is constant in time will develop. This field distribution depends mainly on the cavity size, the product geometry and the dielectric properties of the material to be processed. In contrast to single mode application, normally this non-uniform field distribution, which would result in non-uniform heating pattern, is not desired, since it is difficult to control. An undesired non-uniform heating pattern can be prevented by changing the field configuration either by varying cavity geometries (e.g., mode stirrer) or by moving the product (on a conveyer belt or turntable) [3].

It is expected that the continuous microwave applicators technique will be introduced soon. The reason for this is that energy conservation, labour savings and rationalization of production are

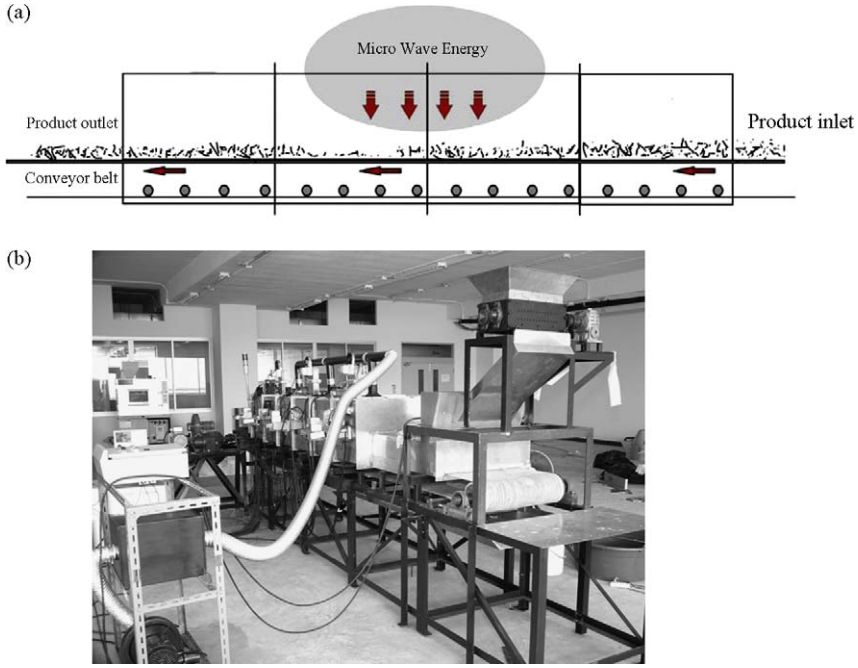

Fig. 1. Experimental equipment: continuous microwave belt drier.

seriously promoted in the high energy consuming wood and rubber industries. Particularly, drying and forming processes in the drying of wood products need a lot of time and energy, which results in a lack of rationality. Only the introduction of some continuous production system through the efficient use of a rational energy source can solve this problem.

4. Experiment procedure

Microwave heating was carried out using a microwave continuous belt drier (Fig. 1). The microwave cavity was a rectangular shape with a cross-sectional area of 94 cm × 47 cm. The drier operates at a frequency of 2.45 GHz with maximum working temperature of 200 °C. The microwave power was generated by means of 14 compressed air-cooled magnetrons. The maximum microwave capacity is 11.2 kW in frequency of 2.45 GHz. The power setting could be adjusted individually in 800 W steps. The magnetrons are fan cooled. The magnetron cover can be adjusted of furnace ventilation by an adjustment wheel. In the continuous processing equipment, two open ends are essential, through which the material to be heated up on the belt conveyer is put in and taken out. The belt conveyor system consists of a drive motor, a tension roller and a belt conveyor. During the heating process, the conveyor speed is adjustable upto 2 m/min and can be set at the potentiometer of control unit.

In this equipment, leakage of microwaves is prevented by the countermeasure in double with a combination of mechanical blocking filter and microwave absorber zone filter is provided at each of the open ends. The microwave leakage was controlled under the DHHS (US Department of Health and Human Services) standard of 5 mW/cm^2. The multiple magnetrons were installed in an asymmetrical position around the rectangular cavity (Fig. 1). The microwave power was then directed into the drier by using waveguides. An infrared camera was used to measure the temperature of the specimens (accurate to ±0.5 °C).

The specimen selected for drying test was a softwood with dimensions of 3 cm × 3 cm × 10 cm which had the initial moisture content of 80% (dry basis) and the initial temperature of 28 °C.

The mechanical characteristics of wood specimens before dried was undergone bending testing, following the BSI, London [31]. While fifteen of the specimens were microwave dried. The microwave dried specimens were weighed before and after they were transferred to the microwave cavity via belt conveyer. The specimens to be dried passed through the drier on an air-permeable microwave transparent conveyor belt. After a certain time, microwave power was applied for a specified period of time. During the heating process, microwaves penetrated the specimen, heating the water until it diffused to the surface. The humid air was then drawn out of the cavity by a suction system. While the drying process proceeded, temperature variations of specimens were measured by using an infrared camera for a specified period of time. The dried specimens left the cavity through another opening for further characterization. The twelve specimens were then removed from the cavity and weighted again to determine the moisture loss. The moisture content of microwave-dried specimen can be calculated based on dry basis from the weight loss of wood specimens before and after microwave drying in order to determine the weight loss. A plastic sheet was wrapped around the specimens to prevent further moisture loss. The other three specimens were capped for bending testing. The 15 conventional dried specimens are covered with plastic sheets after being chopped, removed from the controlled room after one day, and dried in oven at 100 °C, to establish reference strength against which microwave dried specimens can be compared. Finally, the quality of dried specimen was done by SEM (scanning electron microscope).

The dielectric properties for wood specimens were measured at 28 °C using a portable dielectric measurement (network analyzer) over a frequency band ranging from 1.5 to 2.6 GHz as shown in Fig. 2. The portable dielectric measurement kit allows for measurements of the complex permittivity over a wide range of solid, semi-solid, granular and liquid materials. It performs all of the necessary control functions, treatment of the microwave signals, calculation, data processing, and result representation. The software controls the microwave reflectometer to measure the complex reflection coefficient of the material under test (MUT). Then it detects the cavity resonant frequency and quality factor and converts the information into the complex permittivity of the MUT. Finally, the measurement

Table 1
Dielectric properties of wood and penetration depth.

	Data			D_P (m)
	Dielectric constant (ε')	Dielectric loss factor (ε'')	Loss tangent coefficient ($\tan\delta$)	
Present study	1.591	0.033	0.021	1.470
Lehne et al. [28]	2.419	0.036	0.015	1.669
Datta and Anantheswaran [4]	1.5–4	0.015–0.04	0.01	1.946–3.178
Buffer [32]	1.2–5	0.02–0.5	0.017–0.417	0.174–2.090

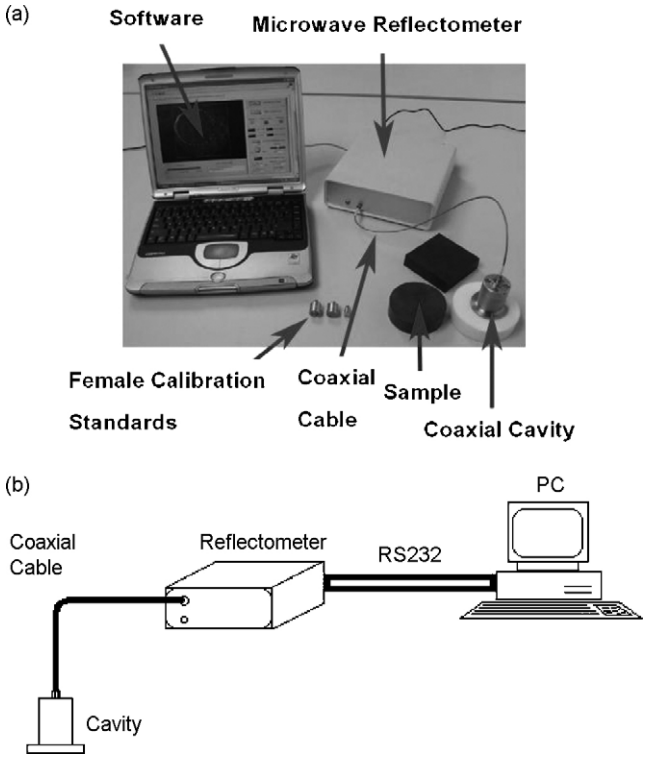

Fig. 2. Portable dielectric measurement (network analyzer).

results are displayed in a variety of graphical formats, or saved to disk. The dielectric properties of wood and its penetration depth obtained from present study and relevant literatures are summarized in Table 1.

5. Results and discussion

Experimental data were analyzed for the drying kinetics for different drying methods and conditions.

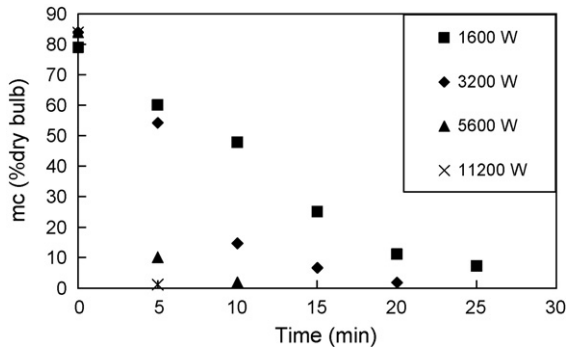

Fig. 3. Moisture profile versus elapsed times for different microwave power levels.

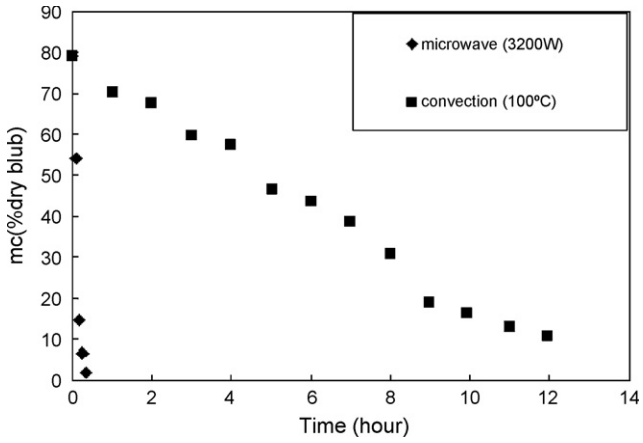

Fig. 4. Comparison of moisture profiles for different drying methods.

Fig. 3 shows moisture profiles with respect to elapsed times for different microwave power levels with constant initial moisture content of 80% (dry basis). It is found that at a high microwave power level the moisture profile of the specimens continuously decreases faster than that in the case of low microwave power level. This is because in the case of higher microwave power level the bulk of this specimen receives the largest amount of microwave energy absorbed. This phenomenon corresponds to the level of absorbed energy in specimens as described in Eq. (1). Furthermore, near the end stage of drying process as the moisture content inside the specimen is reduced, this decreases the microwave energy absorbed. Thus, equilibrium is reached between microwave drying and convective losses by lowering specimen temperature.

Fig. 4 shows the comparison of moisture profiles with respect to elapsed times for different drying methods. It can be observed from Fig. 4 that for microwave drying the specimen dries quickly throughout without the shrinkage phenomena that arises due to uniform heating. It is clear that drying times are drastically reduced compared to conventional drying, from 12 h to less than 1 h. The results show that microwave drying, i.e., microwave continuous belt drier can yield a considerable gain in drying time by a factor of ten or more. In case of conventional drying, as the surface is dried while the interior is still wet the dry layer offered a resistance to the heat transport resulting in a reduction of the evaporation rate as well as drying rate, causing non-uniform shrinkage.

Fig. 5 shows the temperature profile with respect to elapsed times as a parameter of temperature measuring positions with fixed the microwave power level. During the very first period of heating, most of the microwave energy supplied is used to heat the specimen. Wood specimen temperature is raised rapidly up to 100 °C in a few minutes. It is found that only minor temperature differences are observed when microwave energy is applied. This is because an undesired non-uniform heating pattern can be prevented by changing the field configuration either by moving the product on a conveyer belt through the cavity where microwave could be fed at several positions. Besides, considering the multiple magnetron system, the different directions of transmitted wave from different

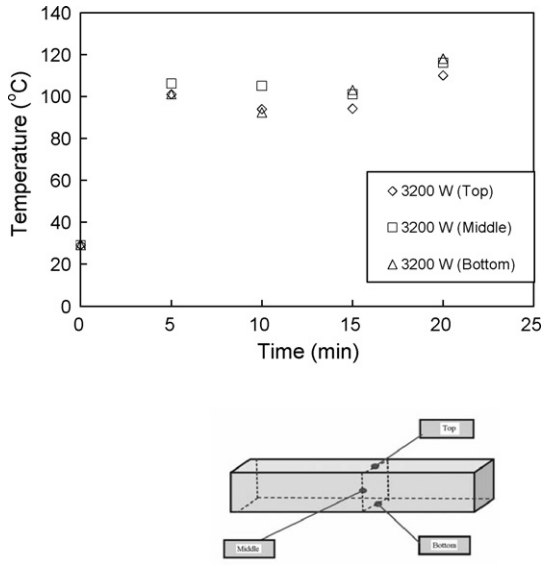

Fig. 5. Temperature variations versus elapsed times for different positions.

magnetron make the uniformity of temperature inside the specimens. This is because of its wave interference and the influence of the wave penetration capability shown in Eq. (2) and Table 1.

Fig. 6 shows the estimation of the efficiency of the applicator (refer to Eq. (6)) where the temperature data used in calculation (averaged value) were directly taken from temperature profile in Fig. 5. It is found that at the same microwave power level (P_{in}) the efficiency of the applicator continuously drops with elapsed times. This is due to the variation of moisture content inside the bulk of specimens (Fig. 4) that results in the variation of microwave absorbed energy. It would correlate to microwave energy absorbed which depends on the change of the configuration of electromagnetic field in the specimens due to the variation of moisture content [19]. Furthermore, near the end stage of drying process as the moisture content inside the bulk of specimens is reduced, the microwave energy absorbed is decreased. Thus, the efficiency of the applicator is reduced. We can conclude again that the heating efficiency largely varies with moisture content inside the bulk of specimens or quantity of dielectric load in microwave applicator. If the moisture content or quantity of dielectric load is decreased, to the contrary, the efficiency rapidly drops. Then, microwaves which could not be absorbed in dielectric load or specimens counterflow to the magnetrons as reflected power and strike its antenna dome. This will largely shorten the life of the magnetrons, and electric discharge may break the magnetron.

As mentioned in the previous work, especially by the authors [22], indicated obviously that the energy consumption by using

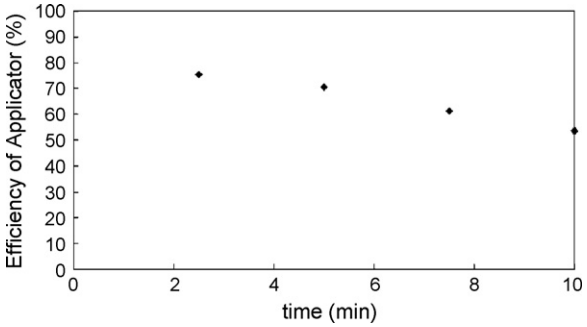

Fig. 6. The estimation of the efficiency of the applicator versus elapsed times.

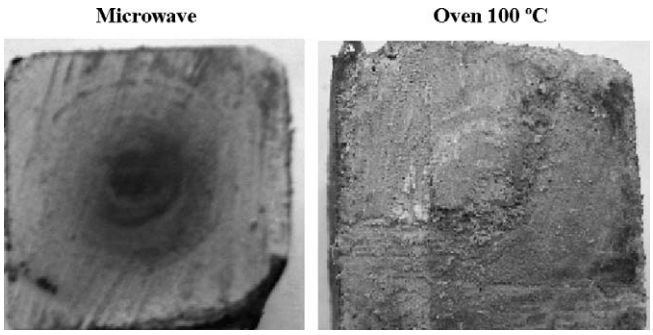

Fig. 7. Comparison of heat pattern in the specimens dried by microwave and oven at 100 °C.

microwave energy can potentially be reduced, Compared to the conventional drying.

Fig. 7 shows a cross section of a wood block after 5 min of microwave irradiation. No significant changes on the surface area were observed after microwave irradiation. The center of wood, however, change to black, indicating that the temperature at the wood core was higher than that at the surface. This is because microwave uniformly irradiated heat from the inside and there is more absorption of the microwave energy at the center of the wood, resulting in temperature at the center being higher than other area. Then, liquid in specimen could be evaporated quickly causing vapor pressure high enough to migrate the moisture which was condensed to cover the entire surface. This phenomenon which does not occur in the conventional drying process could protect the surface to be burnt comparing to the conventional drying process.

In Fig. 8, the quality of specimens dried by microwave is observed to be better than that of conventional dried specimen. The color of specimens dried by microwave remains, whereas the color of the convectional-dried specimen deteriorates.

In the following discussion, the internal structures of wood specimen are investigated base on an analysis of the mechanical properties after drying. Fig. 9 shows the texture overview of the wood specimens under various dried processes by using SEM technique. It is found that the dried specimens in all cases seem to have a similar micro structure arrangement. However, the microwave dried specimen has a better micro structure arrangement because of uniform energy absorption and less shrinkage. This leads to offer

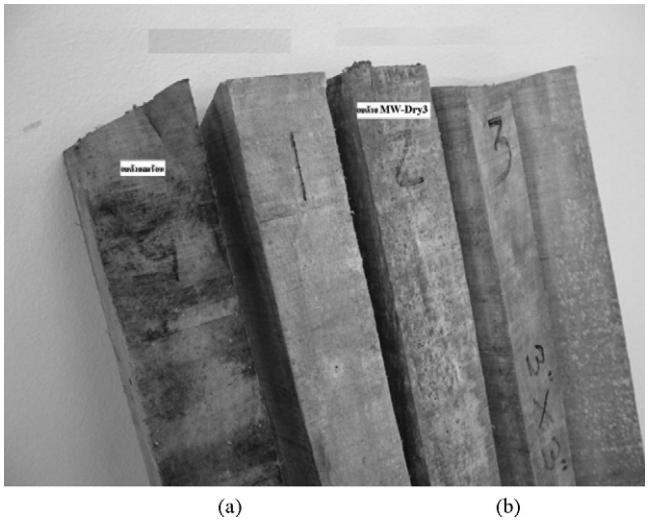

Fig. 8. Comparison of the quality of specimens dried by microwave (a) and oven at 100 °C (b).

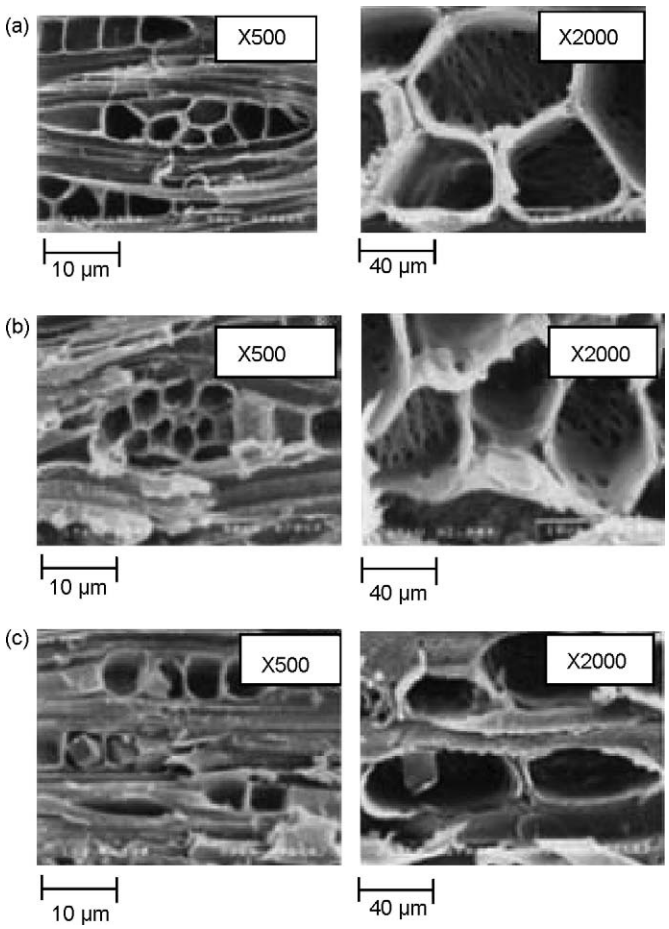

Fig. 9. Microstructure of specimen dried by different methods and conditions: (a) dried by microwave at 3200 W; (b) dried by microwave at 5600 W and (c) dried by oven at 100 °C.

the mechanical properties of dried products. This could be further confirmed by the co-research with material science expert in the following research.

The mechanical characteristics of wood specimens after bending testing based on the BSI, London (Fig. 10) with different drying conditions is shown in Table 1. It is found that the microwave-dried specimens under the conditions presented here seem to have higher strength than those dried at 100 °C in a conventional oven. This is because microwave dried specimens exhibit less shrinkage corresponding to a better micro structure arrangement (Fig. 9). The

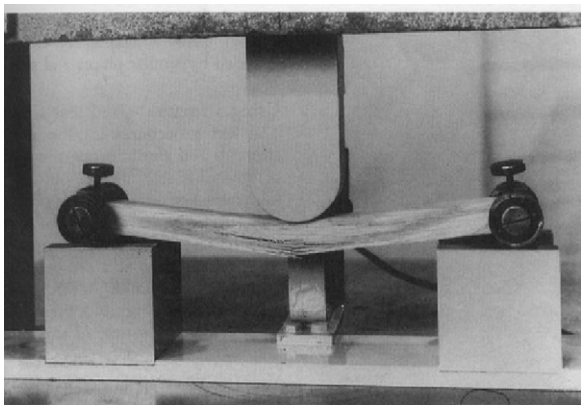

Fig. 10. BSI Standard of static bending test of specimen [31].

Table 2
Comparison of mechanical characteristics (static bending) between specimens dried by microwave and by oven at 100 °C.

Specimen status	Modulus value (MPa)	Stress (MPa)	Toughness (MPa)
Before drying[a]	3112.25	37.23	0.115
Dried by microwave[b]	4464.71	50.73	0.065
Dried by oven at 100 °C[b]	3766.64	45.90	0.064

[a] 80% moisture content (dry basis).
[b] 12–15% moisture content (dry basis).

average strength of microwave and conventional-dried products obtained are 50.73 and 45.90 MPa, respectively (Table 2).

In addition, considering thermal runaway effect, it is well known that the temperature dependence of the dielectric properties that varies according to the material is often very complex and is still unclear. The values of these properties may increase with temperature of decrease with temperature. At room temperature, the wood specimens, exhibits a rapid increase in the loss factor with increasing temperature. In such cases, when this phenomenon known as thermal runaway is apparent, damage such as poor product quality and sample cracking may occur to the product being heated. In this study, great care must be taken to monitor temperatures and turn off the microwave power before the danger period commences. In some instances when this phenomenon cannot be controlled, especially for materials whose the moisture content is close to bone dry or where dried out areas that occur in the product, microwave heating may not be feasible. Understanding, prediction, and preventing or controlling the thermal runaway present a major challenge to the development of microwave processing.

6. Conclusion

Microwave heating using a continuous belt drier provides relatively deeper penetration and displays more uniform heated pattern, compared to that achieved using other simple microwave drying systems or a conventional drying system. The SEM results demonstrated that microwave dried specimens has a better micro structure arrangement because of uniform energy absorption, heat and moisture distribution. In addition, the microwave heating offers better mechanical properties with high strength and little deterioration in its long term performance with higher quality than conventional method do.

Furthermore, in overall, when handling a microwave continuous belt drier correctly, we can conclude the following advantages, over the other heating systems:

(1) Faster, reproducible and more homogeneous heating (high product quality),
(2) Faster heating of thicker layers because the multiple magnetrons are arranged around the cavity, thus the microwaves can penetrate further into the multi-plane of material,
(3) Microwave energy can accelerate the hydration of cement, resulting in rapid strength development of wood in an early period,
(4) Immediately ready for operation and control of heat capacity without delay,
(5) No heat storage losses,
(6) Low specific energy consumption.

The next steps of the research in this problem will be to develop the control system and optimal drying schedules for combined microwave and hot air drying of wood in a microwave continuous belt drier.

Acknowledgement

The authors gratefully acknowledge Thailand Research Fund (TRF) under The Royal Golden Jubilee Ph.D. Program for supporting this research project.

References

[1] A.S. Mujumdar, Handbook of Industrial Drying, 2nd ed., Marcel Dekker, New York, 1995.
[2] A.C. Metaxas, R.J. Meridith, Industrial Microwave Heating, Peter Peregrinus, Ltd, London, 1983.
[3] H. Schubert, M. Regier, The Microwave Processing of Foods, Woodhead Publishing Limited and CRC Press, Cambridge, 2005.
[4] A.K. Datta, R.C. Anantheswaran, Handbook of Microwave Technology for Food Applications, Marcel Dekker, New York, 2001.
[5] P. Ratanadecho, K. Aoki, M. Akahori, Experimental and numerical study of microwave drying in unsaturated porous material, Int. Commun. Heat Mass Trans. 28 (2001) 605–616.
[6] M. Moller, H. Linn, Microwave drying of refractory materials, CN Refractories Special Issues 5 (2001) 79–80.
[7] P. Ratanadecho, K. Aoki, M. Akahori, A numerical and experimental study of microwave drying using a rectangular wave guide, Drying Technol. 19 (2001) 2209–2234.
[8] C. Saltiel, A. Datta, Heat and mass transfer in microwave processing, Adv. Heat Transfer 30 (1997) 1–94.
[9] C.K. Wei, H.T. Davis, E.A. Davis, J. Gordon, Heat and mass transfer in water-laden sand stone, microwave heating, AIChE J. 31 (5) (1985) 842–848.
[10] D. Atong, D.E. Clark, The Effect of Reaction Parameters on Microwave Induced Combustion Synthesis of Al203TiC Composite Powders, Microwave and Radio Frequency Applications, American Ceramics Society, Westerville, OH, 2003, pp. 207–220.
[11] D.A. Brosnan, G.C. Robinson, Introduction to Drying of Ceramics with Laboratory Exercises, The American Ceramic Society (2003) 253.
[12] G. Roussy, A. Bennani, J.M. Thiebaut, Temperature runaway of microwave irradiated materials, J. Appl. Phys. 62 (4) (1987) 1170–1967.
[13] G.A. Kriegsmann, Thermal runaway in microwave heated ceramics: a one-dimensional model, J. Appl. Phys. 71 (4) (1992) 1960–1966.
[14] I.W. Turner, M. Ilic, Combined microwave and convective drying of a porous material, Drying Technol. 9 (5) (1991) 1209–1269.
[15] J. Wang, T. Schmugge, An empirical model for the complex dielectric permittivity of soil as a function of water content, IEEE Trans. Geosci. Remote Sens. GE-18 (4) (1980) 288–295.
[16] J. Monzó-Cabrera, J.M. Catalá-Civera, A.J. Canós, E. De Los Reyes, Simulation of temperature distributions in pressure-aided microwave rubber vulcanization processes, Journal of Microwave Power and Electromagnetic Energy 37 (2) (2002) 73–88.
[17] P. Holl, Two ideal applications for the low energy electron-beam accelerator: vulcanization of pressure-sensitive adhesives and controlled through-curing of coatings on parquet, Radiat. Phys. Chem. 46 (4-6 II) (1995) 953–958.
[18] P. Perre, W. Turner, Microwave drying of softwood in an oversized waveguide, AIChE J. 43 (10) (1997) 2579–2595.
[19] P. Ratanadecho, K. Aoki, M. Akahori, Influence of irradiation time, particle sizes and initial moisture content during microwave drying of multi-layered capillary porous materials, ASME J. Heat Transfer 124 (1) (2002) 151–161.
[20] P. Ratanadecho, K. Aoki, M. Akahori, The characteristics of microwave melting of frozen packed bed using a rectangular wave guide, IEEE Trans. Microwave Theory Tech. 50 (2002) 1487–1494.
[21] P. Rattanadecho, The simulation of microwave heating of wood using a rectangular wave guide (influence of frequency and sample size), Chem. Eng. Sci. 61 (2006) 4798–4811.
[22] P. Rattanadecho, N. Suwannapum, A. Watanasungsuit, A. Duangduen, Drying of dielectric materials using microwave-continuous belt furnace, ASME J. Manuf. Sci. Eng. 129 (1) (2007) 157–163.
[23] P. Rattanadecho, N. Suwannapum, B. Chatveera, D. Atong, N. Makul, Development of compressive strength of cement paste under accelerated curing by using a continuous microwave belt drier, Mater. Sci. Eng. A 472 (2008) 299–307.
[24] P. Perre, I.W. Turner, The use of numerical simulation as a cognitive tool for studying the microwave drying of softwood in an over-sized waveguide, Wood Sci. Technol. 33 (1999) 445–464.
[25] A.L. Antti, Microwave drying of wood: simultaneous measurements pressure, temperature, and weight reduction, Forest Products J. 42 (1992) 49–54.
[26] M. Masakasu, K. Harumi, S. Akihiko, K. Toyoji, T. Keji, Rapid pyrolysis of wood block by microwave heating, J. Anal. Appl. Pyrol. (2003) 1–13.
[27] A. Oloyede, P. Groombridge, The influence of microwave heating on the mechanical properties of wood, J. Mater. Process. Technol. (2000) 67–73.
[28] M. Lehne, G.W. Barton, T.A.G. Langrish, Comparison of experimental and modeling studies for the microwave drying of ironbank timber, Drying Technol. (1999) 2219–2235.
[29] I.W. Turner, A study of the power density distribution generated during the combined microwave and convection drying of softwood, in: Proceedings of the 9th International Drying Symposium, Gold Coast, Australia, August, 1994, pp. 1–4.
[30] H.W. Lee, Combined microwave and convective drying of Korean wood species, in: Proceedings of the 8th International IUFRO Wood Drying Conference, 2003, pp. 146–149.
[31] J. Bodig, B.A. Jayne, Mechanics of Wood and Wood Composites, Van Nostrand Reinhold, Working-Ham, UK, 1982, pp. 106–115.
[32] C.R. Buffer, Microwave Cooking and Processing, Engineering Fundamentals for the Food Scientist, AVI book, Van Nostand Reinhold, New York, 1993.
[33] S. Curet, O. Rouaud, L. Boillereaux, Microwave tempering and heating in a single-mode cavity: numerical and experimental investigations, Chem. Eng. Process.: Process Intensification 47 (9–10) (2008) 1656–1665.

Numerical Analysis of Specific Absorption Rate and Heat Transfer in the Human Body Exposed to Leakage Electromagnetic Field at 915 MHz and 2450 MHz

Teerapot Wessapan

Siramate Srisawatdhisukul

Phadungsak Rattanadecho
e-mail: ratphadu@engr.tu.ac.th

Department of Mechanical Engineering,
Research Center of Microwave Utilization in Engineering (RCME),
Faculty of Engineering,
Thammasat University (Rangsit Campus),
Pathumthani 12120, Thailand

In recent years, society has increased utilization of electromagnetic radiation in various applications. This radiation interacts with the human body and may lead to detrimental effects on human health. However, the resulting thermophysiologic response of the human body is not well understood. In order to gain insight into the phenomena occurring within the human body with temperature distribution induced by electromagnetic field, a detailed knowledge of absorbed power distribution is necessary. In this study, the effects of operating frequency and leakage power density on distributions of specific absorption rate and temperature profile within the human body are systematically investigated. This study focuses attention on organs in the human trunk. The specific absorption rate and the temperature distribution in various tissues, obtained by numerical solution of electromagnetic wave propagation coupled with unsteady bioheat transfer problem, are presented. [DOI: 10.1115/1.4003115]

Keywords: microwave, temperature distribution, specific absorption rate, human body

1 Introduction

Electromagnetic (EM) energy is a one heat source that is attractive over conventional heating methods because an electromagnetic wave that penetrates the surface is converted into thermal energy within the material volumetrically. High speed startup, selective energy absorption, instantaneous electric control, nonpollution, high energy efficiency, and high product quality are several advantages of microwave heating. Therefore, this technology is used in many industrial and household applications such as heating process [1] and drying process [2]. Rapid development of electromagnetic energy applications causes an increase in public concern about health risks from electromagnetic energy emitted from various sources [3].

Increasing use of high power electromagnetic energy results in the necessity to identify the limits of safe exposure with respect to thermal hazards. The amount of energy absorbed by tissue depends on many factors including frequency, dielectric property of the tissue, irradiating time exposure, intensity of electromagnetic radiation, and water content of the tissue. For this reason, public organizations throughout the world have established safety guidelines for electromagnetic wave absorption values [3]. For human exposure to electromagnetic fields, these guidelines are based on peak spatial-average specific absorption rate (SAR) for human body tissues.

The power absorption in human tissues induces temperature increase inside tissues. The severity of the physiological effect produced by small temperature increases can be expected to worsen in sensitive organs. An increase in approximate 1–5 °C in human body temperature can cause numerous malformations, temporary infertility in males, brain lesions, and blood chemistry changes. Even a small temperature increase in human body (approximately 1 °C) can lead to altered production of hormones and suppressed immune response [4].

In the past, the experimental data on the correlation of SAR levels to the temperature increases in human body are sparse. There is a research on SAR distribution of three-layer human body, which simulates three-layer physical models of skin, fat, and muscle tissues [5]. There are limited data available on thermal properties and dielectric properties of human tissues, as very few epidemiological studies have been conducted. There are some experimental studies in animals such as rat [6], cow [7], and pig [8]. However, the results may not represent the practical behavior of human tissues. Most previous studies of human body exposed to electromagnetic field did not consider heat transfer, resulting in an incomplete analysis. Therefore, modeling of heat transport in human tissues is needed in order to completely explain. The modeling of heat transfer in human tissues has been investigated. Earlier studies of heat transfer in human tissues utilized the general bioheat equation [9]; thereafter, the coupled model of general bioheat equation and Maxwell's equation were used to model human tissues exposed to electromagnetic field [10]. Other researches have been done for temperature distribution over the surface, and the various biotissues exposed to an electric field have been studied [11,12]. Furthermore, few reports have suggested thermal interactions for microwave frequency fields [13]. Researchers also carried out temperature increases in human head exposed to a handheld cellular phone [14–17].

However, most studies of temperature increases induced by electromagnetic waves have not been considered in a realistic domain of the human body with complicated organs of several types of tissues. There are few studies on the temperature and electromagnetic field interaction in realistic physical model of the human

Contributed by the Heat Transfer Division of ASME for publication in the JOURNAL OF HEAT TRANSFER. Manuscript received January 6, 2010; final manuscript received November 17, 2010; published online January 31, 2011. Assoc. Editor: Darrell W. Pepper.

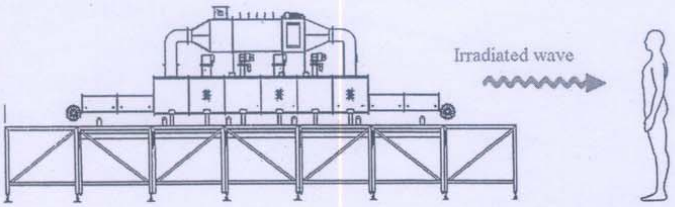

Fig. 1 Wave leakage from an electromagnetic radiation device

body due to the complexity of the problem, even though it is directly related to the thermal injury of tissues. Therefore, in order to provide information on levels of exposure and health effects from electromagnetic radiation adequately, it is essential to simulate the coupled electromagnetic field and heat transfer within an anatomically based human body model to represent the actual process of heat transfer within the human body.

This research is a pioneer work that simulates the SAR distribution and temperature distribution over an anatomically based human body. In this research, a two-dimensional human cross section model [18] was used to simulate the SAR distribution and temperature distribution over the human body at different frequencies. Electromagnetic wave propagation in tissues was investigated by using Maxwell's equations. An analysis of heat transfer in human tissues exposed to microwaves was investigated by using the bioheat equation. The effects of operating frequency (915 MHz and 2450 MHz) and leakage power density (5 mW/cm^2, 10 mW/cm^2, 50 mW/cm^2, and 100 mW/cm^2) on distributions of specific absorption rate and temperature profile within the human body are systematically investigated. The 915 MHz and 2450 MHz frequencies were chosen for simulations in this study as they have wavelengths in the microwave band and are used most frequently in the application of industrial high power microwave heating. The obtained values provide an indication of limitations that must be considered for temperature increases due to localized electromagnetic energy absorption.

2 Formulation of the Problem

Electromagnetic fields emitted by high power radiation devices are harmful. Figure 1 shows the leakage of electromagnetic energy from the industrial microwave drying system to a human body. It is known that a human body exposed to intense electromagnetic waves can cause significant thermal damage in sensitive tissues within the human trunk. Therefore, it is necessary to investigate the temperature distributions due to exposure to electromagnetic waves in order to investigate the hot spot zones within the human body especially in abdominal and thoracic cavities.

Due to ethical consideration, exposing a live human body to electromagnetic fields for experimental purposes is difficult. It is more convenient to develop a realistic model through numerical simulation. The next section, an analysis of specific absorption rate and heat transfer in the human body exposed to electromagnetic field is illustrated. The system of governing equations as well as initial and boundary conditions are solved numerically using the finite element method (FEM).

3 Methods and Model

The first step in evaluating the effects of a certain exposure to radiation in the human body is the determination of the induced internal electromagnetic field and its spatial distribution. Thereafter, electromagnetic energy absorption, which results in temperature increases within particular parts of the human body and other interactions, can be considered.

3.1 Human Model. From Fig. 2, a two-dimensional human body model used in this study is obtained by the image processing technique from the work of Shiba and Higaki [18]. The model has

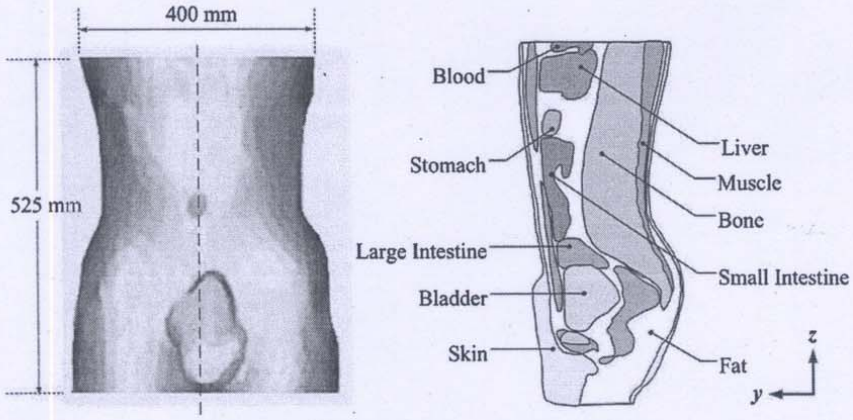

Fig. 2 Human body vertical cross section [16]

Table 1 Dielectric properties of tissues

Tissue	ρ (kg/m^3)	915 MHz σ (S/m)	915 MHz ε_r	2450 MHz σ (S/m)	2450 MHz ε_r
Skin	1125	0.92	44.86	2.16	41.79
Fat	916	0.09	5.97	0.13	5.51
Muscle	1047	1.33	50.44	1.60	46.40
Bone	1038	2.10	44.80	2.10	44.80
Large intestine	1043	2.04	53.90	2.04	53.90
Small intestine	1043	3.17	54.40	3.17	54.40
Bladder	1030	0.69	18.00	0.69	18.00
Blood	1058	2.54	58.30	2.54	58.30
Stomach	1050	2.21	62.20	2.21	62.20
Liver	1030	1.69	43.00	1.69	43.00

Table 2 Thermal properties of tissues

Tissue	k (W/m K)	C_p (J/kg K)	ω_b	Q_{met} (W/m^3)
Skin	0.35	3437	0.02	1620
Fat	0.22	2300	4.58×10^{-04}	300
Muscle	0.6	3500	8.69×10^{-03}	480
Bone	0.436	1300	4.36×10^{-04}	610
Large intestine	0.6	3500	1.39×10^{-02}	9500
Small intestine	0.6	3500	1.74×10^{-02}	9500
Bladder	0.561	3900	0.00×10^{00}	
Blood	0.45	3960		
Stomach	0.527	3500	7.00×10^{-03}	
Liver	0.497	3600	0.017201	

a dimension of 400 mm in width and 525 mm in height. This model comprises ten types of tissues, which are skin, bone, muscle, fat, nerve, blood, and so forth. These tissues have different dielectric and thermal properties. The thermal properties and dielectric properties of tissues at the frequencies of 915 MHz and 2450 MHz are given in Tables 1 and 2, respectively. As very few studies associated with human tissue properties have been conducted, some of the tissue properties are not quantified. It is also difficult to directly measure tissue properties of a live human. Therefore, we used an assumption of comparing them to animal tissues (it should be noted that the properties based on animal experiments are used for most thermal parameters because no actual data are available for the parameters of the human model). Figure 2 shows a vertical cross section through the middle plane of the human trunk model.

3.2 Equations for Electromagnetic Wave Propagation Analysis. Mathematical models were developed to predict the electric field, SAR, and temperature distribution within the human body. To simplify the problem, the following assumptions were made.

1. Electromagnetic wave propagation is modeled in two dimensions over the y-z plane.
2. The human body in which electromagnetic waves and human body interact proceeds in the open region.
3. The computational space is truncated by scattering boundary condition.
4. In the human body, an electromagnetic wave is characterized by transverse electric fields (TE mode).
5. The model assumes that dielectric properties of tissues are constant.

The electromagnetic wave propagation in the human body is calculated by Maxwell's equations [10], which mathematically describe the interdependence of the electromagnetic waves. The general form of Maxwell's equations is simplified to demonstrate the electromagnetic field of microwaves penetrated in the human body as the following equations:

$$\nabla\times\left(\frac{1}{\mu_r}\nabla\times E\right)-k_0{}^2\left(\varepsilon_r-\frac{j\sigma}{\omega\varepsilon_0}\right)E=0 \tag{1}$$

$$\varepsilon_r=n^2 \tag{2}$$

where E is the electric field intensity (V/m), μ_r is the relative magnetic permeability, n is the refractive index, ε_r is the relative dielectric constant, $\varepsilon_0=8.8542\times10^{-12}$ F/m is the permittivity of free space, and σ is the electric conductivity (S/m), $j=\sqrt{-1}$.

3.2.1 Boundary Condition for Wave Propagation Analysis. Microwave energy is emitted by a microwave high power device and strikes the human body with a particular power density. Therefore, boundary condition for electromagnetic wave, as shown in Fig. 3, is considered as follows.

It is assumed that the uniform wave flux strikes the left side of the human body. Therefore, at the left boundary of the considered domain, an electromagnetic simulator employs TE wave propagation port with a specified power density,

$$S=\int(E-E_1)\cdot E_1/\int E_1\cdot E_1 \tag{3}$$

Boundary conditions along the interfaces between different media, for example, between air and tissue or tissue and tissue, are considered as a continuity boundary condition,

$$n\times(H_1-H_2)=0 \tag{4}$$

The outer sides of the tissue boundaries are considered as a scattering boundary condition,

$$n\times(\nabla\times E_z)-jkE_z=-jk(1-k\cdot n)E_{0z}\exp(-jk\cdot r) \tag{5}$$

3.3 Interaction of Electromagnetic Waves and Human Tissues. Interaction of electromagnetic fields with biological tissues can be defined in terms of SAR. Human tissues are generally lossy mediums for EM waves with finite electric conductivity. They are usually neither good dielectric materials nor good con-

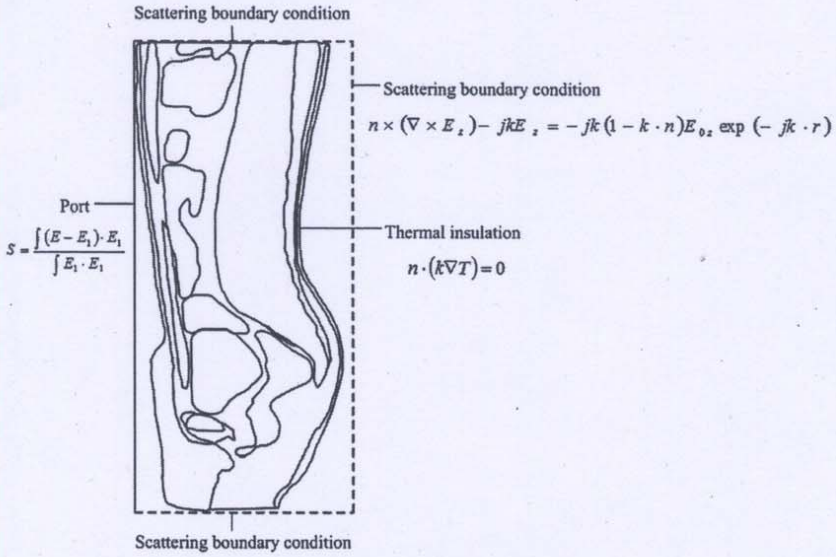

Fig. 3 Boundary condition for analysis

ductors. When EM waves propagate through the human tissues, the energy of EM waves is absorbed by the tissues. The specific absorption rate is defined as a power dissipation rate normalized by material density [8]. The specific absorption rate is given by

$$\mathrm{SAR} = \frac{\sigma}{\rho}|E|^2 \tag{6}$$

where E is the root mean square electric field (V/m), σ is the conductivity (S/m), and ρ is the mass density of the tissue ($\mathrm{kg/m^3}$).

3.4 Equations for Heat Transfer Analysis. The electric field within the model attenuates due to energy absorption. The absorbed energy is converted to thermal energy, which increases the tissue temperature. To solve the thermal problem, the temperature distribution in the human body has been evaluated by the coupled bioheat and Maxwell equations. The temperature distribution corresponded to the specific absorption rate. This is because the specific absorption rate within the human body distributes, owing to energy absorption. Thereafter, the absorbed energy is converted to thermal energy, which increases the tissue temperature.

Heat transfer analysis of the human body is modeled in two dimensions over the y-z plane. To simplify the problem, the following assumptions were made.

1. Human tissues are biomaterial with constant thermal properties.
2. No phase change in substance occurs within the tissues.
3. There is no energy exchange throughout the human body model.
4. There is no chemical reactions occur within the tissues.
5. Local thermodynamic equilibrium is considered.

Corresponding electromagnetic field and temperature profiles can also be assumed to be two dimensional in the y-z plane. There is a continuity boundary condition between the organs within the human body. The temperature distribution inside the human model is obtained by using Pennes' bioheat equation [19]. The transient bioheat equation effectively describes how transfer occurs within the human body, and the equation can be written as

$$\rho C\frac{\partial T}{\partial t} = \nabla \cdot (k\nabla T) + \rho_b C_b \omega_b (T_b - T) + Q_{\mathrm{met}} + Q_{\mathrm{ext}} \tag{7}$$

where ρ is the tissue density ($\mathrm{kg/m^3}$), C is the heat capacity of tissue (J/kg K), k is the thermal conductivity of tissues (W/m K), T is the temperature (°C), T_b is the temperature of blood (°C), ρ_b is the density of blood before entering ablation region ($\mathrm{kg/m^3}$), C_b is the specific heat capacity of blood (J/kg K), ω_b is the blood perfusion rate (1/s), Q_{met} is the metabolism heat source ($\mathrm{W/m^3}$), and Q_{ext} is the external heat source (microwave heat-source density) ($\mathrm{W/m^3}$).

In the analysis, heat conduction between tissues and blood flow is approximated by the term $\rho_b C_b \omega_b (T_b - T)$. The metabolism heat source is negligible, and therefore $Q_{\mathrm{met}}=0$.

The external heat source is equal to the resistive heat generated by electromagnetic field (microwave power absorbed), which defined as

$$Q_{\mathrm{ext}} = \tfrac{1}{2}\sigma_{\mathrm{tissue}}|\bar{E}|^2 \tag{8}$$

where $\sigma_{\mathrm{tissue}}=2\pi f \varepsilon_r' \varepsilon_0$

3.4.1 Boundary Condition for Heat Transfer Analysis. The heat transfer analysis is considered only in the human body domain, which does not include parts of the surrounding space. As shown in Fig. 3, the boundaries of the human body are considered as an insulated boundary condition,

$$n \cdot (k\nabla T) = 0 \tag{9}$$

It is assumed that no contact resistance occurs between the internal organs of the human body. Therefore, the internal boundaries are assumed to be a continuity boundary condition,

$$n \cdot (k_u \nabla T_u - k_d \nabla T_d) = 0 \tag{10}$$

3.4.2 Initial Condition for Heat Transfer Analysis. For this analysis, the temperature distribution within the human body is assumed to be uniform. Therefore, the initial temperature of the human body is defined as

$$T(t_0) = 37\,^\circ\mathrm{C} \tag{11}$$

The thermoregulation mechanisms and the metabolic heat generation of each tissue have been neglected to illustrate the clear temperature distribution. At the skin-air interface, the insulated boundary condition has been imposed to clearly illustrate the temperature distribution.

3.5 Calculation Procedure. To date, there are three principal techniques within computation electromagnetic (CEM): finite difference time domain method (FDTD) [2], method of moments (MOM) [10], and FEM. FEM has been extensively used in the simulation of electromagnetic field. Moreover, FEM models can provide users with quick and accurate solutions to multiple systems of differential equations.

In this research, the finite element method is used to analyze the transient problems. The computational scheme is to assemble finite element model and compute a local heat generation term by performing an electromagnetic calculation using tissue properties. In order to obtain a good approximation, a fine mesh is specified in the sensitive areas. This study provides a variable mesh method for solving the problem, as shown in Fig. 4. The coupled model of electromagnetic field and thermal field is solved by the FEM model, which was implemented using COMSOL™ MULTIPHYSICS 3.4, to demonstrate the phenomenon that occurs within the human body exposed to electromagnetic field. The study employs an implicit time step scheme to solve the electric field and temperature field. In this research, a time step of 10^{-2} s and 10^{-12} s are used to solve Maxwell's equations and bioheat equation, respectively. These are found to be practical to achieve each time step convergence. The temperature distribution has been evaluated by taking into account the specific absorption rate due to the electromagnetic field exposure at a particular frequency. Until the steady state is reached, the temperature at each time step is collected.

The 2D model is discretized using triangular elements, and the Lagrange quadratic is used to approximate temperature and SAR variation across each element. The convergence test of the frequency of 2450 MHz are carried out to identify the suitable number of elements required. The number of elements where solution is independent of mesh density is found to be 92,469. Higher numbers of elements are not tested due to lack of computational memory and performance. The convergence curve resulting from the convergence test is shown in Fig. 5.

4 Results and Discussion

In this study, the coupled mathematical model of bioheat transfer and electromagnetic wave propagation as well as the initial temperature of 37°C for all cases are used for the analysis. For the simulation, the thermal and dielectric properties are directly taken from Tables 1 and 2, respectively. The exposed leakage power density used in this study refers to the ICNIRP standard for safety level at the maximum SAR value of 2 W/kg [3]. However, there are frequently exceeded values of leakage power density in the industrial working area due to the leakage of microwave from the microwave high power devices [3]. In the drying industry, only two microwave frequencies of 915 MHz and 2450 MHz are available. In this analysis, the effects of operating frequency (915 MHz and 2450 MHz) and leakage power density (5 $\mathrm{mW/cm^2}$, 10 $\mathrm{mW/cm^2}$, 50 $\mathrm{mW/cm^2}$, and 100 $\mathrm{mW/cm^2}$) on distributions of specific absorption rate and temperature profile within the hu-

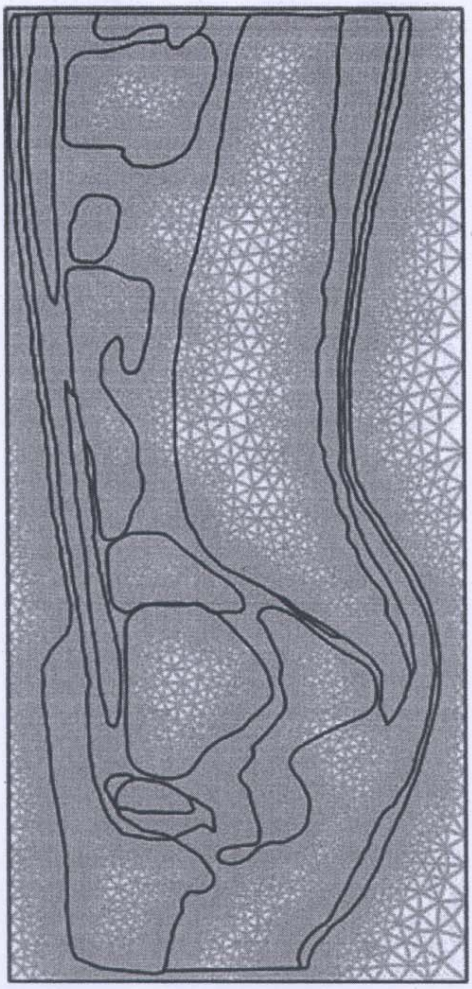

Fig. 4 An initial two-dimensional finite element mesh of human cross section model

man body are systematically investigated. The influences of frequencies and leakage power density on human body subject to electromagnetic wave are discussed in detail.

4.1 Verification of the Model. It must be noted in advance that it is not possible to make a direct comparison of the model in this study and the experimental results. In order to verify the accuracy of the present numerical model, the simple case of the simulated results is then validated against the numerical results

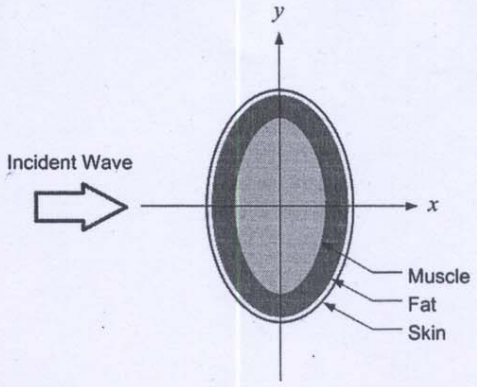

Fig. 6 Geometry of the validation model obtained from the paper [3]

with the same geometric model obtained by Nishizawa and Hashimoto [5]. The horizontal cross section of three-layer human tissues as shown in Fig. 6 is used in the validation case. In the validation case, the leakage power density exposed to the electromagnetic frequency of 1300 MHz is 1 mW/cm^2. The results of the selected test case are illustrated in Fig. 7 for SAR distribution in the human body. Table 3 clearly shows a good agreement in the maximum value of the SAR of tissues between the present solution and that of Nishizawa and Hashimoto. This favorable comparison lends confidence in the accuracy of the present numerical model. It is important to note that there may be some errors occurring in the simulations, which are generated by the input dielectric properties and the numerical scheme.

4.2 Distribution of Electric Field. To illustrate the distribution of penetrated electric field inside each organ of the human body, simulation analysis is required. Figure 8 shows the simulation of electric field pattern inside the human body exposed to electromagnetic field of TE mode propagation along the vertical cross section human body model at the frequencies of 915 MHz and 2450 MHz.

Figure 8(*a*) shows the distribution of electric field at the frequency of 915 MHz. It is found that a large part of electromagnetic wave at 915 MHz can penetrate further into the body. This electric field leads to deeper electromagnetic energy absorbed in the organs of human body in comparison to the frequency of 2450 MHz, which will be discussed later. With the lower frequency, a large part of electromagnetic wave is able to penetrate into the human body due to its long wavelength, which corresponds to a larger penetration depth.

Figure 8(*b*) shows the distribution of electric field at the fre-

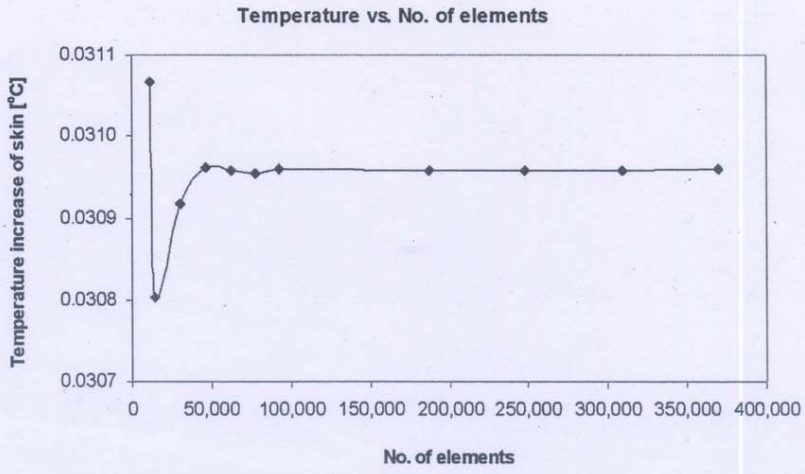

Fig. 5 Grid convergence curve of the 2D model

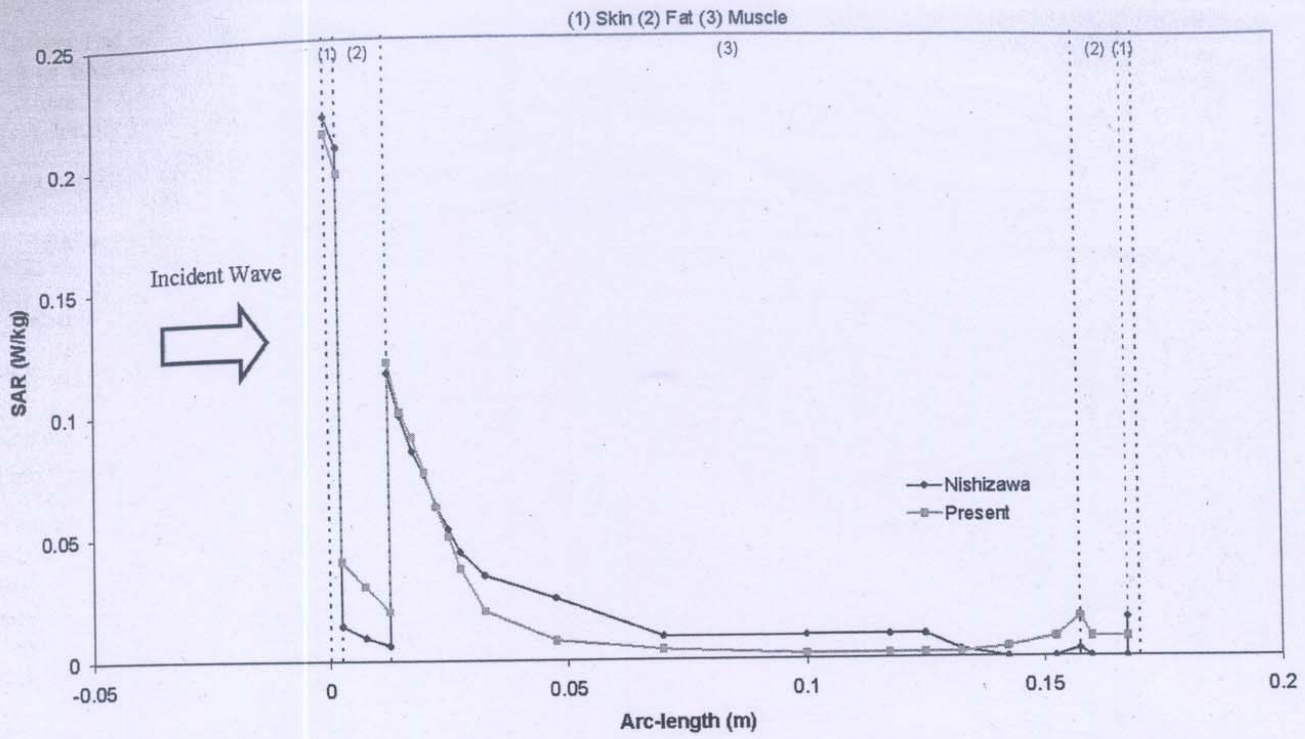

Fig. 7 Comparison of the calculated SAR distribution to the SAR distribution obtained by Nishizawa and Hashimoto [5]

quency of 2450 MHz. A high frequency wave has a short wavelength that corresponds to a small penetration depth of the electromagnetic wave. It is found that the electric field diminishes within very small distances, which results in a low specific absorption rate in organs deep inside the human trunk. This phenomenon explains why the electric field and therefore the specific absorption rate are greatest at the skin and decay sharply along the propagation direction for a short wavelength. It can be seen that the distribution of electric field for the higher frequency occurs in the outer parts of the body, especially in skin, fat, and muscle. The maximum electric field intensities are 91.51 V/m at the frequency of 915 MHz and 56.12 V/m at the frequency of 2450 MHz. The electric field within the human body is extinguished where the electric field attenuates due to absorbed electromagnetic energy and is converted to heat.

Table 3 Comparison of the results obtained in the present study with those of Nishizawa and Hashimoto [5]

	Present work	Published work [5]	% Difference
SAR_{max} in skin	0.212	0.220	3.63
SAR_{max} in fat	0.198	0.206	3.88
SAR_{max} in muscle	0.116	0.120	3.33

4.3 SAR Distribution in Human Tissues. Figure 9 shows the SAR distribution evaluated on the vertical section of the human body in which the maximum SAR value occurs. It is evident from the results that the dielectric properties, as shown in Table 1, can become significant on SAR distribution in human tissues when microwave energy is exposed in these tissues. The magnitude of dielectric properties in each organ will directly affect the amount of SAR within the human body. The highest SAR values are obtained in the region of the skin for the frequency of 915 MHz at 3.43 W/kg and for the frequency of 2450 MHz at 3.02 W/kg. It is found that the SAR distribution in the human model is

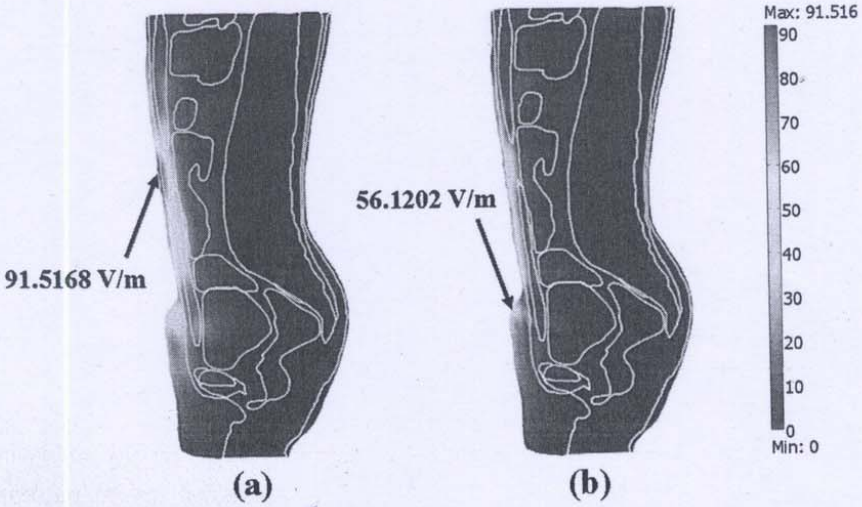

Fig. 8 Electric field distribution in human body (V/m) exposed to the leakage power density of 5 mW/cm^2 at the frequencies of (*a*) 915 MHz and (*b*) 2450 MHz

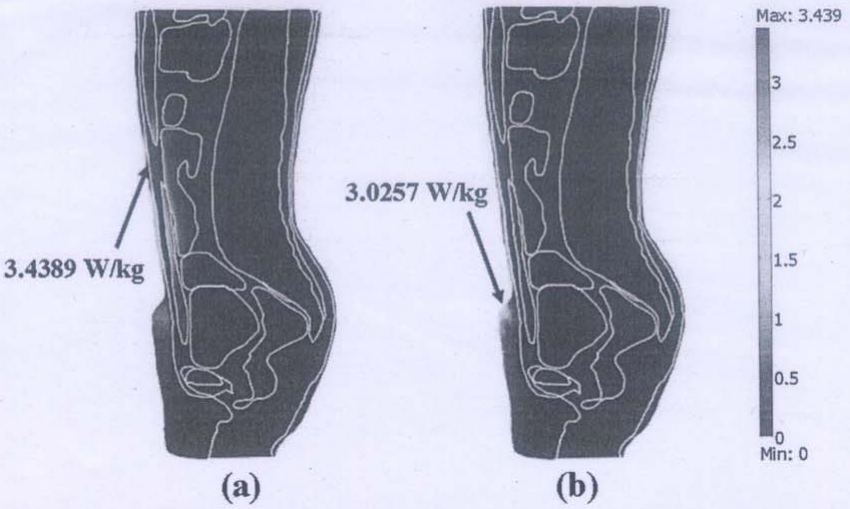

Fig. 9 SAR distribution in human body (W/kg) exposed to the leakage power density of 5 mW/cm^2 at the frequencies of (*a*) 915 MHz and (*b*) 2450 MHz

different due to the effect of the frequency and the dielectric properties of human tissues. From Fig. 9, it appears that for the frequency of 915 MHz, the highest SAR values also occur in the muscle and the small intestine due to the effect of high values of the dielectric properties. Comparing to the ICNIRP limit of SAR values (2 W/kg), the resulting SAR values are exceeded in all cases.

4.4 Temperature Distribution. Figure 10 shows the temperature increase of the organs in human body exposed to electromagnetic waves at various times. For the human body exposed to the leakage of electromagnetic wave from a high power microwave heating device at the frequency of 915 MHz or 2450 MHz for a period of time, the temperature within the human body (Fig. 10) is increased corresponding to the specific absorption rate (Fig. 9). This is because the electric field within the human body attenuates, owing to the energy absorbed, and thereafter the absorbed energy is converted to thermal energy, which increases the human body temperature. It is found that at the different frequencies, the distribution patterns of temperature at a particular time are quite different. The hot spot zone is strongly displayed at the 10 min for the frequency of 915 MHz, owing to the extensive penetration depth and different properties of tissues. To a lesser extent, at the frequency of 2450 MHz, the temperature increases in the human body are always found at the periphery of the body correlated with the electric field and SAR (Figs. 8 and 9). For the case of microwave frequency at 915 MHz, the highest temperature of 37.0487°C occurs in the fat, as shown in Fig. 10(*c*). A different pattern of temperature distribution is obtained at the 2450 MHz frequency, as shown in Fig. 10(*c*), in which the highest temperature of 37.0311°C is presented in the skin. The maximum temperature increases, with the leakage power density of 5 mW/cm^2, at the 915 MHz and 2450 MHz frequencies are 0.048°C and 0.031°C, respectively. These are much lower than the thermal damage temperature within the range of 1–5°C.

An electromagnetic wave exposure (for example, the leakage from microwave heating system) usually lasts only a few minutes; hence, the steady-state temperature rise is rarely reached, except for workers who work in the leakage area. Figures 11 and 12 show the temperature distributions inside the human body at the 915 MHz and 2450 MHz frequencies for different exposure times. At 915 MHz, fat tissue temperature increases slower than the other tissues due to its low lossy behavior. Fat tissue also has maximum steady-state temperature due to its low blood perfusion rate. It is found that at 915 MHz, the internal tissues (fat and bone) reach steady state slower than the external tissues (skin) due to the low thermal conductivity of the fat tissue. However, at 2450 MHz, all of the temperature increases can reach steady state within a short period due to the high thermal conductivity of the skin tissue as well as the low heat capacity of the fat tissue.

4.5 Comparison of SAR Distribution and Temperature Distribution in Human Tissues. Consider the relation of SAR and temperature distribution at the extrusion line (Fig. 13), temperature increases of human tissues are induced by local dissipation of SAR. For a human exposed to the leakage power density of 5 mW/cm^2, Fig. 14 shows the maximum SAR of the 2450 MHz frequency (2.0 W/kg) in the skin region. The maximum SAR value of the 2450 MHz is approximately equal to the maximum SAR value of the 915 MHz frequency (2.0 W/kg) in the skin. However, Fig. 15 shows that the maximum temperature increase of the 2450 MHz frequency in the skin (0.02°C) is lower than the maximum temperature increase of the 915 MHz frequency in the fat (0.03°C). These different behaviors are due to the fact that for the same SAR value at different frequencies, the temperature increase is different. The maximum SAR of the 2450 MHz frequency induces the temperature increase in the skin that is lower than the temperature increase in the fat of the 915 MHz frequency. Consequently, since the interior of the fat region has a lower blood perfusion rate (4.58×10^{-4} 1/s) than the skin (0.02 1/s) and fat is bounded by low thermal conductivity tissue (skin), the heat transfer of fat from blood perfusion is less effective. At the same time, the high blood perfusion is present in the skin.

The localized maximum SAR for the frequencies of 915 MHz and 2450 MHz is shown in Fig. 16. For the value of localized SAR for each organ, it is found that SAR increases as the frequency decreases. For both frequencies, the three highest SARs are shown for skin, muscle, and small intestine. Furthermore, the localized SARs of the 915 MHz frequency are higher than the 2450 MHz frequency in all organs.

The maximum localized temperature increases in all tissues for the frequency of 915 MHz and 2450 MHz are shown in Fig. 17. The maximum temperature increase occurs in fat at the 915 MHz frequency, whereas the maximum temperature increase appears in the skin tissues at the 2450 MHz frequency. Since the penetration depth of the 915 MHz microwave frequency is larger than the 2450 MHz frequency and the inner organs have high dielectric properties, the larger temperature increases of the 915 MHz frequency are particularly high in the inner tissues (small intestine and bladder).

As a result, the human heterogeneous tissues greatly influence the temperature increases in the skin region exposed to the

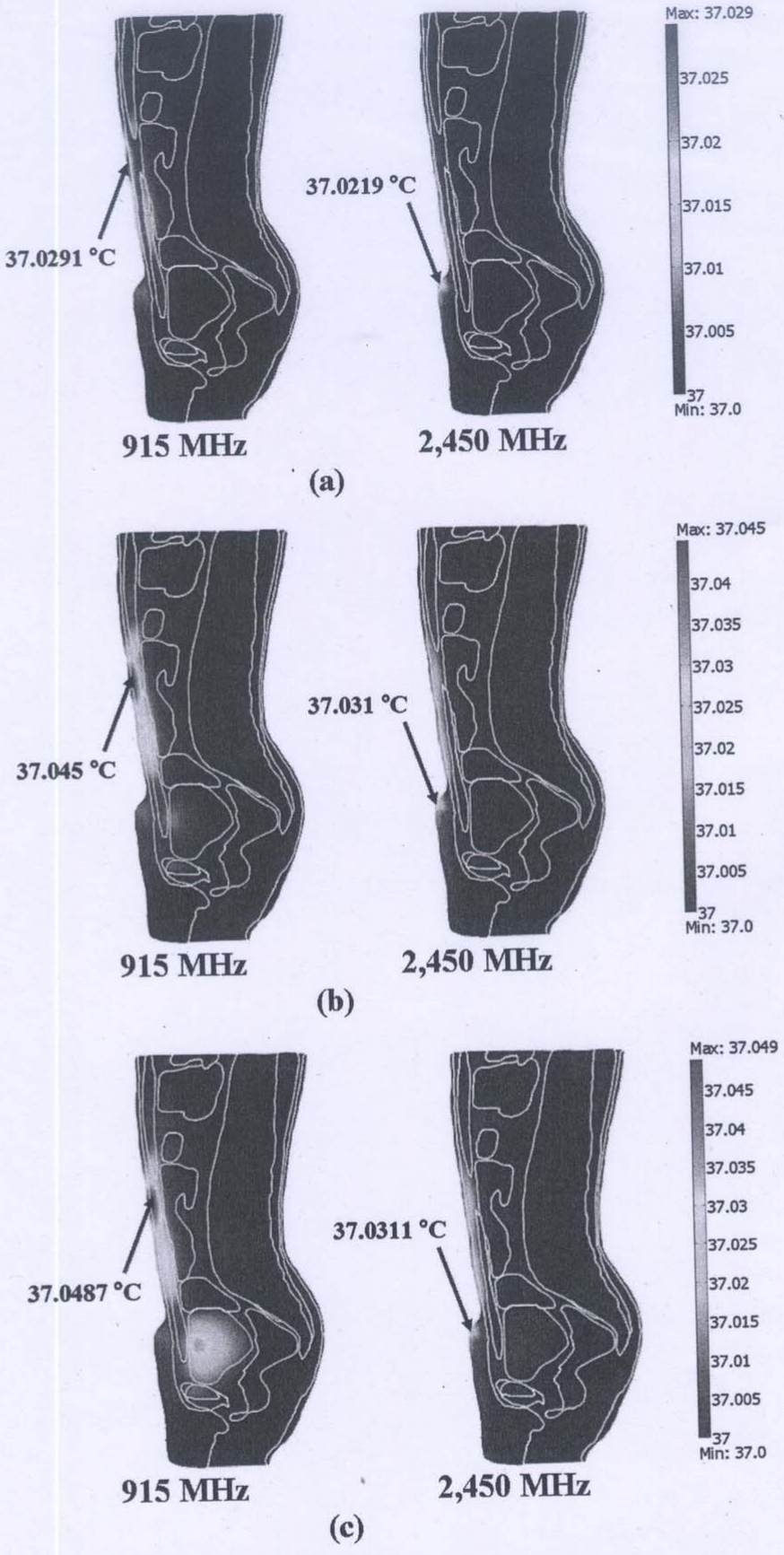

Fig. 10 The temperature distribution of human body exposed to electromagnetic wave at the frequencies of 915 MHz and 2450 MHz: (*a*) 1 min, (*b*) 10 min, and (*c*) steady state

frequency of 2450 MHz and in the fat region for the frequency of 915 MHz. It is found that the temperature distributions are not proportional to the local SAR values. Nevertheless, these are also related to the parameters such as thermal conductivity, dielectric properties, and blood perfusion rate. It is therefore important to use a thermal model couple with electromagnetic wave propagation model to asses the health risk in terms of temperature increase from electromagnetic exposure.

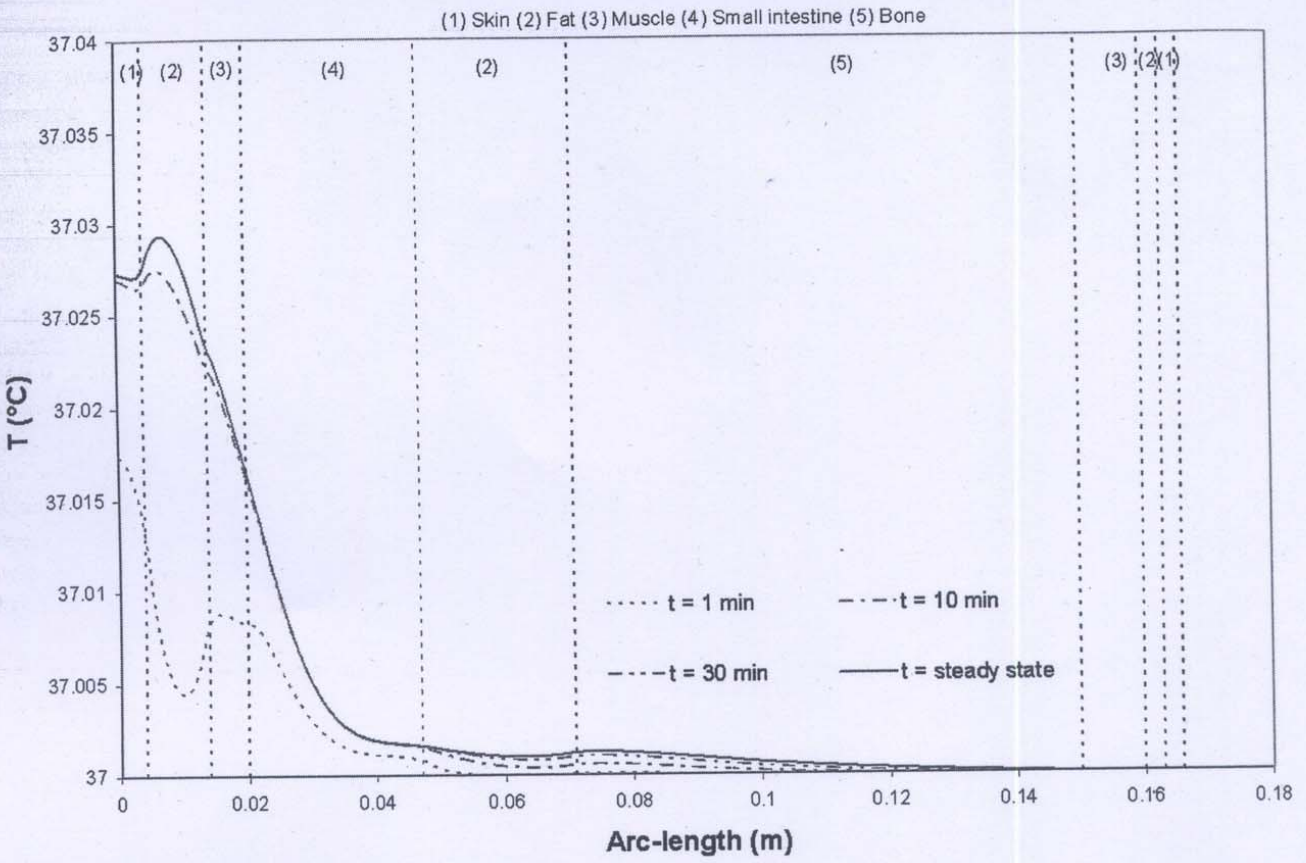

Fig. 11 Temperature distribution versus arc length of human body at various times exposed to the electromagnetic frequency of 915 MHz at the leakage power density of 5 mW/cm^2

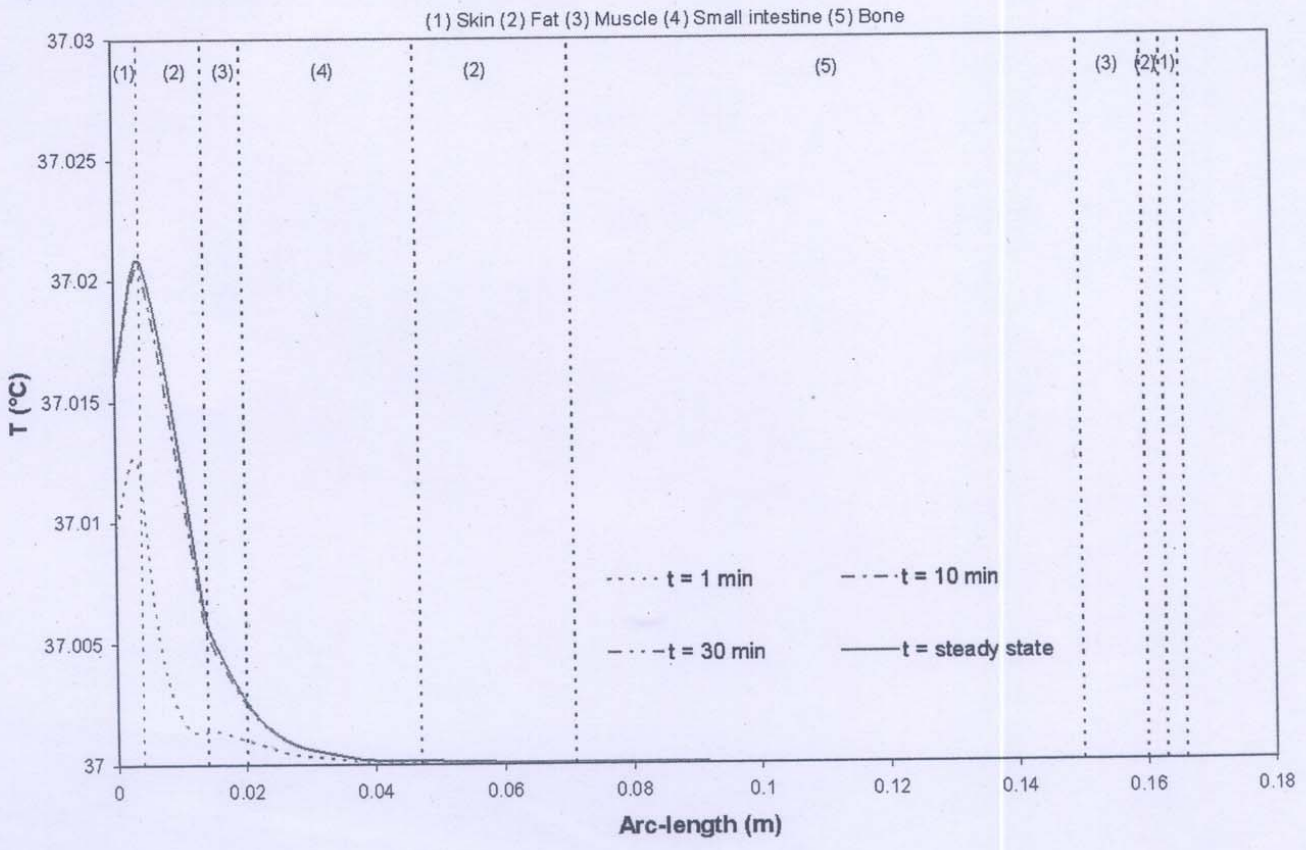

Fig. 12 Temperature distribution versus arc length of human body at various times exposed to the electromagnetic frequency of 2450 MHz at the leakage power density of 5 mW/cm^2

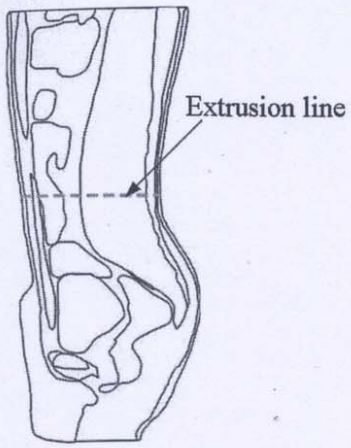

Fig. 13 The extrusion line in the human body where the SAR and temperature distribution are considered

4.6 Effect of Leakage Power Density. The effect of leakage power density (the power irradiated on the human surface) has also been investigated. The incident power and leakage power density are related, as shown in Table 4. Figure 18 shows the comparison of the temperature increase distribution within the human body at various incident powers, at t=1 min, with the frequency of 915 MHz, along the extrusion line (Fig. 13). Figure 19 shows the temperature fields of human body exposed to the electromagnetic frequency of 915 MHz at t=1 min corresponding to leakage power densities, as shown in Table 4. It is found that incident power significantly influences the rate of temperature increase. Greater power provides greater heat generation inside the human body, thereby increasing the rate of temperature rise.

5 Conclusions

This study presents the numerical simulation SAR and temperature distribution in the human body exposed to electromagnetic field at the frequencies of 915 MHz and 2450 MHz with the power densities of 5 mW/cm^2, 10 mW/cm^2, 50 mW/cm^2, and 100 mW/cm^2. The numerical simulations in this study show several important features of the energy absorption in the human body. The results show that the maximum temperatures in various organs are significantly different at different frequencies. The maximum temperature is found at the skin for the frequency of 2450 MHz and is found at the fat for the frequency of 915 MHz. While the maximum SAR value in both frequencies are found at the skin. It is found that greater leakage power density results in a greater heat generation inside the human body, thereby increasing the rate of temperature increase. Moreover, it is found that the temperature distributions in human body induced by electromagnetic fields are not directly related to the SAR distribution due to the effect of dielectric properties, thermal properties, blood perfusion, and penetration depth of the microwave power.

Therefore, health effect assessment of electromagnetic wave at various frequencies requires the utilization of the numerical simulation of SAR model along with the thermal model. However, the dielectric properties of some tissues are not indicated as a function of frequency due to the limited number of human tissue dielectric properties in the literature, and this may affect the accuracy of the simulation results. Future works will focus on the frequency-dependent dielectric properties of human tissue. A study will also be developed for 3D simulations and the study of the temperature dependency of dielectric properties. This will allow a better understanding of the realistic situation of the interaction between the electromagnetic field and the human tissues.

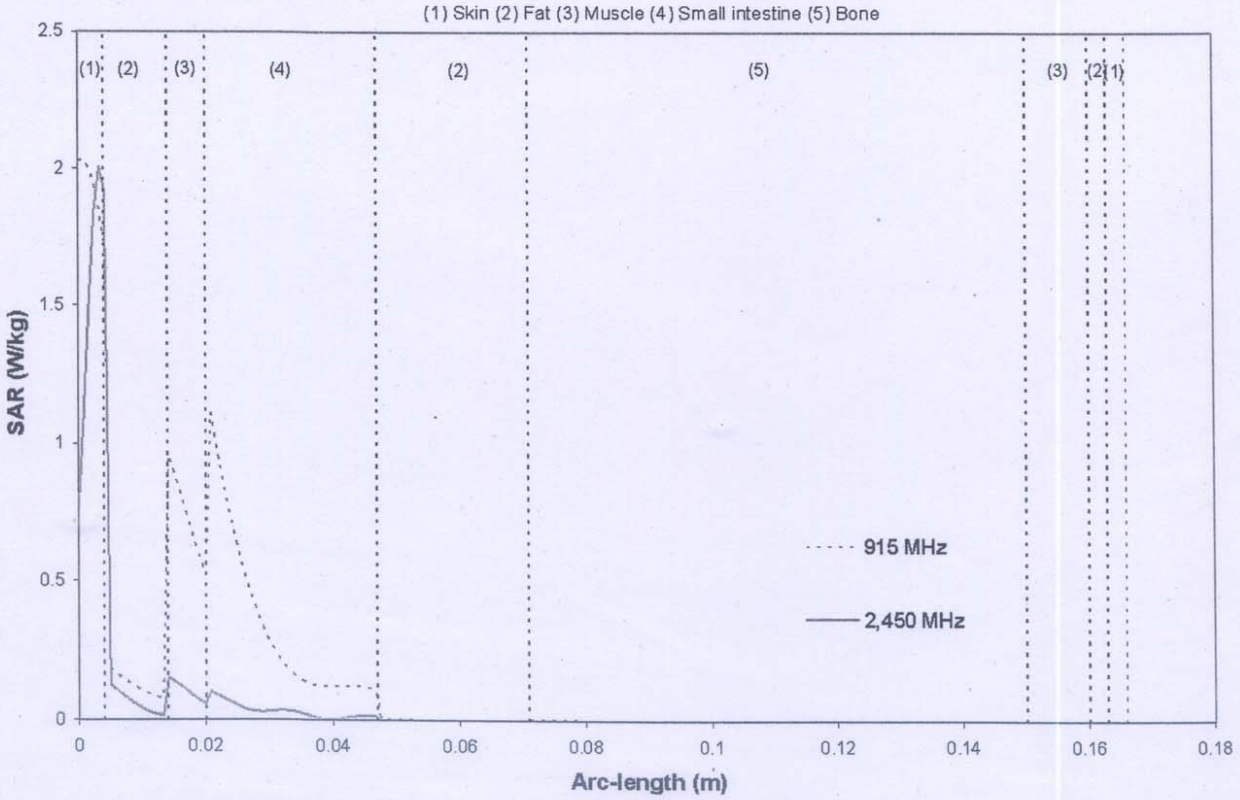

Fig. 14 SAR distribution versus arc length of human body exposed to the leakage power density of electromagnetic field at the 5 mW/cm^2

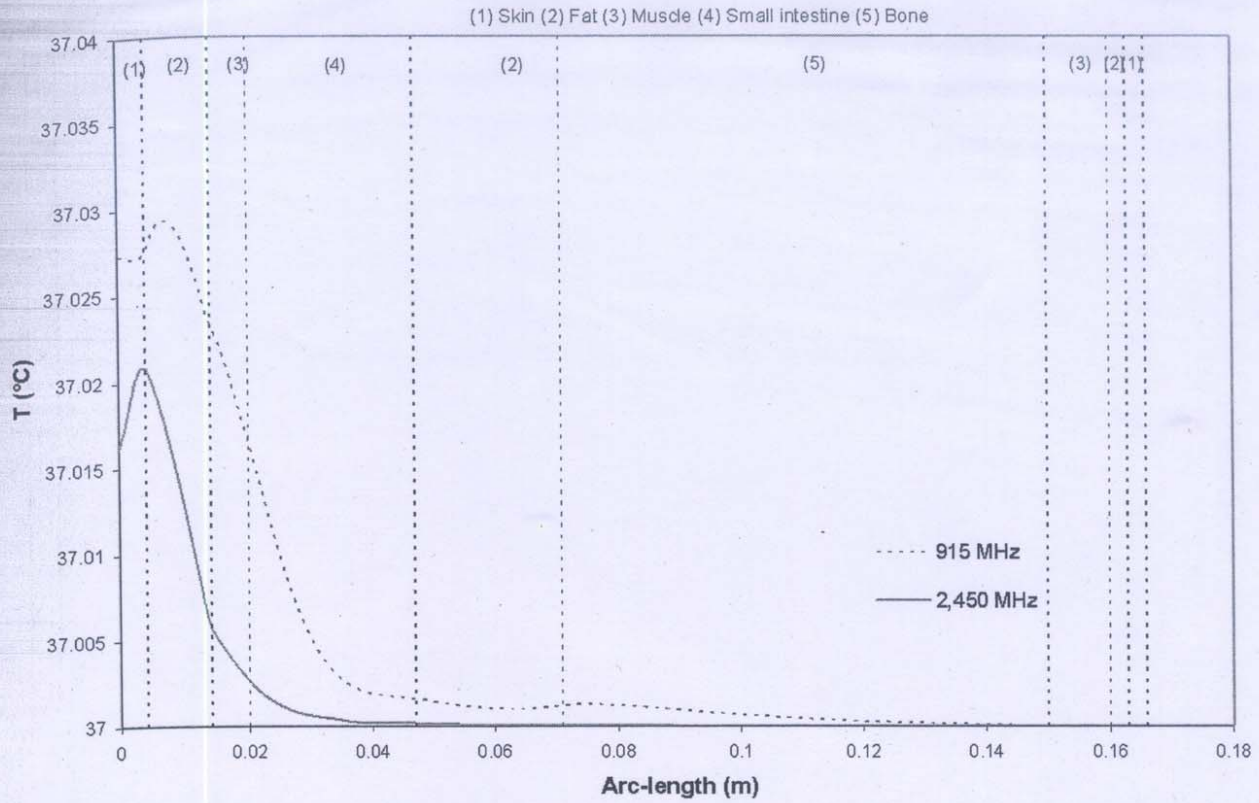

Fig. 15 Temperature distribution versus arc length of the human body exposed to the leakage power density of electromagnetic field at 5 mW/cm^2

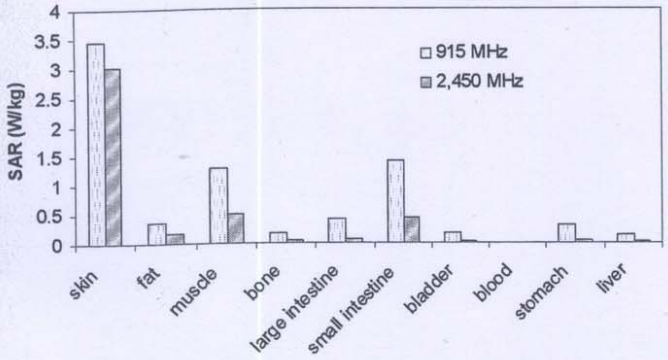

Fig. 16 Comparison of the maximum SAR in human tissues at the frequencies of 915 MHz and 2450 MHz

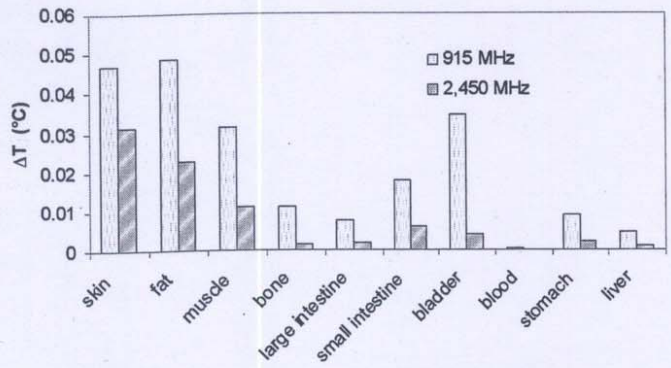

Fig. 17 Comparison of the temperature increases in human tissues at the frequencies of 915 MHz and 2450 MHz

Table 4 The relationship between the incident power and the leakage power density of microwave

Incident power (W)	Power density (mW/cm^2)
10.5	5
21.0	10
105	50
210	100

Acknowledgment

The authors would like to express their appreciation to the Thailand Research Fund (TRF) and the Thai Commission on Higher Education (CHE) for providing financial support for this study.

Nomenclature

C = specific heat capacity (J/(kg K))
E = electric field intensity (V/m)
f = frequency of incident wave (Hz)
j = current density
k = thermal conductivity (W/(m K))
n = refractive index
Q = heat source (W/m^3)
T = temperature (K)
t = time
$\tan \delta$ = loss tangent coefficient

Greek Letters

μ = magnetic permeability (H/m)
ε = permittivity (F/m)
σ = electric conductivity (S/m)
ω = angular frequency (rad/s)

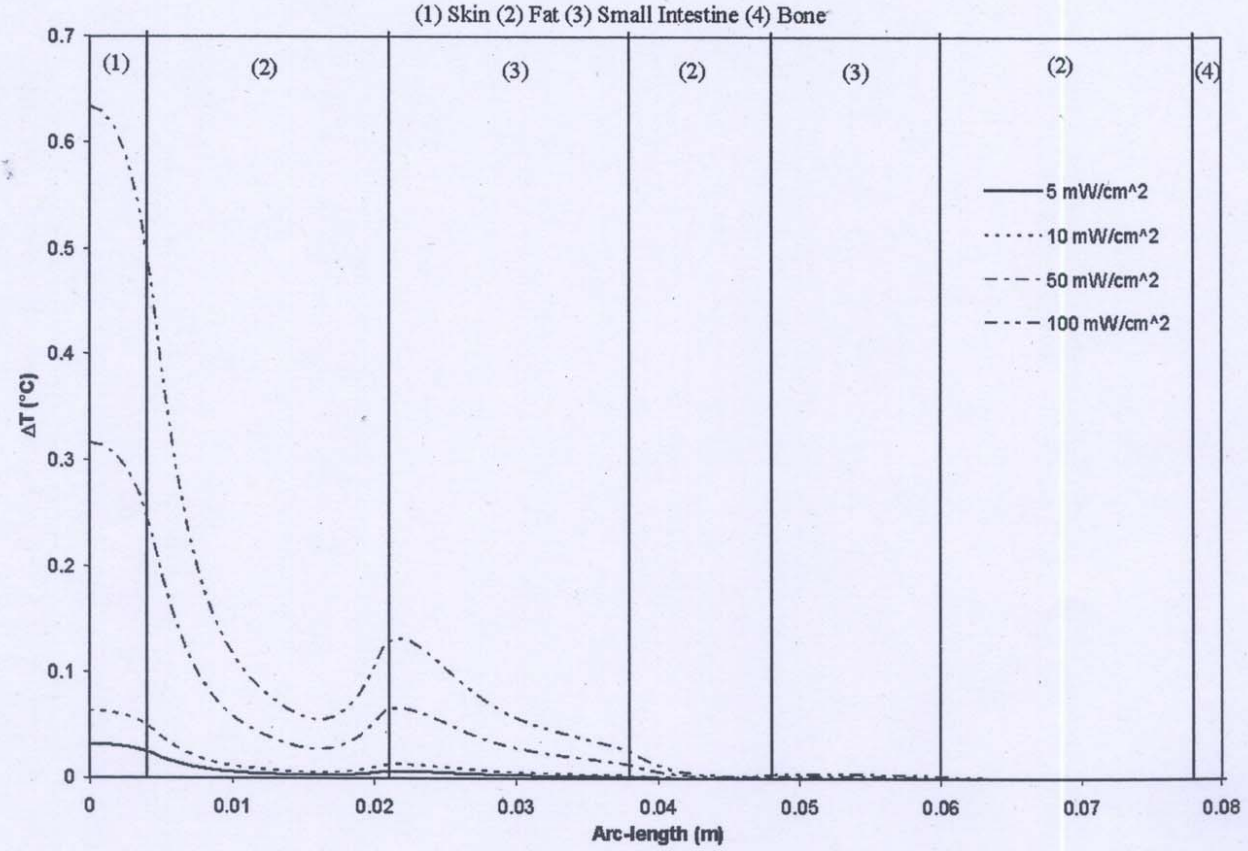

Fig. 18 Temperature increase versus arc length of human body exposed to the electromagnetic frequency of 915 MHz at various leakage power densities, at t=1 min

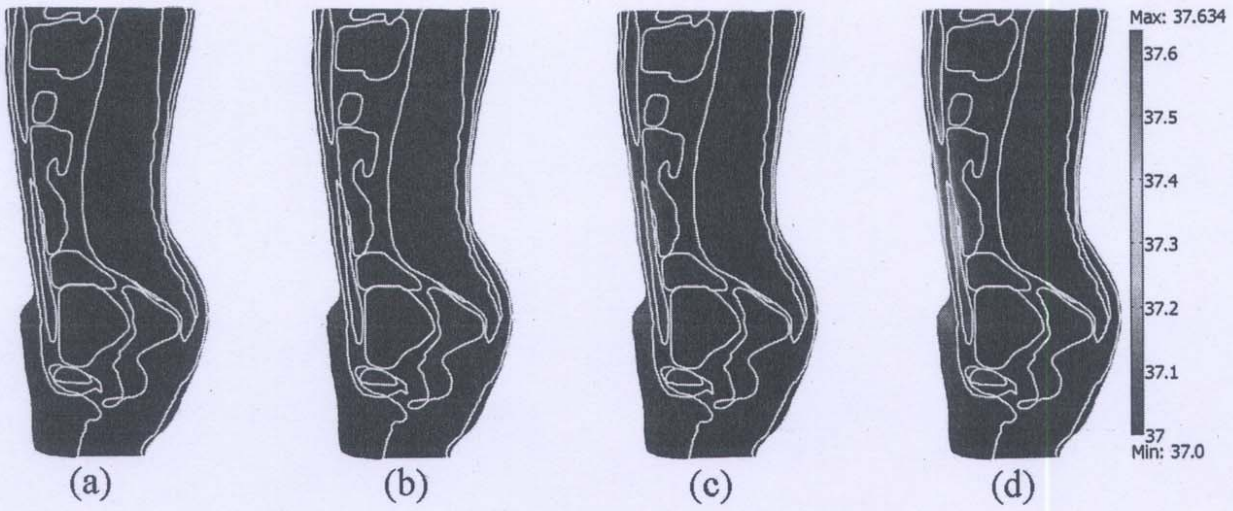

Fig. 19 Temperature distribution of human body exposed to the electromagnetic frequency of 915 MHz at t =1 min at various leakage power densities: (*a*) 5 mW/cm², (*b*) 10 mW/cm², (*c*) 50 mW/cm², and (*d*) 100 mW/cm²

ρ = density (kg/m^3)
ω_b = blood perfusion rate (1/s)

Subscripts

b = blood
ext = external
met = metabolic
r = relative
0 = free space, initial condition

References

[1] Rattanadecho, P., Suwannapum, N., and Cha-um, W., 2009, "Interactions Between Electromagnetic and Thermal Fields in Microwave Heating of Hardened Type I-Cement Paste Using a Rectangular Waveguide (Influence of Frequency and Sample Size)," ASME J. Heat Transfer, **131**, p. 082101.

[2] Ratanadecho, P., Aoki, K., and Akahori, M., 2002, "Influence of Irradiation Time, Particle Sizes, and Initial Moisture Content During Microwave Drying of Multi-Layered Capillary Porous Materials," ASME J. Heat Transfer, **124**, pp. 151–161.

[3] Ziegelberger, G., 2009, "ICNIRP Statement on the 'Guidelines for Limiting Exposure to Time-Varying Electric, Magnetic, and Electromagnetic Fields (up to 300 GHz)'," Health Phys., **97**(3), pp. 257–258.

[4] Stuchly, M. A., 1995, "Health Effects of Exposure to Electromagnetic Fields," IEEE Aerospace Applications Conference Proceedings, pp. 351–368.

[5] Nishizawa, S., and Hashimoto, O., 1999, "Effectiveness Analysis of Lossy Dielectric Shields for a Three-Layered Human Model," IEEE Trans. Microwave Theory Tech., **47**(3), pp. 277–283.

[6] Seufi, A. M., Ibrahim, S. S., Elmaghraby, T. K., and Hafez, E. E., 2009, "Preventive Effect of the Flavonoid, Quercetin, on Hepatic Cancer in Rats via Oxidant/Antioxidant Activity: Molecular and Histological Evidences," J. Exp. Clin. Cancer Res., **28**(1), p. 80.
[7] Yang, D., Converse, M. C., Mahvi, D. M., and Webster, J. G., 2007, "Measurement and Analysis of Tissue Temperature During Microwave Liver Ablation," IEEE Trans. Biomed. Eng., **54**(1), pp. 150–155.
[8] Kanai, H., Marushima, H., Kimura, N., Iwaki, T., Saito, M., Maehashi, H., Shimizu, K., Muto, M., Masaki, T., Ohkawa, K., Yokoyama, K., Nakayama, M., Harada, T., Hano, H., Hataba, Y., Fukuda, T., Nakamura, M., Totsuka, N., Ishikawa, S., Unemura, Y., Ishii, Y., Yanaga, K., and Matsuura, T., 2007, "Extracorporeal Bioartificial Liver Using the Radial-Flow Bioreactor in Treatment of Fatal Experimental Hepatic Encephalopathy," Artif. Organs, **31**(2), pp. 148–151.
[9] Pennes, H. H., 1998, "Analysis of Tissue and Arterial Blood Temperatures in the Resting Human Forearm," J. Appl. Physiol., **85**(1), pp. 5–34.
[10] Spiegel, R. J., 1984, "A Review of Numerical Models for Predicting the Energy Deposition and Resultant Thermal Response of Humans Exposed to Electromagnetic Fields," IEEE Trans. Microwave Theory Tech., **32**(8), pp. 730–746.
[11] Dragun, V. L., Danilova-Tret'yak, S. M., and Gubarev, S. A., 2005, "Simulation of Heating of Biological Tissues in the Process of Ultrahigh-Frequency Therapy," J. Eng. Phys. Thermophys., **78**(1), pp. 109–114.
[12] Ozen, S., Helhel, S., and Cerezci, O., 2008, "Heat Analysis of Biological Tissue Exposed to Microwave by Using Thermal Wave Model of Bio-Heat Transfer (TWMBT)," Burns, **34**(1), pp. 45–49.
[13] Samaras, T., Christ, A., Klingenbock, A., and Kuster, N., 2007, "Worst Case Temperature Rise in a One-Dimensional Tissue Model Exposed to Radiofrequency Radiation," IEEE Trans. Biomed. Eng., **54**(3), pp. 492–496.
[14] Wang, J., and Fujiwara, O., 1999, "FDTD Computation of Temperature Rise in the Human Head for Portable Telephones," IEEE Trans. Microwave Theory Tech., **47**(8), pp. 1528–1534.
[15] Hirata, A., Morita, M., and Shiozawa, T., 2003, "Temperature Increase in the Human Head Due to a Dipole Antenna at Microwave Frequencies," IEEE Trans. Electromagn. Compat., **45**(1), pp. 109–116.
[16] Hirata, A., Wang, J., Fujiwara, O., Fujimoto, M., and Shiozawa, T., 2005, "Maximum Temperature Increases in the Head and Brain for SAR Averaging Schemes Prescribed in Safety Guidelines," IEEE International Symposium on Electromagnetic Compatibility, Chicago, IL, Vol. 3, pp. 801–804.
[17] Garcia-Fernandez, M. A., Valdes, J. F. V., Martinez-Gonzalez, A. M., and Sanchez-Hernandez, D., 2007, "Electromagnetic Heating of a Human Head Model by a Half-Wavelength Dipole Antenna," The Second European Conference on Antennas and Propagation, pp. 1–4.
[18] Shiba, K., and Higaki, N., 2009, "Analysis of SAR and Current Density in Human Tissue Surrounding an Energy Transmitting Coil for a Wireless Capsule Endoscope," 2009 20th International Zurich Symposium on Electromagnetic Compatibility, Zurich, pp. 321–324.
[19] Yang, D., Converse, M. C., Mahvi, D. M., and Webster, J. G., 2007, "Expanding the Bioheat Equation to Include Tissue Internal Water Evaporation During Heating," IEEE Trans. Biomed. Eng., **54**(8), pp. 1382–1388.

International Communications in Heat and Mass Transfer 38 (2011) 255–262

Contents lists available at ScienceDirect

International Communications in Heat and Mass Transfer

journal homepage: www.elsevier.com/locate/ichmt

The effects of dielectric shield on specific absorption rate and heat transfer in the human body exposed to leakage microwave energy ☆

Teerapot Wessapan, Siramate Srisawatdhisukul, Phadungsak Rattanadecho *

Research Center of Microwave Utilization in Engineering (R.C.M.E.), Department of Mechanical Engineering, Faculty of Engineering, Thammasat University (Rangsit Campus), Pathumthani 12120, Thailand

ARTICLE INFO

Available online 16 December 2010

Keywords:
Microwave energy
Numerical methods
SAR
Heat transfer analysis
Dielectric shield

ABSTRACT

This paper proposes a numerical study to simulate the effects of dielectric shield on the specific absorption rate (SAR) and the temperature increase in the human body exposed to leakage microwave energy. In this study, the effects of shield dielectric properties on distributions of SAR and temperature increase within the human body at various operating frequency are systematically investigated. Based on the obtained results, the installed dielectric shield strongly affects the SAR and the temperature increase in human body. The SAR and the temperature increase in human body can be reduced simultaneously by setting the appropriate dielectric properties of the dielectric shield. The appropriate dielectric properties of the dielectric shield greatly depend on the operating frequencies. These fundamental data for the implementations of the radiation protection shielding materials, with focusing on the human organism, are provided as well.

1. Introduction

Microwave is a form of electromagnetic wave with wavelengths ranging from 1 m down to 1 mm, with frequencies between 0.3 and 300 GHz. Microwave energy has proven to be an efficient and reliable form of heating for a wide range of industrial processes such as heating process [1], curing process [2], and melting process [3]. As applications of microwave energy become widespread, adverse effects caused by the leakage microwave energy are increasingly a subject of concern [4,5]. In many countries, various studies on biological effects have been made and many results have been reported. There has been an intensive model analysis of the SAR of the human body [6,7]. The protection is serious for researchers who work with high-power electromagnetic waves. In connection with research on human protection from electromagnetic field exposure, some researches have been carried out on how effectively the human body is protected from unwanted electromagnetic waves [8]. Furthermore, fundamental analysis of shielding effects of lossy dielectric materials located in front of a human body have also been carried out by some researchers [9,10]. However, the heat transfer model has not been included in the modeling analysis.

The computation of the temperature increase is one of the main tasks in the evaluation of the risk related to the exposure of humans to electromagnetic fields [11]. Nevertheless, most studies of human protection from electromagnetic field exposure have not considered the temperature increase within the domain of the human body especially in the human organism. There are few studies on the temperature and electromagnetic field interaction in a realistic physical model of the human body due to the complexity of the problem, even though it is directly related to the thermal injury of tissues [7,12,13]. Therefore, in order to provide information on protection of the human body against electromagnetic fields adequately, it is essential to simulate the coupled electromagnetic field and heat transfer models to represent an actual process of shield protection from possibly harmful effects of electromagnetic fields. This research is a pioneer work on human protection from electromagnetic field exposure that simulates the SAR distribution and temperature distribution over an anatomically based human body.

This work is extended from our previous work [7] in which the human body exposed to leakage electromagnetic field is investigated. This paper mainly analyzes the shielding effect of a dielectric shield being placed in front of a human body. Specifically, lossy dielectric media are chosen as the dielectric shield material. The local SARs and temperature increase of human model are calculated for various operating frequencies. Three shield dielectric properties at microwave frequencies of 300, 915, 1300, and 2450 MHz are selected for the shielding investigation. The system of governing equations, as well as initial and boundary conditions are solved numerically, using finite element method (FEM). Moreover, this research is also focusing on the interaction between electromagnetic field and organs in the human trunk.

2. Formulation of the problem

Fig. 1 depicts a physical model of the problem. The incident plane wave (TE wave) with a microwave power density of 5 mW/cm^2 is

☆ Communicated by W.J. Minkowycz.

* Corresponding author.
E-mail address: ratphadu@engr.tu.ac.th (P. Rattanadecho).

0735-1933/$ – see front matter © 2010 Elsevier Ltd. All rights reserved.
doi:10.1016/j.icheatmasstransfer.2010.12.004

Nomenclatures

C_p	specific heat capacity (J/(kg K))
E	electric fields intensity (V/m)
f	frequency of incident wave (Hz)
k	thermal conductivity (W/m K)
H	magnetic field intensity (A/m)
n	refractive index (-)
Q	heat generation term (W/m^3)
s	Poynting vector (W/m^2)
T	temperature (°C)
t	time (s)
$\tan\delta$	dielectric loss coefficient (-)

Greek letters

ε	permittivity (F/m)
μ	magnetic permeability (H/m)
υ	velocity of propagation (m/s)
ρ	density (kg/m^3)
σ	electric conductivity (S/m)
ω	perfusion rate (1/s)

Subscript

b	blood
ext	external
met	metabolism

incident on the dielectric shield in front of the human model and penetrated into the human model. A human model including ten kinds of organs is used for our analysis.

2.1. Human model

Fig. 2 shows a vertical cross section through the middle plane of the human trunk model. A two-dimensional human body model used in this paper is obtained by image processing technique from the work

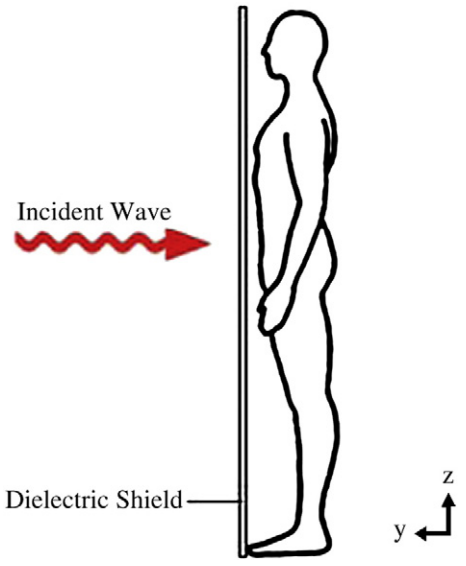

Fig. 1. Human model with dielectric shield.

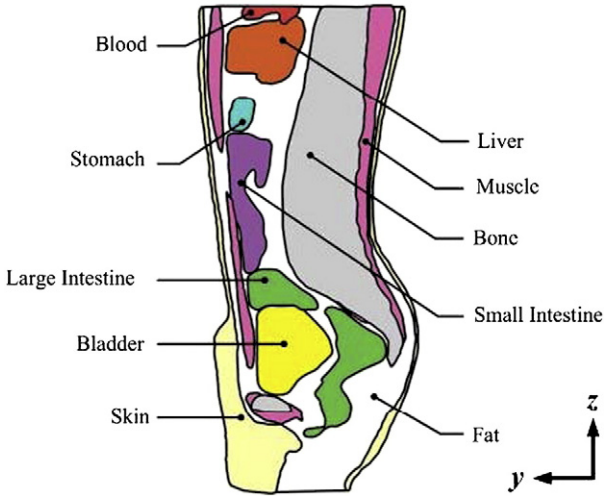

Fig. 2. Human body in vertical cross section plane [12].

of Shiba and Higaki [12]. The human model has a dimension of 300 mm in width and 525 mm in height. This human model comprises 10 types of tissues which are the skin, fat, muscle, bone, large intestine, small intestine, bladder, blood, stomach, and liver, respectively. These tissues have different dielectric and thermal properties. The thermal properties and dielectric properties of these tissues at the frequencies of 300, 915, 1300, and 2450 MHz are given in Table. 1 and Table 2, respectively.

2.2. Modeling of electromagnetic fields

A mathematical model is developed to calculate the electric field, SAR, and temperature distribution within the human model. To simplify the problem, the following assumptions are made; electromagnetic wave propagation is modeled in two dimensions over the y–z plane, in which waves and object interaction proceed in the open region, and the computational space is truncated by scattering boundary condition. The propagation of an electromagnetic wave is characterized by transverse electric fields (TE-Mode). The dielectric properties of human tissues are frequency dependent as shown in Table 1. Since the temperature increase in the human model is slightly changed, the model assumes that the dielectric properties of tissues are independent to temperature change for the specified frequency.

The electromagnetic wave propagation is calculated by Maxwell's equations [6], which mathematically describe the interdependence of

Table 1
Dielectric properties of tissues.

Tissue	300 MHz		915 MHz		1300 MHz		2450 MHz	
	σ (S/m)	ϵ_r	σ (S/m)	ϵ_r	σ (S/m)	ϵ_r	σ (S/m)	ϵ_r
Skin	0.35	48.41	0.92	44.86	1.25	43.56	2.16	41.79
Fat	0.06	6.55	0.09	5.97	0.10	5.80	0.13	5.51
Muscle	1.08	55.45	1.33	50.44	1.42	48.96	1.60	46.40
Bone	2.10	44.80	2.10	44.80	2.10	44.80	2.10	44.80
Large intestine	2.04	53.90	2.04	53.90	2.04	53.90	2.04	53.90
Small intestine	3.17	54.40	3.17	54.40	3.17	54.40	3.17	54.40
Bladder	0.69	18.00	0.69	18.00	0.69	18.00	0.69	18.00
Blood	2.54	58.30	2.54	58.30	2.54	58.30	2.54	58.30
Stomach	2.21	62.20	2.21	62.20	2.21	62.20	2.21	62.20
Liver	1.69	43.00	1.69	43.00	1.69	43.00	1.69	43.00

Table 2
Thermal properties of tissues.

Tissue	ρ (kg/m³)	k (W/m · K)	C_p (J/kg · K)	ω_b	Q_{met} (W/m³)
Skin	1125	0.35	3437	0.02	1620
Fat	916	0.22	2300	4.58E-04	300
Muscle	1047	0.6	3500	8.69E-03	480
Bone	1038	0.436	1300	4.36E-04	610
Large intestine	1043	0.6	3500	1.39E-02	9500
Small intestine	1043	0.6	3500	1.74E-02	9500
Bladder	1030	0.561	3900	0.00E+00	–
Blood	1058	0.45	3960	–	–
Stomach	1050	0.527	3500	7.00E-03	–
Liver	1030	0.497	3600	0.017201	–

the electromagnetic waves. The general form of Maxwell's equations is simplified to demonstrate the electromagnetic field of microwave penetrated into the human model as the following equations:

$$\nabla \times \left(\frac{1}{\mu_r}\nabla \times E\right) - k_0^2\left(\varepsilon_r - \frac{j\sigma}{\omega\varepsilon_0}\right)E = 0 \quad (1)$$

$$\varepsilon_r = n^2 \quad (2)$$

where E is electric field intensity (V/m), μ_r is relative magnetic permeability (H/m), n is refractive index, ε_r is relative dielectric constant, $\varepsilon_0 = 8.8542 \times 10^{-12}$ (F/m) is permittivity of free space, and σ is electric conductivity (S/m), $j = \sqrt{-1}$.

2.2.1. Boundary condition for wave propagation analysis

Microwave energy is emitted by a microwave high power device and strikes the dielectric shield in front of the human model with a microwave power density of 5 mW/cm². The microwave power density in terms of mW/cm² in 2D model can be presumed by dividing the microwave power (mW) by a frontal area of the incident microwave (cm²). Therefore, boundary conditions used for electromagnetic wave, as shown in Fig. 3, are considered in the following.

It is assumed that the uniform wave flux strikes the left side of the human model, where the dielectric shield is located and then penetrates into the human model. From the viewpoint of convergence of the electromagnetic field, only the TE wave is used as the incident wave. Therefore, at the left boundary of the considered domain, an electromagnetic simulator employs TE wave propagation port with specified power density:

$$S = \int (E - E_1)\cdot E_1 \Big/ \int E_1 \cdot E_1. \quad (3)$$

Boundary conditions along the interfaces between different mediums, for example, between air and tissue or tissue and tissue (with different dielectric properties), are considered as continuity boundary condition:

$$n \times (H_1 - H_2) = 0. \quad (4)$$

The outer sides of the tissue boundaries are considered as scattering boundary condition:

$$n \times (\nabla \times E_z) - jkE_z = -jk(1 - k\cdot n)E_{0z}\, exp(-jk\cdot r). \quad (5)$$

2.3. Interaction of electromagnetic waves and human tissues

Interaction of electromagnetic fields with biological tissues can be defined in terms of the SAR. When EM waves propagate through the dielectric shield and then penetrate into the human tissues, the energy of EM waves is absorbed by the tissues. The SAR is defined as the power dissipation rate normalized by tissue density [14]. The SAR is given by:

$$SAR = \frac{\sigma}{\rho}|E|^2 \quad (6)$$

where E is the root mean square electric-field (V/m), σ is the conductivity (S/m) and ρ is mass density of the tissue (kg/m³).

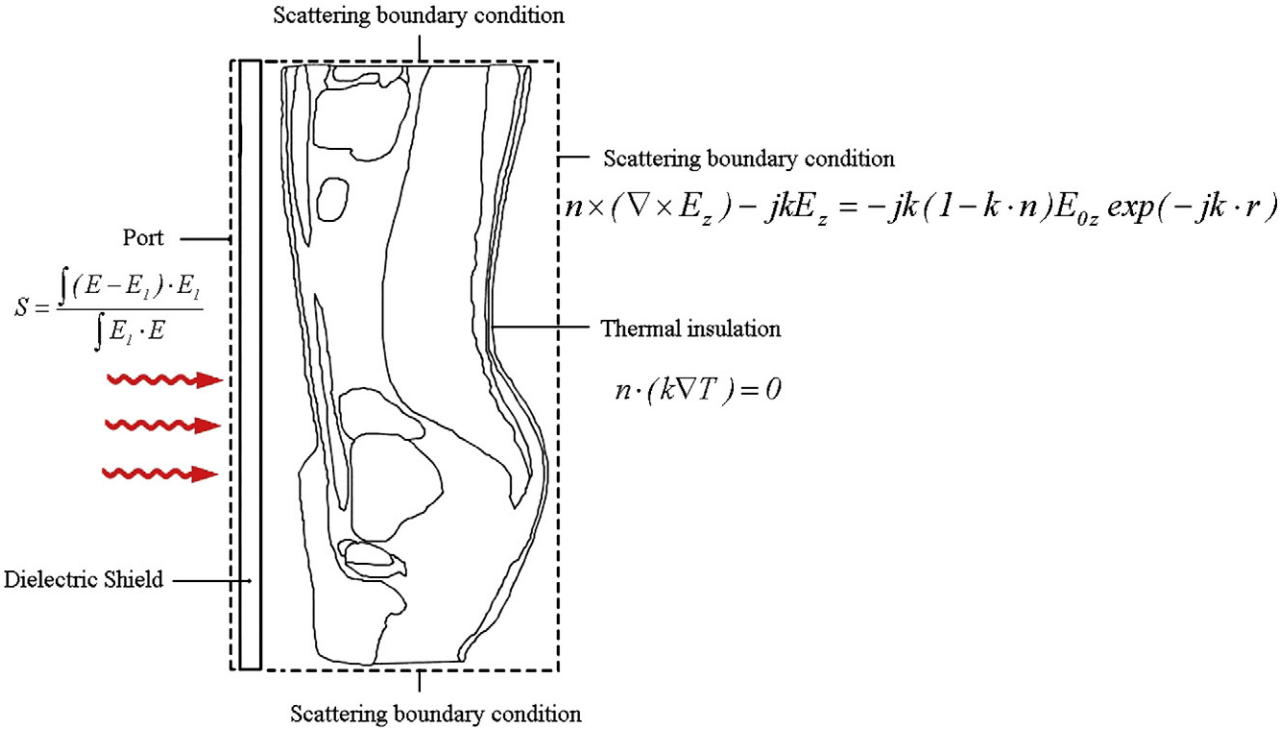

Fig. 3. Physical model and boundary condition used for analysis.

2.4. Modeling of heat transfer

The heat transfer analysis is considered only in the human body domain, which does not include parts of the surrounding space as well as the dielectric shield. To reduce complexity of the problem, the following assumptions have been introduced.

1. There is no phase change and mass transfer in the human model.
2. The human tissues are bio-material with constant thermal properties.
3. There is no chemical reactions occuring within the human model.
4. The initial temperature through the human model is uniform.

The heat transfer analysis of the human model is modeled in two dimensions over the y–z plane. The temperature distribution inside the human model is obtained by using the Pennes' bio-heat equation [15]. The transient bioheat equation effectively describes how heat transfer occurs within the human model, and the equation can be written as:

$$\rho C\frac{\partial T}{\partial t} = \nabla\cdot(k\nabla T) + \rho_b C_b \omega_b (T_b - T) + Q_{met} + Q_{ext} \quad (7)$$

where ρ is the tissue density (kg/m^3),C is the heat capacity of tissue (J/kg · K), k is thermal conductivity of tissue (W/m · K), T is the temperature (°C), T_b is the temperature of blood flow (°C), ρ_b is the density of blood before entering ablation region (kg/m^3), C_b is the specific heat capacity of blood (J/kg · K), ω_b is the blood perfusion rate (1/s), Q_{met} is the metabolism heat source (W/m^3) and Q_{ext} is the external heat source (microwave heat-source density) (W/m^3).

In the analysis, heat conduction between tissue and blood flow is approximated by the term $\rho_b C_b \omega_b (T_b - T)$. In this analysis, the thermoregulation mechanisms and the metabolic heat generation of each tissue have been neglected to illustrate the clear temperature distribution. The metabolism heat source is negligible and therefore $Q_{met} = 0$.

The external heat source is equal to the resistive heat generated by electromagnetic field (microwave power absorbed):

$$Q_{ext} = \frac{1}{2}\sigma_{tissue}|\overline{E}|^2 \quad (8)$$

where $\sigma_{tissue} = 2\pi f \varepsilon'_r \varepsilon_0$.

2.4.1. Boundary condition for heat transfer analysis

At the skin–air interface, the insulated boundary condition has been imposed to clearly illustrate the temperature distribution. As shown in Fig. 3, the boundaries of human body are considered as insulated boundary condition:

$$n.(k\nabla T) = 0. \quad (9)$$

Table 3
Dielectric properties of shield and penetration depth.

Operating frequency	D_p (cm)		
	Low lossy	Medium lossy	High lossy
(MHz)	10-j5	10-j10	20-j20
300	10.36	5.53	3.91
915	3.40	1.81	1.28
1300	2.39	1.28	0.90
2450	1.27	0.68	0.48

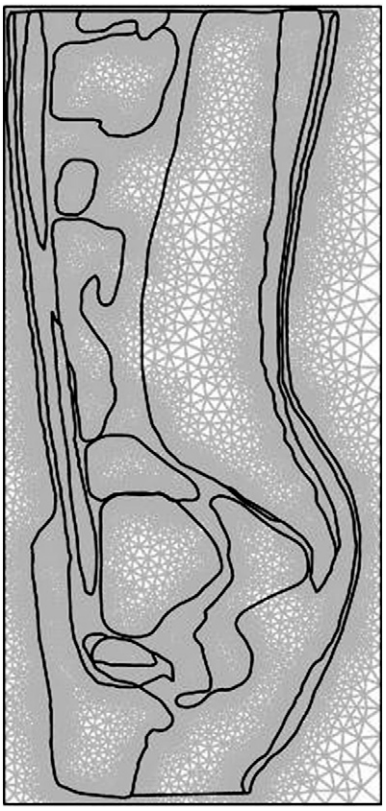

Fig. 4. A two-dimensional finite element mesh of human cross section model.

It is assumed that no contact resistant occurs between the internal organs of the human body. Therefore, the internal boundaries are assumed to be in a continuity boundary condition between the tissue layers within the human model:

$$n\cdot(k_u\nabla T_u - k_d\nabla T_d) = 0. \quad (10)$$

2.4.2. Initial condition for heat transfer analysis

For this analysis, the temperature distribution within the human body is assumed to be uniform. Therefore, initial temperature of human body is defined as

$$T(t_0) = 37°\mathrm{C}. \quad (11)$$

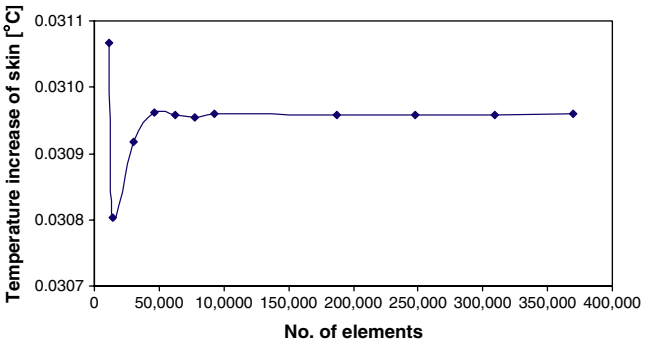

Fig. 5. Grid convergence curve of the 2D model.

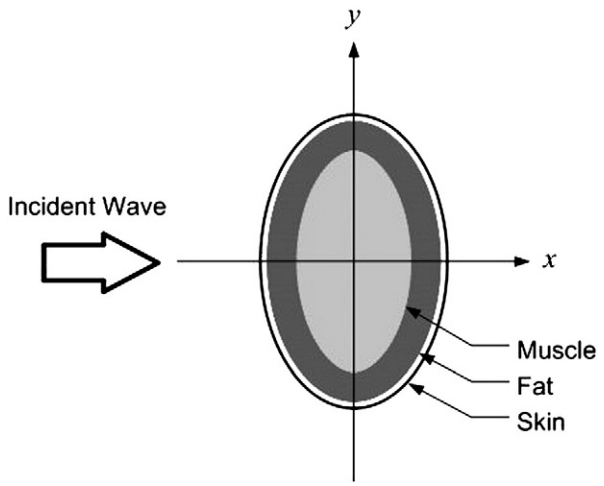

Fig. 6. Geometry of the validation model [9].

2.5. Penetration depth

The penetration depth (D_p) is defined as the distance at which the microwave power density has decreased to 37% of its initial value at the surface [16]:

$$D_p = \frac{1}{\frac{2\pi f}{\upsilon}\sqrt{\frac{\varepsilon_r'\left(\sqrt{1+\left(\frac{\varepsilon_r''}{\varepsilon_r'}\right)^2}-1\right)}{2}}} = \frac{1}{\frac{2\pi f}{\upsilon}\sqrt{\frac{\varepsilon_r'\left(\sqrt{1+(\tan\delta)^2}-1\right)}{2}}} \quad (12)$$

where ε_r'' is the relative dielectric loss factor and υ is the speed of microwave (m/s).

The penetration depth of the microwave power is calculated using Eq. (12), which shows how it depends on the dielectric properties of the dielectric material. The shield dielectric properties and the penetration depth of the dielectric shield are summarized in Table 3.

It is shown that the D_P is greatly dependent on the shield dielectric properties as well as the operating frequency. With high lossy of dielectric shield typically shows greater potential for absorbing microwaves in dielectric shield, while an increase in operating frequency typically decreases in D_P.

3. Numerical procedure

The coupled model of bioheat equation and Maxwell's equation are used to simulate the SAR and temperature increase in the human model. The computational scheme is to first assemble a finite element model and compute a local heat generation term by performing an electromagnetic calculation using tissue properties. In order to obtain a good approximation, a fine mesh is specified in the sensitive areas. This study provides a variable mesh method for solving the problem as shown in Fig. 4. The coupled model of electromagnetic field and thermal field is solved by FEM. The model is implemented using COMSOL™ Multiphysics 3.4, to demonstrate the phenomenon that occurs within the human body exposed to leakage microwave energy. The study employs an implicit time step scheme to solve the electric field and temperature field. The 2D model is discretized using triangular elements and the Lagrange quadratic is used to approximate the temperature and SAR variation across each element. Convergence test of the frequency of 2450 MHz are carried out to identify the suitable number of elements required. The number of elements where solution is independent of mesh density is found to be 92,469. The convergence curve resulting from the convergence test is shown in Fig. 5.

4. Results and discussion

In this section, the couple of the mathematical model of bioheat transfer and electromagnetic wave propagation as well as an initial temperature of 37 °C for all cases is used for the analysis. For the simulation, the thermal properties and dielectric properties are directly taken from Table 1 to Table 3, respectively. The influences of shield dielectric properties and operating frequency on SAR and temperature increase within the human model are clearly investigated.

4.1. Numerical validations

It must be noted in advance that it is not possible to make a direct comparison of the model in this study and the experimental results due to the medical ethics. In order to verify the accuracy of the present numerical model, the simple case of the simulated results is then validated against the numerical results with the same geometric

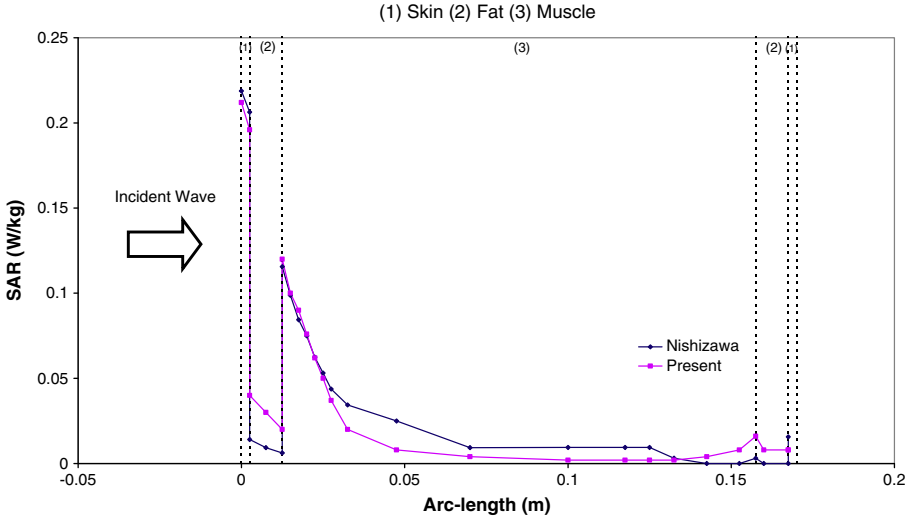

Fig. 7. Comparison of the calculated SAR distribution to the SAR distribution obtained by Nishizawa et al. [9].

Table 4
Comparison of the results obtained in the present study with those of Nishizawa et al. [9].

	Present work	Published work [9]	% Difference
SAR_{max} in skin	0.212	0.220	3.63
SAR_{max} in fat	0.198	0.206	3.88
SAR_{max} in muscle	0.116	0.120	3.33

model presented by Nishizawa et al. [9]. The horizontal cross section of the three layer human tissues as shown in Fig. 6 is used in the validation case. In the validation case, the leakage microwave power density of 1 mW/cm^2 at the electromagnetic frequency of 1300 MHz is considered. The results of the selected test case are illustrated in Fig. 7 for SAR distribution in the human body. Table 4 clearly shows a good agreement of the maximum value of the SAR of tissue between the present solution and that of Nishizawa [9]. This favorable comparison lends confidence in the accuracy of the present numerical model. It is important to note that there may be some errors occurring in the simulations which are generated by the input dielectric properties data base and the numerical scheme.

4.2. The effects of shield dielectric properties and operating frequency

Fig. 8 shows the meshes of the human model as well as the SAR and temperature distribution in the case of unshielded human model exposed to the microwave power density of 5 mW/cm^2 at the frequency of 300 MHz. It is found that the temperature distributions are not proportional to the local SAR values. Nevertheless, these are also related to the parameters such as thermal conductivity, dielectric properties, blood perfusion rate and etc.

In the case of using dielectric shield, the dielectric properties for the shield are chosen as (low-loss; 10-*j*5), (medium-loss; 10-*j*10), and (high-loss; 20-*j*20). The shield gap distance and shield thickness are set to 0.5 cm and 0.3 cm, respectively. Fig. 9 and Fig. 10 show the maximum SAR and maximum temperature increase, respectively, in the human model with the test frequencies of 300 MHz, 915 MHz, 1300 MHz and 2450 MHz.

In this section, we illustrate the maximum value of SAR and temperature increase in the human model without attention to the organism. In the unshielded case, the maximum SAR value appeared at 1300 MHz as shown in Fig. 9, while the maximum temperature increase appeared at 915 MHz as shown in Fig. 10. This is because the differences of dielectric and thermal properties of tissues cause spatial distortions of the resonance excitation.

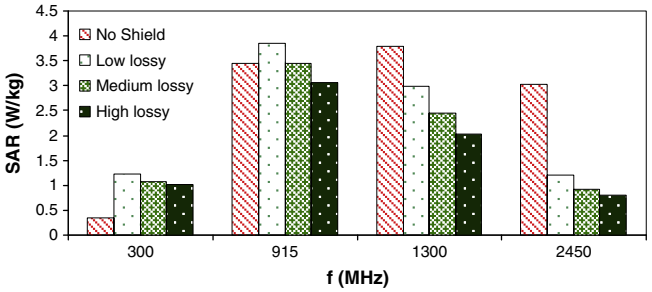

Fig. 9. Comparison of the maximum SAR in the human model at the frequencies of 300 MHz, 915 MHz, 1300 MHz and 2450 MHz.

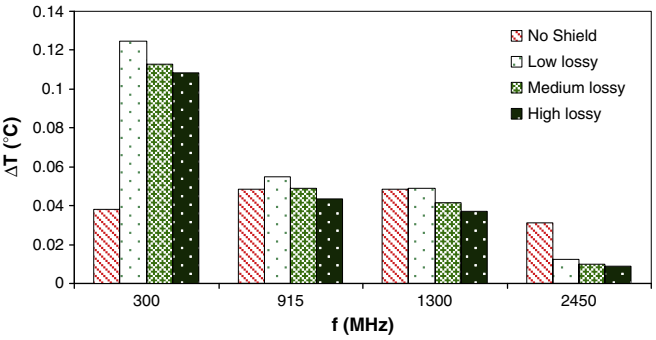

Fig. 10. Comparison of the maximum temperature increases in the human model at the frequencies of 300 MHz, 915 MHz, 1300 MHz and 2450 MHz.

Since in this study, the thickness of the dielectric shield is less than the penetration depth, only a part of the supplied microwave energy is absorbed by the dielectric shield, and the other parts are allowed to penetrate further through the dielectric shield. This causes the interference of waves to penetrate further into the human model to be reflected from the human skin and travel back to the dielectric shield. Consequently, the reflection and transmission components at each interface contribute to the resonance of standing wave within the gap and the human model.

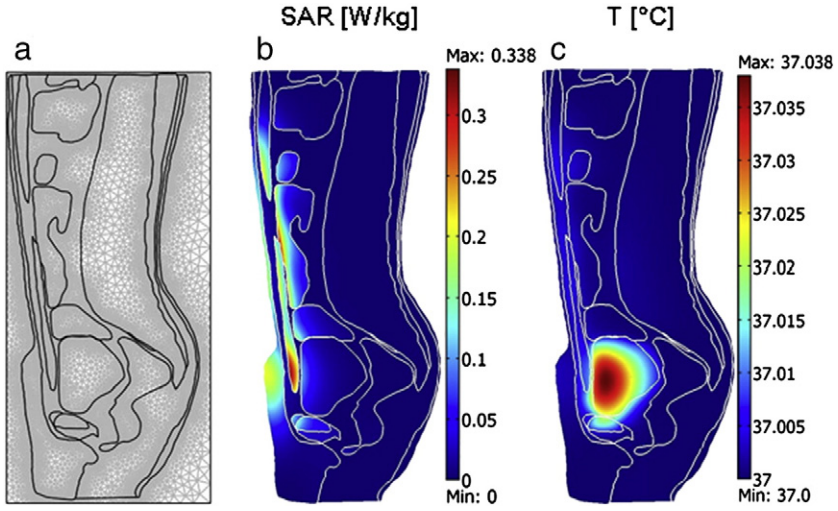

Fig. 8. Analysis of SAR and temperature distribution in the human model exposed to the microwave power density of 5 mW/cm^2 at the frequency of 300 MHz, (a) An initial finite element meshes of human cross section model (b) SAR distribution of the shieldless case (c) Temperature distribution of the unshield case.

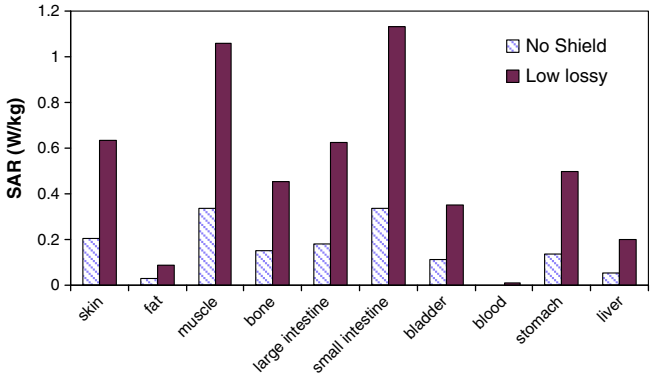

Fig. 11. Comparison of the maximum SAR in human organs of the unshielded and shielded human model at the frequency of 300 MHz.

It is evident from Fig. 9 and Fig. 10 that in the higher frequency of 1300 and 2450 MHz, when using dielectric shield, a significant reduction of SAR and temperature increase within the human model is achieved because of its smaller penetration depth. However, in the lower frequency of 300 MHz corresponding to a long wavelength, the SAR and the temperature increase have higher value than the values of the unshielded case. The reason behind this result is that the penetration depth of the dielectric shield at 300 MHz is much greater than the dielectric shield thickness. This increases a larger part of the incident wave to penetrate further through the dielectric shield and also penetrate into the human model. The great value of SAR and temperature increase in human model is caused by stronger resonance effects that occur at the low frequencies.

While in the frequency of 915 MHz, an insignificant shielding effect of medium lossy dielectric shield is illustrated. It is found that by using low lossy dielectric shield at the frequency of 915 MHz, SAR as well as temperature increase is higher compared to values of the unshielded case. This is because the resonance phenomena between the low lossy dielectric shield and human model is displayed stronger. The multiple reflections within the gap and the human model caused the accumulation of microwave energy in the gap which leads to an increase in the SAR and temperature in human organism by which the reflection rate of microwave strongly depends on the dielectric properties of the dielectric shield. By using the high lossy dielectric shield, the shielding effect is significant. This is because of a large reduction of microwave power density within the human model due to the weakness of resonance, corresponding to the lowering penetration depth of microwave. It is confirmed that the appropriate dielectric properties of the dielectric shield greatly depend on the operating frequencies.

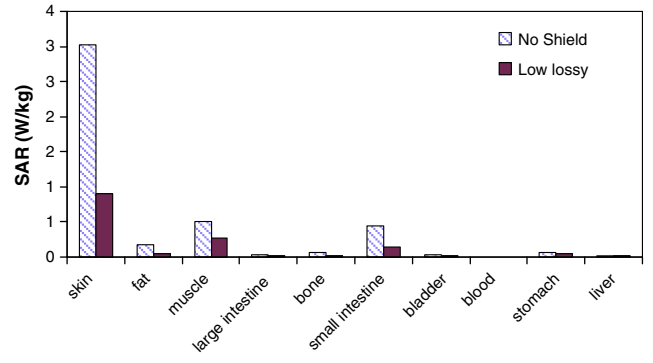

Fig. 12. Comparison of the maximum SAR in human organs of the unshielded and shielded human model at the frequency of 2450 MHz.

4.3. SAR in organs

As shown in Fig. 11, based on the results of the local maximum SAR of the unshielded case, at a low frequency of 300 MHz, peak values of SAR occurred, found both in the small intestine and the muscle. With the use of the low lossy shield, the greater values of SAR occurred as compared to the unshielded case. This is because of a larger part of the incident wave that penetrates further into the gap and human model. This caused the accumulation of microwave energy in the gap and the human model. Fig. 12 shows the maximum SAR in organs at a high frequency of 2450 MHz. It is clearly evident from Fig. 12 that a peak value of local SAR is found only at the skin due to a smaller penetration depth at high frequency range. However, large reduction of the SAR value is achieved when using the same dielectric shield (low-loss shield) with the case of 300 MHz due to the weakness of resonance.

Fig. 11 and Fig. 12 show the maximum SAR and the maximum temperature increase in the human model, while focusing on the human organism. It is found that the SAR and the temperature increase primarily depend on the penetration depth of microwave which corresponds to the operating frequency as well as the dielectric properties of the dielectric shield. As the dielectric properties of a dielectric shield vary, the penetration depth will be changed and the electric field passing through the dielectric shield is altered. If the penetration depth is changing, a fraction of the microwave energy absorbed is also changed which related to the resonance within the model. Consequently, the shielding effect of dielectric shield is changed.

5. Conclusions

This paper presents the simulations of SAR and heat transfer in the human model, where microwave energy strikes the dielectric shield in front of the human model. The SAR and temperature distributions in the human model are governed by the electric field as well as the dielectric properties of tissue.

The results show an interaction between physical parameters: operating frequencies and shield dielectric properties. For human exposure to microwave energy, the installed dielectric shield strongly affects the SAR and the temperature increase in the human body. Actually, the microwaves can transmit through the dielectric shield, and can penetrate into the human model that contribute to the resonance of standing wave within the gap and human model.

Since the frequency increases, the penetration depth for microwave gets smaller and resonance effect becomes weakness. Consequently, the shielding effect is significant. Therefore, the appropriate dielectric properties, which can effectively reduce the SAR and the temperature increase in human body of the dielectric shield, are greatly dependent on the operating frequency. Additionally, this paper presents an interesting viewpoint on the microwave shielding properties of dielectric shields at various operating frequencies, while focusing on the human organism.

Future work will extend the calculations of the SAR and the temperature increase for a three-dimensional model. Moreover, it will be carried out to study the effect of wave pattern, namely, TM wave and TE wave on a realistic model.

Acknowledgments

The authors gratefully acknowledge the financial support provided by The Thailand Research Fund (TRF), and the authors also acknowledge Thammasat University for providing the simulation facilities described in this paper.

References

[1] P. Ratanadecho, N. Suwannapum, W. Cha-um, Interactions between electromagnetic and thermal fields in microwave heating of hardened type I-cement paste using a rectangular waveguide (influence of frequency and sample size), ASME Journal of Heat Transfer 131 (2009) 082101–082112.

[2] N. Makul, P. Ratanadecho, Microwave pre-curing of natural rubber-compounding using a rectangular wave guide, International Communications in Heat and Mass Transfer 37 (7) (2010) 914–923.

[3] P. Ratanadecho, C. Serttikul, Simulation of melting of ice under a constant temperature heat source using a combined transfinite interpolation and partial differential equation methods, Journal of Porous Media 10 (7) (2007) 657–675.

[4] M.A. Stuchly, Health effects of exposure to electromagnetic fields, IEEE Aerospace Applications Conference Proceedings, Aspen, USA, 1995, pp. 351–368.

[5] K.L. Ryan, J.A. D'Andrea, J.R. Jauchem, P.A. Mason, Radio frequency radiation of millimeter wave length: Potential occupational safety issues relating to surface heating, Health Physics 78 (2000) 170–181.

[6] R.J. SPIEGEL, A review of numerical models for predicting the energy deposition and resultant thermal response of humans exposed to electromagnetic fields, IEEE Transactions on Microwave Theory and Techniques 32 (1984) 730–746.

[7] T. Wessapan, S. Srisawatdhisukul, P. Rattanadecho, Numerical analysis of specific absorption rate and heat transfer in the human body exposed to leakage electromagnetic field at 915 MHz and 2,450 MHz, ASME Journal of Heat Transfer, xx (2011) xxx-xxx. (Accepted).

[8] A.W. Guy, C.-K. Chou, J.A. McDougall, C. Sorensen, Measurement of shielding effectiveness of microwave-protective suits, IEEE Transactions on Microwave Theory and Techniques 35 (1987) 984–994.

[9] S. Nishizawa, O. Hashimoto, Effectiveness analysis of lossy dielectric shields for a three-layered human model, IEEE Transactions on Microwave Theory and Techniques 47 (1999) 277–283.

[10] O. Hashimoto, S. Nishizawa, Effectiveness analysis of thin resistive sheet for a three-layered elliptical human model, Microwave and Optical Technology Letters 23 (1999) 73–75.

[11] T. Samaras, A. Christ, A. Klingenbck, N. Kuster, Worst case temperature rise in a one-dimensional tissue model exposed to radiofrequency radiation, IEEE Transactions on Biomedical Engineering 54 (2007) 492–496.

[12] K. Shiba, N. Higaki, Analysis of SAR and current density in human tissue surrounding an energy transmitting coil for a wireless capsule endoscope, Proceedings of the 20th International Zurich Symposium on Electromagnetic Compatibility 1 (2009) 321–324, Zurich.

[13] A. Hirata, O. Fujiwara, T. Shiozawa, Correlation between peak spatial-average SAR and temperature increase due to antennas attached to human trunk, IEEE Transactions on Biomedical Engineering 53 (2006) 1658–1664.

[14] A. Hirata, M. Fujimoto, T. Asano, J. Wang, O. Fujiwara, T. Shiozawa, Correlation between maximum temperature increase and peak SAR with different average schemes and masses, IEEE Transactions on Electromagnetic Compatibility 48 (2006) 569–577.

[15] D. Yang, M.C. Converse, D.M. Mahvi, J.G. Webster, Expanding the bioheat equation to include tissue internal water evaporation during heating, IEEE Transactions on Biomedical Engineering 54 (2007) 1382–1388.

[16] T. Basak, K. Aparna, A. Meenakshi, A.R. Balakrishnan, Effect of ceramic supports on microwave processing of porous food samples, International Journal of Heat and Mass Transfer 49 (2006) 4325–4339.

Drying Technology
Publication details, including instructions for authors and subscription information:
http://www.informaworld.com/smpp/title~content=t713597247

Analysis of Energy Consumption in Drying Process of Non-Hygroscopic Porous Packed Bed Using a Combined Multi-Feed Microwave-Convective Air and Continuous Belt System (CMCB)

W. Jindarat[a]; P. Rattanadecho[a]; S. Vongpradubchai[a]; Y. Pianroj[b]
[a] Research Center of Microwave Utilization in Engineering (RCME), Department of Mechanical Engineering, Faculty of Engineering, Thammasat University, Patum Thani, Thailand [b] Plasma and Fusion Research Unit, Sirindhorn International Institute of Technology, Thammasat University, Patum Thani, Thailand

Online publication date: 08 June 2011

To cite this Article Jindarat, W. , Rattanadecho, P. , Vongpradubchai, S. and Pianroj, Y.(2011) 'Analysis of Energy Consumption in Drying Process of Non-Hygroscopic Porous Packed Bed Using a Combined Multi-Feed Microwave-Convective Air and Continuous Belt System (CMCB)', Drying Technology, 29: 8, 926 — 938
To link to this Article: DOI: 10.1080/07373937.2011.560318
URL: http://dx.doi.org/10.1080/07373937.2011.560318

Drying Technology, 29: 926–938, 2011

ISSN: 0737-3937 print/1532-2300 online
DOI: 10.1080/07373937.2011.560318

Taylor & Francis
Taylor & Francis Group

Analysis of Energy Consumption in Drying Process of Non-Hygroscopic Porous Packed Bed Using a Combined Multi-Feed Microwave-Convective Air and Continuous Belt System (CMCB)

W. Jindarat,[1] P. Rattanadecho,[1] S. Vongpradubchai,[1] and Y. Pianroj[2]

[1]*Research Center of Microwave Utilization in Engineering (RCME), Department of Mechanical Engineering, Faculty of Engineering, Thammasat University, Patum Thani, Thailand*
[2]*Plasma and Fusion Research Unit, Sirindhorn International Institute of Technology, Thammasat University, Patum Thani, Thailand*

In this study, the analysis of energy consumption during the drying of non-hygroscopic porous packed bed by combined multi-feed microwave-convective air and continuous belt system (CMCB) was investigated experimentally. By using a combined multi-feed microwave-convective air and continuous belt system drier, the microwave power was generated by means of 12 compressed air-cooled magnetrons of 800 W each that give a maximum of 9.6 kW. The power setting could be adjusted individually in 800 W steps. Hot air with the maximum working temperature of 240°C was generated using 24 units of electric heater where the total power capacity is 10.8 kW. Most importantly, this work focused on the investigation of drying phenomena under industrialized microwave processing. In this analysis, the effects of the drying time, hot air temperature, porous structure (F-Bed and C-Bed), and location of magnetrons on overall drying kinetics and energy consumption were evaluated in detail. The results showed that the overall drying and energy consumption depend upon the porous structure, hot air temperature, and location of magnetrons. Furthermore, using the continuous microwave application technique had several advantages over the conventional method, such as shorter processing times, volumetric dissipation of energy throughout a product, and less energy consumption. The results presented here provided fundamental understanding for the drying process using a combined multi-feed microwave-convective air and continuous belt system in industrial size.

Keywords Continuous belt system; Microwave energy; Non-hygroscopic porous packed bed; Specific energy consumption

INTRODUCTION

During the past decade, there have been many successful examples of microwave application including the heating and drying of foods, heating and drying of ceramics, heating and curing of concrete, etc. The microwave heating process takes place inside the material, the penetrated depth of which governs how strongly the microwaves are absorbed. It is known that heat dissipated from the microwave energy depends on many parameters, such as configuration and structure of porous packed bed samples, microwave power level, microwave field distribution, the location of feed ports, and dielectric properties of porous packed bed samples. A number of analyses of the microwave heating process have appeared in the recent literature.[1–31] An excellent review of the drying techniques in porous material using microwave energy has been presented by Mujumdar,[1] Metaxas,[2] Datta and Anantheswaran,[3] and Schubert and Regier.[4]

The objective of drying is simply to remove water from the dried sample, i.e., porous packed bed without causing any damage. The process must be done both efficiently and economically. Water can leave the surface of the porous packed bed at a given rate depending on many parameters, such as microwave power level and air temperature, etc. In order to accomplish good drying of product, it requires a method that removes the water from the inside of the dried sample to the outside surface at the same rate as the evaporation of surface water.

The reasons for the interest in the interaction of microwaves with porous materials are reported by several investigators in the recent literature.[5–21] The microwave energy can lower the drying temperature in several porous materials by several hundred degrees, shorten drying times, reduce drying defects, provide greater throughput, increase energy efficiency because of the microwave source known as "magnetron", which is capable of very high power output; moreover, it has an efficiency to convert from electricity to microwave energy of 80%[22] and lessen floor-space requirements in comparison with conventional

Correspondence: P. Rattanadecho, Faculty of Engineering, R.C.M.E., Department of Mechanical Engineering, Thammasat University (Rangsit Campus), Patum Thani 12120, Thailand; E-mail: ratphadu@engr.tu.ac.th

drying methods. It is also environmentally friendly and easily integrates into flexible, automated manufacturing systems. It appears that microwaves increase the heating efficiency by concentrating the heating process within porous material rather than in the cavity in which the porous material is placed.

Currently, the major concern of the drying process is increasing productivity while reducing energy cost. Conventional drying processes of porous material usually take a long time (1–6 hr). The major problem of conventional drying processes is long drying time, which results in increased energy consumption. Thus, there have been many attempts to enhance the rate of drying of porous material in order to decrease drying time as well as energy consumption.

For an analysis of microwave energy consumption in heating and drying processes, we refer to Sharma and Prasad;[23] this study examined specific energy consumption in microwave drying of garlic cloves. The comparative study of specific energy consumption with two different drying methods, namely microwave-hot air and hot air drying, was carried out. Other related papers present microwave energy and hot air heating processes. Varith et al.[24] studied the combined microwave and hot air drying of peeled longan. The influence of moisture content on specific energy consumption (SEC) was examined. The other important paper, written by Lakshmi et al.,[25] presented a comparison of SEC in cooking rice among the microwave oven, electric rice cooker, and pressure cooker.

Investigations of energy efficiency of microwave drying of porous material have been performed since the late 1950s. Many authors (Alibas,[26] Poli et al.,[27] Cheng et al.,[28] Holtz et al.,[29] Soysol et al.,[30] Leiker and Adamska,[31] and Prommas et al.[32]) have placed emphasis on the advantages of microwave drying over convective drying. Varith et al.[24] point out the suitability of combined microwave and hot drying of peeled longan. However, there still remain obstacles to be overcome in applying microwave drying technology to the drying industry. One of the difficulties is that the microwave power absorbed by moist porous material depends mainly on the moisture content and it is necessary to move the porous material for uniform power distribution with an on-off type microwave system at fixed power output.

Although a number of studies have been conducted to investigate a microwave heating process, most of them were carried out using a domestic or housing microwave oven and a single or multimode cavity with a non-movable material. Those studies showed that the result may be dependent on the method used to carry out the curing or heating process. The objective of this study is to demonstrate the applicability of microwave energy as an energy-saving when compared with drying processes, electrical consumption, and production-cost-reducing technology. The microwave drying of a non-hygroscopic porous packed bed in a combined multi-feed microwave-convective air and continuous belt system, where a series of 12 magnetrons, 800 W each with total power of 9.6 kW, were installed, was developed. The experimental results from this study could help to identify some of the potential problems during the practical design stage. This study was of great importance from the practical point of view because it showed the possibility of application of microwave heating-drying of porous materials on an industrial scale, especially in a continuous system.

EXPERIMENTAL PROCEDURE

Microwave-convective air drying was carried out using a combined multi-feed microwave-convective air and continuous belt system (CMCB) (Fig. 1(a)). The shape of the microwave cavity is rectangular with a cross-sectional area

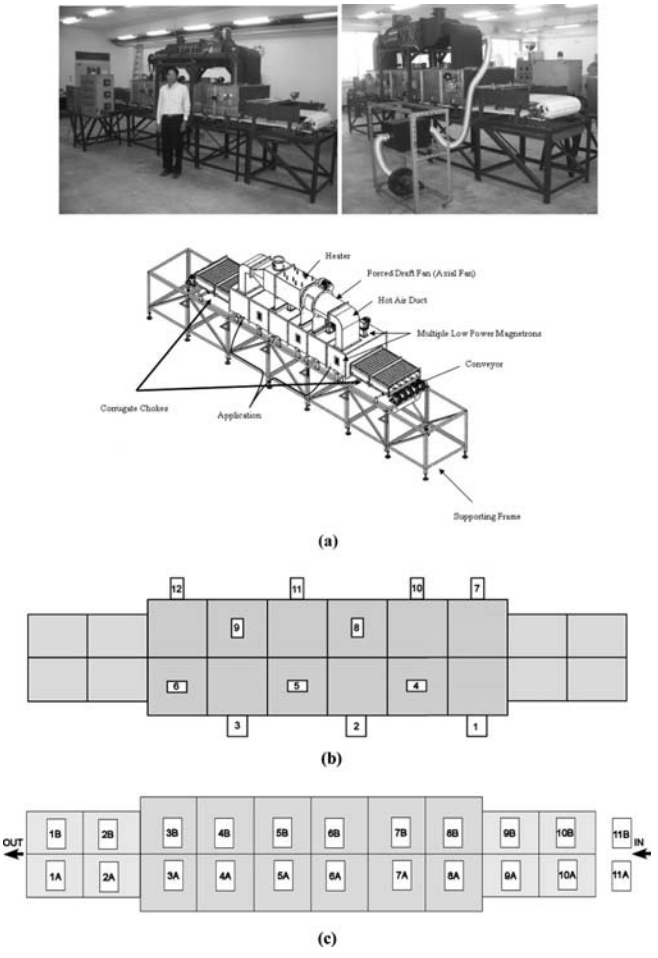

FIG. 1. Schematic diagram of experimental set-up. (a) A combined multi-feed microwave-convective air and continuous belt system; (b) Feed magnetrons positioned of 12 units and (c) Feed samples positioned of 22 packed beds.

of 90 cm × 45 cm × 270 cm. The drier was operated at a frequency of 2.45 GHz with maximum working temperature of 180°C. The microwave power was generated by means of 12 compressed air-cooled magnetrons. The maximum microwave capacity was 9.6 kW with a frequency of 2.45 GHz. The power setting could be adjusted individually in 800 W steps. In the continuous processing equipment, two open ends are essential, in which the material is to be heated up on the belt conveyer where it was put in and taken out. In this equipment, leakage of microwaves was prevented by the countermeasure in duplicate with a combination of mechanical blocking filter (corrugate choke) and microwave absorber zone filter was provided at each of the open ends. The microwave leakage was controlled under the DHHS (US Department of Health and Human Services) standard of 5 mW/cm^2. The multiple magnetrons (12 units) were installed in an asymmetrical position on the rectangular cavity (Fig. 1(b)). The microwave power was then directly supplied into the drier by using waveguides. An infrared thermometer (located at the opening ends) was used to measure the temperature of the specimens (accurate to ±0.5°C).

The magnetrons and transformers used in this system were cooled down by a fan. In the continuous heating/drying equipment, two open ends were essential to feed in and feed out the product, through which the material to be heated up on the belt conveyer was arranged in certain position, as shown in Fig. 1(c). The belt conveyor system consisted of a drive motor, a tension roller, and a belt conveyor. During the drying process, the conveyor speed was adjusted to 0.54 m/min (at the frequency 40 Hz) and the motor speed was controlled by the VSD control unit. Hot air was generated using the 24 units of electric heaters with the maximum capacity of 10.8 kW and the maximum working temperature of 240°C. The hot air was provided by blower fan with 0.4 kW power through the air duct into the cavity. The hot air temperature was measured using a thermocouple.

As shown in Fig. 2, the drying samples were in a non-hygroscopic porous packed bed, which was composed of glass beads and water ($S_0 = 1$). A sample container was made from polypropylene with a thickness of 2 mm (with dimension of 14.5 cm × 21 cm × 5 cm). The polypropylene did not absorb microwave energy. In this study, the voids occupied from a fraction up to 38 percent of the whole volume of packed beds. The samples were prepared in two configurations: a fine single-layered packed bed ($d = 0.15$ mm, $dp = 11.5$ mm) and a coarse single-layered packed bed ($d = 0.40$ mm, $dp = 11.5$ mm). The sample selected for the drying test was a non-hygroscopic porous packed bed with dimensions of 14.5 cm × 21 cm × 1.15 cm. The 22 porous packed beds had total weight of 11 kg, which had initial water saturation (S_0) of 1.0 and the initial temperature was equal to the ambient temperature.

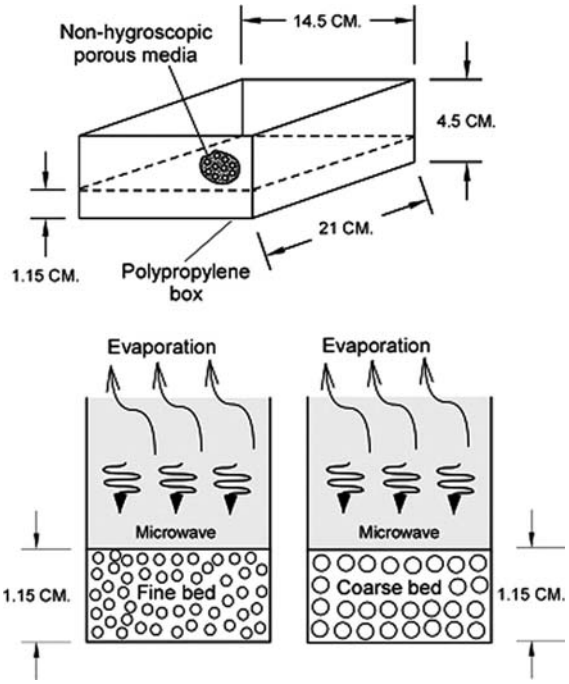

FIG. 2. Schematic of drying sample (porous packed bed).

The water saturation in the non-hygroscopic porous packed bed was defined as the fraction of the volume occupied by water to volume of the pores. It was obtained by weighing dry and wet mass of the sample. The water saturation formula can be described in the following from:[15]

$$S = \frac{M_p \cdot \rho_s \cdot (1 - \phi)}{\rho_w \cdot \phi \cdot 100} \tag{1}$$

where S is water saturation, ρ_s is density of solid, ρ_w is density of water, ϕ is porosity, and M_p is particle moisture content dry basis. During the experimental microwave drying processes, the uncertainty of our data might come from the variations in humidity and room temperature. The uncertainty in drying kinetics was assumed to result from errors in the measured weight of the sample. The calculated drying kinetic uncertainties in all tests were less than 3%. The uncertainty in temperature was assumed to result from errors in measured input power, ambient temperature, and ambient humidity. The calculated uncertainty associated with temperature was less than 2.85%. Three test runs were repeatedly carried out in order to obtain the accurate data.

RELATED THEORIES

Microwave Heat Generation

Microwave heating involves heat dissipation and microwave propagation which causes the dipoles to vibrate and rotate. When the microwave energy emitting from a

microwave oscillator (P_{in}) is irradiated inside the microwave applicator, the dielectric material, which has a dielectric loss factor, absorbs the energy and is heated up. Then the internal heat generation takes place. The basic equation calculates the density of microwave power absorbed by dielectric material (P_1) is given by:[16]

$$P_1 = \omega \varepsilon_0 \varepsilon_r'' E^2 = 2\pi \cdot f \cdot \varepsilon_0 \cdot \varepsilon_r' (\tan \delta) E^2 \tag{2}$$

where E is electromagnetic field intensity, f is microwave frequency, ω is angular velocity of microwave, ε_r' is relative dielectric constant, ε_0 is dielectric constant of air, and tan δ is loss tangent coefficient.

From equation (2), P_1 is directly proportional to the frequency of the applied electric field, loss tangent coefficient, and root-mean-square value of the electric field. It means that an increase of tan δ of specimen, energy absorption and heat generation are also increased. While tan δ is smaller, microwave will penetrate into the specimen without heat generation. However, the temperature increase depends on other factors, such as specific heat, size, and characteristics of specimen.

When the material is heated unilaterally, it is found that as the dielectric constant and loss tangent coefficient vary, the penetration depth will be changed and the electric field within the dielectric material is altered. The penetration depth is used to denote the depth at which the power density has decreased to 37% of its initial value at the surface:[16]

$$D_p = \frac{1}{\frac{2\pi f}{\upsilon}\sqrt{\frac{\varepsilon_r'\left(\sqrt{1+\left(\frac{\varepsilon_r''}{\varepsilon_r'}\right)^2}-1\right)}{2}}} = \frac{1}{\frac{2\pi f}{\upsilon}\sqrt{\frac{\varepsilon_r'\left(\sqrt{1+(\tan\delta)^2}-1\right)}{2}}} \tag{3}$$

where D_P is penetration depth, ε_r'' is relative dielectric loss factor, and υ is microwave speed. The penetration depth of the microwave power is calculated according to Eq. (3), which shows how it depends on the dielectric properties of the material. It is noted that products with huge dimensions and high loss factors may occasionally be overheated to a considerably thick layer on the outer layer. To prevent such phenomenon, the power density must be chosen so that enough time is provided for the essential heat exchange between boundary and core. If the thickness of the material is less than the penetration depth, only a fraction of the supplied energy will become absorbed. Furthermore, the dielectric properties of porous material specimens typically show moderate loss depending on the actual composition of the material. With large amount of moisture content, it reveals a greater potential for absorbing microwaves. For typical porous packed bed specimens, a decrease in the moisture content typically decreases ε_r'', accompanied by a slight increment in D_p.

In the analysis, energy P_2 is required to heat up the dielectric material, which is placed in a microwave applicator. The temperature of material, initially (T_1), is raised to T_2. The energy (P_2) can be estimated by the following calorific equation:[16]

$$P_2 = \frac{4.18 \cdot W \cdot C_p \cdot \Delta T}{t} \tag{4}$$

where W is weight of the dielectric material, C_p is specific heat of the dielectric material, ΔT is the increment of temperature ($T_2 - T_1$), and t is heating time.

Assuming an ideal condition, all of the oscillated microwave energy (P_{in}) is absorbed into the dielectric material, so internal heat generation as Eq. (2) takes place. In this case, the relation between P_{in} and P_2 is shown below:[16]

$$P_{in} = P_2 \tag{5}$$

In a practical point of view, the transformation energy in the applicator exists due to Eq. (2), the rate of microwave energy absorbed by means of the dielectric loss factor of the sample, and Eq. (3) the energy loss in the microwave devices. Accordingly, by taking into account this transformation efficiency, the microwave oscillation output can be calculated by the following equations:[16]

$$P_{in} = \frac{P_2}{\eta_m} \tag{6}$$

$$\eta_m = \frac{P_2}{P_{in}} \tag{7}$$

where

$$P_2 = \frac{Q \cdot S_p \cdot C_P \cdot \Delta T \cdot 4.18}{60 \cdot \eta_m \cdot 10^3} \tag{8}$$

where η_m is efficiency of microwave devices, Q is weight per meter of dielectric material (porous packed bed), S_p is a rate at which the dielectric material is put on the belt conveyer, C_P is specific heat of dielectric material, and ΔT is heat-up range of $T_1 - T_0$.

Mass and Energy Balance Equation for the Drying Process

The conservation of mass for the control volume of cavity is shown in Fig. 3. The mass balance equation can be written as:[33]

$$\frac{dm_{cv}}{dt} = \dot{m}_{g1} - \dot{m}_{g2} \tag{9}$$

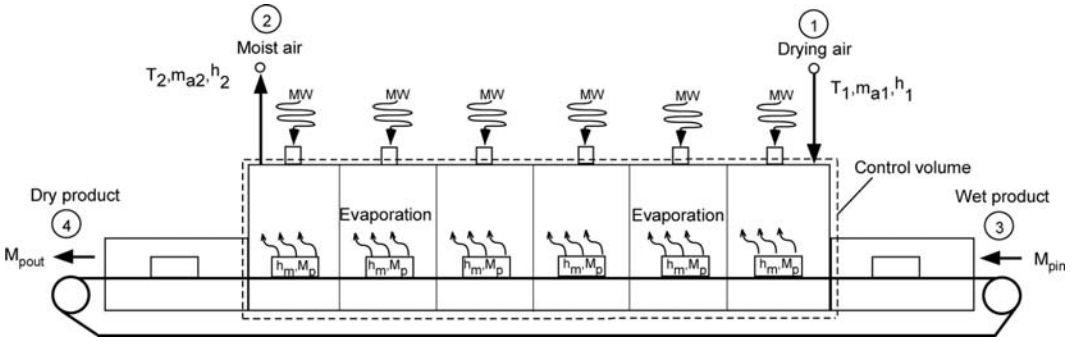

FIG. 3. Schematic of control volume representing drying process using a combined multi-feed microwave-convective air and continuous belt system (CMCB).

Here, Eq. (9) is the mass rate balance for the control volume where $\dot{m}_{g1}$ and $\dot{m}_{g2}$ denote the mass flow rate at inlet (1) and at exit (2), respectively. Similarly, a balance of water in air flowing through the drying cavity leads to:[33]

$$W_d \frac{dM_p}{dt} = \dot{m}_a(X_1 - X_2) \tag{10}$$

where W_d is weight of dry material and M_p is particle moisture content in dry basis. This can be expressed as:[33]

$$M_p = \frac{W_b - W_d}{W_d} \tag{11}$$

where W_b is weight of material before drying, $\dot{m}_a$ is the mass flow rate of dry air, X_1 and X_2 denote absolute humidity of inlet and exit air, respectively. The left-hand side of the mass balance equation, Eq. (10), is the mass flow rate of water in the air flowing from cavity. It can be written as:[33]

$$\dot{m}_w = \dot{m}_a(X_2 - X_1) \tag{12}$$

In the drying process, we apply the first law of thermodynamics (the conservation of energy) for the control volume as shown in Fig. 3. The significant heat transfer is due to the heat of evaporation between the solid and the drying air, and there is also heat rejection to the surroundings. The energy rate balance is simplified by ignoring kinetic and potential energies. Since the mass flow rate of the dry air and the mass of dry material within the control volume remain constant with time, the energy rate balance can be expressed as:

$$\frac{W_d(h_{m2} - h_{m1})}{\Delta t} = \dot{Q}_{evap} + \dot{m}_a(h_1 - h_2) + \dot{Q}_{MW} - \dot{Q}_{loss} \tag{13}$$

where $\dot{Q}_{evap}$ is heat transfer rate due to water evaporation, $\dot{Q}_{MW} = P_{in}$ is microwave energy, h_m is enthalpy of material, t is time, $\dot{m}_a$ is mass flow rate of dry air, h is enthalpy of dry air, and $\dot{Q}_{loss}$ is heat transfer rate to the environment.

Assuming air as an ideal gas, the differences in specific enthalpy are as follows:[33]

$$h_{m1} - h_o = c_m(T_{m1} - T_o) \tag{14}$$

$$h_{m2} - h_o = c_m(T_{m2} - T_o) \tag{15}$$

The enthalpy term of material in Eq. (13) can be written as:[33]

$$h_{m2} - h_{m1} = c_m(T_{m2} - T_{m1}) \tag{16}$$

where c_m represents the specific heat of the material. The enthalpy of moist air can be calculated by adding the contribution of each component as it exists in the mixture; thus the enthalpy of moist air is:[33]

$$h = h_a + Xh_v \tag{17}$$

The heat transfer rate due to phase change is:[33]

$$\dot{Q}_{evap} = \dot{m}_w h_{fg} \tag{18}$$

where h_{fg} is latent heat of vaporization.

Specific Energy Consumption and Energy Efficiency in Drying Process

The drying of a non-hygroscopic porous packed bed is a process of simultaneous heat and mass transfer. The specific energy consumption during the drying process using a combined multi-feed microwave-convective air and continuous belt system and convective drying processes was estimated. The drying conditions are total electrical power supplied in the drying process; convective air temperatures of 30, 50, and 70°C; convective air velocity of 0.5 m/s; total microwave power of 4.8 kW. The specific energy

TABLE 1
Drying time and electrical power under various drying conditions (C-bed)

Testing condition	Power of magnetrons (W)	Position of magnetrons	Air temperature (°C)	Drying time (min)	Electrical power (Kw-hr)	Cost (US$)*
Case 1	800×6	Side (1-10-2-11-3-12)	Ambient Air, 30	80	10.5	1.1
Case 2	800×6	Top (7-4-8-5-9-6)	Ambient Air, 30	70	8.9	0.91
Case 3	800×6	Side (1-10-2-11-3-12)	Hot Air 70	70	16	1.65
Case 4	800×6	Top (7-4-8-5-9-6)	Hot Air 70	70	13.5	1.39
Case 5	800×6	Side (1-10-2-11-3-12)	Hot Air 50	70	11.9	1.23
Case 6	800×6	Top (7-4-8-5-9-6)	Hot Air 50	70	11.8	1.22
Case 7	800×6	Screw (7-4-2-5-9-12)	Hot Air 50	70	12.2	1.26
Case 8	–	–	Hot Air 70	360	33	3.41

*Remark: Baht foreign exchange reference rates as at 15–27 January 2011 (Unit: Baht per 1 unit of U.S. dollar).

consumption (SEC) equation is represented by:

$$SEC = \frac{\text{Total electrical power supplied in drying process}}{\text{Amount of water removed during drying}}, \left[\frac{kW - hr}{kg}\right] \quad (19)$$

$$SEC = \frac{P_{total}}{\text{Amount of water removed during drying}}, \left[\frac{kJ}{kg}\right] \quad (20)$$

where P_{total} is a total electrical power supplied the in drying process; this term can be calculated from:

$$P_{total} = P_{mg} + P_{heater} + P_{exfan} + P_{blfan} + P_{cofan} + P_{con}, \quad [kW \times 3600s] \quad (21)$$

where P_{mg} is the electrical power supplied in the magnetron, P_{heater} is the electrical power supplied in the heater, P_{exfan} is the electrical power supplied in the exhaust fan, P_{blfan} is the electrical power supplied in the blower fan, P_{cofan} is the electrical power supplied in the cooling fans, and P_{con} is the electrical power supplied in the conveyor.

From,[33] the energy efficiency (η_e) for the drying process is defined as:

$$\eta_e = \frac{W_d[h_{fg}(M_{p1} - M_{p2}) + c_m(T_{m2} - T_{m1})]}{\dot{m}_{da}(h_1 - h_o)\Delta t + \Delta t \dot{Q}_{MW}} \quad (22)$$

RESULTS AND DISCUSSIONS

Experimental data are analyzed to obtain the drying kinetics for different drying cases and conditions as listed in Tables 1 and 2. The details of the analysis are as outlined in the following.

Drying Kinetics

Figures 4–7 show the temperature and moisture variations versus elapsed times for C-bed and F-bed with constant initial moisture content of 25% (dry basis). It is found that in the case of microwave–convective air drying

TABLE 2
Drying time and electrical power under various drying conditions (F-bed)

Testing condition	Power of magnetrons (W)	Position of magnetrons	Air temperature (°C)	Drying time (min)	Electrical power (Kw-hr)	Cost (US$)*
Case 1	800×6	Side (1-10-2-11-3-12)	Ambient Air, 30	90	11.4	1.17
Case 2	800×6	Top (7-4-8-5-9-6)	Ambient Air, 30	80	9.9	1.02
Case 3	800×6	Side (1-10-2-11-3-12)	Hot Air 70	80	15.7	1.64
Case 4	800×6	Top (7-4-8-5-9-6)	Hot Air 70	80	16	1.65
Case 5	800×6	Side (1-10-2-11-3-12)	Hot Air 50	80	12.6	1.3
Case 6	800×6	Top (7-4-8-5-9-6)	Hot Air 50	80	11.1	1.18
Case 7	800×6	Screw (7-4-2-5-9-12)	Hot Air 50	80	12.7	1.31
Case 8	–	–	Hot Air 70	420	35.5	3.67

*Remark: Baht foreign exchange reference rates as at 15–27 January 2011 (Unit: Baht per 1 unit of U.S. dollar).

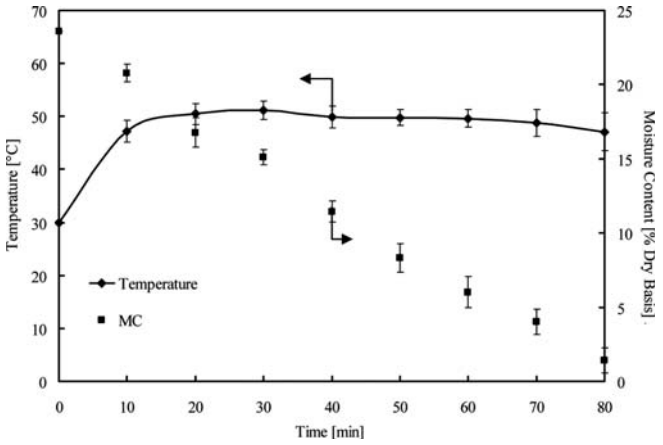

FIG. 4. Temperature and moisture variations versus elapsed times in case drying using CMCB ($T_1 = 30°C$) (C-bed, case 1).

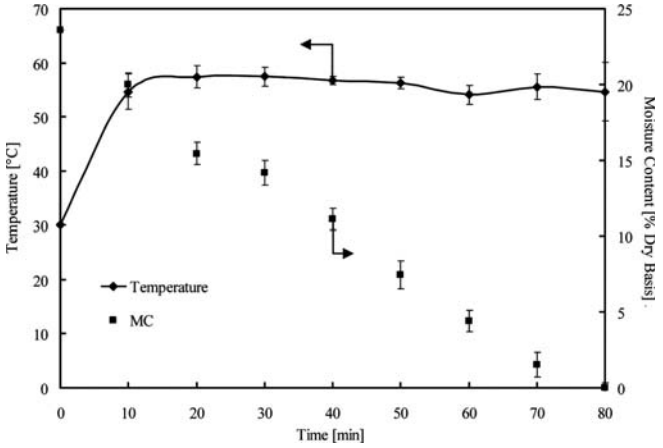

FIG. 5. Temperature and moisture variations versus elapsed times in case drying using CMCB ($T_1 = 30°C$) (case 2, C-bed).

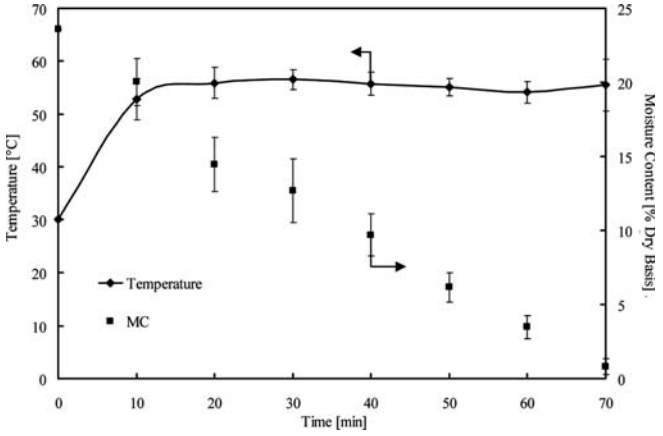

FIG. 6. Temperature and moisture variations versus elapsed times in case drying using CMCB ($T_1 = 70°C$) (case 4, C-bed).

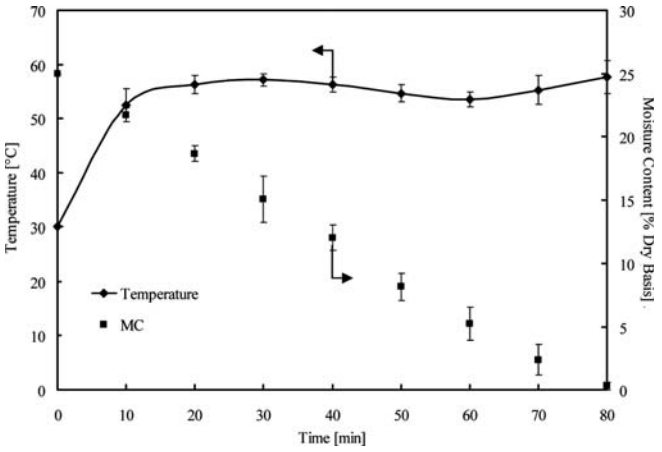

FIG. 7. Temperature and moisture variations versus elapsed times in case drying using CMCB ($T_1 = 70°C$) (case 4, F-bed).

(30 and 70°C) the moisture profile of the sample continuously decreases faster than the case of convective drying, as shown in Figs. 8 and 9. This phenomenon occurred in the case of convective drying (30 and 70°C) combined with microwave energy; thus the bulk of this sample absorbs the largest amount of microwave energy, which corresponds to the level of absorbed energy in samples as described in Eq. (2). Furthermore, when the process nearly reaches the end stage of drying, the moisture content inside the sample reduces and the absorption of microwave energy decreases.[15] Thus, during this period, microwave power should be optimized to control in order to reduce power consumption in the drying systems.

The temperature and moisture variations versus elapsed times are known as the parameters of the microwave power level 4.8 kW. During the first period of heating, most of the microwave energy supplied is used to heat the sample. The

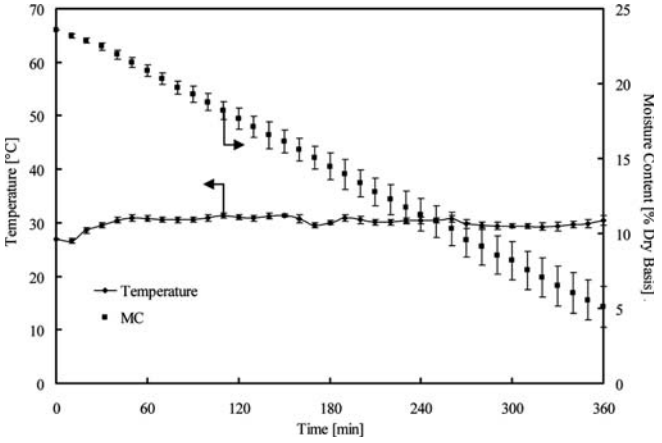

FIG. 8. Temperature and moisture variations versus elapsed times in case using convective drying ($T_1 = 70°C$) (case 8, C-bed).

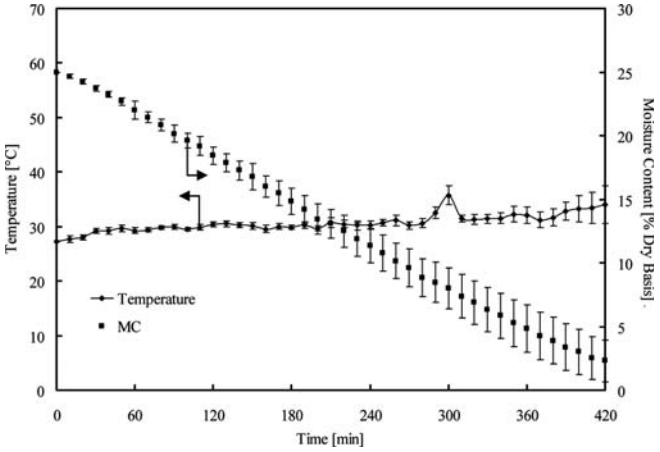

FIG. 9. Temperature and moisture variations versus elapsed times in case using convective drying ($T_1 = 70°C$) (case 8, F-bed).

temperature of the sample is raised rapidly up to 60°C in few minutes. It is found that the temperature increases in the narrow range after the convective air is applied since, at this period, the sample is filled with the moisture, which rapidly responses to the microwave energy at this frequency. Therefore, the major increasing of temperature comes from the microwave energy. However, undesired non-uniform heating patterns can be prevented either by changing the field configuration or by moving the product on a conveyer belt through the cavity where the microwave could be fed at several positions. In addition, considering the multiple magnetron system, the different directions of transmitted waves from different magnetrons make the uniformity of temperature inside the samples. This is because of its wave interference and the influence of the wave penetration capability, as shown in Eq. (2).

Figures 4–9 show the temperature and moisture variations versus elapsed times with respect to different drying methods. It can be observed from these figures that in a combined multi-feed microwave-convective air and continuous belt system, the sample is dried quickly without the residual moisture content in the sample due to the uniform heating. It is clear that the microwave-convective air drying times are drastically reduced compared to convective drying, from 420 min to less than 80 min. This investigation combined that microwave drying; i.e., microwave continuous belt drying can yield a considerable gain in drying time by a factor of ten or more. In the case of convective drying (Figs. 8 and 9), as the surface is dried while the interior is still wet, the dry layer offers a resistance to the heat transport, resulting in a reduction of the evaporation rate as well as drying rate, causing non-uniform heating.

As shown in Fig. 1(b), microwaves oscillated from the magnetron are fed into the cavity. The transmitted wave passes the wave guide (unit numbers 1–12) to heat up the non-hygroscopic porous packed bed. It is found in Figs. 5–7 that the feed magnetrons positioned on the top of the cavity show the influence of microwave power absorbed within the sample, and the temperature relation. Within the sample, the electric field attenuates owing to energy absorption, which is converted to the thermal energy, thus the sample temperature increases. However, the feed magnetrons positioned on the side of the cavity show a lower absorbed microwave power, as shown in Fig. 4. This is because of no direct wave irradiated on the sample; therefore, the influence of the absorbed energy converted to the sample temperature is lower. This phenomenon corresponds to the level of absorbed energy in samples, as explained earlier.

Figures 6 and 7 show the temperature variations and moisture content with respect to elapsed times at different testing conditions. It is found that at a microwave-convective air drying (30 and 70°C) the temperature profile of the sample continuously rises while the moisture content profile rapidly decreases. The electric field distribution in the cavity is uniform. The temperature and moisture content profiles are also depicted in Figs. 6 and 7. It is observed that the increase of temperature and the decrease of moisture content between packed beds A and B are uniform.

Electrical Energy Consumption and Drying Time

The electrical energy consumption during microwave-convective air drying and convective drying of a combined multi-feed microwave-convective air and continuous belt system is given in Figs. 10 and 11. When the two drying methods are compared in terms of electrical energy consumption, it is noted that the lowest electrical energy consumption is observed from the microwave-convective air drying method and this is followed by convective drying methods. The best result with regard to electrical energy

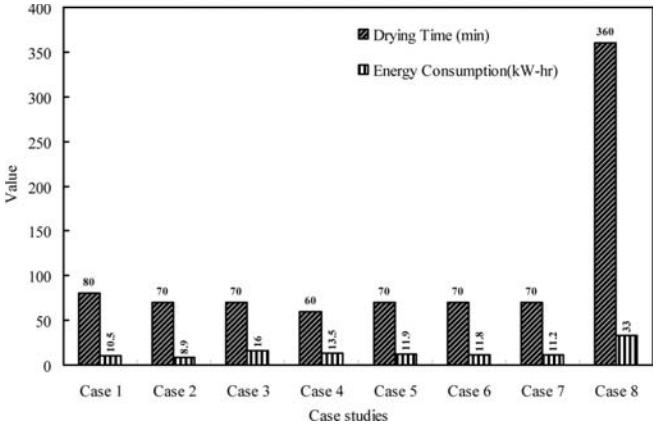

FIG. 10. Variations in drying time and electrical energy consumption in a different case (C-bed).

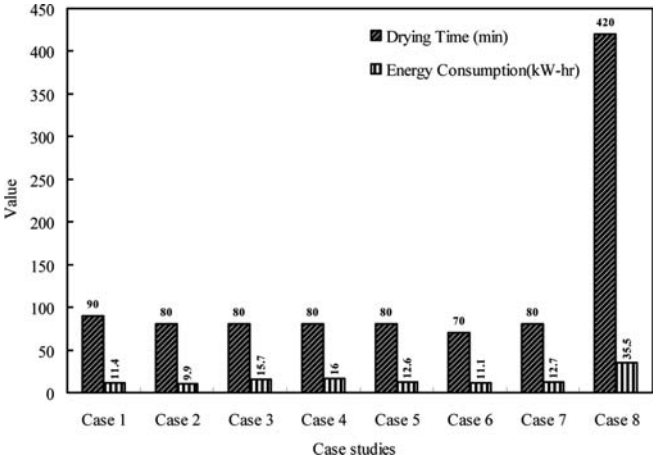

FIG. 11. Variations in drying time and electrical energy consumption in a different case (F-bed).

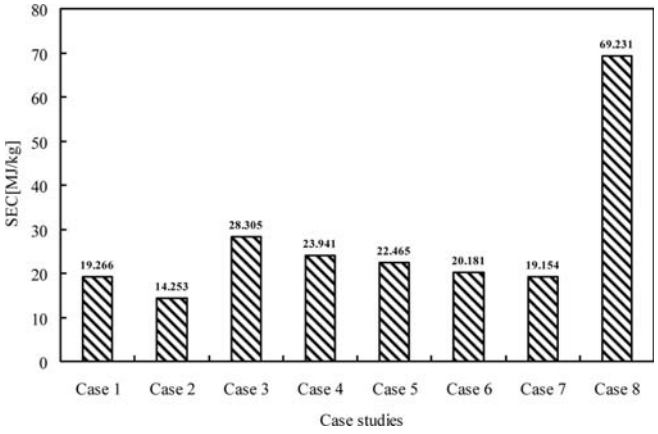

FIG. 12. Variations in specific energy consumption in a different case (C-bed).

consumption is obtained from a microwave power level of 4.8 kW among all drying methods. Electrical energy consumptions at this microwave power level are 8.9 kW-hr (case 2; C-bed) and 9.9 kW-hr (case 2; F-bed). The highest value in all drying methods regarding electrical energy consumption is noted in the convective drying process at temperature 70°C with of 33 kW-hr (case 8; C-bed) and 35.5 kW-hr (case 8; F-bed).

The drying time of convective drying along the drying process is given in Figs. 10 and 11. The highest value in all drying methods regarding the drying time is noted in the convective drying process operating at the temperature of 70°C with 360 minutes (case 8; C-bed) and 420 minutes (case 8; F-bed).

Analysis of Specific Energy Consumption (SEC)

Figures 12 and 13 show the specific energy consumption with the variation of the sample particles.

To obtain the experimental results, the microwave power level is set at 4.8 kW, and the thickness of the layers with C particles and F particles is fixed. Figures 12 and 13 show the specific energy consumption with the variation of the sample thickness. It can be seen in the first period of drying (around 0–120 min) that the packed bed can absorb a lot of microwave power due to the high moisture content, and thus the specific energy consumption is low in this period.

Microwave-convective air drying can be used to efficiently dry the sample. A non-hygroscopic porous packed bed dried using microwave energy required 5 times less specific energy consumption than the bed dried by a convective drying method at 70°C. Similar result are also observed in Figs. 12 and 13; the non-hygroscopic porous packed bed dried by microwave–convective air drying can be rapidly dried due to the uniform heating of the drying system as described in the previous section. The drying times of the microwave–convective air drying is less than 80 min, which is drastically reduced from the convective drying time of 420 min (Fig. 13). The results show that microwave drying can yield a considerable gain in drying time by a factor of two or more. In the case of convective drying, the surface is dried while the interior is still wet; the dry layer offers resistance to the heat transport, resulting in a reduction of the evaporation rate as well as drying rate and also causing high specific energy consumption.

The drying time of the drying trials is carried out by two different drying methods. No marked difference is found between the methods with and without hot air supplied in the cavity. Specific energy consumption depends on the power absorbed by the cavity and the drying time. In this study, the specific energy consumptions at microwave power levels of 4.8 kW are investigated. These short drying times may be due to a result of microwave power levels.

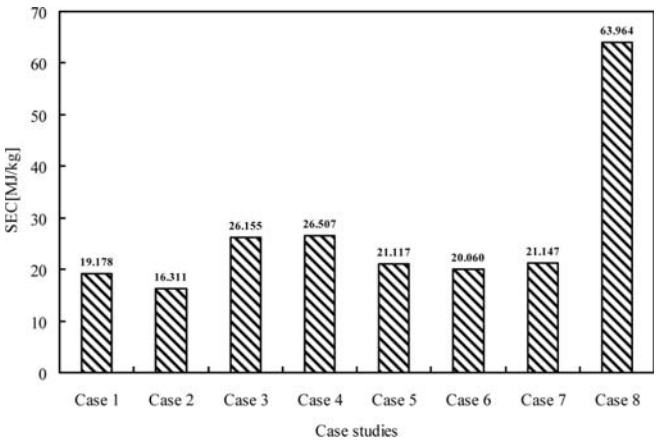

FIG. 13. Variations in specific energy consumption in a different case (F-bed).

However, for convective drying, the drying times are long because the convective heat transfer coefficient of the non-hygroscopic porous packed bed is low. The reduction of specific energy consumption observed during drying and the reduction of drying time is caused by the decrease in convective air levels. The specific energy consumptions of microwave-convective air drying at ambient temperature are 14.253 MJ/kg (case 2; C-bed) and 16.311 MJ/kg (case 2; F-bed), whereas the specific energy consumptions of convective drying at 70°C are 69.231 MJ/kg (case 2; C-bed) and 63.964 MJ/kg (case 2; F-bed). The specific energy consumptions of the combination drying (microwave–convective air drying) give similar trends at all drying processes. The reduction of specific energy consumption is achieved by decreasing the hot air temperature level supplied to cavity. Figures 12 and 13, respectively, show the comparison of specific energy consumption of different drying cases for C-bed and F-bed. The results show that the lowest specific energy consumption is found from the microwave–convective air drying method (ambient air), and followed by convective drying methods (Figs. 12 and 13).

Energy Efficiency

Figures 14 and 15 show the energy efficiency with respect to the drying time in different cases. It is found that the energy efficiency during drying of C-bed and F-bed at the starting period (0–15 min) is high due to the high quantity of moisture content in the non-hygroscopic porous packed bed, which leads to high value of dielectric loss factor; thus the wave absorption is more converted by the non-hygroscopic porous packed bed. The results are high energy efficiency after the vapor moves from the surface of the non-hygroscopic porous packed bed. This causes the moisture content to decrease quickly and the low quantity of absorbed waves because of the decreased energy consumption and decreased efficiency of absorbed microwave power, therefore the energy efficiency depends on the level of absorbed microwave power.

In Fig. 14, the energy efficiency profile for the sample in the case of C-bed rises up quickly in the early stages of drying (between 10–15 min). However, the efficiency rises slowly after this stage (between 45–70 min). It is evident from the figure that the moisture content inside the sample reducing at the final stages of drying causes the decreases in the absorbed microwave power. Consequently, the energy efficiency profiles decrease in this stage of drying.

Figures 14 and 15 show the energy efficiency values during microwave-convective air drying of a combined multi-feed microwave-convective air and continuous belt system in case 1 and case 2 (C-bed and F-bed). It can be observed that when the drying methods are compared in

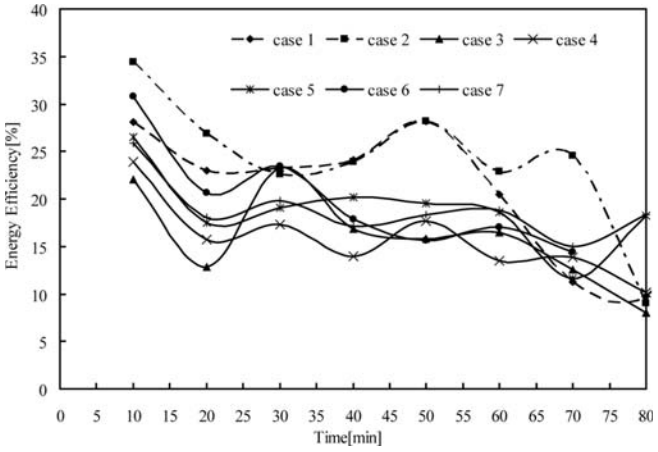

FIG. 15. Energy efficiency profiles with respect to elapsed time in a different case (F-bed).

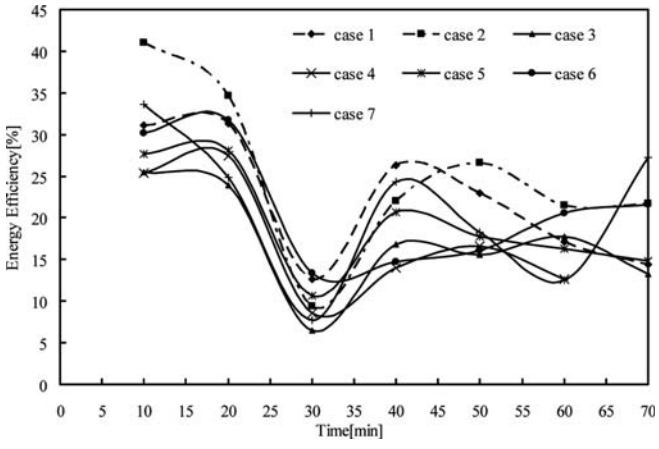

FIG. 14. Energy efficiency profiles with respect to elapsed time in a different case (C-bed).

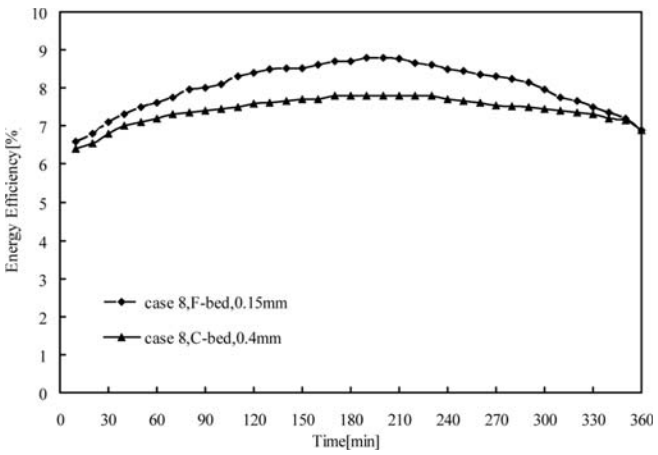

FIG. 16. Energy efficiency profiles with respect to elapsed time in case 8.

terms of energy efficiency, the highest energy efficiency is presented in case 1 and case 2 (Table 1 and Table 2: C-bed and F-bed). No marked difference is found between the supplied hot air into the cavity, since the drying time values obtained in the drying are also not different. The result shows that the microwave–convective air drying is not significant to decrease the drying time and to waste more energy consumption.

Figure 16 shows the energy efficiency with respect to the drying time. The low energy efficiency of convective drying is presented (case 8; C-bed and F-bed). Energy efficiency depends on the temperature in the cavity and the drying time. However, the drying times of convective drying, due to the convective heat transfer of the non-hygroscopic porous packed bed, are low.

Microwave technology is one of the most interesting heating methods because microwave processing requires lower energy consumption for the same or better results than conventional equipment. However, if we consider the capital and operating cost, it is found that microwave technology is capital-intensive and the economics of a particular application must be thoroughly examined before equipment is installed in industry.

CONCLUSIONS

A combined multi-feed microwave-convective air and continuous belt system permits quicker drying at lower temperature, resulting in a 30% reduction in energy consumption for what is normally an energy-intensive process. A non-hygroscopic porous packed bed dried using microwave energy required 5 times less specific energy consumption than the packed bed, which dried by a convective drying method at 70°C in a convective cavity. Moreover, this work depicts the technique that combined the conventional heating with the microwave heating and the continuous belt system. It shows the potential to reduce electrical energy consumption. If this technology is implemented to industry, it will decrease the production costs due to the lower electrical energy consumption.

Overall, when handling a combined multi-feed microwave-convective air and continuous belt system correctly, we can conclude that it will realize the following advantages over other drying systems:

1. Better heat distribution.
2. Faster product heating because the multiple magnetrons are placed around the rectangular cavity; this advantage corresponds to the better microwave power distribution, which can penetrate further into the multi-plane of the material.
3. Can immediately be ready for operation and control of heat capacity without delay.
4. Can continuously supply the material into the system.
5. The cavity is designed to prevent magnetron damage.
6. No heat storage losses.
7. Low specific energy consumption and high energy efficiency.

The next steps of the research related to this work will be done to develop the control system and optimal drying schedules for a combined multi-feed microwave-convective air and continuous belt system of hygroscopic porous material, especially biomaterial.

NOMENCLATURE

C_p	specific heat of the dielectric material (kJ/kg K)
c_m	material specific heat (kJ/kg K)
D_p	penetration depth (m)
d_p	depth of packed bed (mm)
E	electromagnetic field intensity (V/cm)
f	microwave frequency (Hz)
h	enthalpy (kJ/kg)
h_m	enthalpy of material (kJ/kg)
h_{fg}	latent heat of vaporization (kJ/kg_{water})
M_p	particle moisture content dry basis (kg_{water} / kg_{solid})
$\dot{m}$	mass flow rate (kg/s)
$\dot{m}_a$	mass flow rate of dry air (kg/s)
$\dot{m}_w$	mass flow rate of water in the air flowing from cavity (kg/s)
P_{in}	microwave energy emitted from a microwave oscillator (kW)
P_1	density of microwave power absorbed by dielectric material (kW/cm^3)
P_2	energy is required to heat up the dielectric material (kW)
P_{total}	total electrical power supplied in drying process (kJ)
P_{mg}	electrical power supplied in magnetron (kW-hr)
P_{heater}	electrical power supplied in heater (kW-hr)
P_{exfan}	electrical power supplied in exhaust fan (kW-hr)
P_{blfan}	electrical power supplied in blower fan (kW-hr)
P_{cofan}	electrical power supplied in cooling fans (kW-hr)
P_{con}	electrical power supplied in conveyor (kW-hr)
$\dot{Q}_{evap}$	heat transfer rate due to water evaporation (kW)
$\dot{Q}_{MW}$	microwave energy (kW)
$\dot{Q}_{loss}$	heat transfer rate to the environment (kW)
Q	weight per meter of dielectric material (non-hygroscopic porous packed bed) (g/m)
SEC	Specific Energy Consumption (kJ/kg)
S	water saturation
S_p	rate at which the dielectric material is put on the belt conveyer (m/min)
T	temperature (°C)
t	time (s)
tan δ	loss tangent coefficient (-)
W	weight of the dielectric material (kg)
W_d	weight of dry material (kg)

W_b weight of material before drying (kg)
X absolute humidity ($kg_{vapor}/kg_{dry\ air}$)

Greek Letters

ε_r'' relative dielectric loss factor
ε_r' relative dielectric constant
ε_0 permittivity of air (F/m)
ΔT increment temperature (°C)
η_e energy efficiency (%)
η_m efficiency of microwave device (%)
ρ_s density of solid (glass bead) (kg/m^3)
ρ_w density of water (kg/m^3)
ϕ porosity (m^3/m^3)
υ velocity of propagation (m/s)
ρ density (kg/m^3)
ω angular velocity of microwave (rad/s)

Subscripts

o standard state value; surroundings; reference environment
1 inlet
2 outlet
a air
b before
da drying air
d dry material
fg difference in property between saturated liquid and saturated vapor
g gas
in input
m material
s solid
w water
total total
mg magnetron
heater heater
exfan exhaust fan
cofan cooling fan
blfan blower fan
con conveyor

ACKNOWLEDGMENT

This work was supported by the Thailand Research Fund (TRF) and by the National Research University Project of Thailand Office of the Commission on Higher Education (CHE).

REFERENCES

1. Mujumdar, A.S. *Handbook of Industrial Drying*, 2nd ed.; Marcel Dekker: New York, 1995.
2. Metaxas, A.C.; Meridith, R.J. *Industrial Microwave Heating*; Peter Peregrinus, Ltd.: London, 1983.
3. Datta, A.K.; Anantheswaran, R.C. *Handbook of Microwave Technology for Food Applications*; Marcel Dekker: New York, 2001.
4. Schubert, H.; Regier, M. *The Microwave Processing of Foods*; Woodhead Publishing Limited and CRC Press: Cambridge, 2005.
5. Ratanadecho, P.; Aoki, K.; Akahori, M. Experimental and numerical study of microwave drying in unsaturated porous material. International Communications in Heat and Mass Transfer **2001**, *28*, 605–616.
6. Sander, A. Thin-layer drying of porous materials: Selection of the appropriate mathematical model and relationships between thin-layer models parameters. Chemical Engineering and Processing **2007**, *46*, 1324–1331.
7. Salagnac, P.; Dutournié, P.; Glouannec, P. Optimal operating conditions of microwave-convective drying of a porous medium. Industrial and Engineering Chemistry Research **2008**, *47*, 133–144.
8. Abbasi Souraki, B.; Mowla, D. Simulation of drying behaviour of a small spherical foodstuff in a microwave assisted fluidized bed of inert particles. Food Research International **2008**, *41*, 255–265.
9. Zhang, Y.; Liu, R.; Hu, Y.; Li, G. Microwave heating in preparation of magnetic molecularly imprinted polymer beads for trace Triazines analysis in complicated samples. Analytical Chemistry **2009**, *81*, 967–976.
10. Markowski, M.; Bondaruk, J.; Błaszczak, W. Rehydration behavior of vacuum-microwave-dried potato cubes. Drying Technology **2009**, *27*, 296–305.
11. Mihoubi, D.; Bellagi, A. Drying-induced stresses during convective and combined microwave and convective drying of saturated porous media. Drying Technology **2009**, *27*, 851–856.
12. Ratanadecho, P.; Aoki, K.; Akahori, M. A numerical and experimental study of microwave drying using a rectangular wave guide. Drying Technology **2001**, *19*, 2209–2234.
13. Atong, D.; Clark, D.E. Ignition behavior and characteristics of microwave-combustion synthesized AI203-T:C powders. Ceramics International **2004**, *30*(7), 1909–1912.
14. Turner, I.W.; Ilic, M. Combined microwave and convective drying of a porous material. Drying Technology **1991**, *9*(5), 1209–1269.
15. Ratanadecho, P.; Aoki, K.; Akahori, M. Influence of irradiation time, particle sizes and initial moisture content during microwave drying of multi-layered capillary porous materials. ASME Journal of Heat Transfer **2002**, *124*(1), 151–161.
16. Vongpradubchai, S.; Rattanadecho, P. The microwave processing of wood using a continuous microwave belt drier. Chemical Engineering and Processing **2009**, *33*, 472–481.
17. Ratanadecho, P.; Aoki, K.; Akahori, M. The characteristics of microwave melting of frozen packed bed using a rectangular wave guide. IEEE Transactions on Microwave Theory and Techniques **2002**, *50*, 1487–1494.
18. Rattanadecho, P.; Suwannapum, N.; Watanasungsuit, A.; Duangduen, A. Drying of dielectric materials using microwave-continuous belt furnace. ASME Journal of Manufacturing Sciences and Engineering **2007**, *129*(1), 157–163.
19. Rattanadecho, P.; Suwannapum, N.; Chatveera, B.; Atong, D.; Makul, N. Development of compressive strength of cement paste under accelerated curing by using a continuous microwave belt drier. Material Science and Engineering **2008**, *472*, 299–307.
20. Buffer, C.R. *Microwave Cooking and Processing, Engineering Fundamentals for the Food Scientist*; Van Nostand Reinhold: New York, 1993.
21. Curet, S.; Rouaud, O.; Boillereaux, L. Microwave tempering and heating in a single-mode cavity: Numerical and experimental investigations. Chemical Engineering and Processing: Process Intensification **2008**, *47*(9–10), 1656–1665.
22. Pozar, D.M. *Microwave Engineering*; John Wiley & Sons: New York, 2005.

23. Sharma, G.P.; Prasad, S. Specific energy consumption in microwave drying of garlic cloves. Journal of Food Engineering **2005**, *31*, 1921–1926.
24. Varith, J.; Dijkanarukkul, P.; Achariyaviriya, A.; Achariyaviriya, S. Combined microwave-hot air drying of peeled longon. Journal of Food Engineering **2007**, *31*, 459–468.
25. Lakshmi, S.; Chakkaravarthi, A.; Subramanian, R.; Singh, V. Energy consumption in microwave cooking of rice and its comparison with other domestic appliances. Journal of Food Engineering **2005**, *78*, 715–722.
26. Alibas, I. Energy consumption and colour characteristics of nettle leaves during microwave, vacuum and convective drying. Biosystems Engineering **2007**, *96*(4), 495–502.
27. Poli, G.; Sola, R.; Veronesi, P. Microwave-assisted combustion synthesis of NiAl intermetallics in a single mode applicator: Modeling and optimization. Materials Science and Engineering **2006**, *A 441*, 149–156.
28. Cheng, J.; Zhou, J.; Li, Y.; Liu, J.; Cen, K. Improvement of coal water slurry property through coal physicochemical modifications by microwave irradiation and thermal heat. Energy & Fuels **2008**, *22*, 2422–2428.
29. Holtz, E.; Ahrné, L.; Karlsson, T.H.; Rittenauer, M.; Rasmuson, A. The role of processing parameters on energy efficiency during microwave convective drying of porous materials. Drying Technology **2009**, *27*, 173–185.
30. Soysal, Y.; Öztekin, S.; Eren, Ö. Microwave drying of parsley: Modelling, kinetics, and energy aspects. Biosystems Engineering **2006**, *93*(4), 403–413.
31. Leiker, M.; Adamska, M.A. Energy efficiency and drying rates during vacuum microwave drying of wood. Holz als Roh-und Werkstoff **2004**, *62*, 203–208.
32. Prommas, R.; Rattanadecho, P.; Cholaseuk, D. Energy and exergy analyses in drying process of porous media using hot air. International Communications in Heat and Mass Transfer **2010**, *37*, 372–378.
33. Jindarat, W.; Rattanadecho, P.; Vongpradubchai, S. Analysis of energy consumption in microwave and convective drying process of multi-layered porous material inside a rectangular wave guide. Experimental Thermal and Fluid Science **2011**, *35*(4), 728–737.